

Electronic Thesis and Dissertation Repository

12-14-2011 12:00 AM

Transition Metal Complexes with Reactive Trimethylsilylchalcogenolate Ligands: Precursors for the Preparation of Ternary Nanoclusters

Chhatra Bahadur Khadka
The University of Western Ontario

Supervisor
Prof. Dr. J. F. Corrigan
The University of Western Ontario

Graduate Program in Chemistry
A thesis submitted in partial fulfillment of the requirements for the degree in Doctor of Philosophy
© Chhatra Bahadur Khadka 2011

Follow this and additional works at: <https://ir.lib.uwo.ca/etd>

 Part of the [Inorganic Chemistry Commons](#), and the [Materials Chemistry Commons](#)

Recommended Citation

Khadka, Chhatra Bahadur, "Transition Metal Complexes with Reactive Trimethylsilylchalcogenolate Ligands: Precursors for the Preparation of Ternary Nanoclusters" (2011). *Electronic Thesis and Dissertation Repository*. 336.
<https://ir.lib.uwo.ca/etd/336>

This Dissertation/Thesis is brought to you for free and open access by Scholarship@Western. It has been accepted for inclusion in Electronic Thesis and Dissertation Repository by an authorized administrator of Scholarship@Western. For more information, please contact wlsadmin@uwo.ca.

Transition Metal Complexes with Reactive
Trimethylsilylchalcogenolate Ligands: Precursors for the
Preparation of Ternary Nanoclusters

(Spine title: Manganese containing Semiconductor Nanoclusters)

(Integrated-Article Format)

by

Chhatra B. Khadka

Graduate Program in Chemistry

A thesis submitted in partial fulfillment
of the requirements for the degree of
Doctor of Philosophy

The School of Graduate and Postdoctoral Studies
The University of Western Ontario
London, Ontario, Canada

© Chhatra B. Khadka 2011

Certificate of Examination

The University of Western Ontario, School of Graduate and
Postdoctoral Studies

Supervisor

Dr. John F. Corrigan

Examiners

Dr. Ignacio Vargas Baca

Dr. Mahi Singh

Dr. Philip A. W. Dean

Dr. Nicholas C. Payne

The Thesis by

Chhatra Bahadur Khadka

entitled

Transition Metal Complexes with Reactive Trimethylsilylchalcogenolate
Ligands: Precursors for the Preparation of Ternary Nanoclusters

is accepted in partial fulfillment of the
requirements for the degree of
Doctor of Philosophy

Date

Chair of the Thesis Examination Board

ABSTRACT

The Co^{2+} and Mn^{2+} complexes $(N,N'\text{-tmeda})\text{Co}(\text{ESiMe}_3)_2$ ($\text{E} = \text{S}$, **1a**; $\text{E} = \text{Se}$, **1b**), $(3,5\text{-Me}_2\text{C}_5\text{H}_3\text{N})_2\text{Co}(\text{ESiMe}_3)_2$ ($\text{E} = \text{S}$, **2a**; $\text{E} = \text{Se}$, **2b**), $[\text{Li}(N,N'\text{-tmeda})]_2[(N,N'\text{-tmeda})\text{Mn}_5(\mu\text{-ESiMe}_3)_2(\text{ESiMe}_3)_4(\mu_4\text{-E})(\mu_3\text{-E})_2]$ ($\text{E} = \text{S}$, **3a**; $\text{E} = \text{Se}$, **3b**), $[\text{Li}(N,N'\text{-tmeda})]_2[\text{Mn}(\text{SSiMe}_3)_4]$ (**4**), $[\text{Li}(N,N'\text{-tmeda})]_4[\text{Mn}_4(\text{SeSiMe}_3)_4(\mu_3\text{-Se})_4]$ (**5**), and $[\text{Li}(N,N'\text{-tmeda})]_4[\text{Mn}(\text{Se}_4)_3]$ (**6**) have been isolated from reactions of $\text{Li}[\text{ESiMe}_3]$ and the chloride salts of these metals. The treatment of $(N,N'\text{-tmeda})\text{CoCl}_2$ with two equivalents of $\text{Li}[\text{ESiMe}_3]$ ($\text{E} = \text{S}$, Se) yields **1a** and **1b**, respectively, whereas similar reactions with MnCl_2 yield the polynuclear complexes **3a** ($\text{E} = \text{S}$) and **3b** ($\text{E} = \text{Se}$). The selective preparation of the mononuclear complex **4** is achieved by increasing the reaction ratios of $\text{Li}[\text{SSiMe}_3]$ to MnCl_2 to 4:1. Single crystal X-ray analysis of **1–5**, confirms the presence of potentially reactive trimethylsilylchalcogenolate moieties and distorted tetrahedral geometry around the metal centers in each of these complexes. These compounds could potentially be utilized as a convenient source of paramagnetic ions for the synthesis of ternary clusters.

The ternary clusters $(N,N'\text{-tmeda})_6\text{Zn}_{14-x}\text{Mn}_x\text{S}_{13}\text{Cl}_2$ (**7a-d**) and $(N,N'\text{-tmeda})_6\text{Zn}_{14-x}\text{Mn}_x\text{Se}_{13}\text{Cl}_2$ (**8a-d**) and the binary clusters $(N,N'\text{-tmeda})_6\text{Zn}_{14}\text{E}_{13}\text{Cl}_2$ ($\text{E} = \text{S}$, **9a**; Se , **9b**) have been synthesized by reacting $(N,N'\text{-tmeda})\text{Zn}(\text{ESiMe}_3)_2$ with Mn^{2+} and Zn^{2+} salts. Single crystal X-ray analysis of the complexes confirms the presence of the six ' $(N,N'\text{-tmeda})\text{ZnE}_2$ ' units as capping ligands that stabilize the clusters, and distorted tetrahedral geometry around the metal centers. Mn^{2+} is incorporated into the ZnE matrix by substitution of Zn^{2+} ions in the cluster core. Complexes **7a**, **8a** and **8d** represent the first examples of 'Mn/ZnE' clusters with structural characterization and indications of the

local chemical environment of the Mn^{2+} ions. DFT calculations indicate that replacement of Zn with Mn is perfectly feasible and at least partly allows for the identification of some sites preferred by the Mn^{2+} metals. These calculations, combined with luminescence studies suggest a distribution of the Mn^{2+} in the clusters. The room temperature emission spectra of clusters **7c-d** display a significant red shift relative to the all zinc cluster **9a**, with a peak maximum centered at 730 nm. Clusters **8c-d** have a peak maximum at 640 nm in their emission spectra.

The chalcogenolate complexes **3a** and **4** have been utilized as molecular precursors for the isolation of ternary nanoclusters, with approximate formulae $[\text{Mn}_{35/36}\text{Ag}_{118/116}\text{S}_{94}(\text{P}^{\text{n}}\text{Pr}_3)_{30}]$, **10** and $[\text{Mn}_{19/20}\text{Ag}_{150/148}\text{S}_{94}(\text{P}^{\text{n}}\text{Pr}_3)_{30}]$, **11** respectively. Mn^{2+} is incorporated into the Ag_2S matrix by substitution of two Ag^+ ions in the cluster core.

Keywords:

Nanocluster, ternary, quantum confinement, paramagnetic, chalcogen, chalcogenolate, chalcogenide, X-ray crystallography, nanomaterials, photoluminescence, semiconductor, silylated reagents, dilute magnetic semiconductor, quantum dot, doping, Group 6, Group 2.

In memory of my late father

ACKNOWLEDGEMENTS

Foremost, I would like to express my sincere gratitude to my supervisor Dr. John F. Corrigan for all his patience, motivation, enthusiasm and important support throughout this work. You have been a great teacher and have provided me with ample guidance during my studies here. I cannot thank you enough for your kind support, all the opportunities, constant encouragement and endless corrections of my thesis.

During my six long years at Western, I have had the privilege of meeting many people. I thank them all for their friendship and support that have made those six years fun and memorable. I would like to take this opportunity to thank all the graduate and undergraduate students with whom I had the privilege of working with. I would like to thank Siawash Ahmar, Taylor Battista, Aneta Borecki, Mahmood Fard, Diane Medeiros, Brian Nikkel, Dr. Christian Nitschke, Bahar Khalili, Tetyana Levchenko, Dr. Dan Macdonald, Dr. Deeb Taher and Dr. Elizabeth Turner. I owe a special thanks to Aneta Borecki who taught me the all important Schlenk line and other techniques at the beginning of my graduate studies and Dan for solving my crystal structures. Special thanks go out to Siawash, Dan, Ashlee Howarth, Terry Lebold, Dave Dodd, Dwayne Dias and Pellumb Jakupi for great friendship and all those memorable times we had over the years.

I would like to thank the members of the Chemistry Staff that have provided support during my graduate studies. Firstly, Yves Rambour, our glass blower, for all the glassware he has made and repaired. I would like to thank the NMR facility, Matt Willians, Chris Kirby and Kyle Pollard for their assistance with the NMR instruments. Doug Hairsine is thanked for obtaining all mass spectra for this research and repairing

our vacuum pumps. I have to thank all the helpful staff at ChemBio Stores and electronic shops for meeting my requests for chemicals, keeping our glove boxes running properly and taking care of our computers and other electrical equipment. I would also like to thank our graduate coordinators present (Darlene McDonald) and past (Cheryl O'Meara) for all their help.

I would like to take this moment to thank all the people who have made contributions to this research. Dr. Annie K. Powell (KIT, Germany) is thanked for allowing me to be a part of her lab during the ASPIRE exchange program and Dr. Yanhua Lan (KIT, Germany) for her help with magnetic studies. Dr. Andreas Eichhöfer (KIT, Germany) and Dr. Florian Weigend (KIT, Germany) are thanked for invaluable suggestions, critical input and DFT calculations, respectively. Dr. Robert Hudson (UWO) is thanked for allowing access to his fluorimeter. Dr. Mike Jennings and Dr. Guerman Popov are thanked for their help with crystallography. I would also like to thank Dr. Nick Payne (UWO) for teaching me X-ray crystallography and helping me with crystallographic problems as well.

Finally, I have to give a special thanks to my family: although, I have been away from them most of my life, I have always felt their love and support. Without their never-ending support and constant encouragement, I would have never accomplished this.

TABLE OF CONTENTS

CERTIFICATE OF EXAMINATION	ii
ABSTRACT	iii
EPIGRAPH	v
ACKNOWLEDGEMENTS	vi
TABLE OF CONTENTS	viii
CO-AUTHORSHIP	xi
LIST OF TABLES	xii
LIST OF FIGURES	xiii
LIST OF SCHEMES	xv
LIST OF APPENDICES	xv
LIST OF ABBREVIATIONS	xvii
CHAPTER ONE: INTRODUCTION	1
<i>Manganese Doped Semiconductor Nanoclusters</i>	
1.1. Semiconductor Nanomaterials and the Quantum Confinement Effect....	1
1.2. Optical Properties of Quantum Confined Nanoparticles	5
1.3. Doping in Quantum Dots	8
1.3.1. Electronic structure of Mn ²⁺ in II-VI Semiconductor Lattice	9
1.3.2. Synthesis of Mn ²⁺ doped II-VI semiconductor QDs.....	12
1.4. Molecular Precursor Route to Mn ²⁺ Doped II-VI Nanoparticles.....	13
1.5. Molecular Precursor Route to Ternary MM'E Nanoclusters.....	15
1.5.1. Synthesis of Chalcogenolate Precursors	15
1.5.2. Reaction of Chalcogenolate Precursor with other Metal salts	17
1.6. Scope of the Thesis	19
1.7. References	21
CHAPTER TWO:	27
<i>Trimethylsilylchalcogenolates of Co(II) and Mn(II): From Mononuclear Coordination Complexes to Clusters Containing –ESiMe₃ Moieties (E= S, Se)</i>	
2.1. Introduction.....	27
2.2. Results and Discussion	28
2.2.1. Synthesis of Cobalt(II) Chalcogenolate Complexes	28
2.2.2. X-ray Crystallographic Structural Characterization	30
2.2.3. Synthesis and Characterization of Manganese(II) Chalcogenolate Complexes.....	34

2.2.3.1. Magnetic Measurement.....	46
2.3. Conclusions.....	49
2.4. Experimental Section.....	50
2.4.1. General Experimental.....	50
2.4.2. Syntheses.....	52
2.4.2.1. Synthesis of $(N,N'$ -tmeda)Co(SSiMe ₃) ₂ , 1a	52
2.4.2.2. Synthesis of $(N,N'$ -tmeda)Co(SeSiMe ₃) ₂ , 1b	52
2.4.2.3. Synthesis of (3,5-Me ₂ C ₅ H ₃ N) ₂ Co(SSiMe ₃) ₂ , 2a	53
2.4.2.4. Synthesis of (3,5-Me ₂ C ₅ H ₃ N) ₂ Co(SeSiMe ₃) ₂ , 2b	53
2.4.2.5. Synthesis of [Li(N,N' -tmeda)] ₂ [(N,N' -tmeda)Mn ₅ (SSiMe ₃) ₆ (S) ₃], 3a	54
2.4.2.6. Synthesis of [Li(N,N' -tmeda)] ₂ [(N,N' -tmeda)Mn ₅ (SeSiMe ₃) ₆ (Se) ₃], 3b	54
2.4.2.7. Synthesis of [Li(N,N' -tmeda)] ₂ [Mn(SSiMe ₃) ₄], 4	54
2.4.2.8. Synthesis of [Li(N,N' -tmeda)] ₄ [Mn ₄ (SeSiMe ₃) ₄ (Se) ₄], 5	55
and [Li(N,N' -tmeda)] ₄ [Mn(Se ₄) ₃], 6	55
2.5. References.....	56

CHAPTER THREE:.....59

***Zinc Chalcogenolate Complexes as Molecular Precursors to Mn²⁺
Containing ZnE (E= S, Se) Nanoclusters***

3.1. Introduction.....	59
3.2. Results and Discussion.....	61
3.2.1. Synthesis and Characterization of Chalcogenide Complexes.....	61
3.2.2. Photoluminescence Properties.....	71
3.3. Metal type Assignment by Quantum Chemical Calculations.....	77
3.4. Conclusions.....	85
3.5. Experimental Section.....	86
3.5.1. General Experimental.....	86
3.5.2. Syntheses.....	88
3.5.2.1. Synthesis of [(N,N' -tmeda) ₆ Zn _{12.3} Mn _{1.7} S ₁₃ Cl ₂], 7a	88
3.5.2.2. Synthesis of [(N,N' -tmeda) ₆ Zn _{10.9} Mn _{3.1} S ₁₃ Cl ₂], 7b	88
3.5.2.3. Synthesis of [(N,N' -tmeda) ₆ Zn ₁₀ Mn ₄ S ₁₃ Cl ₂], 7c	89
3.5.2.4. Synthesis of [(N,N' -tmeda) ₆ Zn _{6.2} Mn _{7.8} S ₁₃ Cl ₂], 7d	89
3.5.2.5. Synthesis of [(N,N' -tmeda) ₆ Zn ₁₂ Mn ₂ Se ₁₃ Cl ₂], 8a	90
3.5.2.6. Synthesis of [(N,N' -tmeda) ₆ Zn _{10.8} Mn _{3.2} Se ₁₃ Cl ₂], 8b	90
3.5.2.7. Synthesis of [(N,N' -tmeda) ₆ Zn _{10.7} Mn _{3.3} Se ₁₃ Cl ₂], 8c	91
3.5.2.8. Synthesis of [(N,N' -tmeda) ₆ Zn _{8.2} Mn _{5.8} Se ₁₃ Cl ₂], 8d	91
3.5.2.9. Synthesis of [(N,N' -tmeda) ₆ Zn ₁₄ S ₁₃ Cl ₂], 9a	91
3.5.2.10. Synthesis of [(N,N' -tmeda) ₆ Zn ₁₄ Se ₁₃ Cl ₂], 9b	92
3.6. References.....	93

CHAPTER FOUR:	98
<i>Manganese Chalcogenolate Complexes as Molecular Precursors to Mn²⁺ Containing Ag₂S Nanoclusters</i>	
4.1. Introduction.....	98
4.2. Results and Discussion	100
4.2.1. Synthesis and characterization of [Mn _x Ag _{188-2x} S ₉₄ (P ⁿ Pr ₃) ₃₀], 10-11	100
4.2.2. Optical Properties of MnAgS Clusters	111
4.3. Conclusions.....	114
4.4. Experimental Section	114
4.4.1. General Experimental	114
4.4.2. Syntheses.....	116
4.4.2.1. Synthesis of [Mn ₃₆ Ag ₁₁₆ S ₉₄ (P ⁿ Pr ₃) ₃₀], 10	116
4.4.2.2. Synthesis of [Mn ₂₀ Ag ₁₄₈ S ₉₄ (P ⁿ Pr ₃) ₃₀], 11	116
4.4.2.3. Synthesis of [Ag ₁₈₈ S ₉₄ (P ⁿ Pr ₃) ₃₀], 12	117
4.5. References	118
 CHAPTER FIVE:	122
<i>Summary and Future work</i>	
5.1. Summary	122
5.2. References.....	126
 APPENDIX A:	127
X-ray Crystallographic Data Parameters and Atomic Positions For Compounds 1-10	
 APPENDIX B:	161
Magnetic data for Compound 3b Uv-Visible, PL and PLE for Compound 7b, 7c, 8b and 8c Quantum chemical calculations data for Compound 7-8 Copyright information and permissions	
 CURRICULUM VITAE	177

Co-Authorship

Chapter 2 was based on a manuscript authored by Chhatra Khadka, Daniel MacDonald, Yanhua Lan, Annie Powell, Dieter Fenske and John Corrigan. All the experimental work and majority of writing was performed by Chhatra Khadka with the exception of X-ray crystallographic analyses which were performed by Daniel Macdonald and John Corrigan. The magnetic studies (Section 2.2.2.3.1) were performed together with Annie Powell and Yanhua Lan at KIT, Karlsruhe, Germany.

Chapter 3 was based on a manuscript authored by Chhatra Khadka, Andreas Eichhöfer, Florian Weigend and John Corrigan. All the experimental work and majority of writing was performed by Chhatra Khadka and X-ray crystallographic analyses which were performed by John Corrigan. The DFT calculations (Section 3.3) were performed by Florian Weigend at KIT, Karlsruhe, Germany.

LIST OF TABLES

Table 2.1.	Selected bond lengths (Å) and Angles (°) for Complexes 1-2	34
Table 2.2.	Selected bond lengths (Å) and Angles (°) for Complexes 3a, 3b	38
Table 2.3.	Selected bond lengths (Å) and Angles (°) for Complex 4	40
Table 2.4.	Selected bond lengths (Å) and angles (°) for Complex 5	43
Table 2.5.	Selected bond lengths (Å) and Angles (°) for Complex 6	45
Table 3.1.	Selected bond lengths (Å) Complexes 9a, 9b	64
Table 3.2.	Selected bond Angles (°) for Complexes 9a, 9b	66
Table 3.3.	Atomic ratio of Zinc and Manganese using ICP-AES 7-8	68
Table 3.4.	Selected bond lengths (Å) and angles (°) for Complex 8d	70
Table 3.5.	Frequency (%) of Mn found at positions 1-8 for isomers that are higher in energy than the most stable one of each composition by less than 3 kJ/mol	83
Table 3.6.	Most favorable isomers for each composition, 7-8	84
Table 4.1.	X-ray Crystallographic Data parameters for Complex 10	106
Table 4.2.	Atomic ratio of Mn:S:Ag obtained using EDX analyses for 10 and 11	109
Table 4.3.	Molecular formula calculated using the metal ratio from ICP-AES, 10 and 11	110
Table 4.4.	Selected Bond Distances (Å) for 3a and 10	111

LIST OF FIGURES

Figure 1.1.	Schematic representation of the electronic structure of bulk semiconductors, quantum dot and molecule.....	3
Figure 1.2.	Schematic diagram representing the origin of band-edge and deep trap emissions	6
Figure 1.3.	Representative normalized photoluminescence spectra of typical II-VI thiol-capped nanocrystals	7
Figure 1.4.	Tanabe-Sugano ligand field energy level diagram for Mn^{2+} (d^5) in a cubic ligand field	10
Figure 1.5.	Schematic illustration of non-radiative and radiative relaxation process in Mn^{2+} doped II-VI QDs.....	11
Figure 1.6.	Molecular structure of the cluster $[Cd_4Mn_6Se_4(SePh)_{12}(P^rPr_3)]$...	14
Figure 1.7.	Some examples of M-ESiMe ₃ complexes used as precursor for MM'E cluster synthesis.....	16
Figure 1.8.	Molecular structure of $Hg_{15}Cu_{20}Se_{25}(P^rPr_3)_{18}$	18
Figure 1.9.	Molecular structure of $(tmeda)_5Zn_5Cd_{11}Se_{13}(SePh)_6$	18
Figure 2.1.	The molecular structure of $(N,N'-tmeda)Co(SSiMe_3)_2$, 1a and $(N,N'-tmeda)Co(SeSiMe_3)_2$, 1b	31
Figure 2.2.	The molecular structures of, $(3,5-Me_2-C_5H_3N)_2Co(SSiMe_3)_2$, 2a and $(3,5-Me_2-C_5H_3N)_2Co(SeSiMe_3)_2$, 2b	32
Figure 2.3.	Molecular structure of $[Li(N,N'-tmeda)]_2$ $[(N,N'-tmeda)Mn_5(\mu-SSiMe_3)_2(SSiMe_3)_4(\mu_4-S)(\mu_3-S)_2]$, 3a	36
Figure 2.4.	The Mn_5Se_9 framework in the molecular structure of $[(N,N'-tmeda)Mn_5(\mu-SeSiMe_3)_2(SeSiMe_3)_4(\mu_4-Se)(\mu_3-Se)_2]^{2-}$, 3b	37
Figure 2.5.	Molecular structure $[Li(N,N'-tmeda)]_2[Mn(SSiMe_3)_4]$, 4	39
Figure 2.6.	Molecular structure of $[Li(N,N'-tmeda)]_4$ $[Mn_4(SeSiMe_3)_4(\mu_3-Se)_4]$, 5	41
Figure 2.7.	The molecular structure of $[Li(N,N'-tmeda)]_4[Mn(Se_4)_3]$, 6	44

Figure 2.8.	Plots of χT vs T (top) and M vs H (bottom) for Complex 3a	47
Figure 2.9.	Plots of χT vs T (top) and M vs H (bottom) for Complex 5	48
Figure 3.1.	Molecular structure of $[(N,N'-tmeda)_6Zn_{14}E_{13}Cl_2]$, 9a	63
Figure 3.2.	The stereo pair images of $[(N,N'-tmeda)_6Zn_{14}E_{13}Cl_2]$, 9a-b	67
Figure 3.3.	Molecular structure of $[(N,N'-tmeda)_6Zn_{10}Mn_4Se_{13}Cl_2]$, 8d	69
Figure 3.4.	Normalized room temperature solution state UV-visible absorption, photoluminescence excitation (PLE) and photoluminescence (PL), 9a , 7a and 7d	72
Figure 3.5.	Normalized room temperature solution state UV-visible absorption, photoluminescence excitation (PLE) and photoluminescence (PL), 9b , 8a and 8d	74
Figure 3.6.	Normalized room temperature solid state photoluminescence (PL), 9a , 8a and 8d	76
Figure 3.7.	$(N,N'-tmeda)_6Zn_{14-x}Mn_xS_{13}Cl_2$. The eight positions labeled by numbers are occupied by either Mn or Zn	79
Figure 3.8.	Estimated relative energies versus explicitly calculated energies for selected isomers of $Zn_{10}Mn_4$	82
Figure 4.1.	Dynamic light scattering measurements of 10 and 11	102
Figure 4.2.	Depiction of the polyhedra defined by sulfide ligands in 12	104
Figure 4.3.	Molecular structure and space filling model of 10	105
Figure 4.4.	Disordered core of compound 10	108
Figure 4.5.	Picture of single crystals of 10	108
Figure 4.6.	EDX spectrum of cluster $[Mn_{35/36}Ag_{118/116}S_{94}(P^nPr_3)_{30}]$, 10	109
Figure 4.7.	Normalized room temperature UV-visible absorption spectra of $Ag_{188}S_{94}(P^nPr_3)_{30}$, 10 , 11	113

LIST OF SCHEMES

- Scheme 1.1.** General outline of the reaction of M-ESiR₃ complexes with M'X_n salts in the formation of M-E-M' bridging interactions.... 15
- Scheme 2.1.** Synthesis of (N,N'-tmeda)Co(ESiMe₃)₂ and (3,5Me₂C₅H₃N)₂Co(ESiMe₃)₂28
- Scheme 3.1.** Synthesis of (N,N'-tmeda)₆Zn_{14-x}M_xE₁₃Cl₂ (**7a-9b**).....61

LIST OF APPENDICES

- Appendix A.1.** Crystal data and structure refinement for (N,N'-tmeda)Co(SSiMe₃)₂ **1a**..... 128
- Appendix A.2.** Crystal data and structure refinement for (N,N'-tmeda)Co(SSiMe₃)₂ **1b**..... 130
- Appendix A.3.** Crystal data and structure refinement for (3,5-Me₂-C₅H₃N)₂Co(SeSiMe₃)₂ **2a**..... 132
- Appendix A.4.** Crystal data and structure refinement for (3,5-Me₂-C₅H₃N)₂Co(SeSiMe₃)₂ **2b**..... 134
- Appendix A.5.** Crystal data and structure refinement for [Li(N,N'-tmeda)]₂ [(N,N'-tmeda)Mn₅(SSiMe₃)₂(SSiMe₃)₄(μ₄-S)(μ₃-S)]₂, **3a** 136
- Appendix A.6.** Crystal data and structure refinement [Li(N,N'-tmeda)]₂ [(N,N'-tmeda)Mn₅(SeSiMe₃)₂(SeSiMe₃)₄(μ₄-Se)(μ₃-Se)]₂, **3b** 138
- Appendix A.7.** Crystal data and structure refinement for [Li(N,N'-tmeda)]₂[Mn(SSiMe₃)₄], **4**..... 140
- Appendix A.8.** Crystal data and structure refinement for [Li(N,N'-tmeda)]₄[Mn₄(SeSiMe₃)₄(μ₃-Se)]₄, **5**..... 142
- Appendix A.9.** Crystal data and structure refinement for [Li(N,N'-tmeda)]₄[Mn(Se₄)₃], **6**..... 144
- Appendix A.10.** Crystal data and structure refinement for (N,N'-tmeda)₆Zn_{12.3}Mn_{1.7}S₁₃Cl₂, **7a**..... 146
- Appendix A.11.** Crystal data and structure refinement for (N,N'-tmeda)₆Zn_{6.2}Mn_{7.8}S₁₃Cl₂, **7d**..... 148

Appendix A.12.	Crystal data and structure refinement for (<i>N,N'</i> -tmeda) ₆ Zn ₁₂ Mn ₂ S ₁₃ Cl ₂ , 8a	150
Appendix A.13.	Crystal data and structure refinement for (<i>N,N'</i> -tmeda) ₆ Zn _{8.2} Mn _{5.8} S ₁₃ Cl ₂ , 8d	152
Appendix A.14.	Crystal data and structure refinement for (<i>N,N'</i> -tmeda) ₆ Zn ₁₄ S ₁₃ Cl ₂ , 9a	154
Appendix A.15.	Crystal data and structure refinement for (<i>N,N'</i> -tmeda) ₆ Zn ₁₄ Se ₁₃ Cl ₂ , 9b	156
Appendix A.16.	Crystal data and structure refinement for Mn _{35/36} Ag _{116/118} S ₉₄ (P ⁿ Pr ₃) ₃₀ , 10	158
Appendix B.1.	Plots of χT vs T (top) and M vs H (bottom) for Complex 3b .	161
Appendix B.2.	Normalized room temperature solution state UV-visible absorption, photoluminescence excitation (PLE) and photoluminescence (PL), 7b and 7c	162
Appendix B.3.	Normalized room temperature solution state UV-visible absorption, photoluminescence excitation (PLE) and photoluminescence (PL), 8b and 8c	163
Appendix B.4.	Quantum chemical calculations data for 7-8	164
Appendix B.5.	Copyright information and permissions	169

LIST OF ABBREVIATIONS

μL	microliter	min	minute
$^{\circ}\text{C}$	degree Celsius	mL.....	millilitre
\AA	angstrom	mm	millimetre
AES	atomic emission spectroscopy	mmol	millimole
B.....	Racah parameter	${}^n\text{Bu}$	<i>n</i> -butyl
CB	conduction band	nm	nanometer
CCDC.....	Cambridge Crystallographic Datacentre	${}^n\text{Pr}$	<i>n</i> -propyl
DCM	dichloromethane	OAc	acetate
DFT	density functional theory	<i>Oe</i>	Oerstad
DLS	dynamic light scattering	Ph	phenyl
DMF.....	dimethylformamide	PL.....	photoluminescence
DMS.....	dilute magnetic semiconductor	PLE	photoluminescence excitation
DMSO.....	dimethylsulfoxide	ppm	parts per million
E	chalcogen (S,Se,Te)	Py	pyridine
<i>E</i>	energy	QD.....	quantum dot
EDX	energy dispersive X-ray	R.....	organic side group
Et.....	ethyl	SQUID	superconducting quantum interference device
eV	electron volts	St	sterate
g.....	gram	T	temperature
<i>H</i>	magnetic field	${}^t\text{B}$	tert-butyl
Hex	hexyl	THF.....	tetrahydrofuran
HOMO	highest occupied molecular orbital	TMEDA	tetramethyl ethylenediamine
ICP	inductively coupled plasma	UV.....	ultraviolet
${}^i\text{Pr}$	<i>iso</i> -propyl	UV.....	ultraviolet
IR.....	infrared	VB	valence band
K.....	Kelvin	Vis.....	visible
LED.....	light emitting diode	Δ	Crystal field splitting parameter
LUMO.....	lowest unoccupied molecular orbital	μ_{B}	magnetic moment
M.....	d-block metal atom	χ	magnetic susceptibility
<i>M</i>	magnetization		
Me	methyl		

CHAPTER ONE

INTRODUCTION: MANGANESE DOPED SEMICONDUCTOR NANOCLUSTERS

1.1. Semiconductor Nanomaterials and the Quantum Confinement Effect

Nanomaterials are a class of materials having at least one dimension in the range of 1-100 nm. As such, their size is intermediate between a typical molecule and extended bulk solids. Nanomaterials continue to attract significant research interest from multiple scientific disciplines, which can be attributed to their unique size-dependent optoelectronic, magnetic and catalytic properties, phenomena not observed in bulk solids or molecular materials.¹⁻⁸ Understanding the properties of nanomaterials and exploring their potential applications are the two major driving forces behind the synthesis of a large variety of nanomaterials with diverse physiochemical properties. Magnetic nanomaterials of transition metals and transition metal oxides (e.g. Mn, Co, Fe₃O₄)^{9,10} have proven to be useful in various biomedical applications.¹¹ The possibility of designing catalysts with high activity, greater selectivity and high stability by tailoring the size, shape, morphology and composition of nanomaterials has led to an emerging field of 'nanocatalysts'.¹²⁻¹⁴ Amongst nanomaterials, semiconductors represent the most extensively studied class. Semiconductors are a class of materials which have conductivity values between those of conductors (metals) and insulators (glass) and whose band gap energies typically lie between 0.5 to 3.5 eV.¹⁵ The characteristic feature of a semiconductor is its intrinsic band gap (E_g), the energy that separates the filled valence band (VB) and empty conduction band (CB) (Figure 1.1). Semiconductors can be

pure elements (eg. Si, Ge), binary compounds (eg. GaAs, CdSe) and ternary compounds (eg. $Zn_xCd_{1-x}Se$, $Hg_xCd_{1-x}Te$).

When electrons absorb energy greater than that of the band gap of the semiconductor, they are excited across the band gap and into the conduction band. This transition creates a positively charged hole in the valence band and leads to the formation of an electron-hole pair, known as an exciton. The separation of an optically excited electron-hole pair is referred to as the excitonic Bohr radius, which is on the order of a few nanometers in semiconductors. The electron-hole pair can recombine releasing energy, often as a photon, approximately equal to the band gap of the material. This process is called a radiative recombination. Alternatively, an exciton can recombine non-radiatively without releasing a photon. The energy is often released through lattice vibrations or heat and is usually caused by defects in the crystal lattice or surface defects.¹⁶

As the size of semiconductor crystals becomes small enough that it approaches the size of the material's exciton Bohr radius, the exciton is confined by the dimension of the crystal, causing the nanomaterials to exhibit a quantum confinement effect.^{1,8} A nanomaterial can be quantum confined along one, two or all three dimensions. A quantum well describes the system confined in one dimension while a system confined in two dimensions is called quantum wire. A system confined in all three dimensions is called a quantum dot (QD). Well defined semiconducting quantum dots are the subject of this thesis. Colloidal quantum dots are made by organometallic chemical methods and have an inorganic core that is stabilized by a layer of organic molecules.¹⁷ Colloidal quantum dots emerged from a number of research labs in the early 1980s, with Louis

Brus being recognized as a pioneer in this field.^{18a} As the nanomaterials are reduced to the quantum confined size regime, the electronic energy levels can no longer be treated as continuous, as in a bulk semiconductor, but rather the quantization of energy levels occurs together with an increase in the band gap energy with decreasing particle size (Figure 1.1).

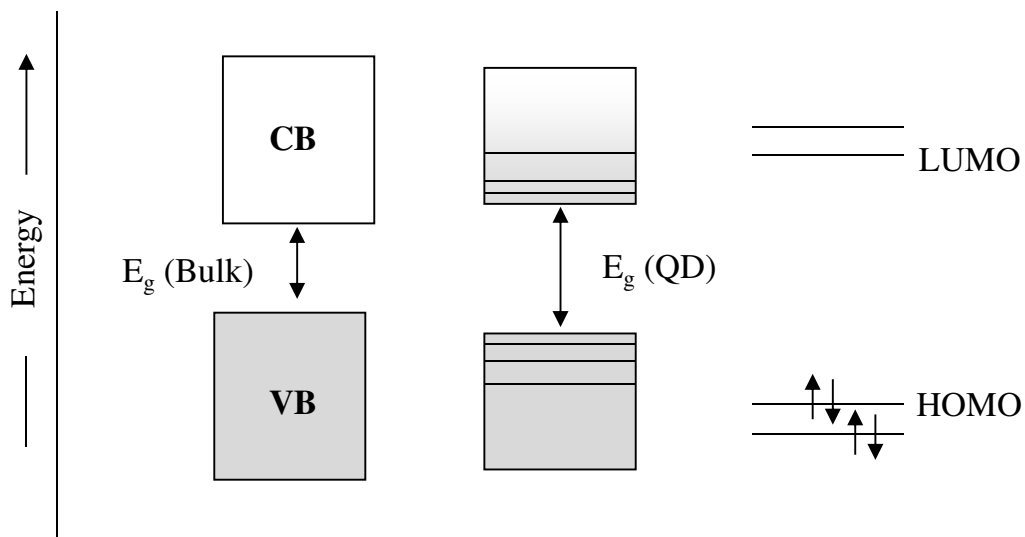


Figure 1.1. Schematic representation of the electronic structure of bulk semiconductors (left), quantum dot (middle) and molecules (right) showing the band gap (E_g).^{18b}

For each of the energy levels, the electronic state could be described by an atom-like wave function, that is, a probability distribution in space and time similar to the electrons bound to the nucleus. For this reason, quantum confined semiconductors are also called ‘artificial atoms’. In a bulk semiconductor, the dimensions of the system are essentially infinite compared to the dimensions of the carriers (negative electrons and positive holes). The wave functions, which are the standing waves in the materials, are spread over an infinite number of unit cells. Confinement in three dimensions based on the physical size of the material changes the boundary conditions imposed on the wave

function resulting in a transformation in the electronic structure from the continuous density of states in the bulk to the discrete levels in a quantum dot. The discrete structure of energy states leads to the discrete absorption observed in the absorption spectrum of the quantum dots, which is in contrast to the continuous spectrum of a bulk semiconductor. This is analogous to the ‘particle in a box’ model which predicts that the size dependent contribution to the energy gap is simply proportional to $1/R^2$. The energy associated with an electron and a hole pair in quantum dot is given by equation 1.1, derived using the parabolic band model, where E_R is the lowest excited state energy of the nanoparticle, E_g is the band gap energy of the bulk semiconductor, \hbar is the reduced Planck’s constant, R is the radius of the particle and m_e and m_h are the effective masses of the electron and hole, respectively.

$$E_R = E_g + \frac{\hbar^2 \pi^2}{2R^2} \left[\frac{1}{m_e} + \frac{1}{m_h} \right] \quad (1.1)$$

A more accurate correlation between the excitation energy and the particle size warrants the inclusion of the coulombic interaction that exists between the charge carriers in these confined systems. The appropriate relationship as proposed by Efros and Efros,^{18a} Brus¹⁹ and Kayanuma²⁰ is thus obtained by modifying equation 1.1 to account for the coulombic interaction and is given in equation 1.2.

$$E_R = E_g + \frac{\hbar^2 \pi^2}{2R^2} \left[\frac{1}{m_e} + \frac{1}{m_h} \right] - \frac{1.8e^2}{\epsilon R} - 0.248E_{Ry}^* \quad (1.2)$$

The coulombic interaction of an exciton is accounted by the second term in the equation 1.2 where ϵ is the dielectric constant of the semiconductor, while the third term is a

spatial correlation correction (E_{Ry}^* is the effective Rydberg energy). The latter term is not dependant on size and is typically very small, but may become significant for materials with a small dielectric constant. Besides effective mass approximation approach, empirical pseudopotential approach and tight-binding models are also used to gain reasonable estimation of the relationship between the excitonic energy with decreasing particle size in these quantum confined systems.²¹

1.2. Optical Properties of Quantum Confined Nanoparticles

The optical properties of semiconducting nanomaterials are strongly affected by their surface characteristics due to the presence of a higher fraction of surface atoms as the particle sizes decreases.²² Due to the consequence of quantum confinement, the particle size distribution of these nanomaterials has a significant impact on the optical properties. These effects can be observed in the emission spectra using photoluminescence (PL) spectroscopy. Photoluminescence of quantum dots can occur as either band edge PL or deep trap PL emission (Figure 1.2).²³ The capping of QD with organic ligands provides ‘electronic’ passivation by terminating dangling bonds present on the surface. The unterminated dangling bonds can affect the QD emission efficiency leading to a loss mechanism wherein electrons are trapped at the surface before emitting a photon. Band edge emission occurs from the recombination of the exciton from the shallow trap and is usually only slightly red shifted from the absorption energy with a narrow band width. On the other hand, the deep trap emission is characterised by a broad line width with significant red shift.

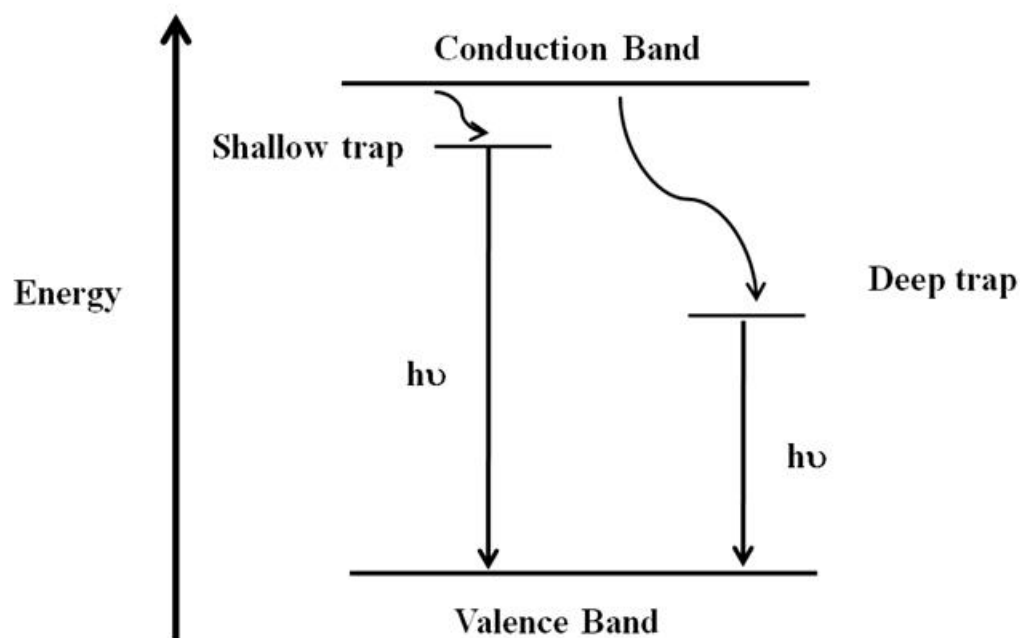


Figure 1.2. Schematic diagram representing the origins of band-edge (left) and deep trap emissions (right).²³

It is essential to control the surface chemistry of QDs to understand the direct interrelation between the nanocrystals and their unique physical and chemical properties. The surface passivation of QDs is usually carried out by using surface bound organic ligands or a secondary inorganic shell, which are capable of effectively eliminating the surface defect sites. It is well established that certain ligands (phosphines, phosphine oxides, amines, thiols) can be effectively used to reduce the surface defects, thereby enhancing the band-edge emission. On the other hand, growth of a secondary shell of a material with higher band gap energy than that of the core material introduces physical barrier between the surface ligands and the core eliminating the surface defects. A variety of so called ‘core-shell’ quantum dots, including CdSe/ZnSe,²⁴ CdSe/ZnS,^{25,26} and InAs/InP²⁷ have been extensively studied. Both of these passivation techniques enhance

the probability of electron-hole recombination by localizing the exciton on the discrete valence and conduction band energy levels.²⁴⁻²⁶ The synthesis of surface passivated monodisperse quantum dot is achieved via variety of synthetic pathways but the pyrolysis of metal-organic precursors in hot coordinating solvents (120-360°C) is the most successful in terms of monodispersity of the nanoparticles.²⁸ These preparative routes involve a temporally discrete nucleation event followed by relatively rapid growth from solution-phase and finally slower growth by Ostwald ripening. The disappearance of broad red shifted deep-trap emission and enhancement of sharp band-edge emission are indicative of effective passivation of the surface (Figure 1.3).²⁹

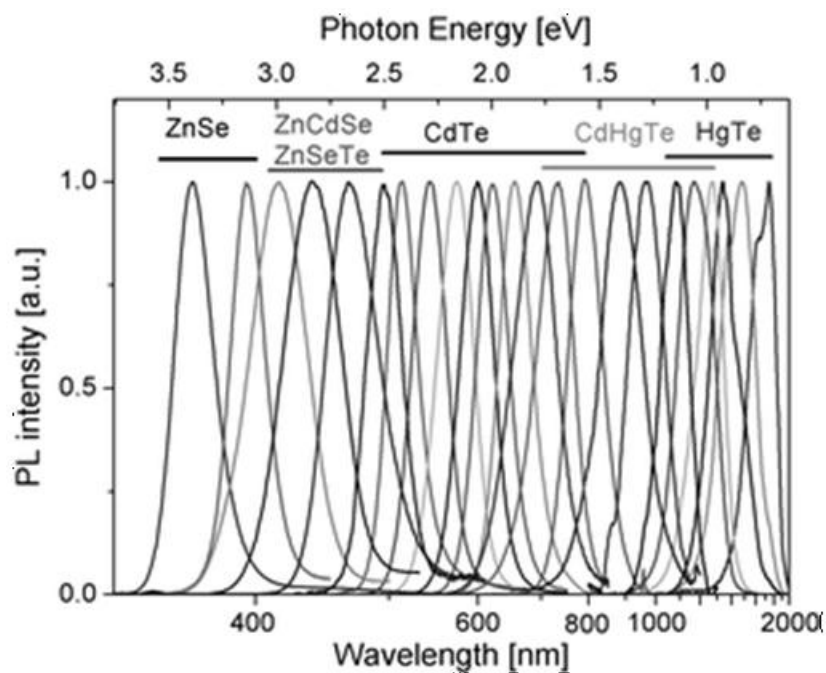


Figure 1.3. Representative normalized photoluminescence spectra of typical II-VI thiol-capped nanocrystals.²⁹ Reproduced with permission from The Royal Society of Chemistry.

More problematic and an area that has received less attention, however, has been the goal of controllably incorporating atomic impurities into semiconducting quantum dots. This technique is also known as doping. It is well known from present semiconductor technologies that the incorporation of impurities (dopants) or defects into semiconductor lattices is the primary means of controlling electrical conductivity, and may also have an immense effect on the optical, luminescent, magnetic, or other physical properties of the semiconductor.³⁰ Thus, doping is a critical step for tailoring properties for specific applications and to gain fundamental scientific understanding of the doping process in nanoparticles.

1.3. Doping in Quantum Dots

Doping semiconductor quantum dots with desired atomic impurities allows the possibility of tuning the emission to longer wavelengths that otherwise could not be possible from their undoped bulk counterparts.³¹ Doped QD can also be used to impart magnetic functionality into the semiconductor for the development of magneto-optical materials, whose optical properties can be tuned by an external magnetic field making them a potential candidate for spintronic applications. Spintronics (spin based electronics) will add the spin degree of freedom to conventional semiconductor charge-based electronics thereby enhancing the capability and performance of the electronic product. The potential advantages of these new devices could be increased processing speed and improved power efficiency compared with conventional semiconductor devices.³² Paramagnetic ions doped into nanoscale semiconductors (eg. ZnS, CdSe) at low concentrations, often referred to as dilute magnetic semiconductors (DMS),³² have

attracted significant interest due to their potential applications as well as fundamental physical properties.³³⁻⁴⁵ This is due to the unique size specific magnetic and optical properties, such as the giant Zeeman splitting of electronic states and carrier-induced ferromagnetism, that arises from the coexistence of the quantum confinement effect and its influence on the sp-d exchange interactions between magnetic ions and the semiconducting host.^{32,44,60} Doped QD not only retain all the advantages of QD, but can also eliminate the self-quenching from non-radiative recombinations. The energy of the excitons can be efficiently transferred to the dopant centres, suppressing undesirable radiation pathways, resulting in higher quantum yield combined with narrow emission line width.⁴⁶

Mn^{2+} is by far the most commonly used dopant and it acts both as luminescent center and localized spins in semiconductor nanoparticles.^{30,46} Mn^{2+} doped semiconductors have comparable emission efficiency as their undoped counterpart and can also have better thermal, chemical and photochemical stability.^{36,44} Further exploration into these robust and efficient emitters could lead to applications such as lasers,⁴⁷ light emitting diodes,⁴⁸ and in bioimaging.³⁴ Furthermore, as a source of magnetic centers, they have potential to find application in magneto-optics and magneto-electronic devices.⁴⁹

1.3.1. Electronic Structure of Mn^{2+} in II-VI Semiconductor Lattice

The local electronic structure of Mn^{2+} ions in a II-VI semiconductor crystal lattice has been successfully described by ligand field theory.⁵⁰⁻⁵² In the high spin state, Mn^{2+} , with five *3d* orbitals filled with one electron each, has a free ion ground state with six

fold spin degeneracy (6S). The tetrahedral or pseudo-tetrahedral cation geometries in a II-VI semiconductor lattice removes the five fold degeneracy of the $3d$ orbitals into a three fold degenerate t_2 set (d_{xy} , d_{yz} and d_{xz}) and a two fold degenerate e set ($d_{x^2-y^2}$, d_z^2). The energy difference between the more stable e and less stable t_2 set for a given cation depends on the crystal field splitting parameter. The splitting of the free ion ground state, as interpreted using a simplified Tanabe-Sugano diagram (Figure 1.4) for Mn^{2+} , gives rise to the ground state 6A_1 and the lowest-energy excited state. 4T_1 . The ${}^4T_1 \rightarrow {}^6A_1$ ligand field transition (Figure 1.4) is responsible for the characteristic luminescence of Mn^{2+} ions into doped II-VI semiconductor lattices.⁴⁶

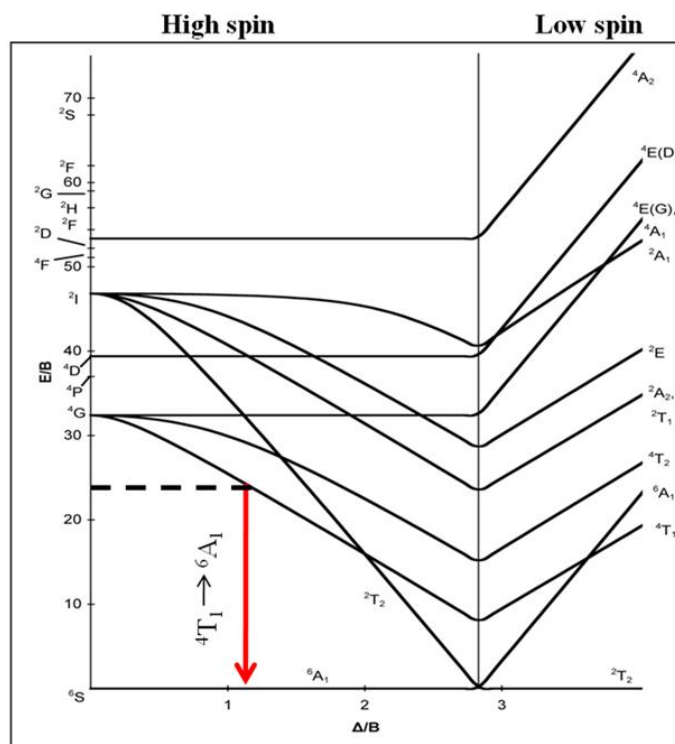


Figure 1.4. Tanabe-Sugano ligand field energy level diagram for Mn^{2+} (d^5) in a cubic ligand field, showing several spin forbidden lowest ligand field excited states, and indicating the emissive ${}^4T_1 \rightarrow {}^6A_1$ transition (orange arrow) observed in many Mn^{2+} doped II-VI semiconductor nanocrystals.⁵³ Reproduced from wikipedia as information available on the public domain (08/22/2011).

Although the spin selection rule forbids the ${}^4T_1 \rightarrow {}^6A_1$ transition, it is partially overcome by the spin-orbit coupling at the Mn^{2+} and to a lesser extent at the coordinated anions.⁵⁴ At higher Mn^{2+} concentrations, exchange interactions between $Mn^{2+}-Mn^{2+}$ also provide a mechanism that circumvents the spin forbiddness because the transition only needs to conserve the total spin of the “cluster”.^{55,56} The dynamics of electron-hole recombination in most Mn^{2+} doped II-VI semiconductor systems can be described based on the processes illustrated in Figure 1.5.

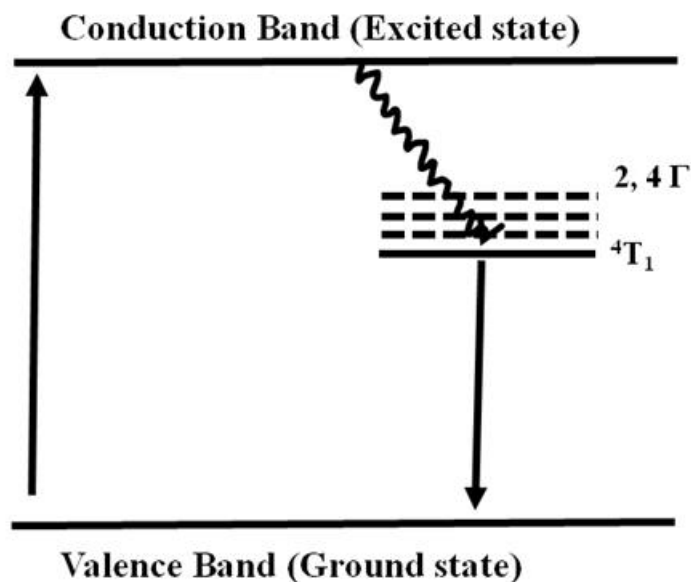


Figure 1.5. Schematic illustration of non-radiative (curly arrow) and radiative (straight arrow) relaxation process in Mn^{2+} doped II-VI QDs.⁴⁶ Reproduced with permission from Elsevier.

When an electron in the valence band of the Mn^{2+} doped II-VI host undergoes photo-excitation, it subsequently is transferred to the 4T_1 state. Following electron transfer, internal relaxation to the 4T_1 state occurs rapidly because of the large density of states. This is followed by a radiative ‘atomic like’ transition (${}^4T_1 \rightarrow {}^6A_1$) between the $3d$

orbital of Mn^{2+} . The ${}^4\text{T}_1 \rightarrow {}^6\text{A}_1$ ligand field excitation energy ($\sim 2.1\text{eV}$) is characteristic of Mn^{2+} doped II-VI semiconductors that have higher band gap energy than 2.1eV . Although the luminescence intensity of Mn^{2+} doped QDs varies with temperature and distribution of dopants, the energy transfer to Mn^{2+} which is very fast relative to excitonic emission, plays a vital role in the enhanced luminescence intensity observed in these systems.⁴⁶

1.3.2. Synthesis of Mn^{2+} Doped II-VI Semiconductor QDs

The importance of doping in bulk semiconductors has stimulated research efforts to develop synthetic methods to incorporate magnetic dopants into semiconducting nanoparticles. To date, a variety of semiconductor hosts have been doped with Mn^{2+} together with other magnetic impurities. The main challenge in the synthesis of doped QDs has been to introduce the impurity in the core (not on the surface or interface) of the nanoparticle without compromising the high crystallinity, monodispersity and well controlled size.⁵⁷ Most of the best characterized doped QDs investigated to date have been prepared using physical methods like molecular beam epitaxy, lithography and related techniques.⁵⁸⁻⁶¹ Along with the physical methods, chemical methods for the synthesis of analogously doped QDs have advanced considerably in recent years.⁶²⁻⁶⁴ The rapid exploration of a different experimental parameters (composition, size, shape etc.), easy processibility, scale-up capacity and the possibility of synthesizing unique heterostructures that the physical methods cannot are some of their advantages.^{46,65} With a brief overview of the literature, it becomes evident that molecular precursor decomposition, hot-injection, autoclave synthetic technique and inverse micelle are the

most commonly used chemical synthetic strategies.^{28,46,62-64} Although much progress has been made in the synthesis of doped QDs by chemical routes, there are still some puzzling questions. It remains difficult to incorporate Mn^{2+} into semiconductors (<6 nm) beyond 1-2% despite the high bulk solubility of these ions.^{29,66} To this day, reports on a complete and accurate structural characterization of the local environment of the magnetic ions within the semiconductor host is minimal.^{38,67} The accurate structural characterization of doped QDs is vital to gain insights into the unique phenomena that occur in quantum confined Mn^{2+} doped semiconductors and to establish structure property relationships. Almost all of the doped semiconductors studied to date are nanoparticles. As such, they are usually less well characterized and are often associated with a certain degree of size distribution. Although, there exists no distinct differentiation between the terms nanoparticle, nanomaterial and nanocluster in the literature, nanoclusters are considered (in this thesis) as nanoscale materials whose composition and structure can be determined accurately using X-ray crystallography. The synthesis of Mn^{2+} containing semiconductor nanoclusters could provide alternative synthetic techniques that would add to the ever growing knowledge of doping semiconductors at the nanoscale.

1.4. Molecular Precursor Route to Ternary Mn^{2+} Doped II-VI Nanoparticles

The molecular precursor approach to synthesize Mn^{2+} doped II-VI nanoparticles was first employed by the O'Brien group, who prepared Mn^{2+} doped ZnS and CdS by thermolysis using $\text{Zn}(\text{S}_2\text{CNEt}_2)_2$ or $\text{Cd}(\text{S}_2\text{CNMe}^n\text{Hex})_2$ as precursors in the presence of MnCl_2 .⁶⁸ Subsequently, the decameric cluster $[\text{Cd}_{10}\text{Se}_4(\text{SPh})_{16}]^{4-}$ was utilized as a

precursor in the presence of MnCl_2 to obtain Mn^{2+} doped CdSe nanoparticles via cluster thermolysis.⁴² Colloidal $\text{Mn}^{2+}:\text{CdSe}$ nanoparticles were synthesized in a thermolysis reaction using $[\text{Cd}_4(\text{SPh})_{10}]^{2-}$ in the presence of MnCl_2 and elemental selenium.⁶⁹ Similarly, $\text{Mn}^{2+}:\text{ZnSe}$ nanoparticles have been prepared by the use of $[\text{Zn}_4(\text{SPh})_{10}]^{2-}$ as molecular precursor in the presence of MnCl_2 salt and elemental selenium.⁷⁰ $[\text{Zn}_{10}\text{Se}_4(\text{SPh})_{16}]^{4-}$ has also been used in presence of $\text{Mn}(\text{stearate})_2$ to obtain Mn doped ZnSe nanowires.⁷¹ Despite the developments in preparation of Mn^{2+} doped II-VI nanoparticles employing different transition metal chalcogen complexes as precursors, analogous nanoclusters of these systems have received little attention. To our knowledge, the only published Mn^{2+} doped II-VI nanoclusters reported to date are $[\text{Cd}_4\text{Mn}_6\text{Se}_4(\text{SePh})_{12}(\text{PPr}_3)_4]$ (Figure 1.6) and $[\text{Cd}_4\text{Mn}_4\text{S}(\text{SePh})_{14}(\text{PPr}_3)_2]$ obtained using $\text{Cd}(\text{N}(\text{SiMe}_3)_2)$ and $\text{Mn}(\text{N}(\text{SiMe}_3)_2)$ as precursors in the presence of PhSeH and the addition of $\text{Se}(\text{SiMe}_3)_2$.⁷²

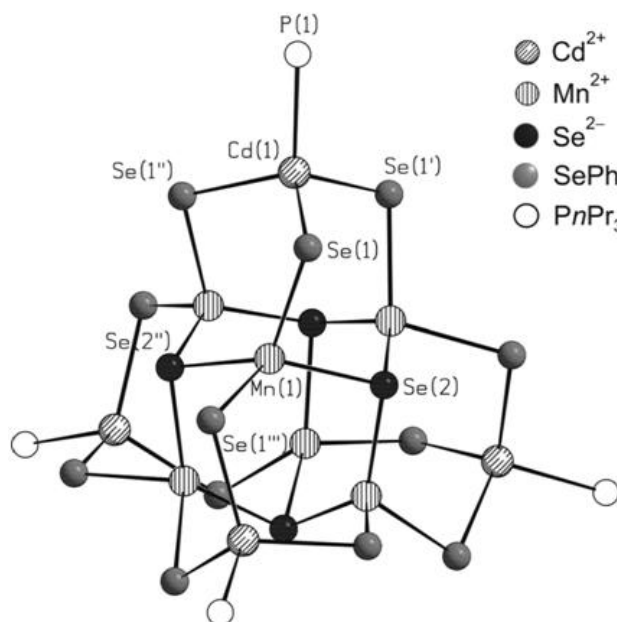
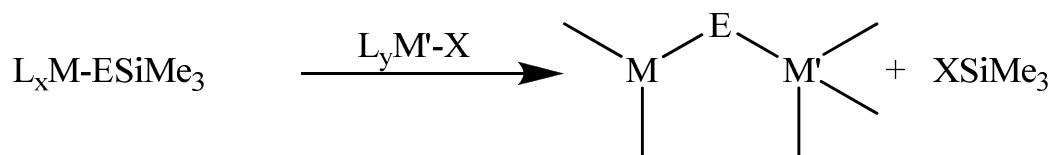


Figure 1.6. Molecular structure of the cluster $[\text{Cd}_4\text{Mn}_6\text{Se}_4(\text{SePh})_{12}(\text{P}^n\text{Pr}_3)_4]$.⁷² C and H atoms are omitted for clarity. Reproduced with permission from the American Chemical Society.

1.5. Molecular Precursor Route to Ternary MM'E (E= S, Se,Te) Nanoclusters

Previous works have proven that transition metal complexes coordinated with a silylchalcogenolate ligand represent practical precursors for synthesis of polynuclear MM'E nanoclusters.⁷³⁻⁸⁰ The principle of this designed methodology is focused on the synthesis of metal complexes with pendant reactive trimethylsilylchalcogenolate ligands. The $-\text{ESiMe}_3$ moieties of these complexes undergo substitution reactions with other metal salts leading to the formation of ternary MM'E as outlined in Scheme 1.1 below.



Scheme 1.1. General outline of the reaction of M-ESiR₃ complexes with M'X_n salts in the formation of M-E-M' bridging interactions (M, M' = d-block metals).⁷⁷

1.5.1. Synthesis of Chalcogenolate Precursors

The use of silylated chalcogen reagents (RESiMe_3 and $\text{E}(\text{SiMe}_3)_2$) in metal chalcogen nanocluster synthesis has been well developed by Fenske and coworkers.⁷⁹ These species react readily with a wide range of metal salts including main group and transition metals to form either metal chalcogenide (M-E-M') or metal chalcogenolate (M-ER) bonding interactions. The driving force for the reaction is the thermodynamically favorable formation of an X-Si bond and the elimination of XSiMe_3 (X= halide, acetate etc.). The synthesis of low nuclearity transition metal chalcogenolate complexes is complicated by the strong preference of chalcogenolate ligands to adopt bridging

coordination modes, thus leading to the formation of polymeric structures or infinite lattice structures. Typical strategies to overcome this tendency involve the use of sterically demanding (“bulky”) substituents ‘R’ on the chalcogenolate group and/or additional, strongly donating or chelating ancillary ligands around the metal centres.⁷⁹ The incorporation of large ligands to increase the steric bulk can prohibit further reactivity of these complexes. Thus, a delicate balance is needed to isolate M-ESiR₃ complexes in which the pendant -SiR₃ groups are still reactive.⁷⁹ The rationale for the synthesis of silyl-functionalized metal chalcogenolate is that the E-Si bonds are substantially weaker and can be more readily cleaved than E-C bonds. The elimination of the pendant -SiR₃ can be readily induced by reacting M-ESiR₃ complexes with M’X_n salts leading to M-E-M’ bridging interactions via elimination of XSiR₃. Some of the mononuclear transition metal chalcogenolates previously synthesized in the Corrigan laboratories that have been utilized as precursors for ternary nanocluster synthesis are shown in Figure 1.6.

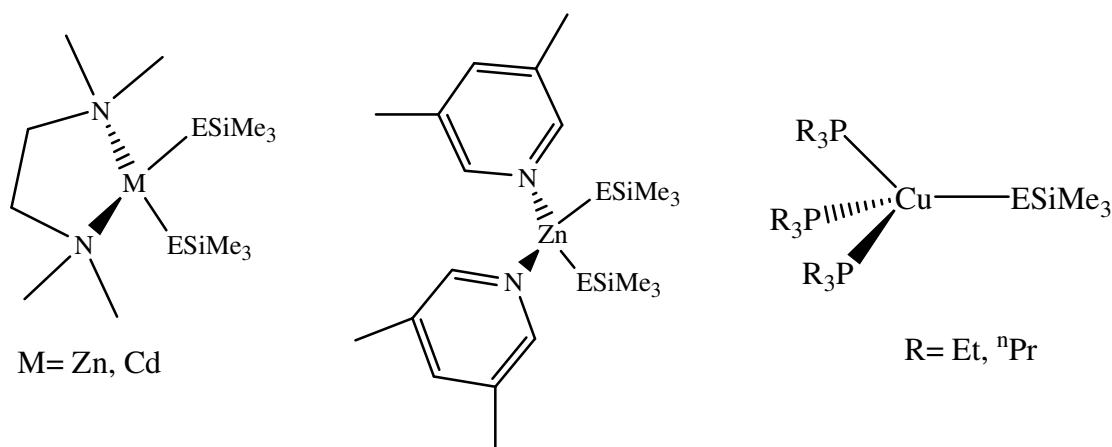


Figure 1.7. Some examples of M-ESiMe₃ complexes used as precursor for MM'E cluster synthesis.

1.5.2. Reaction of a Chalcogenolate Precursor with Other Metal Salts

The utility of the precursors complexes, (${}^n\text{Pr}_3\text{P}$) $_3\text{Cu}(\text{ESiMe}_3)$ ($\text{E} = \text{S}, \text{Se}$) for the synthesis of nanoscopic ternary clusters is demonstrated by the isolation of $[\text{Hg}_{15}\text{Cu}_{20}\text{E}_{25}(\text{P}^n\text{Pr}_3)_{18}]$.^{73a} The principle of this approach is based on the reactivity of the $-\text{SiMe}_3$ moiety, which can be exploited to promote the formation of Cu-E-Hg bonding interactions. Single crystal X-ray crystallographic analysis reveals the ‘pinwheel-shaped’ clusters $[\text{Hg}_{15}\text{Cu}_{20}\text{E}_{25}(\text{P}^n\text{Pr}_3)_{18}]$ ($\text{E} = \text{S}, \text{Se}$) in which the three core elements are intimately mixed within the structure as shown in Figure 1.8. Similarly, $[\text{Zn}_x\text{Cd}_{10-x}\text{E}_4(\text{EPh})_{12}(\text{P}^n\text{Pr}_3)_4]$ ⁷⁵ ($\text{E} = \text{Se}, \text{Te}; x = 2, 3$), and $[\text{Cu}_9\text{Ag}_3\text{S}_6(\text{PEtPh}_2)_8]$ ⁸⁰ have been synthesized using $(3,5\text{-Me}_2\text{C}_5\text{H}_3\text{N})_2\text{Zn}(\text{ESiMe}_3)_2$ and $(\text{PEtPh}_2)_3\text{Cu}(\text{SSiMe}_3)$, respectively. $(N,N'\text{-tmeda})\text{Zn}(\text{SeSiMe}_3)_2$ has also previously been utilized as a molecular precursors for the synthesis of the ternary nanocluster, $[(N,N'\text{-tmeda})_5\text{Zn}_5\text{Cd}_{11}\text{Se}_{13}(\text{SePh})_6(\text{THF})_2]$.^{76b} The molecular structure of this compound is shown in Figure 1.9.

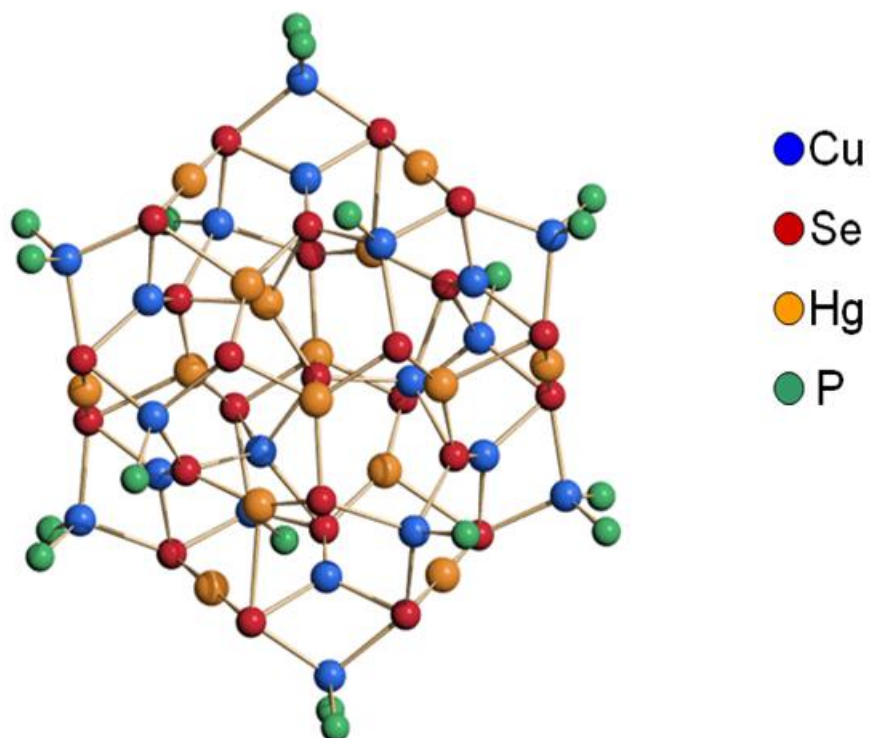


Figure 1.8. Molecular structure of $\text{Hg}_{15}\text{Cu}_{20}\text{Se}_{25}(\text{P}'\text{Pr}_3)_{18}$. The carbon atoms of the phosphine ligands are omitted for clarity.^{73a}

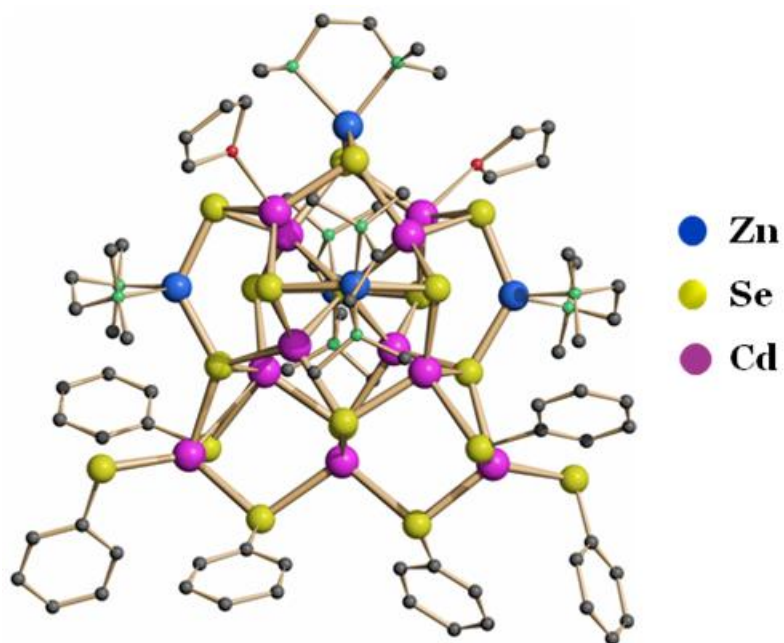


Figure 1.9. Molecular structure of $(\text{N,N}'\text{-tmeda})_5\text{Zn}_5\text{Cd}_{11}\text{Se}_{13}(\text{SePh})_6$.^{76b} Nitrogen (green spheres), Oxygen (Red spheres) and Carbon (Grey spheres). H atoms omitted for clarity.

1.6. Scope of the Thesis

The demonstrated ability of metal-trimethylsilylchalcogenolates to serve as molecular precursors to ternary MM'E nanoclusters and nanoparticles prompted us to develop this class of complex to include the paramagnetic metal ions Mn^{2+} and Co^{2+} . Recent studies on doping at the nanoscale have suggested the propensity for impurities to diffuse to the surface or into the surrounding matrix due to the thermodynamic driving forces, leading to surface doping rather than the desired doping of the nanocrystal core.^{29,57,66} Development of synthetic methods to overcome the problem of dopant exclusion of nanocrystal core and homogenous dopant speciation could provide a platform to investigate the structure-property relationships of doped quantum dots. As discussed in the previous section, the use of silylated chalcogen reagents allows low temperature, controlled formation of structurally characterized polynuclear heterometallic chalcogenolate and chalcogenide nanoclusters. The isolation and structural characterization of ternary nanocluster containing Mn^{2+} , using this methodology, could provide improved and/or additional synthetic route to doped QDs. The nanoclusters benefit from the size homogeneity and the X-ray characterization allows the determination of exact location of the dopants within the semiconductor matrix.

Chapter 2 of this thesis reports on the synthesis and structural characterization of a set of manganese and cobalt trimethylsilylchalcogenolates. The structural characterization and magnetic studies of these compounds suggests that they could be utilized as molecular precursor to isolate ternary nanoclusters containing magnetic impurities in semiconductor matrix. Chapter 3 describes the chemistry of the zinc-trimethylsilylchalcogenolate complexes, $(N,N'\text{-tmeda})\text{Zn}(\text{ESiMe}_3)_2$ ($\text{E} = \text{S}, \text{Se}$) as

molecular precursors to isolate MnZnE ternary nanoclusters which were structurally characterized. Photoluminescence studies, metal ion analysis and X-ray characterization of these nanoclusters confirm the successful incorporation of Mn^{2+} inside the cluster core. The amount of precursors used in the reaction conditions can be altered to vary the metal concentration in the ternary clusters without compromising its size. The utility of Mn^{2+} chalcogenolates as precursor to synthesize Mn^{2+} containing Ag_2S is explored in the fourth chapter. X-ray analysis of such ternary nanoclusters was difficult due to high disorder present within the cluster core. Although Mn^{2+} chalcogenolate complexes successfully delivered ' Mn_xS_y ' in the synthesis of ternary nanoclusters, its effect on the photoluminescence properties was marred due to lack of emission at room temperature. Chapter 5 summarizes the results obtained and provides thoughts on the usefulness of the synthetic approach used and some future research endeavors that could be pursued.

1.7. References

1. Alivisatos, A. P. *J. Phys. Chem.* **1996**, *100*, 13226-13239
2. Weller, H. *Angew. Chem. Int. Ed. Engl.* **1993**, *32*, 41-53
3. Woggon, U. *Optical Properties of Semiconducting Quantum Dots*; Springer Tracts in Modern Physics 136; Springer, New York, NY, **1997**
4. Sapra, S.; Sarma, D. D. *The Chemistry of Nanomaterials: Synthesis, Properties and Applications*; Rao, C. N. R.; Muller, A; Chetham, A. K.; Eds; Wiley-VCH: Weinheim, **2004**; Vol2 pp371-404
5. Murray, C. B.; Kagan, C. R.; Bawendi, M. G. *Annu. Rev. Mater. Sci.* **2000**, *30*, 545-610
6. Efros, A. L.; Rosen, M. *Annu. Rev. Mater. Sci.* **2000**, *30*, 475-521
7. Wang, Y; Herron, N. *J. Phys. Chem.* **1991**, *95*, 525-532
8. Steigerwald, M. L.; Brus, L. E. *Acc. Chem. Res.* **1990**, *23*, 183-188
9. Puntès, V. F.; Krishanan, K. M.; Alivisatos, A.P. *Science.* **2001**, *291*, 2115-2117
10. Park, S.; Kim, S.; Lee, S.; Khim, Z. G.; Char, K.; Hyeon, T. *J. Am. Chem. Soc.* **2000**, *122*, 8581-8582
11. Alexiou, C.; Jurgons, R.; Selinger, C.; Iro, H. *J. Nanosci. Nanotech.* **2006**, *6*, 2762-2768
12. Henkes, A. E.; Vasquez, Y.; Schaak, R. E. *J. Am. Chem. Soc.* **2007**, *129*, 1896-1897
13. Chiang, R. K.; Chaing, R. T. *Inorg. Chem.* **2007**, *46*, 369-371
14. Dhas, N. A.; Suslick, K. S. *J. Am. Chem. Soc.* **2005**, *127*, 2368-2369.
15. Wulfsberg, G. *"Inorganic Chemistry"*. **2000**, University Science Books: California, 620-624.

16. Trindale, T. O.; O'Brien, P.; Pickett, N. L. *Chem. Mater.* **2001**, *13*, 3843-3858
17. Yin, Y.; Alivisatos, A.P. *Nature.* **2005**, *437*, 664-670
18. a) Efros, Al. L.; Efros, A. L. *Sov. Phys. Semicond.* **1982**, *16*, 772-777. b) Rao, C. N. R.; Kulkarni, G. U.; Thomas, P. J.; Edwards, P.P. *Chem. Eur. J.* **2002**, *8*, 29
19. a) Brus, L. E. *J. Chem. Phys.* **1983**, *79*, 5566-5571. (b) Brus, L. E. *J. Chem. Phys.* **1984**, *80*, 4403-4409. (c) Brus, L. E. *J. Phys. Chem.* **1986**, *90*, 2555-2560.
20. Kayanuma, Y. *Solid State Commun.* **1986**, *59*, 405-408.
21. (a) Lippens, P. E.; Lannoo, M. *Phys. Rev. B* **1989**, *39*, 10935-10942. (b) Lippens, P. E.; Lannoo, M. *Mater. Sci. Eng. B* **1991**, *9*, 485-487.
22. Murray, C. B.; Norris, D. J.; Bawendi, M. G. *J. Am. Chem. Soc.* **1993**, *115*, 8706-8715
23. Eychmüller, A.; Hasselbarth, A.; Katsikas, L.; Weller, H. *J. Lumin.* **1991**, 745-749
24. Danek, M.; Jansen, K. F.; Bawendi, M. G. *Chem. Mater.* **1996**, *8*, 173-180
25. Hines, M. A.; Guyot-Sionnest, P. *J. Phy. Chem.* **1996**, *100*, 468-471
26. Talapin, D. V.; Rogach, L. A.; Kornowski, A.; Haase, M.; Weller, H. *Nano. Lett.* **2001**, *1*, 207-211
27. Cao, Y.; Banin, U. *J. Am. Chem. Soc.* **2000**, *122*, 9692-9702
28. Bera, D.; Quian, L.; Tseng, T. K.; Holloway, P. H. *Materials.* **2010**, *3*, 2260-2345
29. Gaponik, N. *J. Mater. Chem.*, **2010**, *20*, 5174-5181
30. Norris, D. J.; Efros, A. L.; Erwin, S. C. *Science.* **2008**, *319*, 1776-1779
31. Norris, D. J.; Yao, N.; Charnock, F.; Kennedy, T. *Nano. Lett.* **2001**, *1*, 3-7
32. Furdyna, J. K., Kossut, J.; Eds *Dilute Magnetic Semiconductors*; Academic Press: New York, **1988**, V25.

33. Alivisatos, A. P.; *Science*. **1996**, *271*, 933-937.
34. Michalet, X.; Pinaud, F. F.; Bentolila, L. A.; Tsay, J. M.; Doose, S., Li, J. J.; Sundaresan, G.; Wu, A. M.; Gambhir, S. S.; Weiss, S.; *Nature*. **2007**, *447*, 441-446.
35. Gur, I.; Fromer, N. A.; Geier, M.L.; Alivisatos, A. P. *Science* **2005**, *310*, 462-465.
36. Bhargava, R. N.; Gallagher, D.; Hong, X.; Nurmikko, A. *Phys. Rev. Lett.* **1994**, *72*, 416-419.
37. Stowell, C. A.; Wiacek, R. J.; Sauders, A. E.; Korgel, B. A. *Nano Lett.* **2003**, *3*, 1441-1447.
38. Santra, S.; Yang, H.; Holloway, P. H.; Stanley, J. T.; Mericle, R. A. *J. Am. Chem. Soc.* **2005**, *127*, 1656-1657.
39. Norberg, N. S.; Parks, G. L.; Salley, G. M.; Gamelin, D. R. *J. Am. Chem. Soc.* **2006**, *128*, 13195-13203.
40. Sapra, S.; Prakash, A.; Ghangrekar, A.; Periasamy, N.; Sarma, D. D. *J. Phys. Chem. B.* **2005**, *109*, 1663-1668.
41. Pradhan, N.; Goorskey, D.; Thessing, J.; Peng, X. *J. Am. Chem. Soc.* **2005**, *127*, 17586-17587.
42. Erwin, S. C.; Zu, L.; Haftel, M. I.; Efros, A. L.; Kennedy, T. A.; Norris, D. J. *Nature* **2005**, *436*, 91-94.
43. Yang, Y.; Chen, O.; Angerhofer, A.; Cao, C. J. *J. Am. Chem. Soc.* **2006**, *128*, 12428-12429.
44. Pradhan, N.; Peng, X. *J. Am. Chem. Soc.* **2007**, *129*, 3339-3347.
45. Nag, A.; Sapra, S.; Nagamani, C.; Sharma, A.; Pradhan, N.; Bhat, S. V.; Sarma, D. *D. Chem. Mater.* **2007**, *19*, 3252-3259.

46. Beaulac, R.; Archer, P. I.; Ochsenein, S. T.; Gamelin, D. R. *Adv. Funct. Mater.* **2008**, *18*, 3873-3891.
47. Klimov, V. I.; Mikhailovsky, A. A.; Xu, S.; Malko, A.; Hollingsworth, J. A.; Leatherdale, C. A.; Eisler, H.; Bawendi, M. G. *Science*. **2000**, *290*, 14-17.
48. Colvin, V. L.; Schlamp, M. C.; Allvisatos, A. P. *Nature*. **1994**, *370*, 354-357.
49. Spin Electronics (ed. D.D. Awschalom), Kluwer Academic Publishing, Boston, **2004**
50. Griffith, J. S. **1961**. '*The Theory of Transition Metal Ions*'. Cambridge: Cambridge University Press
51. Ballhausen, C. J. **1962**. '*Introduction to Ligand Field Theory*'. New York: McGraw-Hill
52. Figgis, B. N.; Hitchman, M. A. **2000**. '*Ligand field Theory and its Applications*'. New York: Wiley
53. Tanabe, Y.; Sugano, S. *J. Phys. Soc. Japan*. **1954**, *753*, 766
54. Boulanger, D.; Parrot, R.; Cherfi, Z. *Phys. Rev. B*. **2004**, *70*, 075209/1-075209/12
55. McClure, D. S. *J. Chem. Phys.* **1963**, *39*, 2850.
56. Pohl, U. W.; Gumlich, H. E. *Phys. Rev. B*. **1989**, *40*, 1194.
57. Shim, M.; Wang, C.; Norris, D. J.; Guyot-Sionnest, P. *MRS Bulletin*, **2001**, *26*, 1005-1008.
58. Lee, S.; Dobrowolska, M.; Furdyna, J. K. *J. Appl. Phys.* **2006**, *99*, 08F702/1-08F702/3.
59. Gould, C.; Slobodskyy, A.; Supp, D.; Slobodskyy, T.; Grabs, P.; Hawrylak, P.; Qu, F.; Schmidt, G.; Molenkamp, L. W. *Phys. Rev. Lett.* **2006**, *97*, 017202/1- 017202/3.

60. Schmidt, T.; Scheibner, M.; Worschech, L.; Forchel, A.; Slobodskyy, T.; Molenkamp, L. W. *J. Appl. Phys.* **2006**, *100*, 123109/1- 123109/5.
61. Oka, Y.; Kayanuma, K.; Shirotori, S.; Murayama, A.; Souma, I.; Chen, Z. *J. Lumin.* **2002**, *100*, 175-190.
62. Bryan, J. D.; Gamelin, D. R. *Prog. Inorg. Chem.* **2005**, *54*, 47-126.
63. Yang, H.; Santra, S.; Holloway, P.H. *J. Nanosci. Nanotechnol.* **2005**, *5*, 1364-1375.
64. Beaulac, R.; Archer, P. I.; Gamelin, D. R. *J. Solid State Chem.* **2008**, *181*, 1582-1589.
65. Scholes, G.D. *Adv. Funct. Mater.* **2008**, *18*, 1157-1172.
66. Nag, A.; Chakraborty, S.; Sarma, D. D. *J. Am. Chem. Soc.* **2008**, *130*, 10605-10611.
67. Graf, C.; Hofmann, A.; Ackermann, T.; Boeglin, C.; Viswanatha, R.; Peng, X.; Rodrigues, A. F.; Nolting, F.; Rühl, E. *Adv. Funct. Mater.* **2009**, *19*, 2501-2510.
68. Azad, M. M.; O'Brien, P.; R, N. *J. Mater. Chem.* **2001**, *11*, 2382-2386.
69. Archer, P. I.; Santangelo, S. A.; Gamelin, D. R. *Nano Lett.* **2007**, *7*, 1037-1043.
70. Vlaskin, V. A.; Beaulac, R.; Gamelin, D. R. *Nano Lett.* **2009**, *9*, 4376-4382.
71. Chin, P. T. K.; Stouwdam, J. W.; Janssen, R. A. J. *Nano Lett.* **2009**, *9*, 745-750.
72. Eichhöfer, A.; Hampe, O.; Lebedkins, S.; Weigend, F. *Inorg. Chem.* **2010**, *49*, 7331-7339.
73. a) Tran, D. T. T.; Taylor, N. J.; Corrigan, J. F. *Agnew. Chem. Int. Ed. Engl.* **2000**, *39*, 935-937 b) Tran, D. T. T.; Beltran, L. M.; Kowalchuk, C. M.; Trefiak, N. R.; Taylor, N. J.; Corrigan, J. F. *Inorg. Chem.* **2002**, *41*, 5693-5698.
74. DeGroot, M. W.; Taylor, N. J.; Corrigan, J. F. *J. Mater. Chem.* **2004**, *14*, 654-660.
75. DeGroot, M. W.; Taylor, N. J.; Corrigan, J. F. *Inorg. Chem.* **2005**, *44*, 5447-5458.

76. a) DeGroot, M. W.; Corrigan, J. F. *Angew. Chem. Int. Ed.* **2004**, *43*, 5355-5357. b) DeGroot, M.W.; Taylor, N. J; Corrigan, J. F. *J. Am. Chem. Soc.* **2003**, *125*, 864-865. c) DeGroot, M. W.; Atkins, K.M.; Borecki, A.; Rösner, H.; Corrigan, J. F. *J. Mater. Chem.* **2008**, *18*, 1123-1130.
77. a) Komuro, T.; Matsuo, T.; Kawaguchi, H.; Tatsumi, K. *J. Chem. Soc., Dalton Trans.* **2004**, *10*, 1618-1625. b) Komuro, T.; Matsuo, T.; Kawaguchi, H.; Tatsumi, K. *J. Chem. Commun.* **2002**, *9*, 988-989. c) Komuro, T.; Matsuo, T.; Kawaguchi, H.; Tatsumi, K. *Angew. Chem. Int. Ed.* **2003**, *42*, 465-468.
78. a) Sommer, H.; Eichhöfer, A.; Drebov, N.; Ahlrichs, R.; Fenske, D. *Eur. J. Inorg. Chem.* **2008**, *32*, 5138-5145. b) Bechlars, B.; Issac, I.; Feuerhake, R.; Clerac, R.; Fuhr, O.; Fenske, D. *Eur. J. Inorg. Chem.*, **2008**, *10*, 1632-1644. c) Feuerhake, R.; Fenske, D. *Z. Anorg. Allg. Chem.* **2003**, *629*, 2317-2324. d) Eichhöfer, A.; Fenske, D. *J. Chem. Soc., Dalton Trans.* **2000**, 941-944.
79. DeGroot, M. W.; Corrigan, J. F. *Z. Anorg. Allg. Chem.* **2006**, *632*, 19-29.
80. Borecki, A.; Corrigan, J. F. *Inorg. Chem.* **2007**, *46*, 2478-2484.

CHAPTER TWO

Trimethylsilylchalcogenolates of Co^{2+} and Mn^{2+} : From Mononuclear Coordination Complexes to Clusters Containing $-\text{ESiMe}_3$ Moieties (E = S, Se).[†]

2.1. Introduction

Despite the continued interest in the fundamental chemistry of nanometer sized polynuclear heterometallic chalcogen clusters, the chemistry of ternary MM'E systems remains under-developed relative to binary systems. This is due in part to a lack of general synthetic routes and suitable, stable precursors although this area of research is burgeoning rapidly.¹ Metal chalcogenolate complexes of the d-block metals with trimethylsilyl functionalities on the chalcogen centers have recently been utilized as precursors for the synthesis of ternary MM'E clusters. The preformed metal-chalcogen bond and high solubility of these complexes in common organic solvents, coupled with the reactivity of the $-\text{ESiMe}_3$ (E = S, Se, Te) ligands towards (ligand stabilized) metal salts, makes these complexes powerful precursors for the formation of M-E-M' bonding interactions and entry into ternary d-block metal MM'E clusters.²⁻⁹ Using these reagents as sources of soluble, protected "metallachalcogenolates" (metal-chalcogenides), the ternary nanoclusters $[\text{Cu}_{20}\text{Hg}_{15}\text{E}_{25}(\text{P}^n\text{Pr}_3)_{18}]$ (E= S, Se),^{2a} $[\text{Zn}_x\text{Cd}_{10-x}\text{E}_4(\text{EPh})_{12}(\text{P}^n\text{Pr}_3)_4]$ (E= Se, Te),⁴ and $[\text{Cu}_9\text{Ag}_3\text{S}_6(\text{PEtPh}_2)_8]$ ⁹ have been synthesized using $(\text{P}^n\text{Pr}_3)_3\text{Cu}(\text{ESiMe}_3)$, $(3,5\text{-Me}_2\text{C}_5\text{H}_3\text{N})_2\text{Zn}(\text{ESiMe}_3)_2$ and $(\text{PEtPh}_2)_3\text{Cu}(\text{SSiMe}_3)$, respectively. The synthesis of heterometallic ternary complexes can be achieved using complexes with less sterically demanding about the chalcogen centers (eg.

[†] Reproduced with permission from *Inorganic Chemistry*, **2010**, *49*, 7289-7297. ©2010 American Chemical Society.

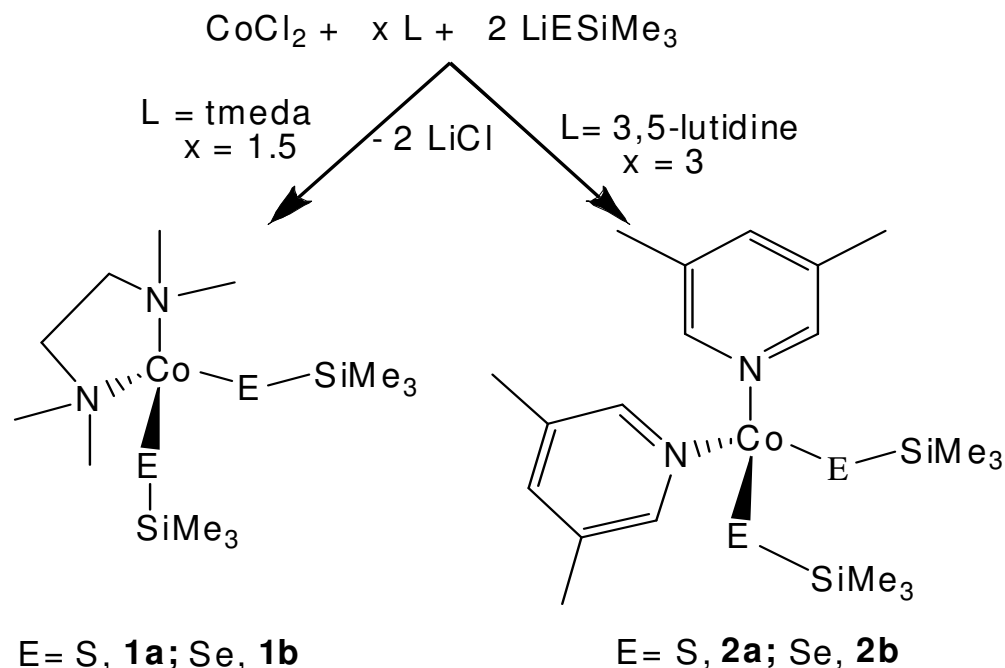
$[\text{SSiMe}_2\text{S}^{2-}]^{6\text{b,c}}$ or $-\text{SiMe}_3^{2-5}$ as larger substituents about the silicon centers can result in non-selective M-E/E-Si bond cleavage reactions.^{6a}

The demonstrated ability of these trimethylsilylchalcogenolates as molecular precursors to ternary MM'E nanoclusters and nanoparticles has prompted us to expand this class of complex to include the paramagnetic metal ions Mn^{2+} and Co^{2+} . Herein, we report the synthesis and structural characterization of a set of manganese and cobalt trimethylsilylchalcogenolates stabilized with 3,5-lutidine and N,N,N',N'-tetramethylethylenediamine ligands: $(N,N'\text{-tmeda})\text{Co}(\text{ESiMe}_3)_2$ (E = S, **1a**; E = Se, **1b**), $(3,5\text{-Me}_2\text{C}_5\text{H}_3\text{N})_2\text{Co}(\text{ESiMe}_3)_2$ (E = S, **2a**; E = Se, **2b**), $[\text{Li}(N,N'\text{-tmeda})]_2[(N,N'\text{-tmeda})\text{Mn}_5(\mu\text{-ESiMe}_3)_2(\text{ESiMe}_3)_4(\mu_4\text{-E})(\mu_3\text{-E})_2]$ (E = S, **3a**; E = Se, **3b**), $[\text{Li}(N,N'\text{-tmeda})]_2[\text{Mn}(\text{SSiMe}_3)_4]$ **4**, $[\text{Li}(N,N'\text{-tmeda})]_4[\text{Mn}_4(\text{SeSiMe}_3)_4(\mu_3\text{-Se})_4]$ **5**.

2.2. Results and Discussion

2.2.1. Synthesis of Cobalt(II) Chalcogenolate Complexes

The cobalt trimethylsilylchalcogenolates **1** and **2** have been prepared by the reaction of CoCl_2 with an appropriate nitrogen donor ligand followed by the addition of freshly prepared lithium salts of the trimethylsilylchalcogenolate anion, $\text{Li}[\text{ESiMe}_3]$, at low temperature as illustrated in Scheme 2.1.



Scheme 2.1. Synthesis of $(N,N'\text{-tmeda})\text{Co}(\text{ESiMe}_3)_2$ and $(3,5\text{Me}_2\text{C}_5\text{H}_3\text{N})_2\text{Co}(\text{ESiMe}_3)_2$

The generation and precipitation of LiCl is the driving force for these reactions, with the resultant formation of metal-chalcogen bonding interactions. Both chalcogenide (E^{2-}) and chalcogenolate (RE^-) ligands tend to adopt bridging coordination modes due to the high polarizability of the chalcogens which often results in the formation of polynuclear species.⁸ To avoid the formation of cluster complexes, the addition of at least 2 equiv. of $\text{Li}[\text{ESiMe}_3]$ to CoCl_2 to promote the terminal coordination of trimethylsilylchalcogenolate ligand and use of excess amount of the tmeda, is vital.¹⁰ Complexes **1** and **2** are highly air sensitive however they can be stored for extended periods as solids at -25°C under an inert atmosphere. The cobalt trimethylsilylselenolates are thermally less stable than their thiolate analogues, with N,N' -tmeda complexes generally being more stable than the related 3,5-lutidine complexes. The observed trend

in the thermal stability of these complexes is consistent with those previously reported for zinc and copper chalcogenolates.^{2a,10}

2.2.2. X-ray Crystallographic Structural Characterization

Single-crystal X-ray diffraction data were collected for all complexes, and the analyses confirmed the monomeric nature of the structures. A summary of the crystal data and structural parameters for **1a**, **1b**, **2a** and **2b** is listed in Appendix A.1-A.4. The isomorphous *N,N'*-tmeda ligated complexes **1a** and **1b**, crystallized in the monoclinic space group, *C2/c* with *Z* = 12. There are 2 independent molecules in the asymmetric unit, one of which resides about a crystallographic two-fold rotation axis whereas the second sits on a general position. Bond lengths and angles refer to the latter. The lutidine complex **2a** crystallizes in orthorhombic space group *Pca2(1)* while **2b** crystallizes in the triclinic space group $P\bar{1}$. The molecular structure of **1a**, **1b**, **2a** and **2b** are shown in Figures 2.1 and 2.2, respectively.

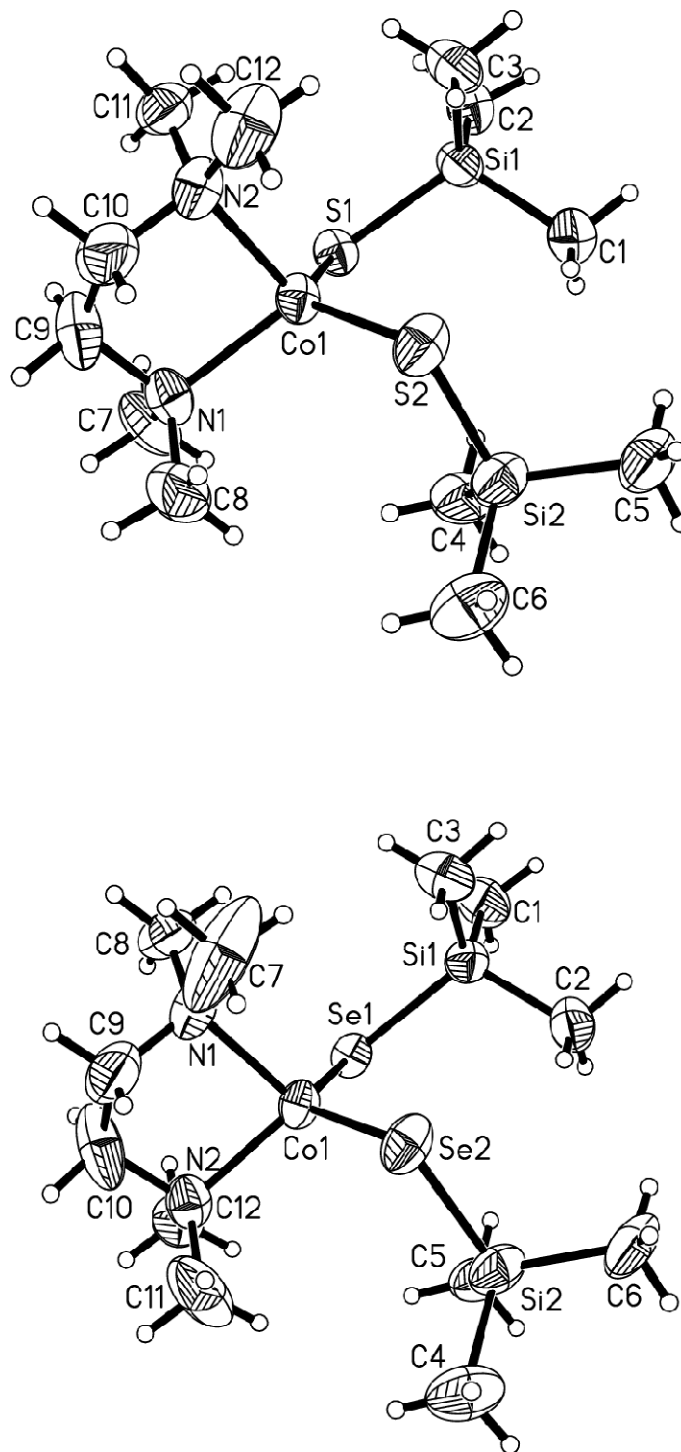


Figure 2.1. The molecular structures of $(N,N'$ -tmeda)Co(SSiMe₃)₂, **1a** (top) and $(N,N'$ -tmeda)Co(SeSiMe₃)₂, **1b** (bottom). Thermal ellipsoids are drawn at 50% probability.

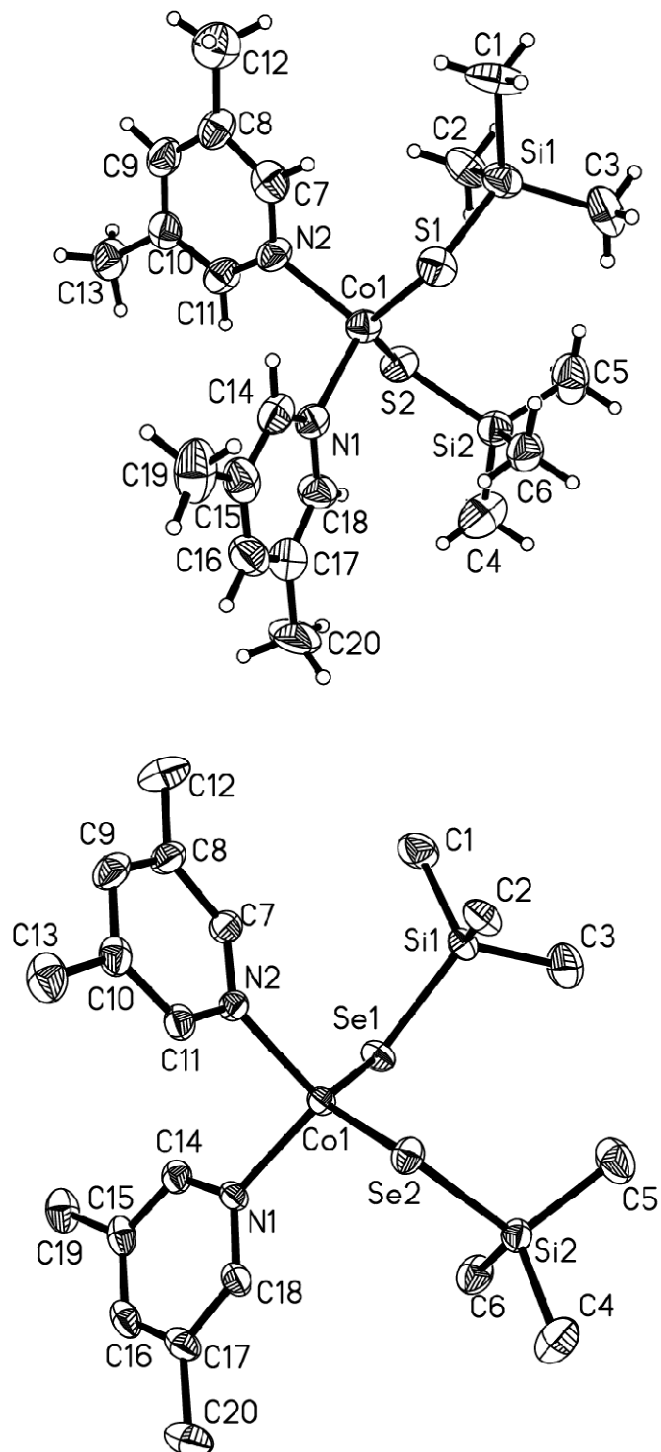


Figure 2.2. The molecular structures of $(3,5\text{-Me}_2\text{C}_5\text{H}_3\text{N})_2\text{Co}(\text{SSiMe}_3)_2$, **2a** (top) and $(3,5\text{-Me}_2\text{C}_5\text{H}_3\text{N})_2\text{Co}(\text{SeSiMe}_3)_2$, **2b** (bottom; hydrogen atoms omitted). Thermal ellipsoids are drawn at 50% probability.

It has been demonstrated that the controlled formation of M-E-M' interactions by the reaction of metal-chalcogenolate complexes M-ESiR₃ with other metals salts (M'-X) via the elimination of a soluble silane R₃Si-X, is adversely affected with the introduction of more sterically demanding substituents on Si and optimized with three methyl groups about silicon (M-ESiMe₃), balanced by the requirements of a suitably stable precursor that is amenable to further reaction chemistry.^{6a} The isolation of the monomeric cobalt chalcogenolate complexes **1** and **2** containing terminal -ESiMe₃ substituents makes them ideal candidates for use as molecular precursors for the controlled synthesis of ternary nanometer sized clusters and particles.^{2,4,9} The common structural features prevalent in all four complexes are the distorted tetrahedral geometry at the Co(II) centre and the presence of terminally bonded trimethylsilylchalcogenolate ligand as depicted in Figures 2.1 and 2.2. The *N,N'*-tmeda ligands are coordinated in a bidentate manner in complexes **1a** and **1b** while two 3,5-lutidine ligands complete the tetrahedral coordination geometry about the cobalt center in **2a** and **2b**. Selected bond distances and angles for complexes **1** and **2** are summarized in Table 2.1.

The 'CoE₂N₂' (E = S, Se) core in complexes **1** and **2** is significantly distorted from an ideal tetrahedral geometry with the E1-Co-E2 angle ranging from 123.69(4)° to 129.48(7)° and N1-Co-N2 ranging from 86.6(2)° to 103.7(2)°. The N1-Co-N2 angle is significantly smaller for the *N,N'*-tmeda ligated complexes than the 3,5-lutidine counterpart. The average Co-S bond distance 2.268(1) Å is slightly shorter compared to the Co-Se average bond distance of 2.384(1) Å, as expected. The same trend is observed for the E-Si bond distances (Table 2.1). The bond angles and distances observed for **1a** are comparable to those previously reported for the four coordinate cobalt thiolato

complexes $(N,N'$ -tmeda)Co(SSiPh₃)₂¹¹ and $(N,N'$ -tmeda)Co(SSiMe₂Bu^t)₂^{6a} and those observed for **2a** are comparable to the previously reported pyridine (py) stabilized cobalt thiolate complex (py)₂Co(S-2,4,6-Pri₃C₆H₂)₂.¹²

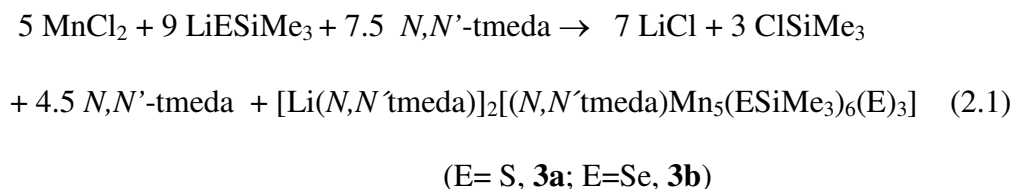
	1a (E = S)	1b (E = Se)	2a (E = S)	2b (E = Se)
Co1-E1	2.275(1)	2.3884(9)	2.285(3)	2.3988(6)
Co1-E2	2.261(1)	2.379(1)	2.285(3)	2.4033(6)
E1-Si1	2.114(2)	2.258(2)	2.121(5)	2.258(1)
E2-Si2	2.112(2)	2.251(2)	2.108(5)	2.262(1)
Co1-N1	2.112(4)	2.113(5)	2.075(9)	2.063(3)
Co1-N2	2.122(4)	2.112(5)	2.057(10)	2.057(3)
N2-Co1-N1	86.65(16)	86.8(2)	103.7(2)	99.86(12)
N2-Co1-E1	112.56(11)	108.44(13)	106.9(3)	110.91(9)
N1-Co1-E1	108.44(11)	112.98(13)	102.9(3)	102.83(9)
N2-Co1-E2	104.22(10)	114.39(13)	103.3(3)	104.73(9)
N1-Co1-E2	114.17(11)	104.38(13)	108.1(3)	108.60(9)
E1-Co1-E2	124.31(5)	123.69(4)	129.48(7)	126.75(2)
Si1-E1-Co1	104.65(6)	102.54(5)	105.88(16)	106.17(3)
Si2-E2-Co1	108.51(7)	105.56(5)	107.60(17)	101.30(3)

Table 2.1. Selected Bond Distances (Å) and Angles (°) for Complexes **1** and **2**

2.2.3. Synthesis and Characterization of Manganese(II) Chalcogenolate Complexes

Similar reaction strategies as used for the preparation of mononuclear complexes **1** and **2** with the manganese salt, MnCl₂, do not result in the isolation of structurally related complexes. The reaction of MnCl₂·tmeda¹³ with two equivalents of Li[ESiMe₃]

led to a dark orange colored solutions almost immediately upon mixing, and the isolation of the pentanuclear manganese chalcogenolate complexes $\text{Li}(\text{N},\text{N}'\text{-tmeda})_2[(\text{N},\text{N}'\text{-tmeda})\text{Mn}_5(\text{ESiMe}_3)_6(\text{E})_3]$ **3a** (E = S) and **3b** (E = Se). The yields for **3a** and **3b** were ultimately optimized by varying the ratios of reagents according to equation 2.1. The tetrameric nature of $\text{MnCl}_2(\text{tmeda})$ and the relative lability of the N-donor ligands for the d^5 metal ion together with the preferred bridging coordination modes of the chalcogen presumably account for the preferred formation of the polynuclear species under these reaction conditions.



A summary of the crystal data is listed in Appendix A.5 and A.6. The cluster **3a** crystallizes in the monoclinic space group $\text{P}2_1/c$ whereas **3b** crystallizes in the space group $\text{C}2/c$, a two-fold rotation axis along the Mn1-Se5 vector relating the two halves of the molecule. Clusters **3a** and **3b** are structurally similar, and are illustrated in Figures 2.3 and 2.4, respectively. The structural features common to both complexes include the presence of six trimethylsilylchalcogenolate ligands as well as three bridging chalcogenides. The defined M_5E_3 core, with five manganese linked via the bridging chalcogenide ligands is unprecedented in Mn-chalcogenide cluster chemistry. The chalcogenide ligands exhibit both μ_3 and μ_4 bridging modes and there are two symmetrical bridging μ_2 - and four terminal $-\text{ESiMe}_3$ ligands. The presence of two N,N' -

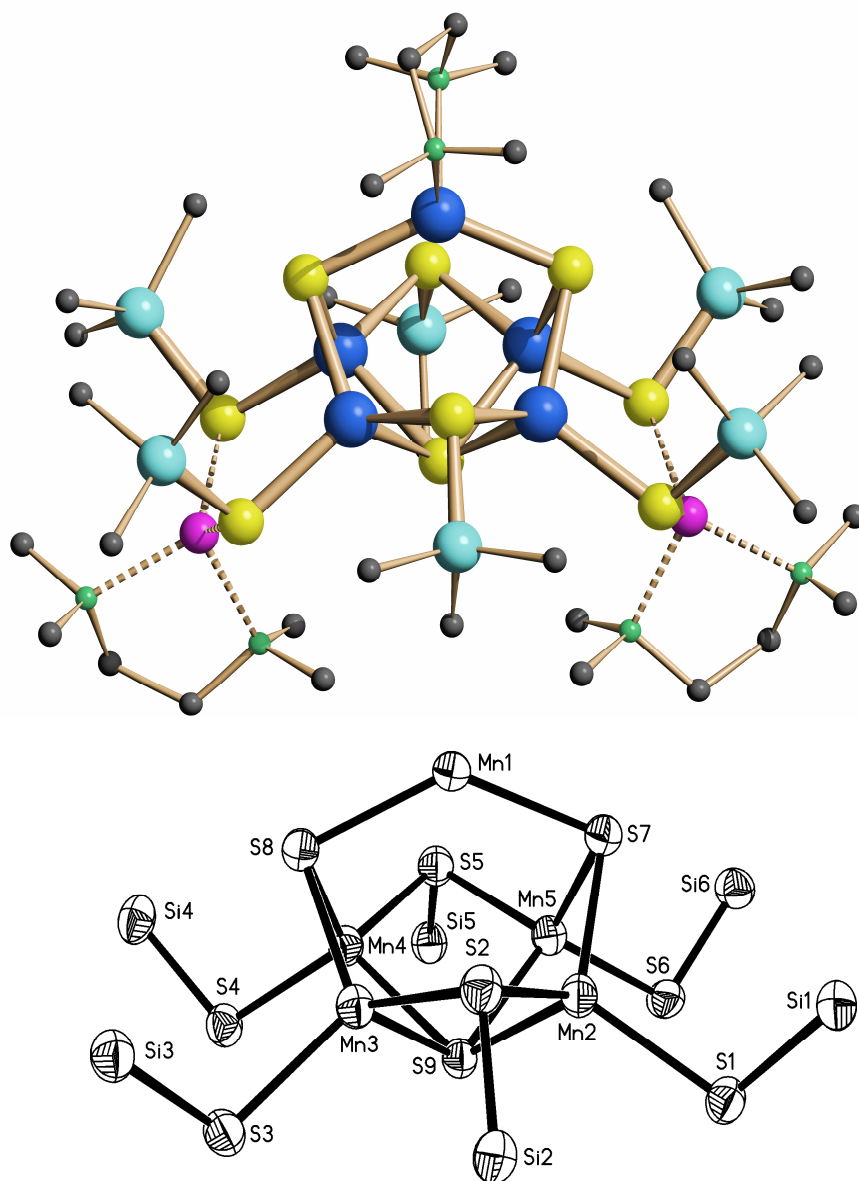


Figure 2.3. The molecular structure of $[\text{Li}(\text{N},\text{N}'\text{-tmeda})]_2[(\text{N},\text{N}'\text{-tmeda})\text{Mn}_5(\mu\text{-SSiMe}_3)_2(\text{SSiMe}_3)_4(\mu_4\text{-S})(\mu_3\text{-S})_2]$ **3a** (top, hydrogen atoms omitted). Mn: blue; S: yellow; Si: aqua; Li: violet; N: green; C: grey. **3a**. Bottom: the Mn_5S_9 framework in **3a** with the numbering system used (thermal ellipsoids drawn at 40%).

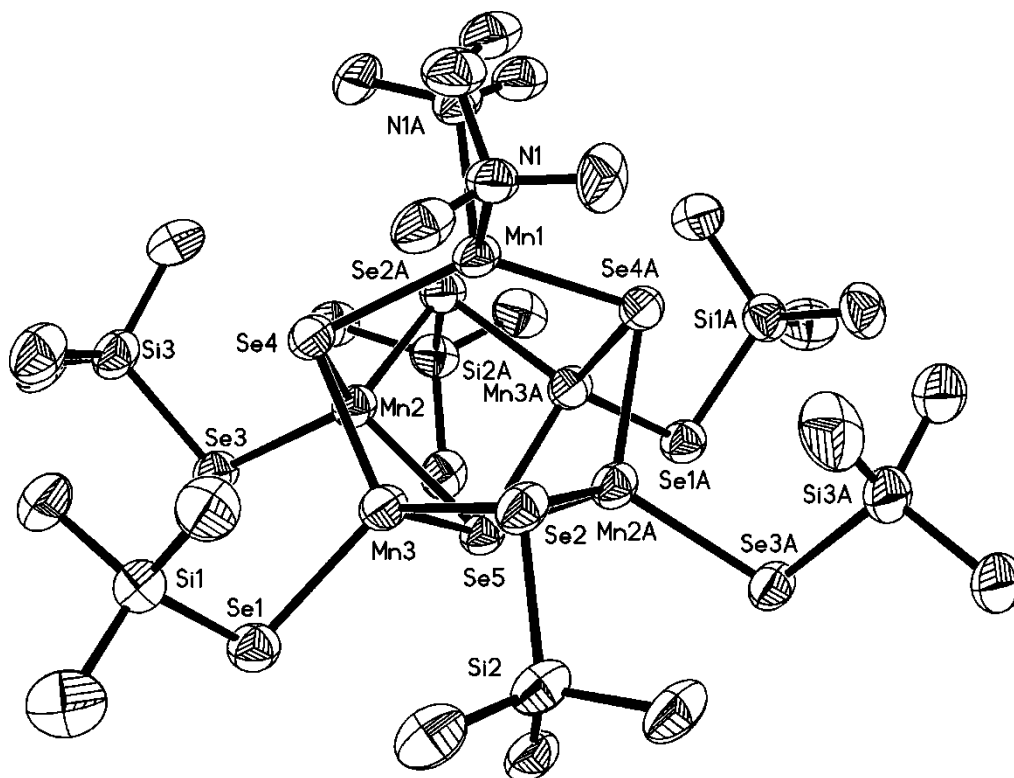


Figure 2.4. The Mn_5Se_9 framework in the molecular structure of $[(N,N'\text{-tmeda})\text{Mn}_5(\mu\text{-SeSiMe}_3)_2(\text{SeSiMe}_3)_4(\mu_4\text{-Se})(\mu_3\text{-Se})_2]^{2-}$ **3b** with the numbering system used (thermal ellipsoids drawn at 40%).

tmeda ligated Li ions together with the magnetic susceptibility measurements (*vide infra*), suggest five Mn(II) centers with an overall charge on the cluster of 2^- .

The five Mn^{2+} define a square pyramid and feature a common distorted tetrahedral ME_4 geometry around each metal center, the angles about the manganese centers deviate significantly from 109.5° , ranging from $100.00(1)$ to $132.89(1)$, as summarized in Table 2.2. The average Mn-sulfide ($2.434(9)$ Å) and Mn-thiolate ($2.434(8)$ Å) bond lengths are, expectedly, shorter than the average Mn-selenide ($2.554(6)$ Å) and Mn-selenolate ($2.557(6)$ Å) bonding interactions (Table 2.2). The $\mu_2\text{-SSiMe}_3$ and $\mu_2\text{-SeSiMe}_3$ bond lengths are similar to those observed in the adamantoid complexes $[\text{Mn}_4(\text{SPri})_6\text{Cl}_4]^{2-}$ and

$[\text{Mn}_4(\text{SePri})_6\text{Br}_4]^{2-}$.¹⁴ In **3**, the two Li ions are sequestered, each bonded with one *N,N'*-tmeda ligand and further bonded to available lone pairs from two $-\text{ESiMe}_3$ ligands (Figure 2.2). The Mn··Mn distances of adjacent metal centers in **3a** range from 2.960(2) to 3.079(2) Å whereas they are slightly expanded in the heavier congener **3b** (3.062(3) to 3.151(3) Å). That both **3a** and **3b** contain six trimethylsilylchalcogenolate ($-\text{ESiMe}_3$) groups suggests the potential to utilize these complexes as precursors for the synthesis of ternary clusters.^{2,4,9}

	3a		3b
Mn1-S7	2.3630(13)	Mn1-Se4A	2.4919(7)
Mn1-S8	2.3676(13)	Mn2-Se2A	2.5854(11)
Mn2-S7	2.4069(13)	Se1-Mn3	2.5291(11)
Mn2-S1	2.4226(13)	Se2-Mn3	2.5798(10)
Mn2-S2	2.4679(13)	Se2-Mn2A	2.5854(11)
Mn2-S9	2.5009(12)	Se3-Mn2	2.5431(10)
Mn3-S8	2.4178(13)	Se4-Mn1	2.4919(7)
Mn3-S3	2.4163(13)	Se4-Mn3	2.5245(10)
Mn3-S2	2.4724(13)	Se4-Mn2	2.5287(11)
Mn3-S9	2.5058(12)	Mn3-Se5	2.6140(10)
Mn4-S4	2.4080(13)	Mn3A-Se5	2.6140(10)
Mn4-S8	2.4122(13)	Mn2A-Se5	2.6311(9)
Mn4-S5	2.4552(13)	Mn2-Se5	2.6311(9)
Mn4-S9	2.5024(12)	Se4A-Mn1-Se4	132.33(5)
Mn5-S6	2.4155(13)	Se4-Mn2-Se3	111.81(4)
Mn5-S7	2.4141(33)	Se4-Mn2-Se2A	112.00(4)
Mn5-S5	2.4621(13)	Se3-Mn2-Se2A	114.14(4)
Mn5-S9	2.5063(12)	Se4-Mn2-Se5	102.19(3)
S7-Mn1-S8	131.69(5)	Se3-Mn2-Se5	112.85(4)
S7-Mn2-S1	113.49(5)	Se2A-Mn2-Se5	102.90(3)
S7-Mn2-S2	112.67(4)	Se4-Mn3-Se1	113.98(4)
S1-Mn2-S2	114.95(5)	Se4-Mn3-Se2	111.94(4)
S7-Mn2-S9	100.15(4)	Se1-Mn3-Se2	114.16(4)
S1-Mn2-S9	112.62(4)	Se4-Mn3-Se5	102.78(3)
S2-Mn2-S9	101.31(4)	Se1-Mn3-Se5	109.21(4)
S8-Mn3-S3	114.22(5)	Se2-Mn3-Se5	103.53(3)

Table 2.2. Selected Bond Distances (Å) and Angles (°) for Complexes **3a** and **3b**.

With the addition of four equivalents of $\text{Li}[\text{SSiMe}_3]$, there was no evidence for the formation of the pentanuclear complex **3a**, and the mononuclear complex $[\text{Li}(\text{N},\text{N}'\text{-tmeda})]_2[\text{Mn}(\text{SSiMe}_3)_4]$, **4** was formed in good yield as the sole product illustrated by equation 2.2 below. Single crystal X-ray diffraction confirmed the monomeric nature of the complex, which is illustrated in Figure 2.5.

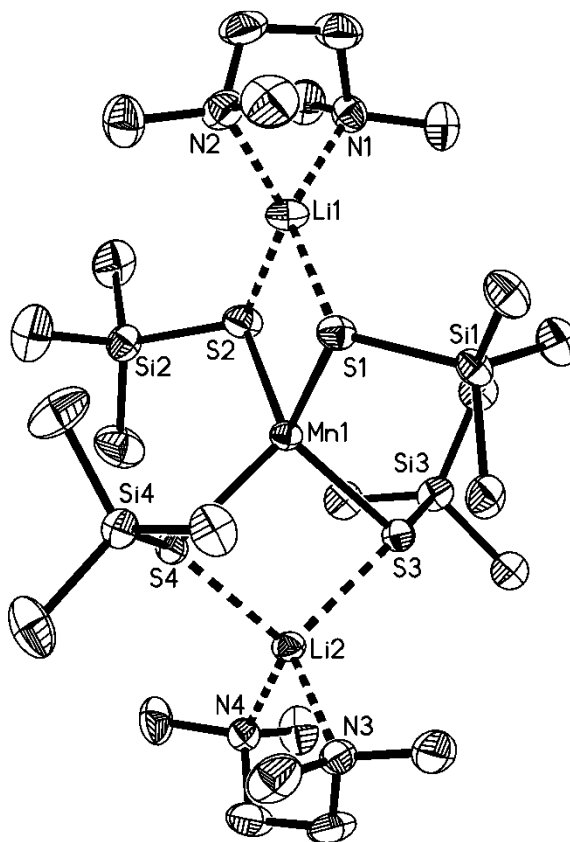
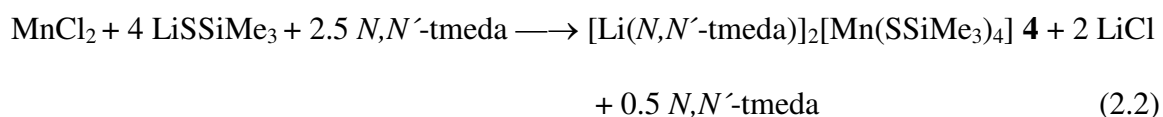


Figure 2.5. The molecular structure of $[\text{Li}(\text{N},\text{N}'\text{-tmeda})]_2[\text{Mn}(\text{SSiMe}_3)_4]$ **4**. Thermal ellipsoids are drawn at 40% probability and H atoms are omitted for clarity.

The tetrathiolate **4** crystallizes in the tetragonal space group P4(1) (Appendix A.7). Distorted tetrahedral geometry is again observed where the angles about Mn1 range from 95.46(4) to 117.13(5) (Table 2.3). The magnitude of this asymmetric arrangement around Mn is more pronounced than that observed in [Et₄N]₂[Mn(S-2-Ph-C₆H₄)₄].¹⁵ The smallest angles (S1-Mn1-S2 and S3-Mn1-S4, 98.12(4) and 95.46(4)°, respectively) arise from the interaction of the two Li ions to two sulfur sites each. The average Mn-S bond distance (2.441(3) Å) in **4** is comparable to that observed in [Mn(S-2-Ph-C₆H₄)₄]²⁻ (2.430(3) Å).¹⁵

Mn1-S1	2.4519(12)	S3-Mn1-S1	117.13(5)
Mn1-S2	2.4468(13)	S4-Mn1-S1	116.11(5)
Mn1-S3	2.4313(14)	S4-Mn1-S2	114.56(5)
Mn1-S4	2.4342(14)	S3-Mn1-S2	116.78(5)
S-Si(avg)	2.106(4)	S3-Mn1-S4	95.46(4)
Li-N (avg)	2.098(18)	S1-Mn1-S2	98.12(4)
Li1-S1	2.462(8)	S1-Li1-S2	93.8(2)
Li1-S2	2.468(8)	N1-Li1-N2	86.9(3)
Li2-S3	2.447(7)	S3-Li2-S4	98.5(2)
Li2-S4	2.439(7)	N3-Li2-N4	87.7(3)

Table 2.3. Selected Bond Distances (Å) and Angles (°) for **4**.

Similar reaction conditions used for the preparation of **4** using four equivalents of the selenium reagent Li[SeSiMe₃] did not lead to the isolation of a related tetraselenolate complex. The addition of MnCl₂(*N,N'*-tmeda) to four equivalents of Li[SeSiMe₃] resulted in an immediate darkening of the reaction solutions from which orange-red

$[\text{Li}(\text{N},\text{N}'\text{-tmeda})]_4[\text{Mn}_4(\text{SeSiMe}_3)_4(\mu_3\text{-Se})_4]$ **5**, and dark-red $[\text{Li}(\text{N},\text{N}'\text{-tmeda})]_4[\text{Mn}(\text{Se}_4)_3]$ **6** were isolated as single crystals. A summary of the crystal data for complexes **5** and **6** is listed in Appendix A.8 and A.9, respectively.

Compound **5** crystallizes in the triclinic space group $P\bar{1}$. The structure of **5** (Figure 2.6) comprises a tetranuclear cubane $[\text{Mn}_4(\mu_3\text{-Se})_4]$ core, with four Mn and four selenido ligands occupying alternate vertices of the cube. A distorted tetrahedral coordination geometry about the metals is completed with four $-\text{SeSiMe}_3$ ligands.

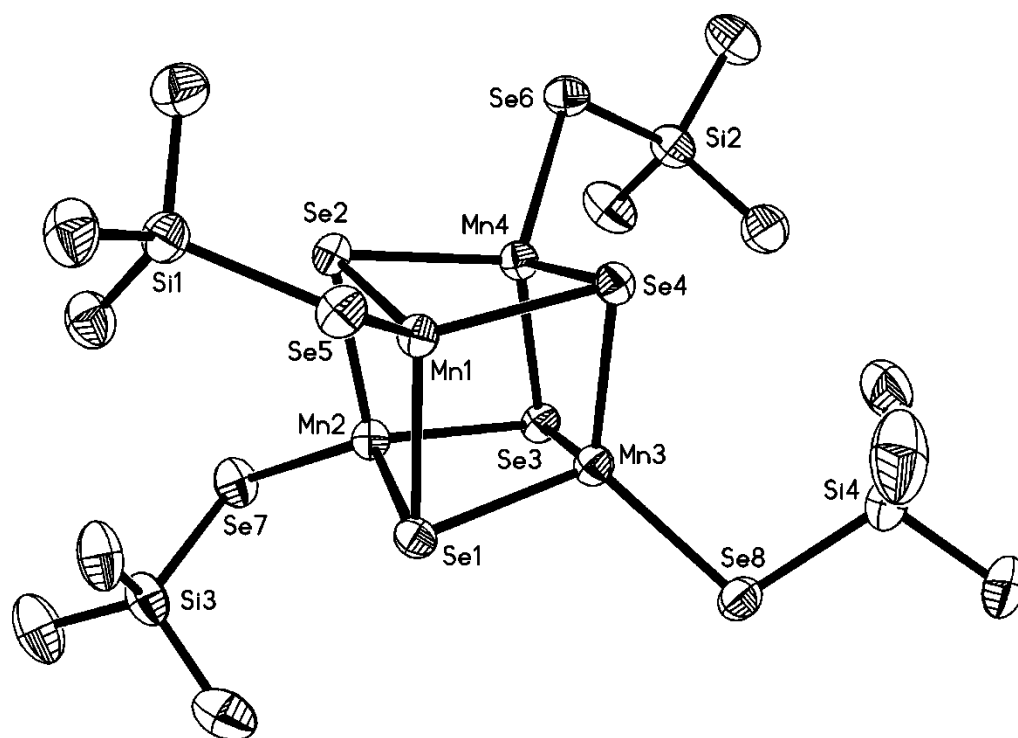


Figure 2.6. The molecular structure of $[\text{Li}(\text{N},\text{N}'\text{-tmeda})]_4[\text{Mn}_4(\text{SeSiMe}_3)_4(\mu_3\text{-Se})_4]$ **5**. Thermal ellipsoids are drawn at 40% probability and H atoms are omitted for clarity.

This cubane structural motif is common to metal-chalcogenide (O/S/Se/Te) M_4 clusters and has been well investigated due in part to its structural relevance in biological

systems.¹⁶ Documented tetranuclear selenido clusters with a cubane-type M_4Se_4 core include those containing the metals Rh, Ir, Co, Fe and Ru.^{2b,17} A manganese(II) cubane cluster with μ_3 -oxo ligands has also been prepared¹⁸ and related telluride-chalcogenolato complexes $[Mn_4Te_4(E\text{Pri})_4]^{4-}$ (E = S, Se, Te)¹⁹ have been reported by Henkel and co-workers. To our knowledge this is the first example of a structurally characterized tetranuclear manganese selenium cluster displaying this structural motif. The Mn_4Se_4 core in **5** is distorted from an ideal cubic geometry as indicated by the variation of Mn-Se bond distances (Table 2.4) and the endohedral angles of the Mn_4Se_4 core. Although there are numerous reports on the incorporation of Mn^{2+} centers into mixed metal MnM_3E_4 (M = transition metal) clusters, the polynuclear complex **5** represents the first example of a homometallic Mn_4Se_4 complex with a cubane core. The selenide ligands in **5** each symmetrically bridge three Mn^{2+} sites with the tetrahedral coordination geometry about the metals completed with the $-SeSiMe_3$ (Table 2.4). The Mn···Mn distances in **5** (3.087(1) to 3.180(1) Å) are contracted compared to those in the telluride/tellorolate complex $[Mn_4Te_4(E\text{Pri})_4]^{4-}$ (3.214(4) to 3.358(4) Å).¹⁹

In contrast to this cubane framework, the polynuclear manganese selenides recently reported by Eichhöfer display adamantane based structures.²⁰ In **5**, four TMEDA ligated Li^+ serve as the counterions present in the crystal for the $[Mn_4(SeSiMe_3)_4(\mu_3-Se)_4]^{4-}$ frame. These Li ions each also form two additional contacts with the Se centers of the trimethylsilylselenolate ligands. The resultant formulation of the cluster with four Mn(II) is consistent with the magnetic measurements (*vide infra*). There is no clear relationship between the structural features of the metal-chalcogen core in **5** and that of the penta-manganese complex **3b**.

Mn(1)-Se(2)	2.5387(10)	Mn(2)-Mn(4)	3.0874(12)
Mn(1)-Se(5)	2.5447(9)	Mn(2)-Mn(3)	3.2171(12)
Mn(1)-Se(4)	2.5716(10)	Mn(3)-Se(4)	2.5326(10)
Mn(1)-Se(1)	2.5944(10)	Mn(3)-Se(8)	2.5424(10)
Mn(1)-Mn(3)	3.1192(11)	Mn(3)-Se(1)	2.5758(10)
Mn(1)-Mn(2)	3.1488(12)	Mn(3)-Se(3)	2.6280(10)
Mn(1)-Mn(4)	3.1801(11)	Mn(3)-Mn(4)	3.1165(12)
Mn(2)-Se(7)	2.5464(11)	Mn(4)-Se(3)	2.5169(9)
Mn(2)-Se(1)	2.5495(10)	Mn(4)-Se(6)	2.5270(10)
Mn(2)-Se(3)	2.5738(10)	Mn(4)-Se(2)	2.5559(10)
Mn(2)-Se(2)	2.5956(10)	Mn(4)-Se(4)	2.6112(10)
Se2-Mn1-Se5	122.75(4)	Se4-Mn3-Se8	122.71(4)
Se2-Mn1-Se4	101.59(3)	Se4-Mn3-Se1	104.90(3)
Se5-Mn1-Se4	115.99(4)	Se8-Mn3-Se1	114.71(4)
Se2-Mn1-Se1	103.20(3)	Se4-Mn3-Se3	103.47(3)
Se5-Mn1-Se1	107.82(3)	Se8-Mn3-Se3	108.72(3)
Se4-Mn1-Se1	103.26(3)	Se1-Mn3-Se3	99.33(3)
Se7-Mn2-Se1	126.33(4)	Se3-Mn4-Se6	125.22(4)
Se7-Mn2-Se3	114.22(4)	Se3-Mn4-Se2	106.04(3)
Se1-Mn2-Se3	101.48(3)	Se6-Mn4-Se2	109.59(4)
Se7-Mn2-Se2	106.09(4)	Se3-Mn4-Se4	104.39(3)
Se1-Mn2-Se2	102.87(3)	Se6-Mn4-Se4	108.64(4)
Se3-Mn2-Se2	103.24(3)	Se2-Mn4-Se4	100.05(3)

Table 2.4. Bond distances (Å) and Angles (°) for Complex **5**.

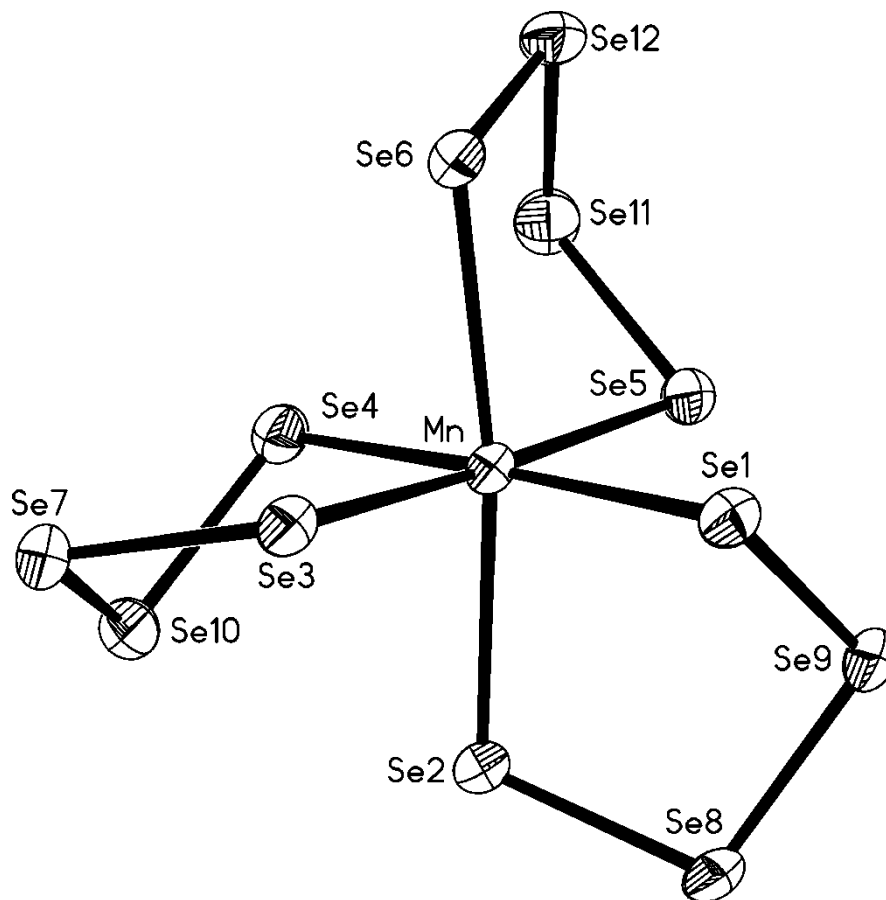


Figure 2.7. The molecular structure of $[\text{Li}(\text{N},\text{N}'\text{-tmeda})]_4[\text{Mn}(\text{Se}_4)_3]$ **6**. Thermal ellipsoids are drawn at 40% probability and H atoms are omitted for clarity.

In addition to the isolation of $[\text{Li}(\text{N},\text{N}'\text{-tmeda})]_4[\text{Mn}_4(\text{SeSiMe}_3)_4(\mu_3\text{-Se})_4]$ **5**, small amounts of dark red crystals were also present from these reactions. A single crystal X-ray analysis indicated the formation of the tris(tetraselenide complex) $[\text{Li}(\text{N},\text{N}'\text{-tmeda})]_4[\text{Mn}(\text{Se}_4)_3]$ **6**. Compound **6** crystallizes in the monoclinic space group $\text{P}2(1)/n$. The structure of **6** (Figure 2.7) consists of a Mn(II) center chelated by three tetraselenide ligands, $(\text{Se}_4)^{2-}$ with a distorted octahedral geometry around the central metal.

The Mn-Se bond lengths vary from 2.647(2) to 2.798(1), each pair of Mn-Se lengths associated with a Se₄ ring displaying one shorter (2.647(2)-2.700(2) Å) and one longer (2.767(2)-2.798(2) Å) bond. These bond lengths are themselves longer than those reported in the tetrahedral bis(tetraselenide) manganese complex [Mn(Se₄)₂]²⁻ (2.537(5)-2.553(5) Å).²¹ [Pt(Se₄)₃]²⁻²² [Ir(Se₄)₃]³⁻²³ and [Sn(Se₄)₃]²⁻^{21,24} represent other examples of structurally characterized octahedral selenometalates containing three tetraselenide ligands. The origin for the reproducible formation of **6** in the reaction is unclear, but requires partial oxidation of Se²⁻ species present in the reaction.⁷⁷Se NMR of Li[SeSiMe₃] displays only one resonance at -518 ppm, with no evidence for any tetraselenide species being present.²⁵

Mn-Se1	2.700(2)	Se1-Mn-Se5	89.57(5)
Mn-Se2	2.798(1)	Se2-Mn-Se3	91.70(4)
Mn-Se3	2.767(2)	Se2-Mn-Se4	85.60(5)
Mn-Se4	2.647(2)	Se2-Mn-Se5	94.84(4)
Mn-Se5	2.685(1)	Se4-Mn-Se5	92.35(5)
Mn-Se6	2.782(1)	Se3-Mn-Se4	95.44(5)
Se1-Mn-Se2	93.09(5)	Se3-Mn-Se6	82.14(4)
Se1-Mn-Se3	82.77(5)	Se4-Mn-Se6	90.15(5)
Se1-Mn-Se6	90.94(5)	Se5-Mn-Se6	91.90(4)

Table 2.5. Bond Lengths (Å) and Angles (°) for Complex **6**.

2.2.3.1. Magnetic Measurements

The temperature dependent magnetic susceptibilities of the clusters **3a**, **3b** and **5** were measured on polycrystalline samples using a superconducting quantum interference device (SQUID) magnetometer. The results for compound **3a** are presented in Figure 2.8 as plots of χT vs T and M vs H . At room temperature, the χT product for **3a** is $5.69 \text{ cm}^3 \text{ K mol}^{-1}$, a much lower value than the calculated one ($21.875 \text{ cm}^3 \text{ K mol}^{-1}$) for five spin-only Mn^{2+} centres ($S = 5/2$, $g = 2$, $\chi T = 4.375 \text{ cm}^3 \text{ K mol}^{-1}$). This type of behavior is indicative of very strong overall antiferromagnetic interactions within this square pyramidal Mn_5 core. This is supported by the temperature dependence of the χT product at 1000 Oe which continuously decreases down to a plateau at $2.36 \text{ cm}^3 \text{ K mol}^{-1}$ at ~ 3.5 K until 1.8 K. The observed χT value of $2.36 \text{ cm}^3 \text{ K mol}^{-1}$ is compatible with a total spin ground state between $S = 3/2$ ($1.875 \text{ cm}^3 \text{ K mol}^{-1}$) and 2 ($3.0 \text{ cm}^3 \text{ K mol}^{-1}$).

Analyzing the spin topology within the structure, the four Mn^{2+} ions in the basal square plane are expected to be antiferromagnetically coupled through the chalcogen bridges and thus the total spin ground state of the compound would be $5/2$, contributed by the lone Mn^{2+} located above the Mn_4 plane. Therefore, the theoretical χT value at 1.8 K should be $4.375 \text{ cm}^3 \text{ K mol}^{-1}$ and the magnitude of the magnetization $5 \mu_B$, which are values in close agreement with the experimentally observed χT value ($2.36 \text{ cm}^3 \text{ K mol}^{-1}$) at 1.8 K and magnetization ($3.1 \mu_B$) at 7 T and 1.8 K. We attribute the discrepancies to the extreme air sensitivity of the samples resulting in the slight oxidation of Mn^{2+} ions. As illustrated in Appendix B.1, the temperature dependent magnetic susceptibility and

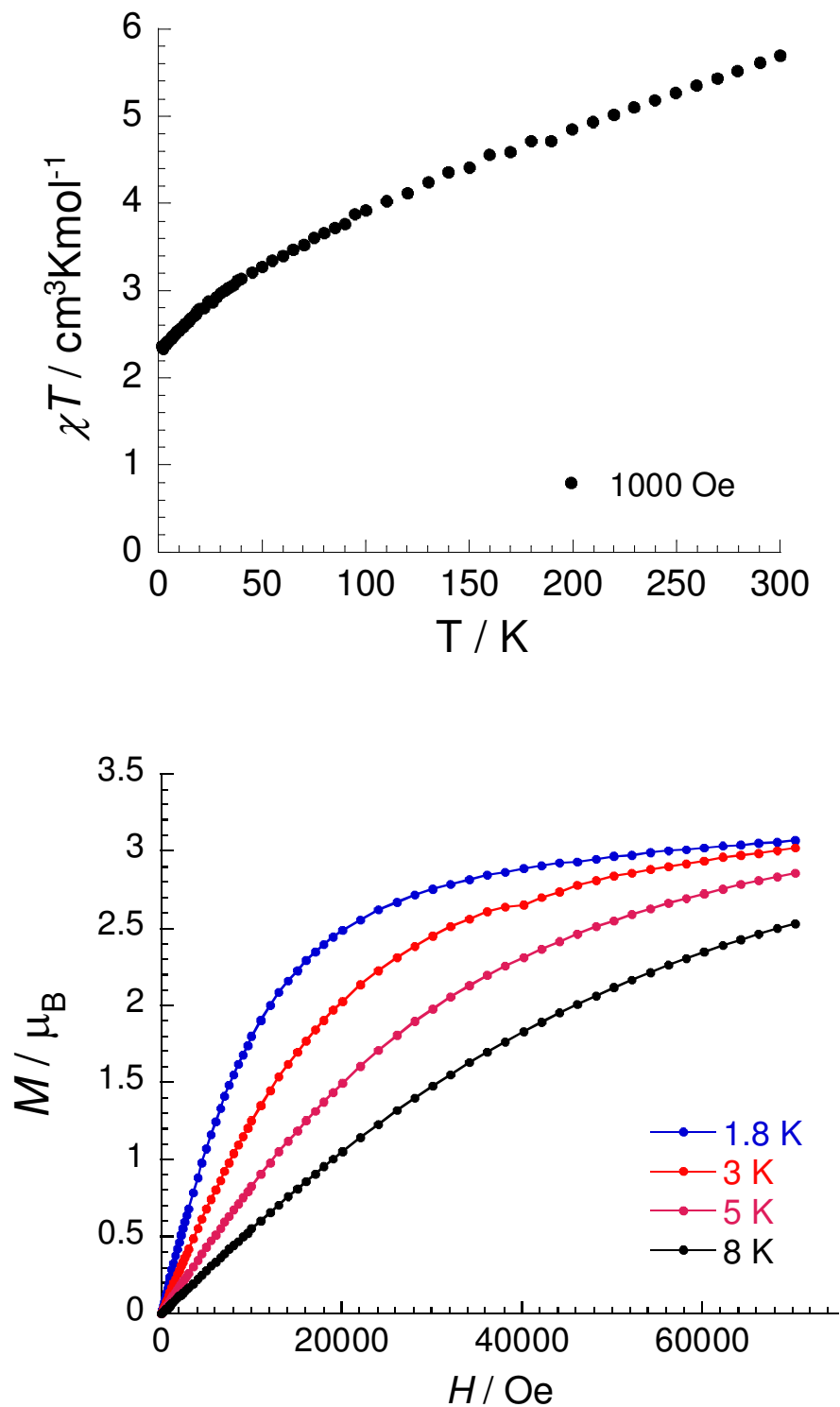


Figure 2.8. Plots of χT vs T (top) and M vs H (bottom) for Complex **3a**.

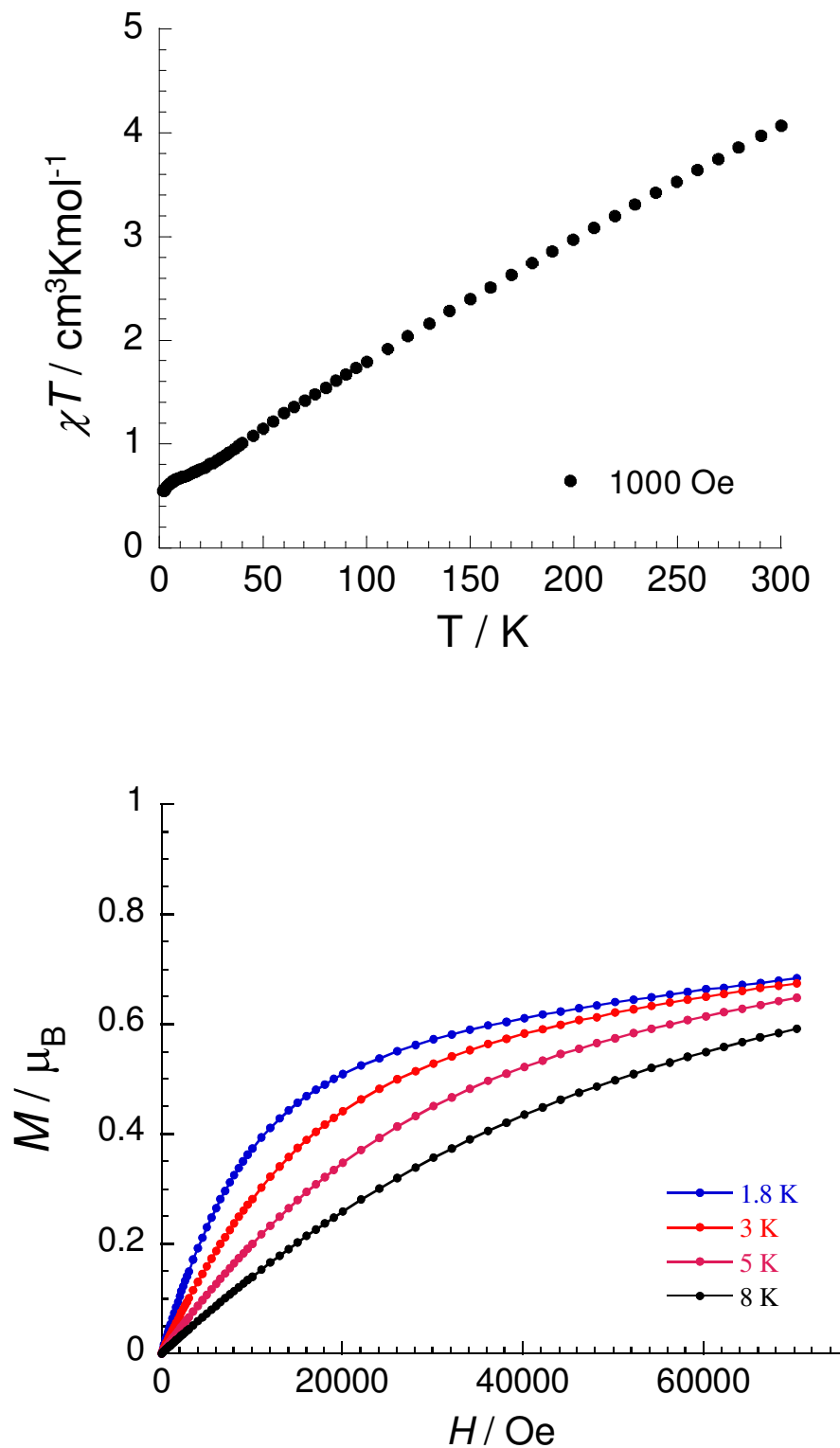


Figure 2.9. Plots of χT vs T (top) and M vs H (bottom) for Complex 5.

the magnetization of the selenium complex **3b** show similar data sets to those of **3a** due to their structural similarities.

At room temperature, the observed χT value for the Mn₄ complex **5** is 4.08 cm³ K mol⁻¹, in much lower comparison to the calculated one (17.5 cm³ K mol⁻¹) for four Mn²⁺ centers (Figure 2.9, top). Again, the very low room temperature χT product indicates the presence of very strong overall antiferromagnetic interactions within the tetranuclear metallic core. This is confirmed by the temperature dependence of the χT product at 1000 Oe that continuously decreases down to 0.52 cm³ K mol⁻¹ until 1.8 K, compatible with a total spin ground state of $S = 1/2$ (0.375 cm³ K mol⁻¹). However, the field dependence of the magnetization at low temperatures as shown in Figure 2.9 (bottom) indicates that the magnetization is only slightly populated with an increase of the applied dc field, suggesting that the total spin ground state of this compound is zero. This discrepancy in the results can again be attributed to the extreme air sensitivity of the sample leading to partial oxidation during sample collection. Taking into consideration the structure, antiferromagnetic couplings between the four Mn²⁺ centers would lead to a total spin ground state of zero. The overall magnetic behavior indicates the presence of dominant antiferromagnetic interactions within this tetranuclear Mn²⁺ compound, as reported for [Mn₄Te₄(TePri)₄]⁴⁻.^{19b,20,26}

2.3. Conclusions

We have been able to synthesize and characterize Mn²⁺ and Co²⁺ complexes with trimethylsilylchalcogenolate ligands. The X-ray crystallographic analysis of these

complexes shows the presence of potentially reactive $-\text{ESiMe}_3$ moieties and suggests that these compounds could potentially be utilized as precursor to the ternary nanocluster synthesis. These compounds should be a convenient source of paramagnetic ions into a semiconductor matrix for the synthesis of ternary clusters that could potentially manifest magnetic as well as semiconducting properties. The reactions to test the utility of these precursors for nanocluster preparation are underway.

2.4. Experimental Section

2.4.1. General Experimental

All experimental procedures were performed using standard double manifold Schlenk line techniques under an atmosphere of dried nitrogen gas or in nitrogen filled glove boxes. The non-chlorinated solvents (THF, hexanes) were dried and collected using a MBraun MB-SP Series solvent purification system with tandem activated alumina (THF) and activated alumina or activated copper redox catalyst (hydrocarbons).²⁷ CH_2Cl_2 was dried and distilled over P_2O_5 . N,N' -tmeda and 3,5-lutidine were dried and distilled over CaH_2 and Na, respectively. MnCl_2 and CoCl_2 were purchased from Aldrich in 98% purity and used as supplied. 1.6 M $^n\text{BuLi}$ in hexanes was purchased from Aldrich. The silylated reagents $\text{E}(\text{SiMe}_3)_2$ (E = S, Se) were synthesized using literature procedures.^{3,28} LiESiMe_3 (E = S, Se) was prepared following a previously published literature procedure.²⁹

X-ray data were collected on a Enraf-Nonius Kappa-CCD diffractometer equipped with graphite-monochromated MoK α ($\alpha = 0.71073\text{\AA}$) radiation. Single crystals of the complexes, were carefully selected, immersed in paraffin oil and mounted on a nylon loop. Crystals were placed in a cold stream of N $_2$ to prevent decomposition. The structures were solved using direct methods and refined by the full-matrix least squares procedure of SHELXTL (G.M.Sheldrick, Madison, WI, 1996). With the exception of disordered carbon atoms of the *N,N'*-tmeda ligands and $-\text{SiMe}_3$ substituents, all non-hydrogen atoms were refined anisotropically, while hydrogen atoms were kept at their calculated distances and refined using a riding model. For **4**, satisfactory refinement of the data was completed with the resolution of a TWIN component (*k*, *h*, *-l*) and resultant BASF values 0.16690 and 0.12390.

The magnetic susceptibility measurements of solid samples **3a**, **3b** and **5** were carried out with the use of a Quantum Design SQUID magnetometer MPMS-XL. This magnetometer works between 1.8 and 400 K for dc applied fields ranging from -7 to 7 T. Ac susceptibility measurements can be measured with an oscillating ac field of 3 Oe and ac frequencies ranging from 1 to 1500 Hz. *M* vs *H* measurements has been performed at 100 K to check for the presence of ferromagnetic impurities in all cases. The magnetic data were corrected for the sample holder and the diamagnetic contribution. Ac susceptibility measurements have been checked with an oscillating ac field of 3 Oe and ac frequencies at 1000 Hz. Measurements were performed on a polycrystalline sample of 12.5 mg (**3a**), 5.6 mg (**3b**) and 31.4 mg (**5**), respectively. The sample bags were prepared in a glove box and measured immediately. It is worth pointing out that the complexes are very air sensitive. Sample bags for SQUID measurements were prepared in a glove box

however noticeable color changes of the samples were observed when during SQUID measurements suggesting partial oxidation.

Elemental analysis of **2a**, **3a**, **3b** and **4** was performed by Guelph Chemical Laboratories, Ltd. (Ontario, Canada) and by Columbia Analytical Services (Tucson, Arizona) for **5**, **6**. Due to the highly air sensitive nature of **1a**, **1b**, and **2b**, elemental analyses were not possible. Sample homogeneity was determined via unit cell measurements on random samplings of the single crystals obtained.

2.4.2. Syntheses

2.4.2.1. Synthesis of $(N,N'$ -tmeda)Co(SSiMe₃)₂, **1a**.

CoCl₂ (0.173g, 1.33 mmol) was dissolved in 20 mL CH₂Cl₂ by adding *N,N'*-tmeda (0.30 mL, 2.00 mmol) to yield a blue solution. This solution was then added to freshly prepared LiSSiMe₃ (2.84 mmol) at 0°C. A suspension was obtained after stirring for 1 hour and raising the temperature to room temperature. **1a** was purified by the removal of solvent in vacuum followed by extraction with hexanes and filtration. Blue needle-like crystals were obtained by the reduction of solvent volume by half and storing at -25°C for a few days. Yield: 0.128g (25% based on CoCl₂).

2.4.2.2. Synthesis of $(N,N'$ -tmeda)Co(SeSiMe₃)₂, **1b**.

CoCl₂ (0.139g, 1.07 mmol) was dissolved in 20mL CH₂Cl₂ by adding *N,N'*-tmeda (0.25mL, 1.67 mmol). This solution was then added to freshly prepared LiSeSiMe₃ (2.30 mmol) at 0°C. A green suspension was obtained after stirring for 20 minutes at 0°C. **1b**

was purified in an analogous manner to **1a** and isolated as green crystals. Yield: 0.102g (20% based on CoCl_2).

2.4.2.3. Synthesis of (3,5-Me₂C₅H₃N)₂Co(SSiMe₃)₂, **2a.**

CoCl_2 (0.145g, 1.12 mmol) was dissolved in 30mL CH_2Cl_2 by adding 3,5-lutidine (0.40mL, 3.50 mmol) to yield a blue solution after stirring overnight. This solution was then added to freshly prepared LiSSiMe_3 (2.37 mmol) at 0°C . A blue suspension was obtained after stirring for 15 minutes at 0°C . **2a** was purified by the removal of solvent in vacuum followed by extraction with hexanes and filtration. Blue crystals were obtained by the reduction of solvent and storing at -80°C freezer for a few weeks. Yield: 0.108g (20% based on CoCl_2). Anal. Calcd for $\text{C}_{20}\text{H}_{36}\text{CoN}_2\text{S}_2\text{Si}_2$: C, 49.66%; H, 7.50%. Found: C, 49.33%; H, 7.24%.

2.4.2.4. Synthesis of (3,5-Me₂C₅H₃N)₂Co(SeSiMe₃)₂, **2b.**

CoCl_2 (0.147g, 1.13 mmol) was dissolved in 30mL CH_2Cl_2 by adding 3,5-lutidine (0.40mL, 3.50 mmol) which was then added to freshly prepared LiSeSiMe_3 (2.30 mmol) at -60°C . A green suspension was obtained after stirring for 15 minutes not allowing the temperature to go above -50°C . The solution was filtered cold. Green crystals were obtained by the reduction of the solvent volume and storing at -45°C . Yield: 0.098g (15% based on CoCl_2)

2.4.2.5. Synthesis of [Li(*N,N'*-tmeda)]₂[(*N,N'*-tmeda)Mn₅(SSiMe₃)₆(S)₃], **3a.**

N,N'-tmeda (0.24mL, 1.56 mmol) was added to a suspension of MnCl₂ (0.131g, 1.04mmol) in 10mL CH₂Cl₂ and stirred at room temperature. After stirring for 1 hour, a pink suspension was obtained. This suspension was then added to freshly prepared LiSSiMe₃ (2.08 mmol) at 0°C and stirred for 2hrs whilst slowly warming to room temperature, to produce an orange-red suspension. The solvent was removed under vacuum and the product was extracted with 20mL hexanes. **3a** was obtained after filtering the extracted orange-red solution through dried Celite. The volume of the solution was reduced by half and stored at -25°C for a few days to afford orange-red X-ray quality crystals of **3a**. Yield: 0.152g (53.5% based on MnCl₂). Anal. Calcd for C₃₆H₁₀₂Li₂Mn₅N₆S₉Si₆: C, 31.68%; H, 7.53%. Found: C, 31.98%; H, 7.75%.

2.4.2.6. Synthesis of [Li(*N,N'*-tmeda)]₂[(*N,N'*-tmeda)Mn₅(SeSiMe₃)₆(Se)₃], **3b.**

The synthesis of **3b** was carried in a similar way as for **3a** by the addition of MnCl₂ (0.155g, 1.23mmol) and *N,N'*-tmeda (0.28mL, 1.85mmol) suspended in 10mL CH₂Cl₂ to freshly prepared LiSeSiMe₃ (2.46mmol). The product **3b** was obtained in the form of orange-red crystals by reducing the volume by half and storing at -25°C for a few days. Yield: 0.090g (20.5% based on MnCl₂). Anal. Calcd for C₃₆H₁₀₂Li₂Mn₅N₆Se₉Si₆: C, 24.20%; H, 5.75%. Found: C, 23.67%; H, 5.72%.

2.4.2.7. Synthesis of [Li(*N,N'*-tmeda)]₂[Mn(SSiMe₃)₄], **4.**

N,N'-tmeda (0.45mL, 3.00 mmol) was added to a suspension of MnCl₂ (0.151g, 1.20 mmol) in 20ml of CH₂Cl₂ and stirred at room temperature. After stirring for 1 hour, a

pink suspension was obtained. This suspension was then added to freshly prepared LiSSiMe_3 (4.82 mmol) at 0°C to form a pale pink colored solution. After removal of the solvent in vacuum, extraction of the residue with hexanes and subsequent filtration over Celite, pale pink crystals were obtained by storing concentrated solutions of **4** at -25°C for a few days. Yield: 0.347g (40.0% based on MnCl_2). Anal. Calcd for $\text{C}_{24}\text{H}_{68}\text{Li}_2\text{MnN}_4\text{S}_4\text{Si}_4$: C, 39.91%; H, 9.49%, Found: C, 39.79%; H, 9.75%.

2.4.2.8. Synthesis of $[\text{Li}(\text{N},\text{N}'\text{-tmeda})]_4[\text{Mn}_4(\text{SeSiMe}_3)_4(\text{Se})_4]$, **5 and $[\text{Li}(\text{N},\text{N}'\text{-tmeda})]_4[\text{Mn}(\text{Se}_4)_3]$, **6**.**

$\text{N},\text{N}'\text{-tmeda}$ (0.35mL, 2.33 mmol) was added to a suspension of MnCl_2 (0.119g, 0.946 mmol) in 20ml CH_2Cl_2 and stirred at room temperature. After stirring for 1 hour, a pink suspension was obtained. This suspension was then added to freshly prepared LiSeSiMe_3 (3.79 mmol) at 0°C to form a deep red solution. The solvent was removed in vacuum and the residue was extracted with hexanes and filtered over Celite. Two different colored crystals were obtained by the reducing the solvent volume and storing the solution at -5°C for a few days. Orange red crystals were characterized as $[\text{Li}(\text{N},\text{N}'\text{-tmeda})]_4[\text{Mn}_4(\text{SeSiMe}_3)_4(\text{Se})_4]$ **5** and dark red/brown crystals were characterized as $[\text{Li}(\text{N},\text{N}'\text{-tmeda})]_4[\text{Mn}(\text{Se}_4)_3]$ **6**. These could be partially separated by hand. Yield: **5**, 0.153g (40% based on MnCl_2). Yield: **6**, 0.071g (5% based on MnCl_2). Anal. Calcd for $\text{C}_{36}\text{H}_{100}\text{Li}_4\text{Mn}_4\text{N}_8\text{Se}_8\text{Si}_4$, **5**: C, 26.40%; H, 6.16%. Found: C, 25.73%; H, 6.16%. Anal. Calcd for $\text{C}_{24}\text{H}_{64}\text{Li}_4\text{MnN}_8\text{Se}_{12}$ **6**: C, 19.28%; H, 4.31%. Found: C, 20.01%; H, 4.00%

2.5. References

1. a) Zhang, Q.F.; Leung, W.H.; Xin, X. *Coord. Chem. Rev.* **2002**, *224*, 35-49. b) DeGroot, M. W.; Corrigan, J. F. *Comprehensive Coordination Chemistry II*; Fujita, M., Powell, A., Creutz, C., Eds.; Elsevier: Oxford, U.K., 2004; Vol. 7, 57-113. c) DeGroot, M. W.; Corrigan, J. F. *The Chemistry of Nanomaterials: Synthesis, Properties and Applications*; Rao, C. N. R.; Muller, A.; Cheetham, A. K.; Eds; Wiley-VCH: Weinheim, Germany, 2004, Vol.2, 418-451. d) Dehnen, S.; Eichhöfer, A.; Fenske, D. *Eur. J. Inorg. Chem.* **2002**, *2*, 279-317 e) Efros, A. I.; Rosen, M. *Ann. Rev. Mater. Sci.* **2000**, *30*, 475-521. f) Hong-Wei, H.; Xin-Quan, X.; Shu, S. *Coord. Chem. Rev.* **1996**, *153*, 25-56. h) Dehnen, S.; Melullis, M. *Coord. Chem. Rev.* **2006**, *251*, 1259-1280.
2. a) Tran, D. T. T.; Taylor, N. J.; Corrigan, J. F. *Angew. Chem. Int. Ed. Engl.* **2000**, *39*, 935-937 b) Tran, D. T. T.; Beltran, L. M.; Kowalchuk, C. M.; Trefiak, N. R; Taylor, N. J.; Corrigan, J. F; *Inorg. Chem.* **2002**, *41*, 5693-5698.
3. DeGroot, M. W.; Taylor, N. J.; Corrigan, J. F. *J. Mater. Chem.* **2004**, *14*, 654-660.
4. DeGroot, M. W.; Taylor, N. J.; Corrigan, J. F. *Inorg. Chem.* **2005**, *44*, 5447-5458.
5. a) DeGroot, M. W.; Corrigan, J. F. *Angew. Chem. Int. Ed.* **2004**, *43*, 5355-5357. b) DeGroot, M.W.; Taylor, N. J; Corrigan, J. F. *J. Am. Chem. Soc.* **2003**, *125*, 864-865.
6. a) Komuro, T.; Matsuo, T.; Kawaguchi, H.; Tatsumi, K. *J. Chem. Soc., Dalton Trans.* **2004**, *10*, 1618-1625. b) Komuro, T.; Matsuo, T.; Kawaguchi, H.; Tatsumi, K. *J. Chem. Commun.* **2002**, *9*, 988-989. c) Komuro, T.; Matsuo, T.; Kawaguchi, H.; Tatsumi, K. *Angew. Chem. Int. Ed.* **2003**, *42*, 465-468.
7. a) Sommer, H.; Eichhöfer, A.; Drebov, N.; Ahlrichs, R.; Fenske, D. *Eur. J. Inorg. Chem.*, **2008**, *32*, 5138-5145. b) Bechlars, B.; Issac, I.; Feuerhake, R.; Clerac, R.; Fuhr, O.; Fenske, D. *Eur. J. Inorg. Chem.*, **2008**, *10*, 1632-1644. c) Feuerhake, R.; Fenske, D. *Z. Anorg. Allg. Chem.* **2003**, *629*, 2317-2324.

8. DeGroot, M. W.; Corrigan, J. F. *Z. Anorg. Allg. Chem.* **2006**, *632*, 19-29.
9. Borecki, A.; Corrigan, J. F. *Inorg. Chem.* **2007**, *46*, 2478-2484.
10. DeGroot, M. W.; Corrigan, J. F. *Organometallics* **2005**, *24*, 3378-3385.
11. Komuro, T.; Kawaguchi, H.; Tatsumi, K. *Inorg. Chem.* **2002**, *41*, 5083-5090.
12. Corwin, D. T.; Gruff, E. S.; Koch, S. A.; *J. Chem. Soc., Chem. Commun.* **1987**, *13*, 966-967.
13. Sobota, P.; Utko, J.; Szafert, S.; Janas, Z.; Glowiak, T. *J. Chem. Soc. Dalton. Trans.* **1996**, *16*, 3469-3473.
14. Stephan, H. O.; Henkel, G. *Polyhedron.* **1996**, *15*, 501-511.
15. Silver, A.; Koch, S. A.; Millar, M. *Inorg. Chim. Acta.* **1993**, *205*, 9-14.
16. a) Krebs, B.; Henkel, G. *Angew. Chem., Int. Ed. Engl.* **1991**, *30*, 769-788. b) Henkel, G.; Krebs, B. *Chem. Rev.* **2004**, *104*, 801-824.
17. a) Seino, H.; Mizobe, Y.; Hidai, M. *Organometallics.* **2000**, *19*, 3631-3639 b) Seino, H.; Mizobe, Y.; Hidai, M. *New J. Chem.* **2000**, *24*, 907-911. c) Christou, G.; Ridge, B.; Rydon, H. N.; *J. Chem. Soc. Dalton*, **1978**, 1423-1425. d) Kern, A.; Nather, C.; Studt, F.; Tuczec, F.; *Inorg. Chem.* **2004**, *43*, 5003-5010.
18. a) Shiga, T.; Oshio, H.; *Sci. Tech. Adv. Mater.* **2005**, *5*, 565-570. b) Stoumpos, C. C.; Gass, I.; Milios, C. J.; Kefallaniti, E.; Raptopoulou, C. P.; Terzis, A.; Lalioti, N.; Brechin, E. K.; Perlepes, S. P.; *Inorg. Chem. Commun.* **2008**, *11*, 196-202.
19. a) Stephan, H. O.; Henkel, G. *Angew. Chem., Int. Ed. Engl.* **1994**, *33*, 2322-2324. b) Stephan, H. O.; Chen, C.; Griesar, K.; Haase, W.; Henkel, G. *J. Chem Soc., Chem. Commun.* **1993**, *10*, 886-888.

20. Eichhöfer, A.; Wood, P. T.; Viswanath, R. N.; Mole, R. A. *Chem. Commun.* **2008**, *13*, 1596-1598.
21. Huang, S. P.; Dhingra, S.; Kanatzidis, M. G. *Polyhedron* **1990**, *9*, 1389-1395.
22. a) Ansari, M. A.; Ibers, J. A. *Inorg. Chem.* **1989**, *28*, 4068-4069. b) McConnachie, J. M.; Ansari, M. A.; Ibers, J. A. *Inorg. Chem.* **1993**, *32*, 3250-3255.
23. Albrecht-Schmitt, T. E.; Cody, J. A.; Hupp, J. T.; Ibers, J. A. *Inorg. Chem.* **1995**, *34*, 5101-5102. b) Albrecht-Schmitt, T. E.; Ibers, J. A. *Inorg. Chem.* **1996**, *35*, 7273-7278.
24. Banda, R. M. H.; Cusick, J.; Scudder, M. L.; Craig, D. C.; Dance, I. G. *Polyhedron* **1989**, *8*, 1999-2001.
25. Cusick, J.; Dance, I. *Polyhedron*, **1991**, *10*, 2629-2640.
26. a) Stephan, H. O.; Kanatzidis, M. G.; Henkel, G. *Angew. Chem., Int. Ed. Engl.* **1996**, *35*, 2135-2137 b) Eichhöfer, A.; Wood, P. T.; Viswanath, R. N.; Mole, R. A. *Eur. J. Inorg. Chem.*, **2007**, *30*, 4794-4799 c) Mellullis, M.; Clérac, R.; Dehnen, S. *Chem. Commun.* **2005**, *48*, 6008-6010.
27. Pangborn, A. B.; Giardello, M. A.; Grubbs, R. H.; Rosen, R. K.; Timmers, F. J. *Organometallics*, **1996**, *15*, 1518-1520.
28. So, J.; Boudjouk, P; *Synthesis* **1989**, 306-307.
29. Taher, D; Wallbank, A. I.; Turner, E. A.; Cuthbert, H. L; Corrigan, J. F. *Eur. J. Inorg. Chem.*, **2006**, *22*, 4616-4620.

CHAPTER THREE

Zinc Chalcogenolate Complexes as Molecular Precursors to Mn²⁺ containing ZnE (E= S, Se) Nanoclusters[†]

3.1. Introduction

Metal chalcogenolate complexes of the d-block metals with trimethylsilyl functionalities on the chalcogen centers have recently been utilized as precursors for the synthesis of ternary MM'E (E = S, Se, Te) nanoclusters. The preformed metal-chalcogen bond and high solubility of these complexes in common organic solvents, coupled with the reactivity of the –ESiMe₃ ligands towards ligand stabilized metal salts, makes these complexes powerful precursors for the formation of M-E-M' bonding interactions and entry into ternary MM'E nanoclusters.¹⁻⁸ Using these reagents as sources of soluble, protected “metallachalcogenolates” (metal-chalcogenides), the ternary nanoclusters [Cu₂₀Hg₁₅E₂₅(PⁿPr₃)₁₈] (E= S, Se),^{1a} [Zn_xCd_{10-x}E₄(EPh)₁₂(PⁿPr₃)₄] (E= Se, Te),³ and [Cu₉Ag₃S₆(PEtPh₂)₈]⁸ have been synthesized using (PⁿPr₃)₃Cu(ESiMe₃), (3,5-Me₂C₅H₃N)₂Zn(ESiMe₃)₂ and (PEtPh₂)₃Cu(SSiMe₃), respectively. (N,N'-tmeda)Zn(SeSiMe₃)₂ has previously been successfully utilized as a molecular precursors for the synthesis of ternary nanocluster, [(N,N'-tmeda)₅Zn₅Cd₁₁Se₁₃(SePh)₆(THF)₂].^{4b} The demonstrated ability of metal-trimethylsilylchalcogenolate complexes as precursors for the controlled assembly of ternary cluster complexes has prompted us to develop this general synthetic route for the assembly of semiconducting systems containing paramagnetic ions, Mn²⁺.

[†] Submitted for publication to *Inorganic Chemistry*, 2011 American Chemical Society.

Paramagnetic ion (e.g. Mn^{2+}) doped semiconductors (eg. ZnE) with dimensions of a few nanometers, often referred to as dilute magnetic semiconductors (DMS),⁹ have attracted significant interest due to potential applications as well as fundamental research.¹⁰⁻²³ This is due to the unique size specific magnetic and optical properties that arise from the coexistence of the quantum confinement effect and its influence on the s-p-d exchange interactions between magnetic ions and the semiconducting host. Mn^{2+} is by far the most commonly used dopant and acts both as luminescent center and localized spins in semiconductor nanocrystals.^{24,25} Mn^{2+} -doped semiconductors are significantly more efficient emitters than their undoped counterpart with better thermal, chemical and photochemical stability.^{13,19} Further exploration into these robust and efficient emitters could lead to applications as lasers,²⁶ LEDs,²⁷ and in bioimaging.¹¹ Furthermore, as a source of magnetic impurity, they have potential to find application in magneto-optics and magneto-electronics.²⁸

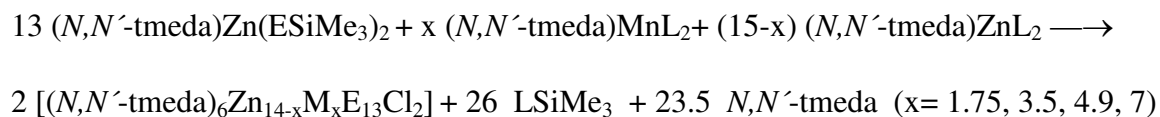
Despite many advances made in synthetic approaches over last decade, it remains difficult to incorporate Mn^{2+} in semiconductors (<6 nm) beyond 1-2% despite their high bulk solubility.^{24,29} To this day, reports on a complete and accurate structural characterization of the local environment of the magnetic ions within the semiconductor host is minimal.^{14,30} The accurate structural characterization of doped QDs is vital to gain insights into the unique phenomena that occur in quantum confined Mn^{2+} doped semiconductors and to establish structure property relationships. Herein, we report the synthesis, complete structural characterization and optical properties of four ZnE nanoclusters containing unusually higher amount of Mn^{2+} , $(N,N'$ -tmeda)₆Zn_{12.3}Mn_{1.7}S₁₃Cl₂ (**7a**), $(N,N'$ -tmeda)₆Zn_{10.9}Mn_{3.1}S₁₃Cl₂ (**7b**), $(N,N'$ -

$(\text{tmeda})_6\text{Zn}_{10}\text{Mn}_4\text{S}_{13}\text{Cl}_2$ (**7c**), $(N,N'\text{-tmeda})_6\text{Zn}_{6.2}\text{Mn}_{7.8}\text{S}_{13}\text{Cl}_2$ (**7d**) and $(N,N'\text{-tmeda})_6\text{Zn}_{12}\text{Mn}_2\text{Se}_{13}\text{Cl}_2$ (**8a**), $(N,N'\text{-tmeda})_6\text{Zn}_{10.8}\text{Mn}_{3.2}\text{Se}_{13}\text{Cl}_2$ (**8b**), $(N,N'\text{-tmeda})_6\text{Zn}_{10.7}\text{Mn}_{3.3}\text{Se}_{13}\text{Cl}_2$ (**8c**), $(N,N'\text{-tmeda})_6\text{Zn}_{8.2}\text{Mn}_{5.8}\text{Se}_{13}\text{Cl}_2$ (**8d**). The photoluminescence properties of these complexes are described and contrasted with isostructural binary clusters, $(N,N'\text{-tmeda})_6\text{Zn}_{14}(\text{E})_{13}\text{Cl}_2$ (E = S, **9a**; E = Se, **9b**).

3.2. Results and Discussion

3.2.1. Synthesis and Characterization of Chalcogenide Complexes

The reaction of the chalcogenolate precursor $(N,N'\text{-tmeda})\text{Zn}(\text{ESiMe}_3)_2$ with $N,N'\text{-tmeda}$ solubilized metal salts as illustrated in Scheme 3.1, afforded the ternary clusters (**7a-d**, **8a-d**) as well as the binary clusters (**9a**, **9b**).



Scheme **3.1**. Synthesis of $(N,N'\text{-tmeda})_6\text{Zn}_{14-x}\text{Mn}_x\text{E}_{13}\text{Cl}_2$ (**7a-9b**). L = Cl, OAc

The generation of ClSiMe_3 and/or AcOSiMe_3 is the driving force for these reactions, which leads to the formation of metal-chalcogen bonding interactions. Exploiting the reactivity of the zinc chalcogenolate precursor and the versatility of the reaction Scheme 3.1, we were able to synthesize ternary clusters containing different amount of Mn^{2+} . Chalcogenide (E^{2-}) ligands tend to adopt bridging coordination modes

due to the high polarizability of these centers, which often results in the formation of polynuclear species.⁷ The isolation of these manganese containing ‘ZnE’ clusters with varying amounts of ‘dopant’, provides an opportunity to study the effect of Mn²⁺ concentration on the photoluminescence properties of these systems. Single-crystal X-ray diffraction data were collected for complexes **7a**, **7d**, **8a**, **8d**, **9a**, **9b** and cell constants were recorded for complexes **7b** and **8b**. A summary of the crystal data and structural parameters for all six complexes is listed in Appendix A.10-A.15.

The common structural feature prevalent in the clusters is the presence of central core that consists of ‘M₁₄E₁₃’ unit that is stabilized by six tmeda and two terminal chloride ligands (Figure 3.1 and Figure 3.3). The chelating tmeda ligands are coordinated to six zinc atoms that are present on the surface of the cluster, thus preventing further condensation of the cluster into bulk solids. This arrangement has previously been observed in the zinc-telluride cluster (N,N'-tmeda)₆Zn₁₄Te₁₃Cl₂³² and a related M₁₄E₁₃ frame has also been displayed with the ternary copper-indium-chalcogenides [Cu₆In₈E₁₃Cl₄(PR₃)₁₂] (E = S, Se; R = alkyl).^{1b, 6d}

The binary clusters (N,N'-tmeda)₆Zn₁₄S₁₃Cl₂ **9a** and (N,N'-tmeda)₆Zn₁₄Se₁₃Cl₂ **9b** can be prepared from a combination of Zn(OAc)₂ with the zinc chalcogenolates (N,N'-tmeda)Zn(SSiMe₃)₂ and (N,N'-tmeda)Zn(SeSiMe₃)₂, respectively, as outlined in Scheme 3.1. The solid state molecular structure obtained from single crystal X-ray diffraction is shown in Figure 3.1 for the sulfide complex (N,N'-tmeda)₆Zn₁₄S₁₃Cl₂ **9a**. Cluster **9a** crystallizes in the triclinic space group, P $\bar{1}$ with Z = 2 and there are nine CH₂Cl₂ solvent molecules present in the asymmetric unit. The isostructural and isomorphous selenide complex **9b** was also isolated in the form of single crystals, and its structure determined.

The molecular structure of both ternary (*vide infra*) and binary clusters shows that the zinc chalcogenolate precursors successfully deliver “ZnE₂” into the cluster core and act as a source of six “tmedaZnE₂” units that stabilize the polyhedron.

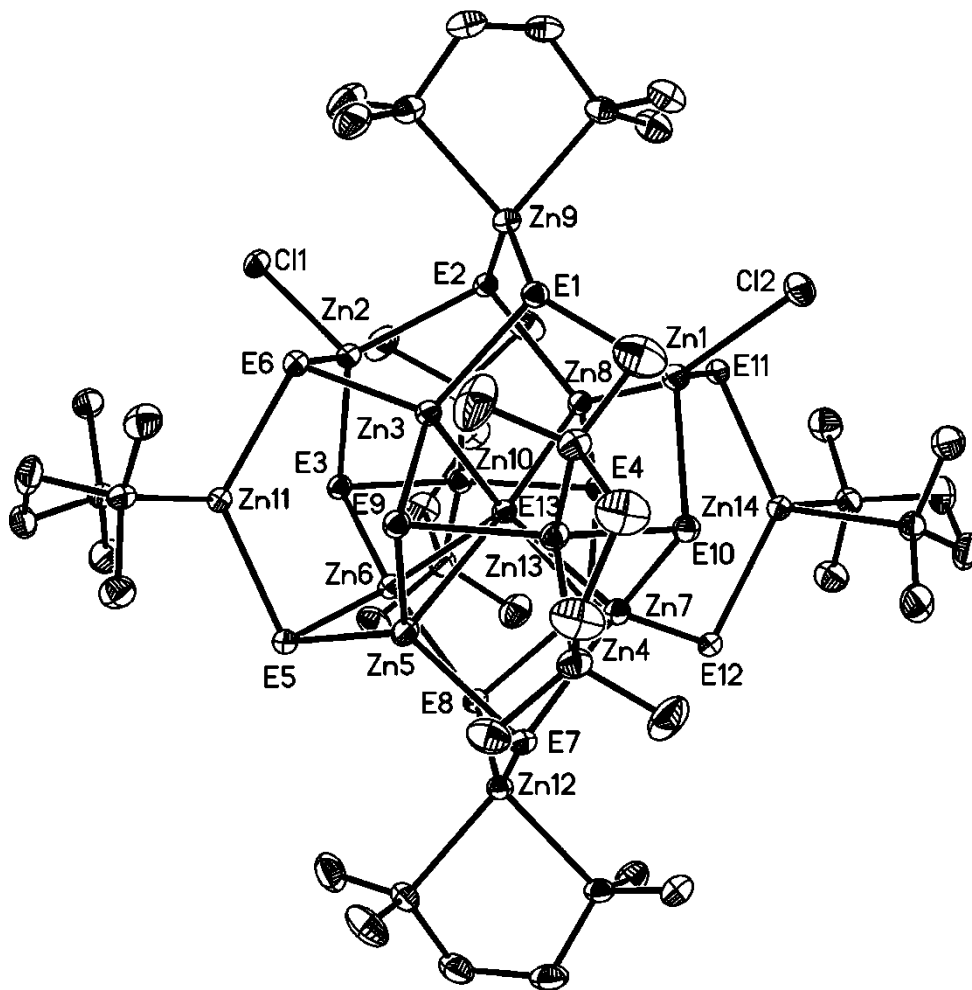


Figure 3.1. The molecular structure of $(N,N'\text{-tmeda})_6\text{Zn}_{14}\text{E}_{13}\text{Cl}_2$ (E = S (illustrated), Se). Thermal ellipsoids are drawn at the 45% probability level. Hydrogen atoms are omitted for clarity.

The geometry around the Zn centers is distorted tetrahedral. Interestingly, there are two chloride ligands bonded to two Zn²⁺ centers at the surface of the cluster (Figures 3.1 and 3.2). Although the source of the chloride ion must be solvent, the syntheses and

yields of **9a** and **9b** using Zn(OAc)₂ are entirely reproducible. Each zinc is four coordinate, with Zn9-14 bonded to a bidentate tmeda ligand and two chalcogenide ions, Zn1 and Zn2 each bonded to one Cl⁻ and three E²⁻ and the six interstitial zinc bonded to four sulfur (**9a**) or selenium (**9b**) centers. Summaries of the bond distances and angles for **9a** and **9b** are listed in Tables 3.1 and 3.2, respectively. Each of the chalcogens bridges three zinc centers with the exception of the central ligand, which is within bonding distance to six metals albeit with four shorter (~ 2.4 Å, **9a**; 2.5 Å, **9b**) and two longer (~ 2.6 Å, **9a**; ~ 2.9 Å, **9b**) contacts.

	9a (E = S)	9b (E = Se)
Zn(1)-E(1)	2.3495(11)	2.4709(11)
Zn(1)-E(10)	2.3580(11)	2.4782(11)
Zn(1)-E(11)	2.3525(11)	2.4529(11)
Zn(1)-Cl(1)	2.3640(11)	2.343(2)
Zn(2)-E(2)	2.3568(11)	2.4658(12)
Zn(2)-E(3)	2.3681(11)	2.4703(11)
Zn(2)-E(6)	2.3454(11)	2.4665(11)
Zn(2)-Cl(2)	2.3567(11)	2.358(2)
Zn(4)-E(4)	2.2851(11)	2.4099(11)
Zn(4)-E(8)	2.2999(11)	2.4120(11)
Zn(4)-E(12)	2.2923(11)	2.4007(12)
Zn(4)-E(13)	2.7974(11)	2.9278(6)
Zn(6)-E(3)	2.3151(11)	2.4249(11)
Zn(6)-E(5)	2.3574(11)	2.4644(11)
Zn(6)-E(8)	2.4112(11)	2.4930(11)
Zn(6)-E(13)	2.4388(11)	2.5287(11)
Zn(7)-E(7)	2.3793(11)	2.5197(11)
Zn(7)-E(10)	2.3158(11)	2.4254(11)
Zn(7)-E(12)	2.3590(11)	2.4681(11)
Zn(7)-E(13)	2.4351(11)	2.5302(11)
Zn(8)-E(2)	2.3167(11)	2.4346(11)
Zn(8)-E(4)	2.3898(11)	2.5138(11)

Zn(8)-E(11)	2.3389(11)	2.4286(11)
Zn(8)-E(13)	2.4620(11)	2.5635(11)
Zn(10)-E(3)	2.2720(11)	2.3884(11)
Zn(10)-E(4)	2.2794(11)	2.4011(12)
Zn(10)-N(3)	2.156(3)	2.156(6)
Zn(10)-N(4)	2.179(3)	2.182(7)
Zn(11)-E(5)	2.3063(11)	2.4059(12)
Zn(11)-E(6)	2.2734(11)	2.3805(11)
Zn(11)-N(5)	2.124(3)	2.171(6)
Zn(11)-N(6)	2.167(3)	2.164(6)
Zn(12)-E(7)	2.2808(11)	2.4013(11)
Zn(12)-E(8)	2.2856(11)	2.3946(11)
Zn(12)-N(7)	2.153(3)	2.157(6)
Zn(12)-N(8)	2.164(3)	2.149(6)
Zn(13)-E(9)	2.2792(11)	2.3998(11)
Zn(13)-E(10)	2.2781(11)	2.3843(11)
Zn(13)-N(10)	2.180(3)	2.182(6)
Zn(14)-E(11)	2.2702(11)	2.3866(11)
Zn(14)-E(12)	2.2921(11)	2.4214(11)
Zn(14)-N(11)	2.177(3)	2.177(6)

Table 3.1. Selected Bond Distances (Å) of Complexes **9a** and **9b**

	9a (E = S)	9b (E = Se)
E(1)-Zn(1)-E(11)	114.03(4)	112.28(4)
E(1)-Zn(1)-E(10)	114.01(4)	115.11(4)
E(11)-Zn(1)-E(10)	115.64(4)	114.96(4)
E(1)-Zn(1)-Cl(1)	105.46(4)	103.49(6)
E(10)-Zn(1)-Cl(1)	102.40(4)	107.31(6)
E(11)-Zn(1)-Cl(1)	103.30(4)	102.10(6)
E(4)-Zn(4)-E(12)	118.67(4)	119.05(4)
E(4)-Zn(4)-E(8)	119.84(4)	118.49(4)
E(12)-Zn(4)-E(8)	120.06(4)	120.47(4)
E(4)-Zn(4)-E(13)	94.23(4)	95.06(4)
E(12)-Zn(4)-E(13)	94.05(4)	95.03(3)

E(8)-Zn(4)-E(13)	93.66(4)	93.99(4)
E(3)-Zn(6)-E(5)	116.42(4)	115.26(4)
E(3)-Zn(6)-E(8)	113.96(4)	114.42(4)
E(5)-Zn(6)-E(8)	112.82(4)	112.60(4)
E(3)-Zn(6)-E(13)	107.57(4)	106.65(4)
E(5)-Zn(6)-E(13)	103.35(4)	103.56(4)
E(8)-Zn(6)-E(13)	100.66(4)	102.66(4)
E(10)-Zn(7)-E(12)	116.83(4)	115.56(4)
E(10)-Zn(7)-E(7)	114.48(4)	113.35(4)
E(12)-Zn(7)-E(7)	112.92(4)	112.34(4)
E(10)-Zn(7)-E(13)	106.74(4)	107.87(4)
E(12)-Zn(7)-E(13)	102.52(4)	104.29(4)
E(7)-Zn(7)-E(13)	101.00(4)	101.92(4)
N(3)-Zn(10)-N(4)	84.20(13)	84.7(3)
N(3)-Zn(10)-E(3)	114.84(9)	110.3(2)
N(4)-Zn(10)-E(4)	109.81(9)	110.48(19)
E(3)-Zn(10)-E(4)	128.23(4)	127.67(4)
N(7)-Zn(12)-N(8)	84.84(13)	84.9(3)
N(7)-Zn(12)-E(7)	112.27(9)	111.84(17)
N(8)-Zn(12)-E(7)	105.77(9)	105.44(19)
N(8)-Zn(12)-E(8)	112.24(9)	111.97(18)
E(7)-Zn(12)-E(8)	127.95(4)	128.46(4)
N(12)-Zn(14)-N(11)	84.26(12)	84.4(2)
N(12)-Zn(14)-E(11)	113.32(9)	112.25(18)
N(11)-Zn(14)-E(11)	109.77(9)	105.78(17)
N(11)-Zn(14)-E(12)	108.50(9)	112.09(17)
E(11)-Zn(14)-E(12)	126.92(4)	126.66(4)
Zn(7)-E(13)-Zn(6)	115.65(4)	114.36(4)
Zn(7)-E(13)-Zn(8)	109.90(4)	108.68(4)
Zn(3)-E(13)-Zn(8)	102.87(4)	103.97(3)
Zn(8)-E(13)-Zn(4)	73.05(3)	72.18(3)
Zn(8)-E(13)-Zn(5)	175.15(4)	176.39(4)
Zn(4)-E(13)-Zn(5)	111.76(3)	111.40(3)

Table 3.2. Selected Bond Angles (°) of Complexes **9a** and **9**

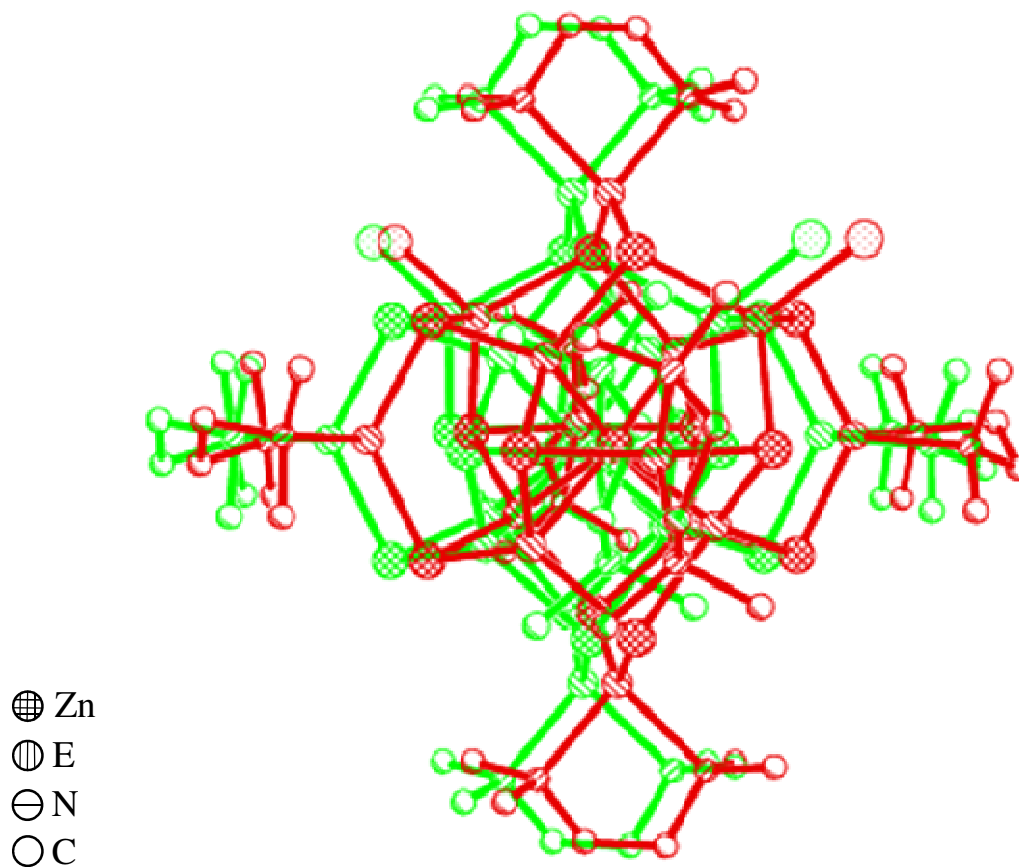


Figure 3.2. The stereo pair images of $(N,N'\text{-tmeda})_6\text{Zn}_{14}\text{E}_{13}\text{Cl}_2$ ($\text{E} = \text{S}$ (illustrated), Se) shown in red and green. Hydrogen atoms are omitted for clarity.

The strategy of using the reagents $(N,N'\text{-tmeda})\text{Zn}(\text{SSiMe}_3)_2$ and $(N,N'\text{-tmeda})\text{Zn}(\text{SeSiMe}_3)_2$ for the preparation of the all Zn^{2+} complexes suggested that mixed metal species could also be prepared by reacting them with a different metal salt. In this vein, adding a defined ratio of $\text{Mn}^{2+}:\text{Zn}^{2+}$ to solutions of $(N,N'\text{-tmeda})\text{Zn}(\text{ESiMe}_3)_2$ led to the formation of similar frameworks, but with varying amounts of manganese present in the clusters as determined by elemental analysis and changes in the luminescence properties, and supported by single crystal X-ray diffraction. Table 3.3 lists the atomic ratio of $\text{Zn}:\text{Mn}$ found in clusters **7-8** as determined via inductively coupled plasma atomic

emission spectroscopy (ICP-AES). The observed values indicate that the ratio between the two metals generally matches that introduced into the reaction mixtures (Scheme 3.1), with the exception of **8c** and **8d**, where the Mn contents in the clusters both lower than were introduced in the reaction scheme.

	7a	7b	7c	7d	8a	8b	8c	8d
Mn	1.7	3.1	4	7.8	2	3.2	3.3	5.8
Zn	12.3	10.9	10	6.2	12	10.8	10.7	8.2

Table 3.3. Atomic ratio of Zinc and Manganese in Compound **7a-d** and **8a-d** using ICP-AES.

Single crystal X-ray analysis of the mixed metal clusters confirmed that, as observed for **9a** and **9b**, all of the metal centers adopt distorted tetrahedral geometries. The slight differences in the scattering power of Zn and Mn together with site disorder of the Mn^{2+} make it difficult to model the occupancies accurately from the diffraction data. However, satisfactory refinement was achieved with the Zn ions occupying the six surface sites ligated by the tmeda ligands (Zn9-Zn14); the two metal sites bonded to the terminal chloride ions were best refined with full occupancy by manganese (Mn1 and Mn2) when the Mn content was greater than 2 atoms per cluster. Refinement of the crystallographic data for **7a** (S) and **8a** (Se) was satisfactorily completed with the two Mn centers with occupancy 0.5 at the two M-Cl sites (Figure 3.3) but the site specific location of remaining Mn^{2+} ions could not be confirmed based on the data. Overall, the local coordination geometries of the individual metal sites do not change drastically from those observed in **9a** and **9b** with increasing Mn content, reflecting the small differences

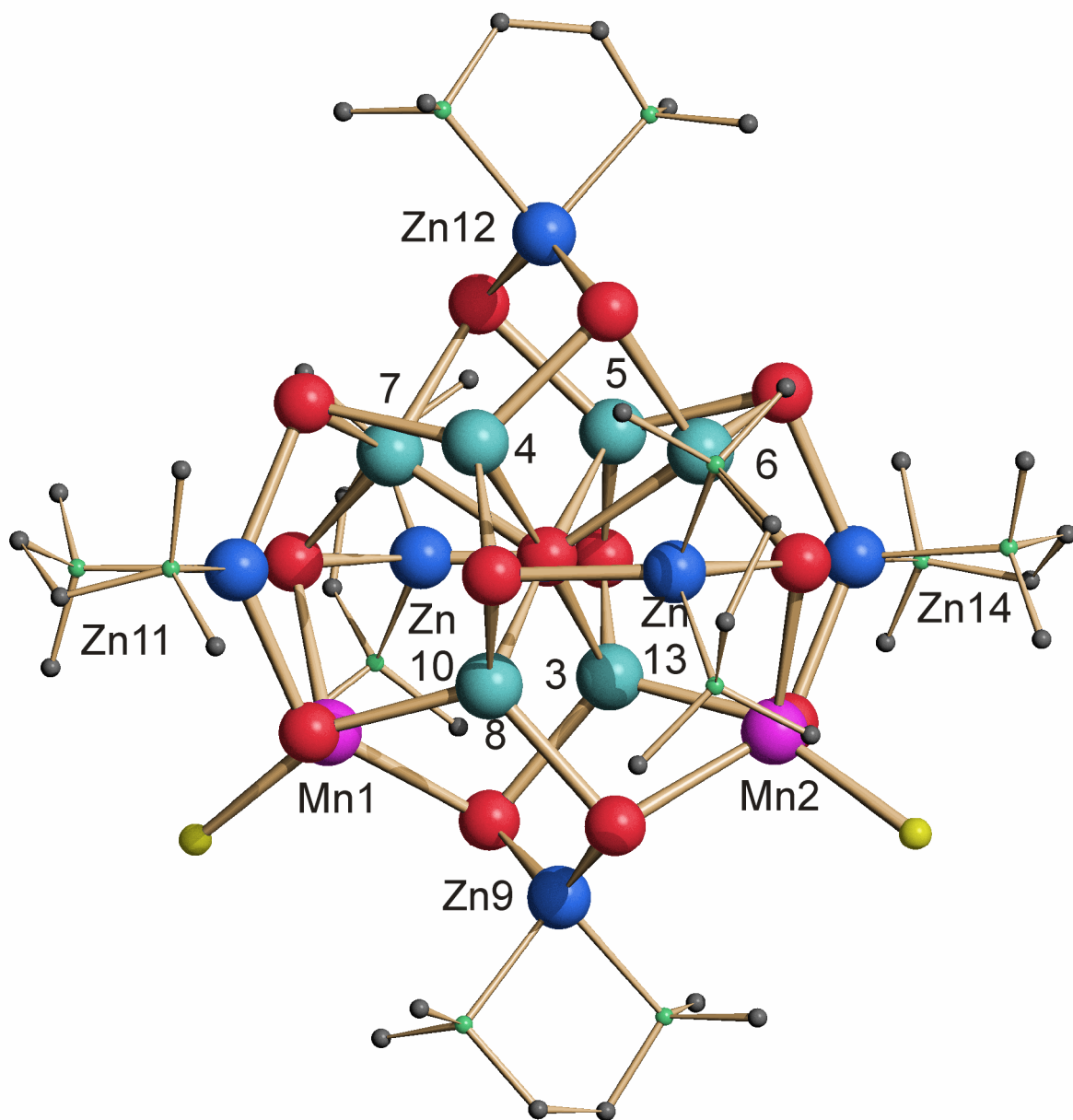


Figure 3.3. Molecular structure of $(N,N'\text{-tmeda})_6\text{Zn}_{10}\text{Mn}_4\text{Se}_{13}\text{Cl}_2$ **8d**. Blue: Zn; violet: Mn; red: Se; green: N; grey: C; yellow: Cl. Cyano colored metal sites represents those with refined partial occupancy of Zn and Mn in **8d**.

Mn1-Cl1	2.386(5)
Mn1-Se	2.546(3)-2.554(3)
Mn2-Cl2	2.395(5)
Mn2-Se	2.532(3)-2.544(3)
M3-Se	2.495(3)2.640(3)
M4-Se	2.453(3)-2.832(3)
M5-Se	2.440(3)-2.841(3)
M6-Se	2.478(3)-2.604(3)
M7-Se	2.461(3)-2.610(3)
M8-Se	2.478(3)2.614(3)
Zn9-N1	2.172(13)
Zn9-N2	2.195(13)
Zn9-Se2	2.378(3)
Zn9-Se1	2.394(3)
Zn10-N3	2.164(14)
Zn10-N4	2.178(13)
Zn10-Se3	2.393(2)
Zn10-Se4	2.401(2)
Zn11-N6	2.188(13)
Zn11-N5	2.200(13)
Zn11-Se6	2.387(2)
Zn11-Se5	2.404(2)
Zn12-N7	2.144(14)
Zn12-N8	2.178(15)
Zn12-Se7	2.394(3)
Zn12-Se8	2.396(2)
Zn13-N10	2.139(14)
Zn13-N9	2.177(12)
Zn13-Se10	2.391(2)
Zn13-Se9	2.402(2)
Zn14-N12	2.166(14)
Zn14-N11	2.170(14)
Zn14-Se11	2.380(3)

Table 3.4. Selected Bond Distances (Å) of **8d**.

in the ionic radii for the two four-coordinate metals (0.74 Å Zn²⁺; 0.80 Å Mn²⁺ high spin).³³ The overall size of the Mn-Zn-E cluster cores is approximately 9 Å × 9 Å × 9 Å.

The cluster (*N,N'*-tmeda)₆Zn_{8.4}Mn_{5.6}Se₁₃Cl₂ **8d** crystallizes in the trigonal space group P3(2)21 with 3.5 molecules of CH₂Cl₂. Selected bond distances for **8d** are summarized in Table 3.4. The two metal sites ligated to Cl were refined with full occupancy of Mn and, excluding the six tmeda ligated Zn sites, the remaining six metal positions present in the cluster core of **8d** were satisfactorily refined with partial occupancy of both zinc and manganese. The molecular structure of **8d** is shown in Figure 3.3. The average Mn-Se bond distance is 2.544(8) Å. The Mn-Cl and Mn-Se bond distances are similar to those observed in the adamantoid complex [Mn₄(SePri)₆Br₄]²⁻.³⁴ The Mn-Se bond distances are also comparable to those observed in [Mn₃₂Se₁₄(SePh)₃₆(PⁿPr₃)₄] and [Mn₈Se(SePh)₁₆]²⁻.³⁵ Refined Zn-Se bond distances are comparable with those observed in **9a** and **9b** and to those previously reported in [Zn₁₀S₇(SO₄)₃(py)₉]³⁶ (py = pyridine), [Zn₁₀S₄(SEt)₁₂(py)₄],³⁷ [Zn₈Se(SePh)₁₂(Cl)₄]²⁻,³⁸ and [(*N,N'*-tmeda)₅Zn₅Cd₁₁Se₁₃(SePh)₆(thf)₂].^{4b}

3.2.2. Photoluminescence Properties of MnZnE Clusters

Room temperature solution UV-visible absorption, photoluminescence (PL) and photoluminescence excitation (PLE) spectra were recorded for the clusters. Figure 3.4 shows the PL, PLE and UV-visible spectra of compounds **9a**, **7a** and **7d** and the same information for compounds **7b** and **7c** is shown in Appendix B.2.

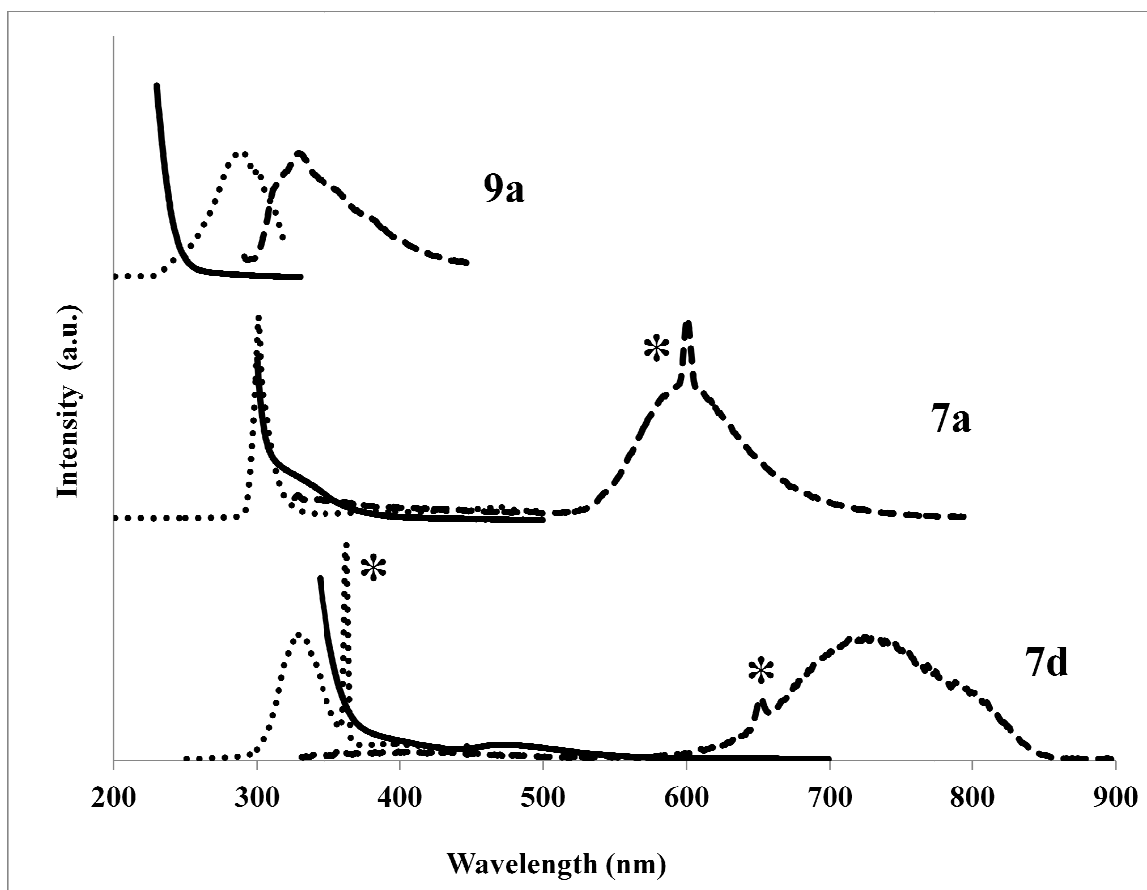


Figure 3.4. Normalized room temperature UV-visible (—), PLE (•••) and PL (---) spectra of Compound **9a**, **7a** and **7d** in DCM, DMSO and DMF respectively. *denotes harmonic vibration and/or solvent peaks. PLE (•••) were recorded using an excitation energy at the observed PL maximum.

The maximum PL emission band for the binary ZnS cluster **9a** is observed at 321nm. Upon incorporation of 2 Mn^{2+} to yield the heterometallic cluster **7a**, a drastically different PL emission spectrum is observed, as shown in Figure 3.4. The complete disappearance of the “band-edge” emission peak from **9a** is accompanied by a large Stokes shift with a PL peak maximum observed at 590 nm. When the amount of Mn was increased to yield cluster **7b**, the maximum PL emission is observed at ~ 600 nm. The peak at ~ 600 nm observed in **7a** and **7b** is no longer observed when the amount of Mn incorporated into the cluster is increased further. For **7c** and **7d** a single PL emission

maximum is observed ~ 730 nm for both compounds. At ambient temperatures, these emissions are very weak, as has been documented for the ternary Cd-Mn-E (E = S, Se) clusters.³¹ For each manganese containing complex, weak absorption transitions are observed centered around ~ 450 nm, consistent with d-d transitions of the tetrahedrally coordinated d^5 metals in Mn-Se clusters.^{31,35}

Figure 3.5 shows the room temperature (solution) UV-visible absorption, PL and PLE spectra of clusters **9b**, **8a** and **8d**. Spectra for **8b** and **8c** are illustrated in Appendix B.3 The PL spectra of the Zn cluster **9b** display a weak maximum at 450 nm when irradiated at 375 nm. However, the emission profile for the ZnSe clusters incorporating Mn^{2+} is again markedly different. A broad PL emission peak centered at 620 nm is observed for cluster **8a** with a smaller shoulder observed at 560 nm. The large Stokes shift observed in **8a** as compared to very small shift displayed by **4** provide evidence in support of successful incorporation of Mn^{2+} into the ZnSe matrix. As observed for the sulfide clusters **7a-7d**, the PL emission profiles of Mn containing ZnSe clusters change with the incorporation of higher amounts of manganese. Thus for sample **8c** and **8d**, the shoulder observed at 560 nm is no longer observed, with the emission at 640 nm being dominant. The origin of two emissions is not certain at present, but it likely reflects a distribution of clusters $(N,N'-tmeda)_6Zn_{14-x}Mn_xSe_{13}Cl_2$ in which the number of Mn^{2+} in the individual clusters is either lower (560 nm) or higher (640 nm). The redistribution of Cd^{2+} and Mn^{2+} has recently been documented for mixed Mn/Cd-selenide nanoclusters in solution.³¹

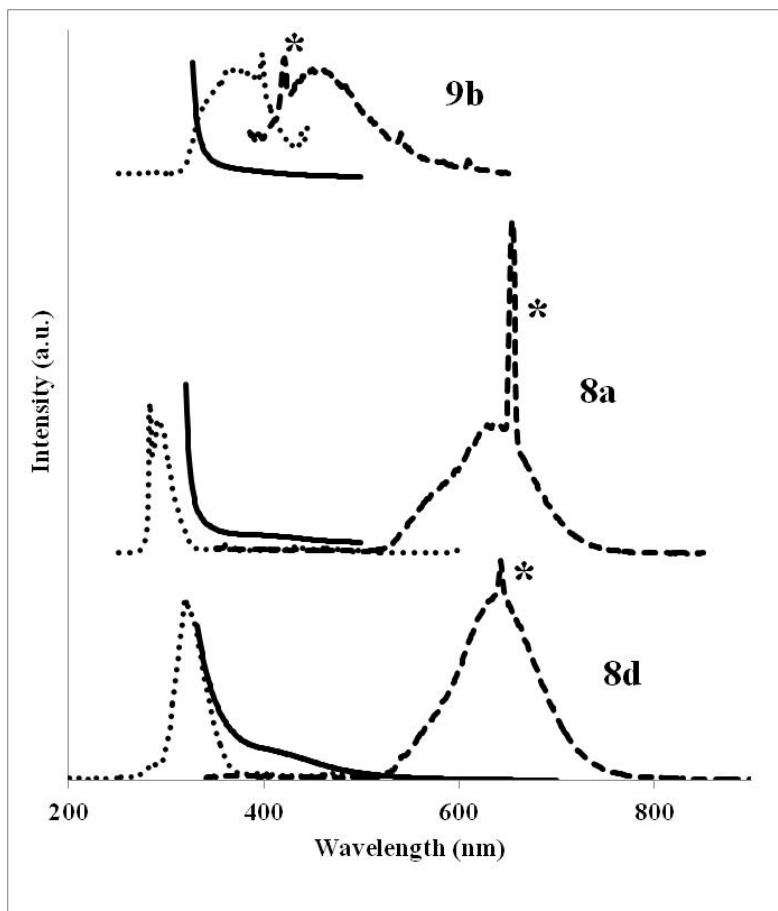


Figure 3.5. Normalized room temperature UV-visible (—), PLE (•••) and PL (---) spectra of Compound **9b**, **8a** and **8d** in DMSO, DCM and DCM respectively. *denotes harmonic vibration and/or solvent peaks. PLE (•••) were recorded using an excitation energy at the observed PL maximum.

The PL emission energies observed for **7c**, **7d** and **8a-d** are significantly red shifted compared to those reported for ZnE nanoparticles with low concentrations of Mn^{2+} dopants (dilute magnetic semiconductors, DMS). It is well established that incorporation of Mn^{2+} into a ZnE nanoparticle host results in the efficient energy transfer into the electronic state of Mn^{2+} , which undergoes atomic like transition from the lowest excited state (${}^4\text{T}_1$) to the ground state (${}^6\text{A}_1$), with a characteristic orange luminescence maximum at ca. 590 nm.^{25,30} In contrast, the emission energies for clusters with high

amounts of manganese, namely $[\text{Cd}_4\text{Mn}_6\text{Se}_4(\text{SePh})_{12}(\text{PPr}_3)_4]$ and $[\text{Cd}_4\text{Mn}_4\text{S}(\text{SePh})_{14}(\text{PPr}_3)_2]$, are observed at 780 and 725 nm, respectively.³¹ The PL emission observed at the yellow-orange region of visible spectrum for clusters with a small number (2-3) of Mn^{2+} centers (**7a-b**, **8a-b**) have emission energies similar to the electronic transition from ${}^6\text{A}_1 \leftarrow {}^4\text{T}_1$ observed in DMS systems. Increasing the number of manganese in the clusters **7** and **8** results in a shift in the emission energies in these clusters to 730 nm (**7c-d**) and 640 nm (**8c-d**). This energy shift from commonly observed yellow-orange to red region of the spectrum could be due to the separation of the ‘ZnMnE’ clusters into separate ‘ZnE’ and ‘MnE’ species. However solid state PL spectra (as nujol mulls between quartz plates) of **7a** are similar to those observed in the solution state (Figure 3.6). The PL data for solid samples of **8d** are also similar to those observed for solution data, with an emission observed at 640 nm. Emission at 640 nm has also been observed in Mn^{2+} doped 12-16 solids,³⁹ as well as in related nanoparticle samples.^{22,40} This phenomenon is usually observed with higher Mn^{2+} content and the close proximity of the paramagnetic centers within the nanoparticle core, resulting in direct Mn-Mn coupling^{22,40} and related Mn-E interactions.⁴¹ O’Brien *et al.* have reported a similar observation with $\text{Mn}_x\text{Cd}_{1-x}\text{S}$ nanoparticles which they reasoned to be due to loss of capping agents.⁴² Recently, due to the lattice strain in MnS-CdS heterostructures, Mn^{2+} ions were found to exhibit a red emission at 650 nm.⁴³

Based on our results and the literature the most plausible explanation for the uncommon red emission observed in our systems could be enhanced Mn-Mn coupling interactions. When the amount of Mn^{2+} is lowest as in **7a**, a single emission is observed at 590 nm. The complete disappearance of emission at 590 nm and the emergence of a

single transition at 720 nm when the amount of Mn^{2+} is increased in the cluster core would arise as a result of Mn-Mn coupling interactions in these clusters. A similar trend is observed for the selenium containing clusters **8a-d** with the only difference being the emission peak maximum at a lower wavelength. The red shift in emission displayed by the clusters **7c-d** (720nm) in comparison with cluster **8c-d** (630nm) is likely due to the change in the tetrahedral ligand field splitting when sulfide ligands are substituted with selenide ligands. Unlike other Mn^{2+} containing ZnE nanoparticles, the nanoclusters **7-8** also have two chloride ligands within the coordination sphere of the manganese centers which may also play a role in the observed PL data.

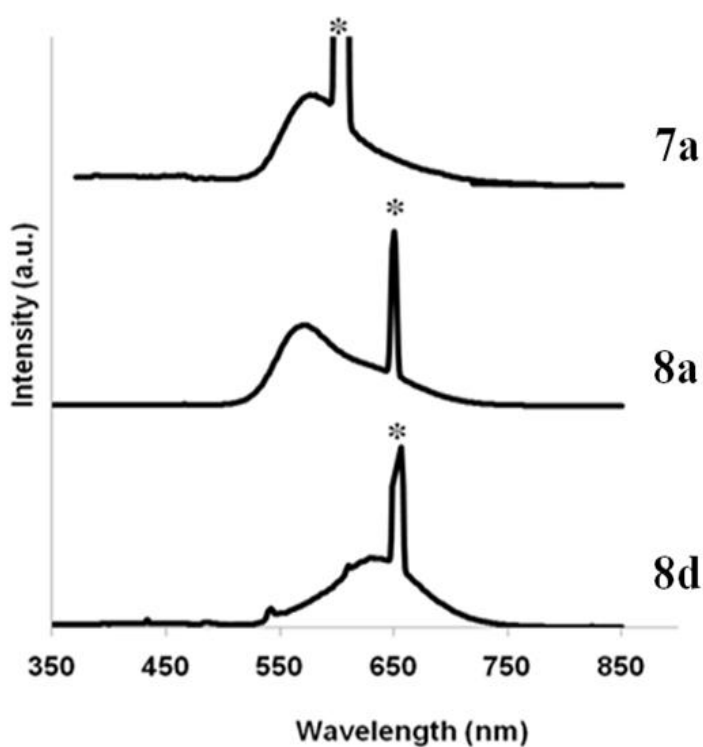
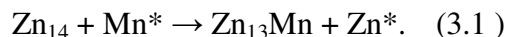


Figure 3.6. Room temperature solid state PL spectra of **7a**, **8a** and **8d**. The peaks labeled *arise from the different mineral oils used for sample preparation.

3.3. Metal type Assignment by Quantum Chemical Calculations

Quantum chemical calculations at DFT level (program system TURBOMOLE⁴⁴, B3-LYP⁴⁵ functional, def-SV(P) bases^{46a} and respective Coulomb fitting bases^{46b}) were carried out to address the following questions. a) Is the facile exchange of Zn²⁺ with Mn²⁺ in $(N,N'$ -tmeda)₆Zn_{14-x}Mn_xE₁₃Cl₂ confirmed by quantum-chemically obtained data of exchange reactions? b) Can we identify preferred sites for Mn²⁺ from calculated energies when neglecting pair interactions like anti-ferromagnetic coupling? c) Do these interactions significantly influence the preferences identified in b)? We restrict considerations to E=S and briefly discuss the case E=Se in the end.

For a), one might calculate exchange reaction energies like



Cl, S and tmeda are omitted here and in the following for simplicity, but not in the calculations. The asterisk means that the respective metal atom may be considered for different situations, e.g. as isolated atom (i), as dichloride (ii), or as dication with correction of solvent effects e.g. by the COSMO model⁴⁷, with the dielectric constant of the solvent as input parameter (iii), e.g. $\epsilon = 9 \approx \epsilon(\text{CH}_2\text{Cl}_2)$ or $\epsilon = 3 \approx \epsilon(\text{tmeda})$. All models might be plausible (MnCl₂ is one of the educts, both CH₂Cl₂ and tmeda are present in the reaction), but unfortunately the reaction energies very much depend on the choice of the model. For (i) one gets 160 kJ/mol, for (ii) 295 kJ/mol, in case of (iii) we find 80 kJ/mol for $\epsilon = 9$ and 35 kJ/mol for $\epsilon = 3$. At least all energies are all negative, indicating that the exchange is possible. This is not unexpected: the bonds situation is ionic in all cases, that is, in all cases electrons are transferred from the 4s orbital of the metal atom to the

(energetically lower) S/Cl valence orbitals. As the energy of the 4s orbital, which in first order is the ionization potential (Koopman's theorem), is higher for Mn^{2+} than for Zn^{2+} (by ca. 1.2 eV at Hartree-Fock level) this is more favorable for Mn than for Zn. Facile exchange of Zn^{2+} with Mn^{2+} also corresponds to low energies for reactions of type



This formulation has the advantage that, in contrast to equation 3.1, M^* does not need to be modeled; on the other hand, the energies of the most stable conformation for each composition are needed, and finding the respective isomers, i.e. b) and c) of the above tasks, has to be done before.

Large clusters with magnetic centers usually are treated within a broken symmetry approach⁴⁸ at DFT level, which also for the present combination of elements (Mn/S) was documented to give reasonable results⁴⁹. For the present problem, a huge number of calculations would be necessary, as for each distribution of atoms and within each distribution for each broken-symmetry spin-state a calculation would have to be done. Even if only the eight positions in question (those labeled only by numbers in Figure 3.3) are considered, this amounts to $3^8 = 6561$ calculations, as each of the eight positions may be occupied by either Zn^{2+} or Mn^{2+} (d^5 -configuration, spin-up) or Mn (d^5 -configuration, spin-down). According to the tasks formulated above, it is reasonable to divide the relative energies of the different distributions in a part that neglects pair-interactions, and a part describing the pair interactions; this dramatically reduces the number of calculations and further allows for estimation of the influence of pair-interactions on the metal distribution. Of course, the quality of this approach has to be

tested by comparison of relative energies obtained this way with those from the broken-symmetry approach for several selected distributions.

We start from Zn_{14} and replace only one Zn atom with Mn, in eight separate single-point calculations (for the X-ray structure parameters) for the eight positions in question, see figure 3.7.

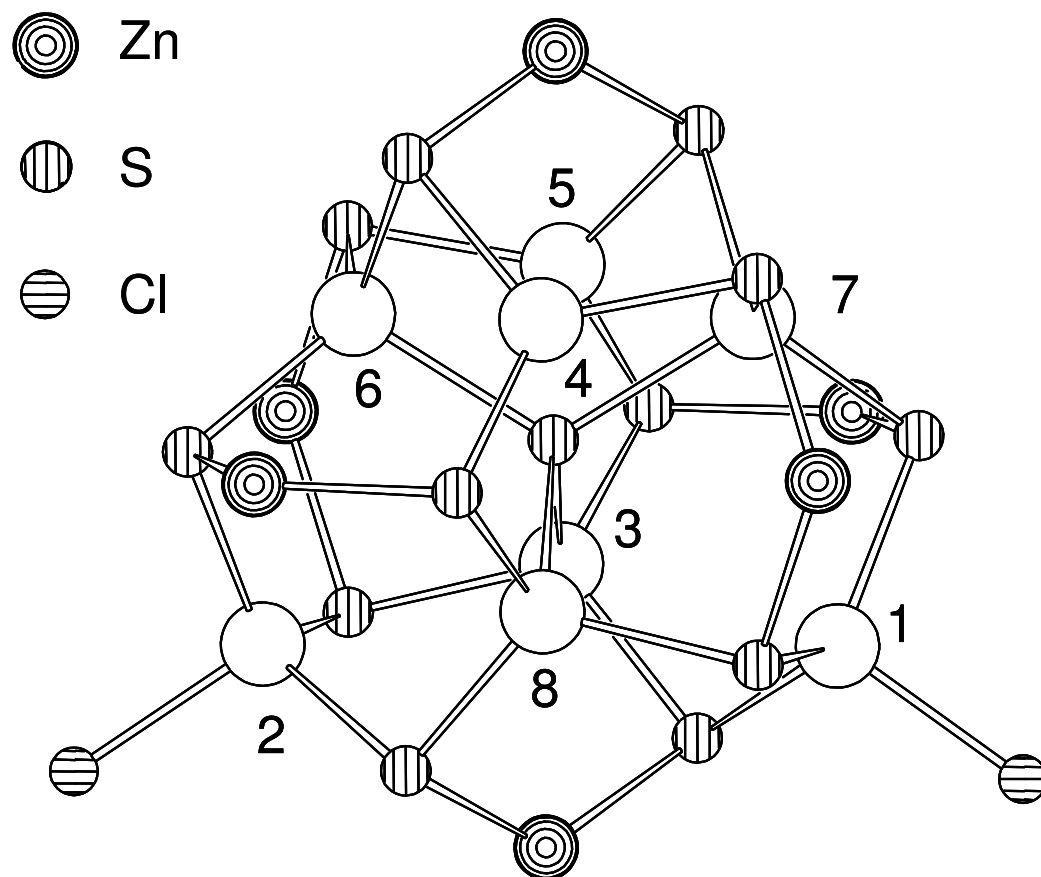


Figure 3.7. $(N,N'\text{-tmeda})_6\text{Zn}_{14-x}\text{Mn}_x\text{S}_{13}\text{Cl}_2$. The eight positions labeled by numbers are occupied by either Mn^{2+} or Zn^{2+} .

In this way one gets the energetic sequence of positions without accounting for pair interactions, i.e. mainly without considering anti-ferromagnetic coupling of different Mn^{2+} atoms. The absolute energies are given in Appendix B.4. The relative energies reveal the following picture: replacement of Zn^{2+} with Mn^{2+} is least favorable for positions 4 and 5, here the metal atom binds to three sulfur atoms (i). For positions 3 and 6 to 8 this replacement is more favorable than for positions 4 or 5 by 12-14 kJ/mol (ii); here the metal atom binds to four sulfur atoms. Replacement is most favorable for positions 1 and 2, 29 and 26 kJ/mol, for which the metal atom binds to three sulfur atoms and one chlorine atom (iii). This trend can be rationalized in the same way as the energy gain for the exchange of Zn^{2+} with Mn^{2+} (*vide supra*): the electron-pulling forces increase from (i) to (ii) as number of electronegative bond partners increases from (i) to (ii), and the electronegativity of one bond partner from (ii) to (iii). This leads to a larger energy gain for Mn than for Zn, as the electron-donating 4s orbital is less stable for Mn than for Zn. So, without regarding pair-interactions one expects positions 1 and 2 occupied by Mn^{2+} first, 3 and 6 to 8 next, and finally 4 and 5. The role of electronegativity of the environment as main reason for preference of specific sites by Mn is confirmed when replacing Cl binding to position 1 with more electronegative F (and reducing the distance by 45 pm, according to the Pauling radii). In this case the replacement of Zn^{2+} with Mn^{2+} at position 1 is more favorable than at position 5 by 41 kJ/mol (instead of 29 kJ/mol in case of Cl).

For the calculation and discussion of pair interactions we introduce the following short-hand notation for the characterization of the isomers. We only denote those of the eight positions that are occupied by Mn; distinguishing between spin-down and spin-up is

done by underlining/not underlining the respective position number. As an example “128” indicates that in the respective isomer positions one and eight are occupied by Mn^{2+} (spin up), position two by Mn^{2+} (spin down) and three to seven by Zn^{2+} . The numbers refer to those in Figure 3.7.

Not all isomers were explicitly calculated, the following screening procedure was applied first, using the structure parameters from the X-ray analysis, i.e. without any structure relaxation: The relative energy of each isomer was approximated by the energy change E_1 when exchanging single Zn atoms by Mn, e.g.

$$E_1(1\underline{2}8) = E_1(1) + E_1(2) + E_1(8)$$

plus the energy gain by the anti-ferromagnetic coupling, E_2 ,

$$E_2(1\underline{2}8) = E_2(12) + E_2(28).$$

$E_1(1)$ to $E_1(8)$ are the energies of the eight different isomers of $\text{Mn}_1\text{Zn}_{13}$ with respect to the least stable one, i.e. the energies discussed in the previous section. $E_2(12)$ to $E_2(78)$ are the energy differences between the high-spin and the broken-symmetry low-spin state of the respective isomer, e.g. $E_2(12) = E(12) - E(\underline{1}2)$ (using the above notation), they are listed in the Table S2. The mean value over all energies E_2 is 4.1 kJ/mol and the maximum value is 11 kJ/mol. This is smaller than e.g. $E_1(1)$ or $E_1(8)$, but not small enough to be negligible. By calculation of $E = E_1 + E_2$ it is possible to estimate the energetic sequence within each given composition. The resulting estimated energies E are listed in Appendix B.4.

For validation of the accuracy of this approximation explicit calculations of the apparently most favorable isomers and (arbitrarily selected) further isomers of the $\text{Mn}_4\text{Zn}_{10}$ species were performed and compared to the estimated data, Figure 3.8.

Accordance obviously is good enough to use the approximation as screening procedure for the selection of the best isomers of each composition and to identify trends for the preference of either Zn^{2+} or Mn^{2+} for each position when including spin-spin coupling.

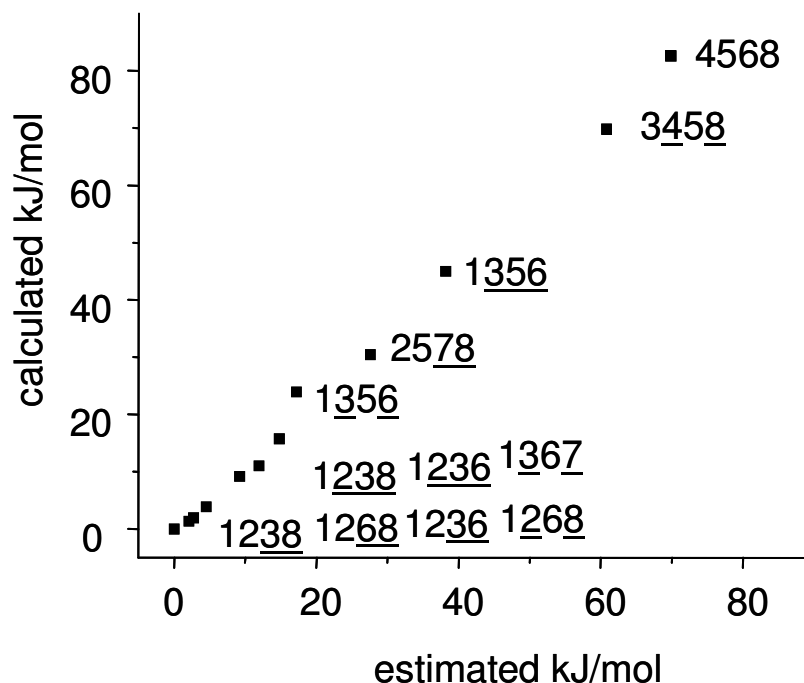


Figure 3.8. Estimated relative energies versus explicitly calculated energies for selected isomers of $\text{Zn}_{10}\text{Mn}_4$. See also text.

We now identify sites preferred by one of the metals by inspection of the energetically low lying configurations. For this purpose the frequency of Mn^{2+} found at each of the eight positions was determined from the data given (Appendix B.4) for the most stable isomers of each composition (those being disfavored by less than 3 kJ/mol towards the respective most stable isomer). The results are given in Table 3.5 and show the following trends: If two Mn atoms are present, they occupy positions 1 and 2. This is in accordance to the assignment based on the crystallographic refinement of **7a** and **8a**. The third Mn

atom most likely is found at position 8, but positions 3, 6 or 7 are also possible with somewhat lower probability. Similar is true for compounds containing four Mn atoms. Only if five or more Mn atoms are present, positions 4 and 5 may be occupied by Mn, otherwise by Zn. These findings are similar to those without accounting for anti-ferromagnetic coupling (position 1 and 2 most favored, 4 and 5 least favored); thus consideration of pair interactions only refines but does not substantially change the picture.

composition	n	frequency of Mn at positions 1-8							
		1	2	3	4	5	6	7	8
Mn ₁ Zn ₁₃	2	50	50	0	0	0	0	0	0
Mn ₂ Zn ₁₂	2	100	100	0	0	0	0	0	0
Mn ₃ Zn ₁₁	8	100	100	12	0	0	25	25	37
Mn ₄ Zn ₁₀	9	100	100	33	0	0	55	44	66
Mn ₅ Zn ₉	23	100	100	52	26	13	73	73	60
Mn ₆ Zn ₈	5	100	100	80	60	40	80	60	80
Mn ₇ Zn ₇	5	100	100	80	80	80	100	80	80

Table 3.5. Frequency (%) of Mn found at positions 1-8 for isomers that are higher in energy than the most stable one of each composition by less than 3 kJ/mol. The compositions are given in the first column, the number of isomers (n) in the second.

We return to question a) and demonstrate that Mn²⁺ and Zn²⁺ are easily exchangeable. This can be seen from energies for reactions according to equation (3.2), calculated on the basis of the (explicitly calculated) total energies of the most stable isomers, Table 3.6. To give an example, for Mn₂Zn₁₂ we considered the 14 reactions leading to $1/3\text{Zn}_{14} + 2/3\text{Mn}_3\text{Zn}_{11}$, ..., $6/7\text{MnZn}_{13} + 1/7\text{Mn}_8\text{Zn}_6$. The relative stability of each composition is then the lowest of all reaction energies for the respective

composition; if this energy is positive, the species is stable with respect to any reaction according to equation 2. For the calculation of the stability of Mn_8Zn_6 the Mn_9Zn_5 species was regarded, which was derived from the most favorable Mn_8Zn_6 isomer by exchanging the Zn atom with Mn at the site closest to position 1. All reaction energies are listed in Appendix 3.4, the lowest for each composition in table 3.6, column 4. All reaction energies are rather small (absolute values typically below 5 kJ/mol), thus Mn^{2+} and Zn^{2+} are easily exchangeable. The comparably high local stability for Mn_8Zn_6 indicates that the presence of more than eight Mn atoms is unfavorable.

Cluster	configuration	E_{tot}	E_{reac}	products
$\text{Mn}_1\text{Zn}_{13}$	1	-32456.9126	1.35	$1/2\text{Zn}_{14}+1/2\text{Mn}_2\text{Zn}_{12}$
$\text{Mn}_2\text{Zn}_{12}$	12	-31828.6580	3.62	$1/2\text{Mn}_1\text{Zn}_{13}+1/2\text{Mn}_3\text{Zn}_{11}$
$\text{Mn}_3\text{Zn}_{11}$	128	-31200.4007	0.83	$1/2\text{Mn}_2\text{Zn}_{12}+1/2\text{Mn}_4\text{Zn}_{10}$
$\text{Mn}_4\text{Zn}_{10}$	1238	-30572.1427	1.16	$4/5\text{Mn}_3\text{Zn}_{11}+1/5\text{Mn}_8\text{Zn}_6$
Mn_5Zn_9	12478	-29943.8821	-5.45	$3/4\text{Mn}_4\text{Zn}_{10}+1/4\text{Mn}_8\text{Zn}_6$
Mn_6Zn_8	124678	-29315.6248	-1.98	$1/2\text{Mn}_4\text{Zn}_{10}+1/2\text{Mn}_8\text{Zn}_6$
Mn_7Zn_7	1234678	-28687.3667	-0.92	$1/4\text{Mn}_4\text{Zn}_{10}+3/4\text{Mn}_8\text{Zn}_6$
Mn_8Zn_6	12345678	-28059.1085	13.8	$1/2\text{Mn}_7\text{Zn}_7+1/2\text{Mn}_9\text{Zn}_5$

Table 3.6. Most favorable isomers for each composition. The configurations of the respective isomers are given in column 2 (for notation see text) and the total energies (E_{tot} , in E_{H}) in column 3 (further: $E_{\text{tot}}(\text{Mn}_0\text{Zn}_{14}) = -33085.1662$, $E_{\text{tot}}(\text{Mn}_9\text{Zn}_5) = -27430.8398 E_{\text{H}}$). Column 4 contains the lowest energies for reactions according to equation 2 (E_{reac} , in kJ/mol) calculated from E_{tot} in column 4, column 5 the corresponding reaction products. A positive energy means that the reaction is endothermic, i.e. that the species is stable with respect to all reactions according to equation 3.2.

For the selenium compounds situation is expected to be very similar, as can be seen from the similarity of the energies for Se and S for the reaction according to

Equation 3.1 (with M^{2+} and $\epsilon=3$), 26 kJ/mol (35 kJ/mol for S, see above) and further from the similarity of e.g. $E_1(1)=23$ kJ/mol (29 kJ/mol for S, see above), and $E_2(56)=10$ kJ/mol (11 kJ/mol for S, see above).

3.4. Conclusions

The chalcogenolate complexes $(N,N'\text{-tmeda})Zn(E\text{SiMe}_3)_2$ ($E = \text{S}, \text{Se}$), have been utilized as molecular precursors for the preparation of the ternary nanoclusters, $(N,N'\text{-tmeda})_6Zn_{14-x}Mn_xE_{13}Cl_2$ where the value of x varies from 1.7 to as high as 7.8. Using a low temperature synthetic method, we have been able to incorporate Mn^{2+} into well defined ZnS and ZnSe cluster frameworks. DFT calculations indicate that the exchange of Zn^{2+} with Mn^{2+} is easily feasible and this is supported by the crystallographic data. The photoluminescence properties of these complexes show marked differences based on the amount of Mn^{2+} incorporated.

3.5. Experimental Section

3.5.1. General Experimental

All experimental procedures were performed using standard double manifold Schlenk line techniques under an atmosphere of dried nitrogen gas or in nitrogen filled glove boxes. The non-chlorinated solvents (Tetrahydrofuran, Pentane) were dried and collected using a MBraun MB-SP Series solvent purification system with tandem activated alumina (Tetrahydrofuran) and activated alumina or activated copper redox catalyst (hydrocarbons).⁵⁰ Dichloromethane (CH_2Cl_2) was dried and distilled over P_2O_5 . *N,N,N',N'*-tetramethylethylenediamine (*N,N'*-tmeda) was dried and distilled over CaH_2 . Spectral grade solvents dimethylsulfoxide (DMSO) and CH_2Cl_2 were purchased from Caledon and dimethylformamide (DMF) from Fisher Chemicals. MnCl_2 and $\text{Zn}(\text{OAc})_2$ were purchased from Aldrich in 98% and 99.99% purity respectively and used as supplied. The silylated reagents $\text{E}(\text{SiMe}_3)_2$ (E = S, Se) were synthesized using literature procedures.^{4b,51} $(\text{N,N}'\text{-tmeda})\text{Zn}(\text{ESiMe}_3)_2$ (E = S, Se) was prepared following a previously published literature procedure.⁵² Room temperature solution photoluminescence and photoluminescence excitation were measured on a Photon Technologies International Inc. Quantum Master equipped with a Xenon lamp. Room temperature UV-visible absorption spectra were recorded on a Varian Cary 300 spectrometer. A Quartz Xone EDX analysis system coupled to a Leo 440 SEM equipped with a Gresham light element detector was used to obtain semi-quantitative analysis of zinc and manganese. Elemental analysis of **7d**, **8d**, **9a**, **9b** performed by Columbia

Analytical Services (Tuscan, AZ, USA) while analysis of **7a**, **8b** performed by Guelph Chemical Laboratories Ltd. (Ontario, Canada) and the analysis of **7b**, **7c**, **8a**, **8c** performed by Laboratoire d'Analyse Élémentaire de l'Université de Montréal (Montréal, Canada). Metal analysis of compound **7** and compound **8** were performed using Inductively Coupled Plasma atomic emission spectroscopy (ICP-AES) by Columbia Analytical Services (Tuscan, AZ, USA).

Single crystal X-ray data were collected on Bruker APEX-II CCD (**7a**, **8a**, **9a**) and Enraf-Nonius Kappa-CCD (**8d**, **9b**) diffractometers equipped with graphite-monochromated MoK α ($\lambda = 0.71073\text{\AA}$) radiation. Highly solvated single crystals of the complexes were carefully selected, immersed in paraffin oil and mounted on a nylon loop. Crystals were placed immediately in a cold stream of N $_2$ to minimize desolvation. The structures were solved using direct methods and refined by the full-matrix least squares procedure of SHELXTL (G. M. Sheldrick, Madison, WI, 1996). All non-hydrogen atoms cluster atoms were refined anisotropically, while hydrogen atoms were kept at their calculated distances and refined using a riding model. Partial site occupancy for Zn and Mn (see text) was evaluated by comparing respective thermal parameters: sites displaying mixed Mn/Zn occupancy. The site disorder was ultimately refined with common positional and thermal parameters for the two metals (EXYZ and EADP commands in SHELX, respectively). The refined Flack parameter for **8d** was -0.009(18).

3.5.2. Syntheses

3.5.2.1. Synthesis of $(N,N'$ -tmeda) $_6$ Zn $_{12.3}$ Mn $_{1.7}$ S $_{13}$ Cl $_2$, **7a**.

MnCl $_2$ (0.022g, 0.174 mmol) was dissolved in 5 mL CH $_2$ Cl $_2$ by adding N,N' -tmeda (0.04 mL, 0.268 mmol) and the pale orange solution was cooled to -75°C. Zn(OAc) $_2$ (0.096g, 0.523 mmol) was dissolved in 5 mL CH $_2$ Cl $_2$ by adding N,N' -tmeda (0.12 mL, 0.805 mmol) and the clear solution was cooled to -75°C. These two solutions were then added to previously prepared colorless solution of $(N,N'$ -tmeda)Zn(SSiMe $_3$) $_2$ (0.274g, 0.699 mmol) in 10 mL of CH $_2$ Cl $_2$ at -75°C. The very pale yellow solution was left stirring overnight letting the temperature to increase slowly to room temperature. Almost colorless crystals were obtained by the reduction of solvent volume by half and slow diffusion of pentane at room temperature after a few days. Yield: 0.093g (43.6%). Anal. Calcd for C $_{36}$ H $_{96}$ Cl $_2$ N $_{12}$ S $_{13}$ Zn $_{12.3}$ Mn $_{1.7}$: C, 20.80%; H, 4.65%. Found: C, 20.99%; H, 4.85%.

3.5.2.2. Synthesis of $(N,N'$ -tmeda) $_6$ Zn $_{10.9}$ Mn $_{3.1}$ S $_{13}$ Cl $_2$, **7b**.

MnCl $_2$ (0.068g, 0.540 mmol) was dissolved in 5 mL CH $_2$ Cl $_2$ by adding N,N' -tmeda (0.12 mL, 0.805 mmol) and the pale orange solution was cooled to -75°C. Zn(OAc) $_2$ (0.098g, 0.534 mmol) was dissolved in 5 mL CH $_2$ Cl $_2$ by adding N,N' -tmeda (0.12 mL, 0.805 mmol) and the clear solution was cooled to -75°C. These two solutions were then added to previously prepared colorless solution of $(N,N'$ -tmeda)Zn(SSiMe $_3$) $_2$ (0.420g, 1.07 mmol) in 10 mL of CH $_2$ Cl $_2$ at -75°C. Analogous experimental procedure as 1a, afforded

pale orange crystals. Yield: 0.140g (38.8%). Anal. Calcd for $C_{36}H_{96}Cl_2N_{12}S_{13}Zn_{10.9}Mn_{3.1}$: C, 20.90%; H, 4.68%. Found: C, 20.97%; H, 4.84%.

3.5.2.3. Synthesis of $(N,N'$ -tmeda) $_6Zn_{10}Mn_4S_{13}Cl_2$, **7c**.

$MnCl_2$ (0.056g, 0.445 mmol,) was dissolved in 5 mL CH_2Cl_2 by adding N,N' -tmeda (0.1mL, 0.671 mmol) and the pale orange solution was cooled to $-75^\circ C$. $Zn(OAc)_2$ (0.035g, 0.191mmol) was dissolved in 5 mL CH_2Cl_2 by adding N,N' -tmeda (0.04 mL, 0.268 mmol) and the clear solution was cooled to $-75^\circ C$. These two solutions were then added to previously prepared colorless solution of $(N,N'$ -tmeda) $Zn(SSiMe_3)_2$ (0.250g, 0.638 mmol) in 10 mL of CH_2Cl_2 at $-75^\circ C$. Analogous experimental procedure as **1a**, afforded orange crystals. Yield: 0.0090g (39.2%). Anal. Calcd for $C_{36}H_{96}Cl_2N_{12}S_{13}Zn_{10.0}Mn_{4.0}$: C, 21.00%; H, 4.70%. Found: C, 21.67%; H, 5.10%.

3.5.2.4. Synthesis of $(N,N'$ -tmeda) $_6Zn_{6.2}Mn_{7.8}S_{13}Cl_2$, **7d**.

The synthesis was carried out in a similar manner as **1a**, with $MnCl_2$ (0.120g, 0.953 mmol), N,N' -tmeda (0.22 mL, 1.50 mmol) and $(N,N'$ -tmeda) $Zn(SSiMe_3)_2$ (0.360g, 0.918 mmol). Orange crystals were obtained by the reduction of solvent volume by half and slow diffusion of pentane at room temperature after a few days. Yield: 0.125g (50.1%). Anal. Calcd for $C_{36}H_{96}Cl_2N_{12}S_{13}Zn_{6.2}Mn_{7.8}$: C, 21.44%; H, 4.80%. Found: C, 21.67%; H, 5.10%.

3.5.2.5. Synthesis of $(N,N'$ -tmeda) $_6$ Zn $_{12}$ Mn $_2$ Se $_{13}$ Cl $_2$, **8a.**

MnCl $_2$ (0.026g, 0.206 mmol) was dissolved in 5 mL CH $_2$ Cl $_2$ by adding N,N' -tmeda (0.05 mL, 0.336 mmol) and the pale orange solution was cooled to -75°C . Zn(OAc) $_2$ (0.113g, 0.616mmol) was dissolved in 5 mL CH $_2$ Cl $_2$ by adding N,N' -tmeda (0.14 mL, 0.939 mmol) and the clear solution was cooled to -75°C . These two solutions were then added to previously prepared solution of $(N,N'$ -tmeda)Zn(SeSiMe $_3$) $_2$ (0.400g, 0.823 mmol) in 10 mL of CH $_2$ Cl $_2$ at -75°C . The pale orange solution was left stirring overnight letting the temperature to increase slowly to room temperature. Almost colorless crystals were obtained by the reduction of solvent volume and slow diffusion of pentane at room temperature after a few days. Yield: 0.120g (42.3%). Anal. Calcd for C $_{36}$ H $_9$ Cl $_2$ N $_{12}$ Se $_{13}$ Zn $_{12}$ Mn $_2$: C, 16.08%; H, 3.60%. Found: C, 15.17%; H, 3.55%.

3.5.2.6. Synthesis of $(N,N'$ -tmeda) $_6$ Zn $_{10.8}$ Mn $_{3.2}$ Se $_{13}$ Cl $_2$, **8b.**

The synthesis was carried out in a similar manner as **7a** MnCl $_2$ (0.047g, 0.373 mmol) was dissolved in 5 mL CH $_2$ Cl $_2$ by adding N,N' -tmeda (0.08 mL, 0.537 mmol) and the orange solution was cooled to -75°C . Zn(OAc) $_2$ (0.068g, 0.371mmol) was dissolved in 5 mL CH $_2$ Cl $_2$ by adding N,N' -tmeda (0.08 mL, 0.536 mmol) and the clear solution was cooled to -75°C . These solutions were then added to previously prepared solution of $(N,N'$ -tmeda)Zn(SeSiMe $_3$) $_2$ (0.360g, 0.740 mmol) in 10 mL of CH $_2$ Cl $_2$ at -75°C . Analogous experimental procedure as **8a**, afforded pale orange crystals Yield: 0.137g (43.8%). Anal. Calcd for C $_{36}$ H $_9$ Cl $_2$ N $_{12}$ Se $_{13}$ Zn $_{10.8}$ Mn $_{3.2}$: C, 16.14%; H, 3.61%. Found: C, 15.61%; H, 3.63%.

3.5.2.7. Synthesis of $(N,N'\text{-tmeda})_6\text{Zn}_{10.7}\text{Mn}_{3.3}\text{Se}_{13}\text{Cl}_2$, **8c**.

MnCl_2 (0.092g, 0.731 mmol) was dissolved in 10 mL CH_2Cl_2 by adding N,N' -tmeda (0.16 mL, 1.07 mmol) and the orange solution was cooled to -75°C . $\text{Zn}(\text{OAc})_2$ (0.058g, 0.316mmol) was dissolved in 5 mL CH_2Cl_2 by adding N,N' -tmeda (0.07 mL, 0.470 mmol) and the clear solution was cooled to -75°C . These solutions were then added to previously prepared solution of $(N,N'\text{-tmeda})\text{Zn}(\text{SeSiMe}_3)_2$ (0.506g, 1.04 mmol) in 10 mL of CH_2Cl_2 at -75°C . Analogous experimental procedure as **8a**, afforded orange crystals. Yield: 0.198g (33.3%). Anal. Calcd for $\text{C}_{36}\text{H}_{96}\text{Cl}_2\text{N}_{12}\text{Se}_{13}\text{Zn}_{10.7}\text{Mn}_{3.3}$: C, 16.14%; H, 3.61%. Found: C, 16.88%; H, 4.12%.

3.5.2.8. Synthesis of $(N,N'\text{-tmeda})_6\text{Zn}_{8.2}\text{Mn}_{5.8}\text{Se}_{13}\text{Cl}_2$, **8d**.

MnCl_2 (0.115g, 0.913 mmol) was dissolved in 10 mL CH_2Cl_2 by adding N,N' -tmeda (0.20 mL, 1.50 mmol) and the orange solution was cooled to -75°C . This solution was then added to previously prepared solution of $(N,N'\text{-tmeda})\text{Zn}(\text{SeSiMe}_3)_2$ (0.435g, 0.895 mmol) in 10 mL of CH_2Cl_2 at -75°C . Analogous experimental procedure as **2a**, afforded orange crystals. Yield: 0.180g (58.0%). Anal. Calcd for $\text{C}_{36}\text{H}_{96}\text{Cl}_2\text{N}_{12}\text{Se}_{13}\text{Zn}_{8.2}\text{Mn}_{5.8}$: C, 16.33%; H, 3.66%. Found: C, 15.61%; H, 3.63%.

3.5.2.9. Synthesis of $(N,N'\text{-tmeda})_6\text{Zn}_{14}\text{S}_{13}\text{Cl}_2$, **9a**.

$\text{Zn}(\text{OAc})_2$ (0.105g, 0.57 mmol) was dissolved in 10 mL CH_2Cl_2 by adding N,N' -tmeda (0.13 mL, 1.50 mmol) and the colorless solution was cooled to -75°C . This solution was then added to previously prepared solution of $(N,N'\text{-tmeda})\text{Zn}(\text{SSiMe}_3)_2$ (0.215g, 0.55 mmol) in 10 mL of CH_2Cl_2 at -75°C . The colorless solution was left stirring overnight

letting the temperature to increase slowly to room temperature. Colorless block crystals were obtained by the reduction of solvent volume by half and slow diffusion of pentane at room temperature after a few days. Yield: 0.080g (45%). Anal. Calcd for $C_{36}H_{96}Cl_2N_{12}S_{13}Zn_{14}$: C, 20.59%; H, 4.61%. Found: C, 19.47%; H, 4.84%.

3.5.2.10. Synthesis of $(N,N'$ -tmeda) $_6Zn_{14}Se_{13}Cl_2$, **9b**.

$Zn(OAc)_2$ (0.140g, 0.76 mmol) was dissolved in 10 mL CH_2Cl_2 by adding N,N' -tmeda (0.17 mL, 1.50 mmol) and the colorless solution was cooled to $-75^\circ C$. This solution was then added to previously prepared pale yellow solution of $(N,N'$ -tmeda) $Zn(SeSiMe_3)_2$ (0.369g, 0.76 mmol) in 10 mL of CH_2Cl_2 at $-75^\circ C$. Analogous experimental procedure as **3a**, afforded colorless block crystals. Yield: 0.125g (40%). Anal. Calcd for $C_{36}H_{96}Cl_2N_{12}Se_{13}Zn_{14}$: C, 15.95%; H, 3.57%. Found: C, 16.80%; H, 3.29%.

3.6. References

1. a) Tran, D. T. T.; Taylor, N. J.; Corrigan, J. F. *Agnew. Chem. Int. Ed. Engl.* **2000**, *39*, 935-937 b) Tran, D. T. T.; Beltran, L. M.; Kowalchuk, C. M.; Trefiak, N. R.; Taylor, N. J.; Corrigan, J. F. *Inorg. Chem.* **2002**, *41*, 5693-5698.
2. DeGroot, M. W.; Taylor, N. J.; Corrigan, J. F. *J. Mater. Chem.* **2004**, *14*, 654-660.
3. DeGroot, M. W.; Taylor, N. J.; Corrigan, J. F. *Inorg. Chem.* **2005**, *44*, 5447-5458.
4. a) DeGroot, M. W.; Corrigan, J. F. *Angew. Chem. Int. Ed.* **2004**, *43*, 5355-5357. b) DeGroot, M. W.; Taylor, N. J.; Corrigan, J. F. *J. Am. Chem. Soc.* **2003**, *125*, 864-865. c) DeGroot, M. W.; Atkins, K. M.; Borecki, A.; Rösner, H.; Corrigan, J. F. *J. Mater. Chem.* **2008**, *18*, 1123-1130.
5. a) Komuro, T.; Matsuo, T.; Kawaguchi, H.; Tatsumi, K. *J. Chem. Soc., Dalton Trans.* **2004**, *10*, 1618-1625. b) Komuro, T.; Matsuo, T.; Kawaguchi, H.; Tatsumi, K. *J. Chem. Commun.* **2002**, *9*, 988-989. c) Komuro, T.; Matsuo, T.; Kawaguchi, H.; Tatsumi, K. *Angew. Chem. Int. Ed.* **2003**, *42*, 465-468.
6. a) Sommer, H.; Eichhöfer, A.; Drebov, N.; Ahlrichs, R.; Fenske, D. *Eur. J. Inorg. Chem.* **2008**, *32*, 5138-5145. b) Bechlars, B.; Issac, I.; Feuerhake, R.; Clerac, R.; Fuhr, O.; Fenske, D. *Eur. J. Inorg. Chem.*, **2008**, *10*, 1632-1644. c) Feuerhake, R.; Fenske, D. *Z. Anorg. Allg. Chem.* **2003**, *629*, 2317-2324. d) Eichhöfer, A.; Fenske, D. *J. Chem. Soc., Dalton Trans.* **2000**, 941-944.
7. DeGroot, M. W.; Corrigan, J. F. *Z. Anorg. Allg. Chem.* **2006**, *632*, 19-29.

8. Borecki, A.; Corrigan, J. F. *Inorg. Chem.* **2007**, *46*, 2478-2484.
9. Furdyna, J. K.; Kossut, J.; Eds *Dilute Magnetic Semiconductors*; Academic Press: New York, **1988**, V25.
10. Alivisatos, A. P.; *Science* **1996**, *271*, 933-937.
11. Michalet, X.; Pinaud, F. F.; Bentolila, L. A.; Tsay, J. M.; Doose, S., Li, J. J.; Sundaresan, G.; Wu, A. M.; Gambhir, S. S.; Weiss, S.; *Nature* **2007**, *447*, 441-446.
12. Gur, I.; Fromer, N. A.; Geier, M.L.; Alivisatos, A. P. *Science* **2005**, *310*, 462-465.
13. Bhargava, R. N.; Gallagher, D.; Hong, X.; Nurmikko, A. *Phys. Rev. Lett.* **1994**, *72*, 416-419.
14. Norris, D. J.; Yao, N.; Charnock, F. T.; Kennedy, T. A. *Nano Lett.* **2001**, *1*, 3-7.
15. Stowell, C. A.; Wiacek, R. J.; Sauders, A. E.; Korgel, B. A. *Nano Lett.* **2003**, *3*, 1441-1447.
16. Santra, S.; Yang, H.; Holloway, P. H.; Stanley, J. T.; Mericle, R. A. *J. Am. Chem. Soc.* **2005**, *127*, 1656-1657.
17. Norberg, N. S.; Parks, G. L.; Salley, G. M.; Gamelin, D. R. *J. Am. Chem. Soc.* **2006**, *128*, 13195-13203.
18. Sapra, S.; Prakash, A.; Ghangrekar, A.; Periasamy, N.; Sarma, D. D. *J. Phys. Chem. B.* **2005**, *109*, 1663-1668.

19. Pradhan, N.; Goorskey, D.; Thessing, J.; Peng, X. *J. Am. Chem. Soc.* **2005**, *127*, 17586-17587.
20. Erwin, S. C.; Zu, L.; Haftel, M. I.; Efros, A. L.; Kennedy, T. A.; Norris, D. J. *Nature* **2005**, *436*, 91-94.
21. Yang, Y.; Chen, O.; Angerhofer, A.; Cao, C. J. *J. Am. Chem. Soc.* **2006**, *128*, 12428-12429.
22. Pradhan, N.; Peng, X. *J. Am. Chem. Soc.* **2007**, *129*, 3339-3347.
23. Nag, A.; Sapra, S.; Nagamani, C.; Sharma, A.; Pradhan, N.; Bhat, S. V.; Sarma, D. *D. Chem. Mater.* **2007**, *19*, 3252-3259.
24. Norris, D. J.; Efros, A. L.; Erwin, S. C. *Science* **2008**, *319*, 1776-1779.
25. Beaulac, R.; Archer, P. I.; Ochsenbein, S. T.; Gamelin, D. R. *Adv. Funct. Mater.* **2008**, *18*, 3873-3891.
26. Klimov, V. I.; Mikhailovsky, A. A.; Xu, S.; Malko, A.; Hollingsworth, J. A.; Leatherdale, C. A.; Eisler, H.; Bawendi, M. G. *Science* **2000**, *290*, 314-317.
27. Colvin, V. L.; Schlamp, M. C.; Allvisatos, A. P. *Nature* **1994**, *370*, 354-357.
28. Spin Electronics (ed. D.D. Awschalom), Kluwer Academic Publishing, Boston, **2004**.
29. Nag, A.; Chakraborty, S.; Sarma, D. D. *J. Am. Chem. Soc.* **2008**, *130*, 10605-10611.

30. Graf, C.; Hofmann, A.; Ackermann, T.; Boeglin, C.; Viswanatha, R.; Peng, X.; Rodrigues, A. F.; Nolting, F.; Rühl, E. *Adv. Funct. Mater.* **2009**, *19*, 2501-2510.
31. Eichhöfer, A.; Hampe, O.; Lebedkins, S.; Weigend, F. *Inorg. Chem.* **2010**, *49*, 7331-7339.
32. Pfistner, H.; Fenske, D. *Z. Anorg. Allg. Chem.* **2001**, *627*, 575-582.
33. CRC Handbook of Chemistry & Physics (18th Ed.) , CRC Press: Boca Raton, FL., **1983**
34. Stephan, H. O.; Henkel, G. *Polyhedron* **1996**, *15*, 501-511.
35. Eichhöfer, A.; Wood, P. T.; Viswanath, R. N.; Mole, R. A. *Chem. Commun.* **2008**, *13*, 1596-1598.
36. Ali, B.; Dance, I. G.; Craig, D. C.; Scudder, M. L. *J. Chem. Soc., Dalton. Trans.*, **1998**, 1661-1667.
37. Nyman, M. D.; Hampden-Smith, M. J.; Duesler, E. N. *Inorg. Chem.* **1996**, *35*, 802-803.
38. Eichhöfer, A.; Fenske, D.; Pfistner, H.; Wunder, M. *Z. Anorg. Allg. Chem.* **1998**, *624*, 1909-1914.
39. Chen, W.; Sammynaiken, R.; Huang, Y.; Malm, J. O.; Wallenberg, R.; Bovin, J. O.; Zwiller, V.; Kotov, N.A. *J. Appl. Phys.* **2001**, *89*, 1120-1129.
40. Suyver, J. F.; Wusiter, S. F.; Kelly, J. J.; Meijerink, A. *Phys. Chem. Chem. Phys.* **2000**, *2*, 5445-5448.

41. Karar, N.; Singh, F.; Mehta, B. R. *J. Appl. Phys.* **2004**, *95*, 656-660.
42. Malik, M. A.; Revaprasadu, N.; O'Brien, P. *J. Mater. Chem.* **2001**, *11*, 2382-2386.
43. Zuo, T.; Sun, Z.; Zhao, Y.; Jiang, X.; Gao, X. *J. Am. Chem. Soc.* **2010**, *132*, 6618-6619.
44. TURBOMOLE V6.1, TURBOMOLE GmbH Karlsruhe, 2010, <http://www.turbomole.de>. TURBOMOLE is a development of University of Karlsruhe and Forschungszentrum Karlsruhe 1989-2007, TURBOMOLE GmbH since 2007.
45. Lee, C.; Yang, W.; Parr, R. G. *Phys. Rev. B* **37**, **1988**, 785-789.
46. a) Weigend, F.; Ahlrichs, R. *Phys. Chem. Chem. Phys.* **2005**, *7*, 3297-3305, b) Weigend, F. *Phys. Chem. Chem. Phys.* **2006**, *8*, 1057.
47. Klamt, A.; Schüürmann, G; *J. Chem. Soc. Perkin Trans.* **1993**, *2*, 799-805.
48. Ruiz, E.; Cano, J.; Alvarez, S.; Alemany, P. *J. Comput. Chem.* **1999**, *20*, 1301-1400.
49. von Hänisch, C.; Weigend, F.; Clérac, R. *Inorg. Chem.* **2008**, *47*, 1460-1464.
50. Pangborn, A. B.; Giardello, M. A; Grubbs, R. H.; Rosen, R. K.; Timmers, F. J. *Organometallics*, **1996**, *15*, 1518-1520.
51. So, J; Boudjouk, P; *Synthesis* **1989**, 306-307.
52. DeGroot, M. W.; Corrigan, J. F. *Organometallics* **2005**, *24*, 3378-3385.

CHAPTER FOUR

Manganese Chalcogenolate Complexes as Molecular Precursors to Mn²⁺ containing Ag₂S Nanoclusters

4.1. Introduction

The synthesis and structural characterization of metal rich clusters of high nuclearity are of increasing interest because of the structural diversity and potential applications of these materials.^{1,2} Metal chalcogenide and chalcogenolate clusters represent one of this class of large metal clusters. These polynuclear metal-chalcogenolates and chalcogenides possess rich photophysical properties and unique structures due to the various coordination modes displayed by the highly polarizable chalcogen centres.² Molecular Ag₂S nanoclusters are of particular interest because their well-defined structures facilitate the study of the structural and physical properties without size polydispersity effects usually encountered in nanoparticles. A number of high nuclearity silver sulfide clusters has been synthesized by Fenske and coworkers by combining silver and sulfur sources in the presence of a variety of phosphine ligands.³⁻⁷ Some examples include [Ag₁₂₃S₃₅(S^tBu)₅₀],³ [Ag₁₈₈S₉₄(PⁿBu₃)₃₀],³ [Ag₁₈₈S₉₄(PⁿPr₃)₃₀],³ [Ag₃₂₀S₁₃₀(S^tBu)₆₀(dppp)₁₂] (dppp = 1,3-Bis(diphenylphosphino)propane),³ [Ag₃₅₂S₁₂₈(S^tC₅H₁₁)₉₆] and [Ag₄₉₀S₁₈₈(S^tC₅H₁₁)₁₁₄].⁶ Silver sulfide (Ag₂S) is a direct band gap semiconductor with a bulk band gap of 1.1 eV with a relatively large absorption coefficient, making it an ideal candidate for use in photovoltaic cells, infrared optical devices and bio-imaging devices.⁷ Even though Ag₂S nanoclusters are expected to have similar interesting optical properties due to quantum confinement effects, there are few

reports on the study of their photoluminescence properties. Recently the first report on room temperature emission from a structurally well defined Ag₂S nanocluster, [Ag₆₂S₁₃(S^tBu)₃₂][(BF₄)₄], was reported.⁸ We are interested in exploring the incorporation of Mn²⁺ into such Ag₂S nanoclusters. Mn²⁺ is by far the most commonly used dopant which acts both as luminescent center and localized spins in semiconductor nanocrystals. Mn(II) doped semiconductors have comparable emission efficiencies as their undoped counterpart and can also have better thermal, chemical and photochemical stability.⁹ The search for compounds combining the properties of semiconductivity and magnetism has evolved into an important field of materials science over the past few decades. In particular, paramagnetic ion (e.g. Mn²⁺) doped II-VI semiconductors (eg. ZnS) with dimensions of a few nanometers, often referred to as dilute magnetic semiconductors (DMS)¹⁰, have attracted significant interest due to potential applications as well as fundamental research.⁹⁻²⁶ To date, there are no studies reported on the incorporation of any magnetic ions into the semiconducting matrix of Ag₂S, despite growing interest in DMS.

We are interested in synthesizing such ternary nanoclusters using a molecular precursor approach. To this end, we have been able to synthesize and characterize trimethylsilylchalcogenolate complexes containing the paramagnetic ion Mn²⁺, [Li(*N,N'*-tmeda)]₂[(*N,N'*-tmeda)Mn₅(SSiMe₃)₆(S)₃] **3a** and [Li(*N,N'*-tmeda)]₂[Mn(SSiMe₃)₄] **4**.²⁷ The molecular structures of these complexes show the presence of potentially reactive -ESiMe₃ moieties and could be utilized as precursor to deliver Mn²⁺ into metal-sulfide nanoclusters. The preformed metal-chalcogen bond and high solubility of these complexes in common organic solvents, coupled with the reactivity of the -ESiMe₃

towards ligand stabilized metal salts, may make these complexes useful as precursors for the formation of Mn-E-M' bonding interactions and serve as an entry into ternary MnM'E nanoclusters.²⁸⁻³⁵

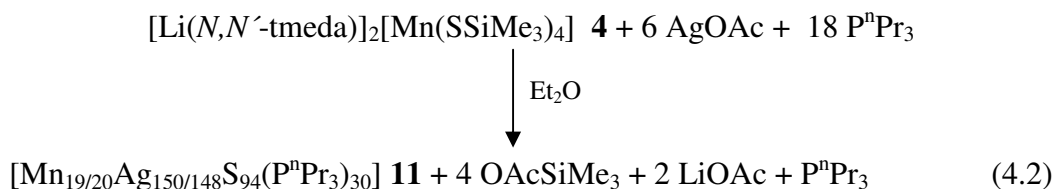
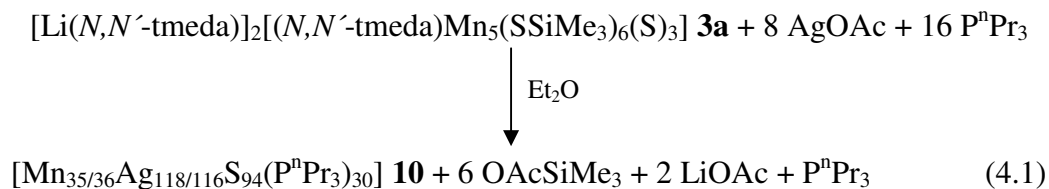
Herein, we report the synthesis, structural characterization and optical properties of two AgS nanoclusters containing Mn²⁺, Mn_{35/36}Ag_{118/116}S₉₄(PⁿPr₃)₃₀ **10** and Mn_{19/20}Ag_{148/150}S₉₄(PⁿPr₃)₃₀ **11** synthesized using [Li(N,N'-tmeda)]₂[(N,N'-tmeda)Mn₅(SSiMe₃)₆(S)₃] **3a** and [Li(N,N'-tmeda)]₂[Mn(SSiMe₃)₄] **4**, as molecular precursors.

4.2. Results and Discussion

4.2.1. Synthesis and Characterization

The approach used to isolate Mn²⁺ containing I-VI clusters involved the use of pentanuclear **3a** as well as the mononuclear manganese chalcogenolate complex **4** as reagents. The synthesis of both clusters was carried out in a similar manner. When a freshly prepared solution of AgOAc solubilized with PⁿPr₃ ligands is reacted with a pink solution of **3a** or colorless solution of **4** at -75°C in ether, an instant color change to yellow is observed. The color of the reaction solution changes to dark brown when the reaction temperature is slowly allowed to increase to -30°C. Dark brown colored, block like crystals suitable for single crystal X-ray crystallography were obtained after storing at -25°C for 24 hours. The pendant -ESiMe₃ moieties present in both manganese precursors drives the reaction forward by forming a thermodynamically favorable

product, AcOSiMe_3 . The propensity of the sulfide to adopt bridging modes favors the formation of high nuclearity complexes which are protected by a shell of phosphine ligands, preventing any further reaction to more stable extended solids. The balanced equations for the formation of the **10** and **11** are given in equations 4.1 and 4.2, respectively.



The molecular structure of cluster **10** was investigated by single crystal X-ray analysis. A complete crystallographic data set was not collected for **11** due to the structural similarity with **10**, confirmed by comparing the cell constants. Both clusters crystallize in the space group $\text{P } \bar{1}$ with one molecule in the unit cell. The cluster **10** is isostructural with the related binary $[\text{Ag}_{188}\text{S}_{94}(\text{P}^n\text{Pr}_3)_{30}]$ **12**, previously synthesized by Fenske and co-workers.³ Cluster **10** has an almost spherical structure (Figure 4.3) with 30 P^nPr_3 acting as capping ligands. The diameter of the cluster core is ~ 2.0 nm, with an overall diameter of ~ 3.0 nm when the surface tripropyl phosphine ligands are taken into consideration. Dynamic light scattering (DLS) measurements suggest the retention of the

size of these clusters in solution (Figure 4.1). The sizes of **10** and **11** are expectedly similar to those reported for the binary analogue.³

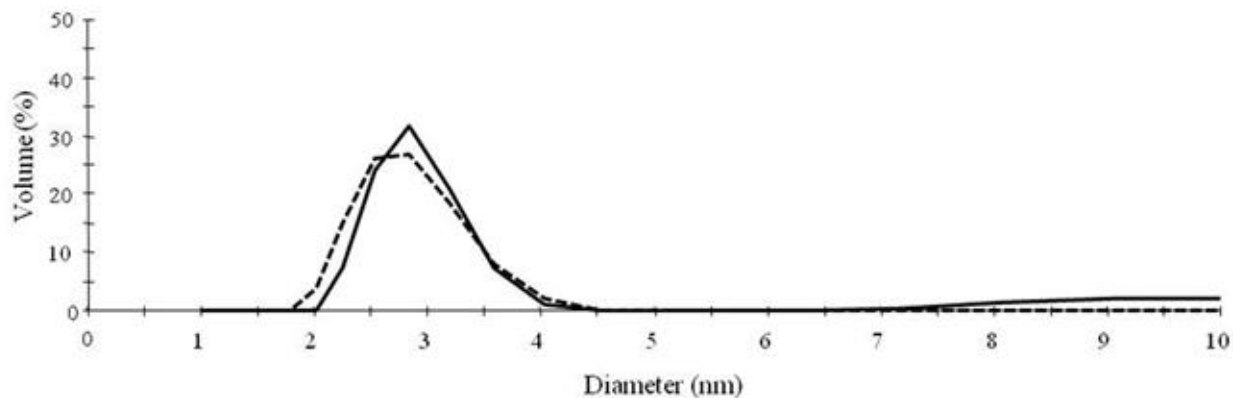


Figure 4.1. Dynamic light scattering (DLS) measurements of **10** (---) and **11** (—) in DCM.

One of the features of large silver sulfide nanoclusters is the difficulty in determining some aspects of their structure from single crystal X-ray analysis due to metal site disorder in the cluster core.³ It has been reported that with nuclearity of up to 100 silver atoms, crystals usually diffract well up to high 2θ values ($50\text{-}60^\circ$ with MoK_α) with no significant disorder as shown by electron density in the difference Fourier maps observed within the clusters.⁷ However, when the nuclearity is greater than 120 silver atoms, the intensities of the reflections decreases sharply above $2\theta\text{-}40^\circ$, with high residual electron density within the clusters. Thus, the structural refinement results in anomalously high agreement factors (R).⁷ The degree of disorder varies within the cluster with the core being highly disordered while the atomic positions on the surface periphery are not typically affected. The observed disorder within the cluster core has been previously reported for similar larger silver chalcogenide clusters, namely $[\text{Ag}_{123}\text{S}_{35}(\text{S}^t\text{Bu})_{50}]$,⁴ $[\text{Ag}_{188}\text{S}_{94}(\text{P}^n\text{Bu}_3)_{30}]$,³ $[\text{Ag}_{188}\text{S}_{94}(\text{P}^n\text{Pr}_3)_{30}]$,³

$[\text{Ag}_{320}\text{S}_{130}(\text{S}^t\text{Bu})_{60}(\text{dppp})_{12}]$,⁶ $[\text{Ag}_{352}\text{S}_{128}(\text{S}^t\text{C}_5\text{H}_{11})_{96}]$ ⁶ and $[\text{Ag}_{490}\text{S}_{188}(\text{S}^t\text{C}_5\text{H}_{11})_{114}]$.⁶ A brief overview of the structure and disorder in cluster **12** is provided due to its structural similarity with the ternary nanoclusters **10** and **11**. The distribution and arrangement of sulfur atoms in **12**, where its spherical structure is evident, is depicted in Figure 4.2. The sulfur centres are distributed over three shells consisting of a central S_{10} polyhedron (orange) which is surrounded by a S_{34} polyhedron (dark yellow) forming the middle shell and a S_{50} polyhedron (bright yellow) forms the outer shell. Along with 50 sulfur centres, the outer shell of **12** consists of 114 silver and 30 phosphorus atoms. The middle shell is completed with 50 silver atoms and the remaining 24 Ag atoms occupy the cluster core. The Ag atoms within the S_{10} polyhedron and on its periphery were found to be highly disordered with relatively high electron density still remaining within the core and between the two inner sulfur polyhedra.³ The disordered silver atoms present within the cluster core were refined with partial occupancy (25%) to obtain a satisfactory result. Those silver atoms present on the middle and the outer shells showed no site disorder and were refined with full occupancy.

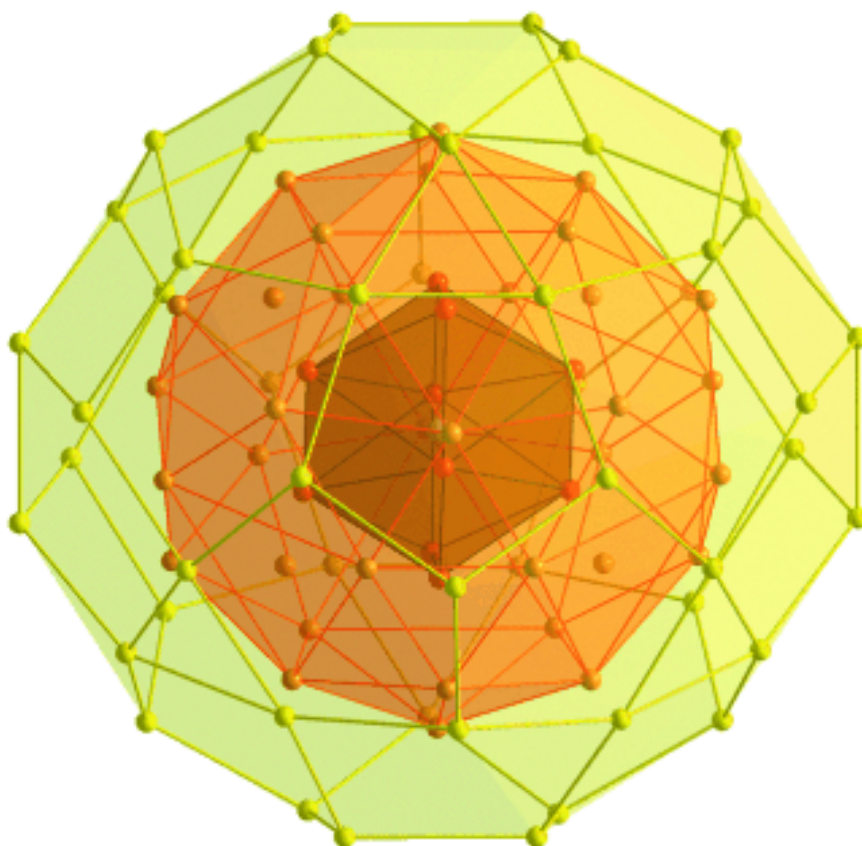


Figure 4.2. Depiction of the polyhedra defined by the sulfide ligands in **12**. S_{10} polyhedron (orange), S_{34} polyhedron (dark yellow) and S_{50} polyhedron (bright yellow).³ Reproduced with permission from WILEY-VCH Verlag GmbH & Co.

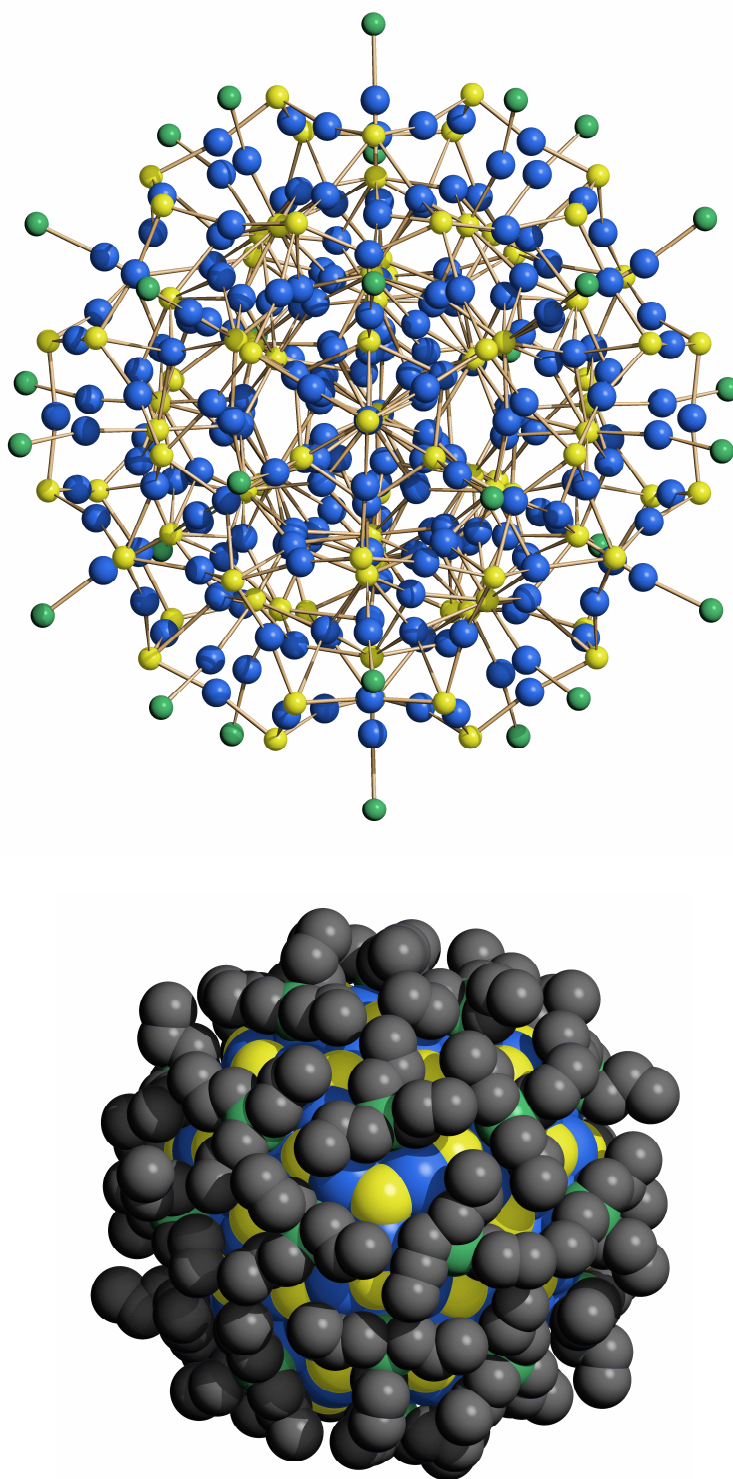


Figure 4.3. Molecular structure of (top) and space filling model (bottom) of **10**. C (gray), P (green), S (yellow) and Ag (Blue). ¹³⁹Pr groups omitted for clarity (top).

Compound	10	
Empirical formula	$\text{Ag}_{188}\text{S}_{94}\text{P}_{30}\text{C}_{277}\text{H}_{640}\text{O}_2$	
Formula weight	14113.10	
Temperature	150(2) K	
Wavelength	0.71073 Å	
Crystal system	Triclinic	
Space group	$P \bar{1}$	
	$a = 27.6264(9) \text{ \AA}$	$\alpha = 61.005(2)^\circ$
	$b = 27.6940(9) \text{ \AA}$	$\beta = 61.9942(12)^\circ$
	$c = 28.3689(14) \text{ \AA}$	$\gamma = 60.873(2)^\circ$
Volume	$15789(5) \text{ \AA}^3$	
Z	1	
Density (calculated)	2.969 Mg/m^3	
Absorption coefficient	6.085 mm^{-1}	
F(000)	13108	
Crystal size	$0.09 \times 0.15 \times 0.20 \text{ mm}^3$	
Theta range for data collection	0.86 to 20.82°	
Index ranges	-27 ≤ h ≤ 23, -27 ≤ k ≤ 0, -28 ≤ l ≤ 24	
Reflections collected	30733	
Independent reflections	30733 [R(int) = 0.137]	
Completeness	92.9 %	
Refinement method	Full-matrix-block least squares on F^2	
Data / restraints / parameters	30733 / 5595 / 1969	
Goodness-of-fit on F^2	1.463	
Final R indices [I > 2σ(I)]	$R_1 = 0.1011$, $wR_2 = 0.3186$	
R indices (all data)	$R_1 = 0.1276$, $wR_2 = 0.3397$	
Largest diff. peak and hole	3.686 and $-6.360 \text{ e. \AA}^{-3}$	

Table 4.1. X-ray Crystallographic Data parameters for Compound 10

The structure of **10** reveals a similar spherical structure observed in **12** (Figure 4.3). The differentiation between the manganese centres and silver centres could not be made mainly due to the disorder present in the cluster. Thus, all the metal sites are assigned as silver centres with varying site occupancies despite manganese centres being present in the cluster. Crystallographic Data parameters for **10** are shown in Table 4.1. The atomic positions on the outer shell of **10** were refined as consisting of Ag, S and P ligands with satisfactory parameters. The refinement of the atomic positions of the inner shells expectedly became problematic due to site disorder. Figure 4.4 shows the highly disordered metal atoms present within the core of the cluster. Ultimately 32 silver atom positions (Ag78-Ag110) were refined with 50% occupancy to obtain satisfactory results. Even with the refinement of silver atom sites with partial occupancy, some silver atoms still show high temperature factors (Appendix A.16). All of the phosphorus sites, sulfur sites and silver sites with full occupancy were refined anisotropically and all the carbon sites and partially occupied silver sites were refined isotropically. After the completion of the structural refinement, high electron density ($6.36e \text{ \AA}^{-3}$) still remains within the core of the cluster. As observed with $[\text{Ag}_{188}\text{S}_{94}(\text{P}^n\text{Pr}_3)_{30}]$ **12**, a more accurate assignment of atomic sites was not possible. Nevertheless, the X-ray analysis of **10**, gives us the clear picture of its spherical nature but the determination of the precise molecular formula from these results should only be considered idealized.

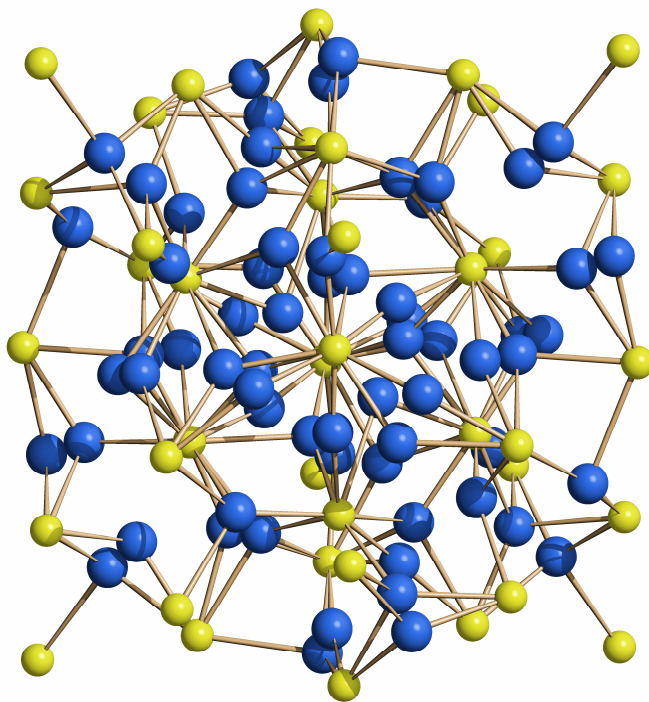


Figure 4.4. Disordered core of Complex **10**. S (yellow) and Ag (Blue).

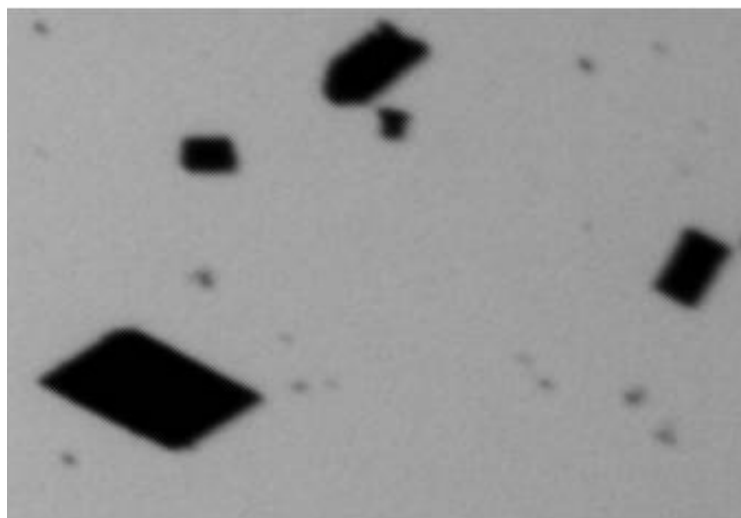


Figure 4.5. Picture of single crystals of **10** taken under a microscope.

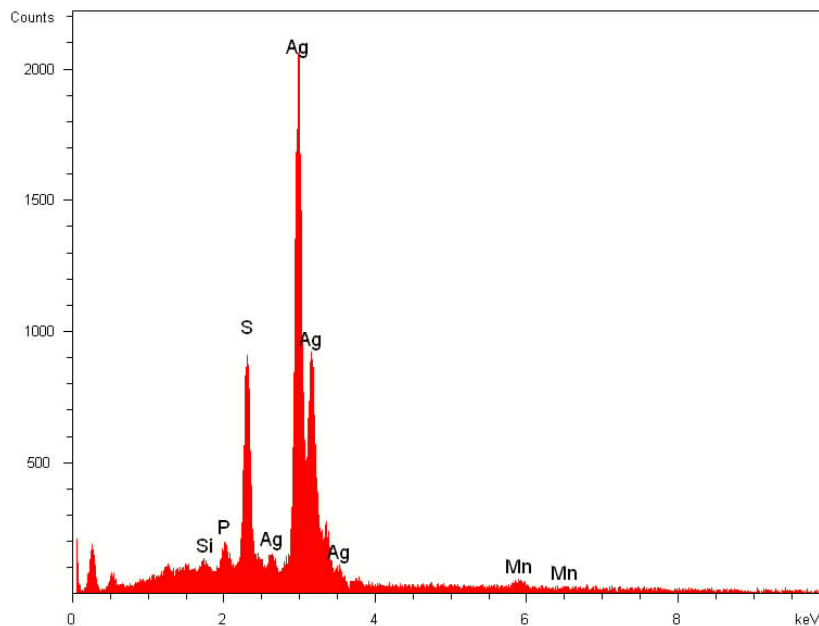


Figure 4.6. EDX spectrum of cluster **10** indicating the mixture of metals (Ag and Mn)

Elemental analysis was carried out on single crystals to determine molecular formulae of **10** and **11**. The initial confirmation of the presence of both manganese and silver atoms in the clusters **10** and **11** was determined by EDX analysis of single crystals. EDX measurements were carried out on five different samples of single crystals of **10** and **11**; a representative spectrum is shown in Figure 4.6 and the ratio of Mn:S:Ag as obtained from EDX analyses is shown in Table 4.2.

Cluster	Mn	Ag	S
10	0.27 ±0.09	1.3 ±0.4	1
11	0.20 ±0.08	1.52±0.32	1

Table 4.2. Atomic ratio of Mn:S:Ag obtained using EDX analyses for **10** and **11**.

The semi-quantitative metal analysis obtained from EDX analysis provided evidence of a mixed metal composition within the cluster. The exact Ag:Mn ratio was further probed by ICP-AES metal analysis. Using the Ag:Mn ratio obtained from ICP-AES, the molecular formulae of the clusters were then calculated. The results are tabulated below.

Cluster	Mn (%)	Ag (%)	Mn: Ag ratio	Molecular formula
10	7.30	46.53	1: 3.25	$\text{Mn}_{35/36}\text{Ag}_{118/116}\text{S}_{94}(\text{P}^n\text{Pr}_3)_{30}$
11	3.17	47.02	1: 7.55	$\text{Mn}_{19/20}\text{Ag}_{150/148}\text{S}_{94}(\text{P}^n\text{Pr}_3)_{30}$

Table 4.3. Molecular formulae of **10** and **11** calculated using the metal ratio from ICP-AES.

The idealized molecular formulae of **10** and **11** were established from the X-ray data obtained and ICP-AES analysis. The overall neutral charge of the clusters is achieved by the substitution of 2 Ag^+ atoms for every Mn^{2+} being incorporated into the cluster assuming the retention of the divalent state of the 3d metal. The feasibility of Mn^{2+} displacing Ag^+ atoms is supported by the similarity of Mn-S and Ag-S bond lengths, typically around 2.3- 2.5 Å.^{3,27} Table 4.4 shows the comparison of the Mn-S bond length of Manganese thiolate cluster, **3a** and Ag-S bond length of cluster **10**.

	3a		10
Mn1-S7	2.3630(13)	Ag1-S17	2.407(8)
Mn1-S8	2.3676(13)	Ag1-S25	2.440(8)
Mn2-S7	2.4069(13)	Ag5-S16	2.416(7)
Mn2-S1	2.4226(13)	Ag5-S28	2.433(7)
Mn2-S2	2.4679(13)	Ag12-S37	2.406(7)
Mn2-S9	2.5009(12)	Ag12-S17	2.414(8)
Mn3-S8	2.4178(13)	Ag18-S33	2.365(8)
Mn3-S3	2.4163(13)	Ag18-S21	2.369(8)
Mn3-S2	2.4724(13)	Ag20-S13	2.401(8)
Mn3-S9	2.5058(12)	Ag20-S31	2.415(8)
Mn4-S4	2.4080(13)	Ag21-S13	2.424(8)
Mn4-S8	2.4122(13)	Ag21-S42	2.435(8)

Table 4.4. Selected Bond Distances (Å) for Complexes **3a** and **10**

Combustion analysis was also carried out (C, H, S) to probe the sample purity. Both **10** and **11** show a lower carbon and sulfur content than the expected value obtained using the idealized formulae. In compound **10** the carbon content is 3.34% lower and sulfur is 2.68% lower than the expected values. In the case of **11** the sulfur content was found to be lower by 3.28%. These results clearly suggest perhaps co-crystallizing species, and ultimately a lack of sample homogeneity during the elemental analysis. Efforts to confirm sample purity using powder X-ray diffraction were marred by the problem of desolvation of the crystalline samples.

The observed ratio of Ag:Mn in **10** and **11**, indicate that the Mn content in the clusters is lower than the amount of Mn introduced via the chalcogenolate precursors in the reaction mixture (Equations 4.1 and 4.2). The Ag:Mn ratio found in the **10** (3.3) is almost twice as high as the ratio used to synthesize the compound (1.6). On the other hand, the Ag:Mn ratio is only 1.3 times higher in case of **11**. The excess Mn present in the reaction mixture would have formed undetermined side products, resulting in the lower Mn content found in both the compounds.

These results nonetheless confirm the utility of the manganese chalcogenolate compounds as a source of paramagnetic ions as well as sulfide ligands, promoting the formation of ternary MnAgS nanoclusters under mild reaction conditions. The results indicate that the mononuclear manganese complex, **4**, is more efficient source of Mn^{2+} than the pentanuclear cluster, **3a**. The instability of **3a** in solution due to the break down of the Mn_5 cluster framework could explain the observed discrepancy between the two precursors.

4.2.2. Optical Properties

Room temperature solution UV-visible absorption, photoluminescence (PL) and photoluminescence excitation (PLE) spectra were recorded for the clusters. Figure 4.7 shows the UV-visible spectra of compounds **10**, **11** and the analogous binary compound **12**. The solution state electronic absorption spectra of complexes **10**, **11** and **12** all show a similar absorption profile with a broad absorption band maximum at 680 nm and a higher energy shoulder at 525 nm (Figure 4.7). The absorption peak detected in the visible spectrum (680 nm) is the lowest energy excitonic absorption peak of the clusters and is assigned to the $\text{S}^{2-} (3p) \rightarrow \text{Ag}^+ (5s)$ electronic transition.³⁷ Relative to the bulk band gap energy of Ag_2S (~1240 nm),¹² the excitonic peak observed for these clusters exhibits a blue shift, indicating the clusters are within the quantum-confinement regime.

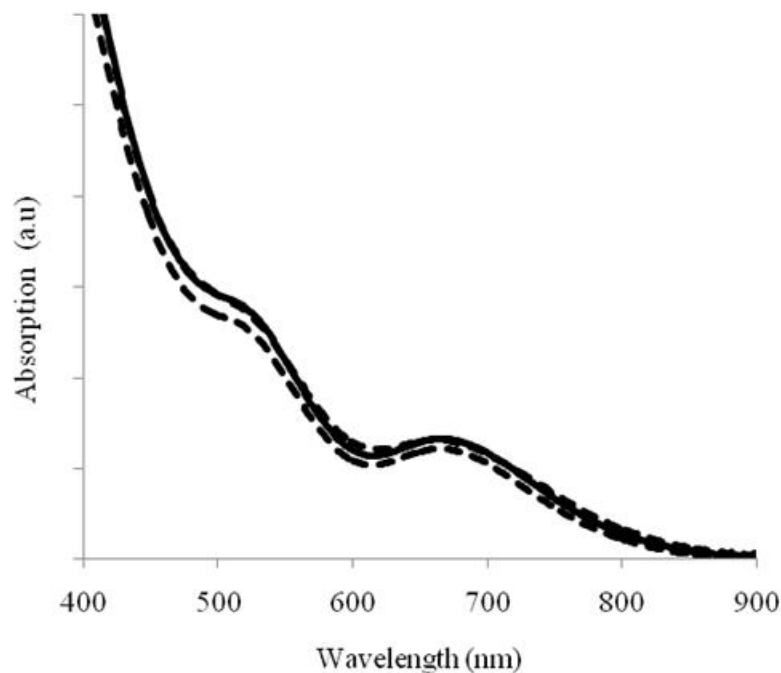


Figure 4.7. Normalized room temperature UV-visible spectra of **12** (—), **10** (---), compound **11** (-.-) in DCM.

The solution and solid state photoluminescence spectra of **10** and **11** at room temperature showed no emission when the excitation wavelength lower than 680 nm was used. The band-edge emission and emission associated with $S^{2-}(3p) \rightarrow Ag^+(5s)$ are expected to occur at distinctly lower energies.⁸ There are reports of Ag_2S nanocrystals with as-expected near infra red emission properties³⁶ as well as the emissions are believed to originate predominantly from a ligand-to-metal charge-transfer LMCT [$(S^{2-}) \rightarrow Ag$] excited state.^{8,37} PL spectra observed for **10**, **11** as well as **12** clearly indicated no such emissions are observed at room temperature.

4.3. Conclusions

The chalcogenolate complexes $[\text{Li}(\text{N},\text{N}'\text{-tmeda})]_2[(\text{N},\text{N}'\text{-tmeda})\text{Mn}_5(\text{SSiMe}_3)_6(\text{S})_3]$ and $[\text{Li}(\text{N},\text{N}'\text{-tmeda})]_2[\text{Mn}(\text{SSiMe}_3)_4]$ have been utilized as molecular precursors for the preparation of the ternary nanoclusters, $[\text{Mn}_{35/36}\text{Ag}_{118/116}\text{S}_{94}(\text{P}^n\text{Pr}_3)_{30}]$ and $[\text{Mn}_{19/20}\text{Ag}_{150/148}\text{S}_{94}(\text{P}^n\text{Pr}_3)_{30}]$ respectively. Using a low temperature synthetic method, we have been able to incorporate Mn^{2+} into a large Ag_2S semiconducting matrix. These clusters show no emission at room temperature. To investigate the effect of Mn^{2+} incorporation on the photoluminescence properties of these clusters, low temperature PLE and PL measurement might provide a better insight.

4.4. Experimental Section

4.4.1. General Experimental

All experimental procedures were performed using standard double manifold Schlenk line techniques under an atmosphere of dried nitrogen gas or in nitrogen filled glove boxes. The non-chlorinated solvents (tetrahydrofuran, pentane) were dried and collected using a MBraun MB-SP Series solvent purification system with tandem activated alumina (tetrahydrofuran) and activated alumina or activated copper redox catalyst (hydrocarbons). *N,N,N',N'*-tetramethylethylenediamine (*N,N'*-tmeda) was dried and distilled over CaH_2 . Spectral grade solvent CH_2Cl_2 was purchased from Caledon and

dimethylformamide (DMF) from Fisher Chemicals. MnCl_2 and AgOAc were purchased from Aldrich in 98% and 99.99% purity respectively and used as supplied. 1.6 M $n\text{BuLi}$ in hexanes was purchased from Aldrich and used as supplied. The silylated reagents $\text{E}(\text{SiMe}_3)_2$ ($\text{E} = \text{S}, \text{Se}$) were synthesized using literature procedures.^{31b, 38} $[\text{Li}(\text{N},\text{N}'\text{-tmeda})]_2[(\text{N},\text{N}'\text{-tmeda})\text{Mn}_5(\text{SSiMe}_3)_6(\text{S})_3]$, $[\text{Li}(\text{N},\text{N}'\text{-tmeda})]_2[\text{Mn}(\text{SSiMe}_3)_4]$ and $[\text{Ag}_{188}\text{S}_{94}(\text{P}^n\text{Pr}_3)_{30}]$ were prepared following a previously published literature procedure.^{3,27} Room temperature solution photoluminescence and photoluminescence excitation were measured on a Photon Technologies International Inc. Quantum Master equipped with a Xenon lamp. Room temperature UV-visible absorption spectra were recorded on a Varian Cary 300 spectrometer. A Quartz Xone EDX analysis system coupled to a Leo 440 SEM equipped with a Gresham light element detector was used to obtain semi-quantitative analysis of silver and manganese. Elemental (C, H, S) analysis of **10**, **11** was performed by Laboratoire d'Analyse Élémentaire de l'Université de Montréal (Montreal, Canada). Metal analysis of compound **10** and **11** were performed using Inductively Coupled Plasma atomic emission spectroscopy (ICP-AES) by Columbia Analytical Services (Tuscan, AZ, USA).

Single crystal X-ray data were collected Enraf-Nonius Kappa-CCD diffractometers equipped with graphite-monochromated MoK_α ($\lambda = 0.71073\text{\AA}$) radiation. Highly solvated single crystals of the complexes were carefully selected, immersed in paraffin oil and mounted on a nylon loop. Crystals were placed immediately in a cold stream of N_2 to minimize desolvation. The structures were solved using direct methods and refined by the full-matrix least squares procedure of SHELXTL (G. M. Sheldrick, Madison, WI, 1996).

4.4.2. Syntheses

4.4.2.1. Synthesis of $\text{Mn}_{35.5}\text{Ag}_{117}\text{S}_{94}(\text{P}^n\text{Pr}_3)_{30}$, **10**.

$[\text{Li}(\text{N},\text{N}'\text{-tmeda})]_2[(\text{N},\text{N}'\text{-tmeda})\text{Mn}_5(\text{SSiMe}_3)_6(\text{S})_3]$ (0.105g, 0.077 mmol) was dissolved in 5 mL Et_2O and the pale orange solution was cooled to -75°C . AgOAc (0.103g, 0.617 mmol) was dissolved in 10 mL Et_2O by adding P^nPr_3 (0.40 mL, 2.01 mmol) and the clear solution was cooled to -75°C . These two solutions were then added to previously prepared pale orange solution of $[(\text{N},\text{N}'\text{-tmeda})\text{Mn}_5(\text{SSiMe}_3)_6(\text{S})_3]^{2-}$ at -75°C . The reaction solution turned pale yellow instantly after the addition of two reagents. The reaction mixture was left stirring for a few hours until the reaction temperature reached -30°C at which point the reaction solution had turned dark brown. Dark brown crystals were obtained by storing the reaction mixture at -25°C for 24 hours. Yield: 0.110g. Anal. Calcd for $\text{C}_{270}\text{H}_{630}\text{P}_{30}\text{S}_{94}\text{Mn}_{35.5}\text{Ag}_{117}$: C, 14.53%; H, 2.85%, S, 13.51%. Found: C, 11.19%; H, 2.26%; S, 10.83%.

4.4.2.2. Synthesis of $\text{Mn}_{19.5}\text{Ag}_{149}\text{S}_{94}(\text{P}^n\text{Pr}_3)_{30}$, **11**.

The synthesis was carried out in a similar manner as **10**, with $[\text{Li}(\text{N},\text{N}'\text{-tmeda})]_2[\text{Mn}(\text{SSiMe}_3)_4]$ (0.100g, 0.138mmol), AgOAc (0.140g, 0.839 mmol) and P^nPr_3 (0.50 mL, 2.52 mmol). Dark brown crystals were obtained after storing the reaction mixture at -25°C for a day.

Yield: 0.150g. Anal. Calcd for $\text{C}_{270}\text{H}_{630}\text{P}_{30}\text{S}_{94}\text{Mn}_{19.5}\text{Ag}_{149}$: C, 13.03%; H, 2.55%, S%, 12.11. Found: C, 12.87%; H, 2.63%; S, 8.83%.

4.4.2.3. Synthesis of $\text{Ag}_{188}\text{S}_{94}(\text{P}^n\text{Pr}_3)_{30}$, 12.

AgOAc (0.120g, 0.718 mmol) was dissolved in 15 mL Et_2O by adding P^nPr_3 (0.43 mL, 2.15 mmol) and the clear solution was cooled to -75°C . Half equivalent of $\text{S}(\text{SiMe}_3)_2$ (0.08mL, 0.336mmol) was then added to the AgOAc solution at -75°C . The reaction solution turned pale yellow instantly after the addition of $\text{S}(\text{SiMe}_3)_2$ reagents. The reaction mixture was left stirring for a few hours until the reaction temperature reached -30°C at which point the reaction solution had turned dark brown. Dark brown crystals were obtained by storing the reaction mixture at room temperature for 24 hours. Yield: 0.150g. Anal. Calcd for $\text{C}_{270}\text{H}_{630}\text{P}_{30}\text{S}_{94}\text{Ag}_{188}$: C, 11.54%; H, 2.26%, S, 10.73%. Found: C, 10.32%; H, 1.94%; S, 11.58%.

4.5. References

1. Schmid, G.; Ed.; *Clusters and Colloids: From Theory to Applications (2nd edition)*; VCH: Weinheim, Germany, **2010**.
2. Corrigan, J. F.; Fuhr, O.; Fenske, D. *Adv. Mater.* **2009**, *21*, 1867-1871
3. Wang, X. J.; Langetepe, T.; Persau, C.; Kang, B. S.; Sheldrick, G. M.; Fenske, D. *Angew. Chem. Int. Ed.* **2002**, *41*, 3818-3822
4. Fenske, D.; Anson, C. E.; Eichhöfer, A.; Fuhr, O.; Ingendoh, A.; Persau, C.; Richert, C. *Angew. Chem. Int. Ed.* **2005**, *44*, 5242-5246
5. Chitsaz, S.; Fenske, D.; Fuhr, O. *Angew. Chem. Int. Ed.* **2006**, *45*, 8055-8059
6. Anson, C. E.; Eichhöfer, A.; Issac, I.; Fenske, D.; Fuhr, O.; Sevillano, P.; Persau, C.; Stalke, D.; Zhang, J. *Angew. Chem. Int. Ed.* **2008**, *47*, 1326-1331
7. a) Terabe, K., Hasegawa, T., Nakayama, T. and Aono, M. *Nature.* **2005**, *433*, 47-50
b) Huxter, V. M., Mirkovic, T., Nair, P. S. and Scholes, G. D. *Adv. Mater.* **2008**, *20*, 2439-2443
c) Xiang, J. H., Cao, H. Q., Wu, Q. Z., Zhang, S. C., Zhang, X. R. and Watt, A. A. R. *J. Phys. Chem. C.* **2008**, *112*, 3580-3584
d) Du, Y.; Xu, B.; Fu, T.; Cai, M.; Li, F.; Zhang, Y.; Wang, Q. *J. Am. Chem. Soc.*, **2010**, *132*, 1470-1471
8. Li, G.; Lei, Z.; Wang, Q. M. *J. Am. Chem. Soc.* **2010**, *132*, 17678-17679
9. Norris, D. J.; Efros, Al. L.; Erwin, S. C. *Science* **2008**, *319*, 1776-1779

10. Furdyna, J. K.; Kossut, J.; Eds *Dilute Magnetic Semiconductors*; Academic Press: New York, **1988**, V25.
11. Alivisatos, A. P.; *Science* **1996**, *271*, 933-937.
12. Michalet, X.; Pinaud, F. F.; Bentolila, L. A.; Tsay, J. M.; Doose, S., Li, J. J.; Sundaresan, G.; Wu, A. M.; Gambhir, S. S.; Weiss, S.; *Nature* **2007**, *447*, 441-446.
13. Gur, I.; Fromer, N. A.; Geier, M.L.; Alivisatos, A. P. *Science* **2005**, *310*, 462-465.
14. Bhargava, R. N.; Gallagher, D.; Hong, X.; Nurmikko, A. *Phys. Rev. Lett.* **1994**, *72*, 416-419.
15. Norris, D. J.; Yao, N.; Charnock, F. T.; Kennedy, T. A. *Nano Lett.* **2001**, *1*, 3-7.
16. Stowell, C. A.; Wiacek, R. J.; Sauders, A. E.; Korgel, B. A. *Nano Lett.* **2003**, *3*, 1441-1447.
17. Santra, S.; Yang, H.; Holloway, P. H.; Stanley, J. T.; Mericle, R. A. *J. Am. Chem. Soc.* **2005**, *127*, 1656-1657.
18. Norberg, N. S.; Parks, G. L.; Salley, G. M.; Gamelin, D. R. *J. Am. Chem. Soc.* **2006**, *128*, 13195-13203.
19. Sapra, S.; Prakash, A.; Ghangrekar, A.; Periasamy, N.; Sarma, D. D. *J. Phys. Chem. B.* **2005**, *109*, 1663-1668.
20. Pradhan, N.; Goorskey, D.; Thessing, J.; Peng, X. *J. Am. Chem. Soc.* **2005**, *127*, 17586-17587.

21. Erwin, S. C.; Zu, L.; Haftel, M. I.; Efros, A. L.; Kennedy, T. A.; Norris, D. J. *Nature* **2005**, *436*, 91-94.
22. Yang, Y.; Chen, O.; Angerhofer, A.; Cao, C. J. *J. Am. Chem. Soc.* **2006**, *128*, 12428-12429.
23. Pradhan, N.; Peng, X. *J. Am. Chem. Soc.* **2007**, *129*, 3339-3347.
24. Nag, A.; Sapra, S.; Nagamani, C.; Sharma, A.; Pradhan, N.; Bhat, S. V.; Sarma, D. *Chem. Mater.* **2007**, *19*, 3252-3259.
25. Beaulac, R.; Archer, P. I.; Ochsenein, S. T.; Gamelin, D. R. *Adv. Funct. Mater.* **2008**, *18*, 3873-3891.
26. Klimov, V. I.; Mikhailovsky, A. A.; Xu, S.; Malko, A.; Hollingsworth, J. A.; Leatherdale, C. A.; Eisler, H.; Bawendi, M. G. *Science* **2000**, *290*, 314-317.
27. Khadka, C. B.; Macdonald, D. G.; Lan, Y.; Powell, A. K.; Fenske, D.; Corrigan, J. F. *Inorg. Chem.* **2010**, *49*, 7289-7297
28. a) Tran, D. T. T.; Taylor, N. J.; Corrigan, J. F. *Angew. Chem. Int. Ed. Engl.* **2000**, *39*, 935-937 b) Tran, D. T. T.; Beltran, L. M.; Kowalchuk, C. M.; Trefiak, N. R.; Taylor, N. J.; Corrigan, J. F. *Inorg. Chem.* **2002**, *41*, 5693-5698.
29. DeGroot, M. W.; Taylor, N. J.; Corrigan, J. F. *J. Mater. Chem.* **2004**, *14*, 654-660.
30. DeGroot, M. W.; Taylor, N. J.; Corrigan, J. F. *Inorg. Chem.* **2005**, *44*, 5447-5458.
31. a) DeGroot, M. W.; Corrigan, J. F. *Angew. Chem. Int. Ed.* **2004**, *43*, 5355-5357. b) DeGroot, M.W.; Taylor, N. J.; Corrigan, J. F. *J. Am. Chem. Soc.* **2003**, *125*, 864-865. c)

- DeGroot, M. W.; Atkins, K.M.; Borecki, A.; Rösner, H.; Corrigan, J. F. *J. Mater. Chem.* **2008**, *18*, 1123-1130.
32. a) Komuro, T.; Matsuo, T.; Kawaguchi, H.; Tatsumi, K. *J. Chem. Soc., Dalton Trans.* **2004**, *10*, 1618-1625. b) Komuro, T.; Matsuo, T.; Kawaguchi, H.; Tatsumi, K. *J. Chem. Commun.* **2002**, *9*, 988-989. c) Komuro, T.; Matsuo, T.; Kawaguchi, H.; Tatsumi, K. *Angew. Chem. Int. Ed.* **2003**, *42*, 465-468.
33. a) Sommer, H.; Eichhöfer, A.; Drebov, N.; Ahlrichs, R.; Fenske, D. *Eur. J. Inorg. Chem.* **2008**, *32*, 5138-5145. b) Bechlars, B.; Issac, I.; Feuerhake, R.; Clerac, R.; Fuhr, O.; Fenske, D. *Eur. J. Inorg. Chem.*, **2008**, *10*, 1632-1644. c) Feuerhake, R.; Fenske, D. *Z. Anorg. Allg. Chem.* **2003**, *629*, 2317-2324. d) Eichhöfer, A.; Fenske, D. *J. Chem. Soc., Dalton Trans.* **2000**, 941-944.
34. DeGroot, M. W.; Corrigan, J. F. *Z. Anorg. Allg. Chem.* **2006**, *632*, 19-29.
35. Borecki, A.; Corrigan, J. F. *Inorg. Chem.* **2007**, *46*, 2478-2484.
36. Du, Y.; Xu, B.; Fu, T.; Miao, C, Li, F.; Zhang, Y.; Wang, Q. *J. Am. Chem. Soc.* **2010**, *132*, 1470-1471
37. Yam, V. W. W.; Lo, K. K. W.; Wang, C. R.; Cheung, K. K. *Inorg. Chem.* **1996**, *35*, 5116-5117
38. So, J; Boudjouk, P; *Synthesis.* **1989**, 306-307

CHAPTER FIVE

CONCLUSIONS AND FUTURE WORK

5.1. Summary

The use of impurities (dopants) to tailor the properties of semiconductor nanoparticles is of key importance to exploit their promise as technological materials. Magnetic dopants have been shown to strongly influence the optical properties of semiconductors due to the enhanced interaction between the host lattice and the magnetic dopants as a result of quantum confinement.¹ It will be imperative to be able to control and understand doping at the nanoscale semiconductors if this class of materials is going to evolve into practical applications. A considerable amount of experimental work has been performed in the past few years to understand doping at the nanoscale. Despite this, the inability to introduce impurities into the core of the nanocrystals due to lattice annealing remains one of the problems in the field of synthesis of doped QDs.^{2,3} Surface bound dopants may hinder the understanding of the origins of the nanocrystals properties or even compromise the desired properties. Development of alternative synthetic methodologies to access doped QDs are desirable as it might circumvent the problem of surface doping and make the elucidation of structure-property more reliable.

Numerous chemical methods have been developed for the synthesis of magnetic ion doped semiconductor nanocrystals, but there are only handful of reports on the synthesis of magnetic ion doped semiconductor nanoclusters.^{4,5} The pursuit of ternary nanoclusters containing magnetic ions is novel and using single crystal X-ray technique as an analytical tool, it could be possible to obtain a more accurate structural characterization of dopants within the semiconductor host. Transition metal complexes

coordinated with silylchalcogenolate ligands have proven to be a practical precursor for the synthesis of polynuclear MM'E nanoclusters.⁶⁻⁸ The research described in this thesis was the development of this synthetic approach to isolate Mn²⁺ containing II-VI and I-VI nanoclusters.

Chapter 2 describes the synthesis of Mn²⁺ and Co²⁺ complexes with reactive –ESiMe₃ (E= S, Se) ligands. Cobalt complexes were synthesized with both chelating *N,N'*-tmeda and monodentate 3,5-lutidine ligands but only the *N,N'*-tmeda ligated complexes were isolated for manganese. Using the same reaction conditions and the ratio of reagents, mononuclear complexes of Co²⁺ were obtained while polynuclear complexes were typically isolated for Mn²⁺. X-ray crystallographic characterization of these complexes reveals the terminally coordinated –ESiMe₃ ligands, rendering them to be a possible candidate for synthesis of ternary nanoclusters containing Mn²⁺ and Co²⁺. The magnetic studies using SQUID provide the evidence of overall paramagnetic nature of pentanuclear manganese complexes.

Chapter 3 explores the reactivity of the previously synthesized complex, (*N,N'*-tmeda)Zn(ESiMe₃)₂ (E = S, Se), with MnCl₂ for the preparation of the ternary nanoclusters, (*N,N'*-tmeda)₆Zn_{14-x}Mn_xE₁₃Cl₂. X-ray crystallographic analysis shows the retention of '(*N,N'*-tmeda)ZnE₂' units which acts as capping ligands preventing the condensation to bulk phases. The reaction scheme utilized allows the incorporation of varying amounts of metals where the value of *x* varies from 1.7 to as high as 7.8. Mn²⁺ was found to be on the surface of the nanoclusters when it was introduced at lower quantities (*x*=1.7) but with increased amount of Mn²⁺ it occupied positions in the cluster

core. DFT calculations indicate that the exchange of Zn with Mn is easily feasible and supports the crystallographic data. Increasing the number of manganese ($x > 1.7$) in the clusters **7** and **8** resulted in a red shift in the emission energies in these clusters from with a characteristic orange luminescence maximum at ~590 nm due to the electronic transition from ${}^6A_1 \leftarrow {}^4T_1$ observed in DMS systems.³ The isolation of cluster **7** and **8**, demonstrates that $(N,N'$ -tmeda)Zn(ESiMe₃)₂ (E = S, Se) complexes are can be successfully utilized as molecular precursors to MnZnE nanoclusters.

The molecular precursor approach to ternary nanocluster was further investigated and is described in Chapter 4, using manganese chalcogenolate complexes. Two manganese complexes synthesized as part of this thesis, [Li(*N,N'*-tmeda)]₂[(*N,N'*-tmeda)Mn₅(SSiMe₃)₆(S)₃] and [Li(*N,N'*-tmeda)]₂[Mn(SSiMe₃)₄] were reacted with tripropyl phosphine solubilized AgOAc to isolate Mn_{35/36}Ag_{116/118}S₉₄(PⁿPr₃)₃₀ and Mn_{19/20}Ag_{148/150}S₉₄(PⁿPr₃)₃₀, respectively. The complete structural characterization of **10** by single crystal X-ray analysis was not possible due to high amount of disorder within the cluster core. Both the EDX analysis and elemental analysis (ICP-AES) of **10** and **11** reveal the incorporation of Mn²⁺ into the Ag₂S semiconductor matrix. Both manganese chalcogenolate complexes proved to be effective precursors for the synthesis of Mn²⁺ containing Ag₂S ternary nanoclusters. The effect of Mn²⁺ incorporation on the Ag₂S semiconductor lattice on the photoluminescence of the ternary nanocluster was hampered by the lack of luminescence from these ternary clusters at room temperature.

The reactivity of manganese chalcogenolate complexes (**3a**, **3b**, **4** and **5**) and cobalt chalcogenolate complexes (**1a**, **1b** and **2a**, **2b**) as precursors to synthesize Mn²⁺ or Co²⁺ doped II-VI ternary nanoclusters were performed by reacting them with salts of

Zn^{2+} , Cd^{2+} and Hg^{2+} without any success in obtaining crystalline samples. Although the color change of the reaction once the reagents were mixed together indicated the reactivity of these complexes, single crystals of X-ray quality was not obtained. Instead these reactions invariably resulted in the formation of powder solids. Alternatively, the chalcogenolate complexes, $(N,N'\text{-tmeda})\text{Zn}(\text{ESiMe}_3)_2$ ($\text{E} = \text{S}, \text{Se}$), **3a** and **4**, proved to be a powerful precursors for the formation of ternary nanocluster containing both semiconducting as well as magnetic properties. With the synthesis and characterization of ternary **7**, **8**, **10** and **11** using metal chalcogenolate precursors, we have been able to expand the scope of our synthetic methodology to include paramagnetic metal ions.

With the success of $(N,N'\text{-tmeda})\text{Zn}(\text{ESiMe}_3)_2$ ($\text{E} = \text{S}, \text{Se}$) the future work could also involve further expansion of this methodology to utilize the tellurium analogue, $(N,N'\text{-tmeda})\text{Zn}(\text{TeSiMe}_3)_2$ as well as $(N,N'\text{-tmeda})\text{Cd}(\text{ESiMe}_3)_2$ ($\text{E} = \text{S}, \text{Se}, \text{Te}$) to isolate doped QDs. The low temperature optical properties and magnetic properties of **7-8**, **10** and **11** should be further investigated. Future work could also include the utilization of doped nanoclusters as precursors to ternary nanoparticles using lyothermal techniques. Transition metals (eg. Cr^{2+} , Fe^{2+} , Co^{2+}) doped II-VI semiconductors have broad absorption and emission bands in the mid- IR region of the optical spectrum making them an ideal candidate for a variety of application including non-invasive medical diagnostics, atmospheric sensing and free space communication and detection of explosives among others.⁹ Such ternary nanocluster could be targeted using a similar methodology employed in this thesis.

5.2. References

1. Bryan, J. D.; Gamelin, D. R. *Prog. Inorg. Chem.* **2005**, *54*, 47-126.
2. Nag, A.; Chakraborty, S.; Sarma, D. D. *J. Am. Chem. Soc.* **2008**, *130*, 10605-10611.
3. Graf, C.; Hofmann, A.; Ackermann, T.; Boeglin, C.; Viswanatha, R.; Peng, X.; Rodrigues, A. F.; Nolting, F.; Rühl, E. *Adv. Funct. Mater.* **2009**, *19*, 2501-2510.
4. Beaulac, R.; Archer, P. I.; Gamelin, D. R. *J. Solid State Chem.* **2008**, *181*, 1582-1589
5. Eichhöfer, A.; Hampe, O.; Lebedkins, S.; Weigend, F. *Inorg. Chem.* **2010**, *49*, 7331-7339
6. DeGroot, M. W.; Taylor, N. J.; Corrigan, J. F. *Inorg. Chem.* **2005**, *44*, 5447-5458.
7. a) DeGroot, M. W.; Corrigan, J. F. *Angew. Chem. Int. Ed.* **2004**, *43*, 5355-5357. b) DeGroot, M.W.; Taylor, N. J; Corrigan, J. F. *J. Am. Chem. Soc.* **2003**, *125*, 864-865. c) DeGroot, M. W.; Atkins, K.M.; Borecki, A.; Rösner, H.; Corrigan, J. F. *J. Mater. Chem.* **2008**, *18*, 1123-1130.
8. DeGroot, M. W.; Corrigan, J. F. *Z. Anorg. Allg. Chem.* **2006**, *632*, 19-29.
9. Mirov, S.; Fedorov, V.; Moskalev, I.; Martyshkin, D.; Kim, C. *Laser and Photon. Rev.* **2010**, *1*, 21-41

APPENDIX A:

**X-ray Crystallographic Data Parameters and
Atomic Positions for Complexes 1-10**

APPENDIX A.1.**Crystal data and structure refinement for (N,N'-tmeda)Co(SSiMe₃)₂, **1a****

Empirical formula	C ₁₂ H ₃₄ Co N ₂ S ₂ Si ₂
Formula weight	385.64
Temperature	150(2) K
Wavelength	0.71073 Å
Crystal system	Monoclinic
Space group	C 2/c
Unit cell dimensions	a = 25.0680(10) Å α = 90°. b = 14.3286(7) Å β = 105.225(2)°. c = 18.7037(9) Å γ = 90°.
Volume	6482.4(5) Å ³
Z	12
Density (calculated)	1.185 Mg/m ³
Absorption coefficient	1.091 mm ⁻¹
F(000)	2484
Crystal size	0.09 x 0.05 x 0.02 mm ³
Theta range for data collection	1.87 to 25.08°.
Index ranges	-29 ≤ h ≤ 23, -16 ≤ k ≤ 17, -22 ≤ l ≤ 22
Reflections collected	19464
Independent reflections	5732 [R(int) = 0.1740]
Completeness to theta = 25.08°	99.6 %
Absorption correction	Semi-empirical from equivalents
Max. and min. transmission	0.9785 and 0.9082
Refinement method	Full-matrix least-squares on F ²
Data / restraints / parameters	5732 / 0 / 273
Goodness-of-fit on F ²	1.029
Final R indices [I > 2σ(I)]	R1 = 0.0584, wR2 = 0.1431
R indices (all data)	R1 = 0.1051, wR2 = 0.1647
Largest diff. peak and hole	0.646 and -0.692 e.Å ⁻³

Atomic coordinates ($\times 10^4$) and equivalent isotropic displacement parameters ($\text{\AA}^2 \times 10^3$)

for (*N,N'*-tmeda)Co(SSiMe₃)₂. U(eq) is defined as one third of the trace of the orthogonalized U^{ij} tensor.

	x	y	z	U(eq)
Co(1)	7424(1)	8590(1)	3381(1)	38(1)
S(1)	6708(1)	8086(1)	3816(1)	41(1)
S(2)	7326(1)	9403(1)	2318(1)	53(1)
Si(1)	6133(1)	9197(1)	3595(1)	45(1)
Si(2)	6906(1)	8556(1)	1423(1)	53(1)
N(1)	8023(2)	7518(3)	3541(2)	49(1)
N(2)	8015(2)	9364(3)	4181(2)	46(1)
C(1)	5771(2)	9271(4)	2597(3)	59(2)
C(2)	5612(2)	8981(4)	4137(3)	61(1)
C(3)	6474(2)	10357(3)	3848(3)	60(2)
C(4)	6612(2)	7483(3)	1745(3)	61(2)
C(5)	6322(2)	9225(4)	800(3)	72(2)
C(6)	7378(3)	8195(5)	858(3)	84(2)
C(7)	7827(2)	6634(3)	3763(4)	70(2)
C(8)	8231(2)	7381(5)	2889(3)	78(2)
C(9)	8479(2)	7877(4)	4184(3)	70(2)
C(10)	8531(2)	8893(5)	4191(3)	79(2)
C(11)	7902(2)	9358(4)	4913(3)	60(2)
C(12)	8051(3)	10376(4)	3984(3)	83(2)
Co(2)	10000	9611(1)	2500	40(1)
S(3)	10345(1)	8896(1)	1652(1)	69(1)
Si(3)	9773(1)	7938(1)	1032(1)	54(1)
N(3)	9434(2)	10690(3)	2059(2)	46(1)
C(13)	9747(3)	8107(5)	39(3)	102(2)
C(14)	10006(2)	6725(4)	1276(4)	98(2)
C(15)	9065(2)	8066(4)	1144(4)	85(2)
C(17)	8873(2)	10550(4)	2176(3)	68(2)
C(18)	9368(2)	10809(4)	1259(3)	56(1)
C(19)	9698(2)	11531(3)	2460(3)	65(2)

APPENDIX A.2.Crystal data and structure refinement for (*N,N'*-tmeda)Co(SeSiMe₃)₂, **1b**

Empirical formula	C ₁₂ H ₃₄ Co N ₂ Se ₂ Si ₂
Formula weight	479.44
Temperature	150(2) K
Wavelength	0.71073 Å
Crystal system	Monoclinic
Space group	C2/c
Unit cell dimensions	a = 25.487(2) Å α = 90°. b = 14.4650(10) Å β = 104.930(3)°. c = 18.8350(10) Å γ = 90°.
Volume	6709.5(8) Å ³
Z	12
Density (calculated)	1.424 Mg/m ³
Absorption coefficient	4.122 mm ⁻¹
F(000)	2916
Crystal size	0.16 x 0.06 x 0.04 mm ³
Theta range for data collection	2.59 to 25.04°.
Index ranges	-25 ≤ h ≤ 30, -17 ≤ k ≤ 16, -22 ≤ l ≤ 21
Reflections collected	25911
Independent reflections	5922 [R(int) = 0.1126]
Completeness to theta = 25.04°	99.6 %
Max. and min. transmission	0.8525 and 0.5584
Refinement method	Full-matrix least-squares on F ²
Data / restraints / parameters	5922 / 0 / 273
Goodness-of-fit on F ²	1.026
Final R indices [I > 2σ(I)]	R1 = 0.0537, wR2 = 0.1127
R indices (all data)	R1 = 0.1098, wR2 = 0.1302
Largest diff. peak and hole	1.042 and -1.027 e.Å ⁻³

Atomic coordinates ($\times 10^4$) and equivalent isotropic displacement parameters ($\text{\AA}^2 \times 10^3$)

for $(N,N'$ -tmeda)Co(SeSiMe₃)₂. U(eq) is defined as one third of the trace of the orthogonalized U^{ij} tensor.

	x	y	z	U(eq)
Co(1)	2545(1)	8642(1)	1586(1)	39(1)
Se(1)	3297(1)	8108(1)	1159(1)	40(1)
Se(2)	2638(1)	9496(1)	2691(1)	53(1)
Si(1)	3882(1)	9307(1)	1426(1)	46(1)
Si(2)	3083(1)	8555(1)	3599(1)	54(1)
C(1)	4396(3)	9114(4)	883(4)	64(2)
C(2)	4225(3)	9356(5)	2423(4)	62(2)
C(3)	3537(3)	10441(4)	1201(4)	64(2)
C(4)	2614(3)	8142(5)	4148(4)	84(3)
C(5)	3378(3)	7534(4)	3245(4)	57(2)
C(6)	3647(3)	9213(5)	4227(4)	75(2)
C(7)	1930(4)	10399(6)	988(5)	142(5)
C(8)	2098(3)	9430(5)	62(4)	67(2)
C(9)	1476(3)	8970(8)	763(5)	111(4)
C(10)	1503(3)	7979(5)	805(6)	86(3)
C(11)	1776(3)	7410(6)	2083(5)	109(4)
C(12)	2133(3)	6720(4)	1148(4)	59(2)
Co(2)	5000	4722(1)	2500	42(1)
Se(3)	5354(1)	3974(1)	1614(1)	97(1)
Si(3)	4742(1)	2965(1)	999(1)	58(1)
N(1)	1977(2)	9406(3)	785(3)	47(1)
N(2)	1957(2)	7582(4)	1420(3)	50(1)
N(3)	4448(2)	5780(3)	2075(3)	48(1)
C(13)	4050(3)	3139(5)	1107(6)	106(4)
C(14)	4728(4)	3091(7)	11(5)	140(4)
C(15)	4953(3)	1797(5)	1280(6)	121(4)
C(16)	4704(3)	6619(4)	2464(4)	67(2)
C(17)	3901(2)	5649(5)	2201(4)	65(2)
C(18)	4367(3)	5901(5)	1270(4)	65(2)

APPENDIX A.3.Crystal data and structure refinement for (3,5-Me₂C₅H₃N)₂Co(SSiMe₃)₂, **2a**

Empirical formula	C ₂₀ H ₃₆ Co N ₂ S ₂ Si ₂	
Formula weight	483.74	
Temperature	150(2) K	
Wavelength	0.71073 Å	
Crystal system	Orthorhombic	
Space group	Pca2(1)	
Unit cell dimensions	a = 16.961(4) Å	α = 90°.
	b = 8.704(2) Å	β = 90°.
	c = 17.945(5) Å	γ = 90°.
Volume	2649.2(11) Å ³	
Z	4	
Density (calculated)	1.213 Mg/m ³	
Absorption coefficient	0.904 mm ⁻¹	
F(000)	1028	
Crystal size	0.15 x 0.06 x 0.04 mm ³	
Theta range for data collection	2.27 to 24.48°.	
Index ranges	-19<=h<=18, -8<=k<=10, -20<=l<=20	
Reflections collected	9122	
Independent reflections	3851 [R(int) = 0.0586]	
Completeness to theta = 24.48°	92.1 %	
Refinement method	Full-matrix least-squares on F ²	
Data / restraints / parameters	3851 / 1 / 254	
Goodness-of-fit on F ²	1.061	
Final R indices [I>2sigma(I)]	R1 = 0.0575, wR2 = 0.1079	
R indices (all data)	R1 = 0.0999, wR2 = 0.1295	
Absolute structure parameter	-0.02(4)	
Largest diff. peak and hole	0.601 and -0.383 e.Å ⁻³	

Atomic coordinates ($\times 10^4$) and equivalent isotropic displacement parameters ($\text{\AA}^2 \times 10^3$)

for (3,5-Me₂C₃H₃N)₂Co(SSiMe₃)₂, 2a. U(eq) is defined as one third of the trace of the orthogonalized U^{ij} tensor.

	x	y	z	U(eq)
Co(1)	1258(1)	11885(1)	7180(1)	38(1)
S(1)	1931(1)	12959(3)	8153(1)	43(1)
S(2)	583(2)	13052(3)	6235(2)	45(1)
Si(1)	1186(3)	14704(5)	8584(2)	45(1)
Si(2)	1320(3)	14765(4)	5783(2)	43(1)
N(1)	2086(6)	10421(11)	6711(5)	35(2)
N(2)	438(6)	10416(12)	7633(5)	39(2)
C(14)	2512(6)	9515(12)	7144(7)	44(2)
C(15)	3114(5)	8567(10)	6876(6)	47(3)
C(19)	3558(6)	7529(11)	7372(7)	68(4)
C(16)	3255(6)	8633(11)	6113(6)	50(3)
C(17)	2817(8)	9597(14)	5663(8)	53(3)
C(18)	2234(7)	10469(14)	5984(7)	45(3)
C(20)	2950(11)	9668(14)	4816(8)	74(5)
C(7)	285(7)	10408(13)	8374(7)	46(3)
C(8)	-304(7)	9562(14)	8702(7)	46(3)
C(9)	-743(5)	8618(10)	8228(6)	48(2)
C(10)	-593(5)	8534(10)	7468(5)	43(2)
C(13)	-1048(6)	7472(10)	6959(5)	54(3)
C(11)	-13(6)	9489(12)	7201(7)	42(2)
C(12)	-470(10)	9664(15)	9517(9)	72(4)
C(3)	1589(8)	16628(12)	8333(7)	72(4)
C(2)	167(8)	14601(12)	8208(9)	50(3)
C(1)	1145(9)	14516(19)	9642(7)	75(4)
C(6)	2343(8)	14720(11)	6180(9)	51(3)
C(4)	1415(9)	14539(18)	4771(8)	72(4)
C(5)	891(7)	16710(12)	5977(8)	67(3)

APPENDIX A.4.**Crystal data and structure refinement for (3,5-Me₂-C₅H₃N)₂Co(SeSiMe₃)₂, **2b****

Empirical formula	C ₂₀ H ₃₆ Co N ₂ Se ₂ Si ₂	
Formula weight	577.54	
Temperature	200(2) K	
Wavelength	0.71073 Å	
Crystal system	Triclinic	
Space group	P-1	
Unit cell dimensions	a = 9.0799(4) Å	α = 95.734(2)°.
	b = 9.9145(5) Å	β = 91.369(2)°.
	c = 16.6353(6) Å	γ = 115.881(2)°.
Volume	1336.79(10) Å ³	
Z	2	
Density (calculated)	1.435 Mg/m ³	
Absorption coefficient	3.462 mm ⁻¹	
F(000)	586	
Crystal size	0.14 x 0.05 x 0.04 mm ³	
Theta range for data collection	2.30 to 27.68°.	
Index ranges	-11 ≤ h ≤ 11, -12 ≤ k ≤ 12, -21 ≤ l ≤ 20	
Reflections collected	14442	
Independent reflections	6176 [R(int) = 0.0635]	
Completeness to theta = 27.68°	98.8 %	
Refinement method	Full-matrix least-squares on F ²	
Data / restraints / parameters	6176 / 0 / 253	
Goodness-of-fit on F ²	1.031	
Final R indices [I > 2σ(I)]	R1 = 0.0461, wR2 = 0.1194	
R indices (all data)	R1 = 0.0618, wR2 = 0.1286	
Largest diff. peak and hole	1.026 and -1.135 e.Å ⁻³	

Atomic coordinates ($\times 10^4$) and equivalent isotropic displacement parameters ($\text{\AA}^2 \times 10^3$)
 for $(3,5\text{-Me}_2\text{-C}_5\text{H}_3\text{N})_2\text{Co}(\text{SeSiMe}_3)_2$. $U(\text{eq})$ is defined as one third of the trace of the orthogonalized U^{ij}
 tensor.

	x	y	z	U(eq)
Co(1)	11990(1)	5002(1)	-2498(1)	20(1)
Se(1)	12301(1)	3052(1)	-1875(1)	27(1)
Se(2)	14107(1)	7078(1)	-3049(1)	25(1)
Si(1)	13198(1)	1861(1)	-2828(1)	27(1)
Si(2)	16262(1)	7675(1)	-2144(1)	24(1)
N(2)	10090(4)	4092(4)	-3387(2)	23(1)
N(1)	10943(4)	5856(4)	-1625(2)	22(1)
C(1)	11623(6)	-148(5)	-3104(3)	41(1)
C(2)	13654(6)	2820(5)	-3765(3)	36(1)
C(3)	15102(7)	1819(6)	-2413(3)	51(1)
C(4)	17618(6)	9753(5)	-2061(3)	43(1)
C(5)	17453(6)	6637(6)	-2506(3)	44(1)
C(6)	15639(5)	7196(5)	-1112(2)	35(1)
C(7)	9323(5)	2602(5)	-3629(2)	26(1)
C(8)	8074(5)	1962(5)	-4245(2)	31(1)
C(9)	7606(5)	2920(5)	-4611(2)	33(1)
C(10)	8358(5)	4465(5)	-4363(2)	28(1)
C(11)	9597(5)	5001(5)	-3748(2)	25(1)
C(12)	7268(7)	277(6)	-4490(3)	50(1)
C(13)	7836(6)	5532(6)	-4738(3)	39(1)
C(14)	9583(5)	4927(5)	-1304(2)	26(1)
C(15)	8854(5)	5438(5)	-695(2)	30(1)
C(16)	9613(5)	6965(5)	-412(2)	31(1)
C(17)	11011(5)	7948(5)	-740(2)	30(1)
C(18)	11627(5)	7339(5)	-1352(2)	26(1)
C(19)	7300(6)	4360(6)	-371(3)	40(1)
C(20)	11845(7)	9614(6)	-455(3)	48(1)

APPENDIX A.5.

Crystal data and structure refinement for [Li(*N,N'*-tmeda)]₂[(*N,N'*-tmeda)Mn₅(SSiMe₃)₆(S)₃], **3a**

Empirical formula	C ₃₆ H ₁₀₂ Li ₆ Mn ₅ N ₂ S ₉ Si ₆
Formula weight	1336.62
Temperature	150(2) K
Wavelength	0.71073 Å
Crystal system	Monoclinic
Space group	P2(1)/c
Unit cell dimensions	a = 16.7280(8) Å α = 90°. b = 17.8065(8) Å β = 93.0000(10)°. c = 29.6483(15) Å γ = 90°.
Volume	8819.2(7) Å ³
Z	4
Density (calculated)	1.007 Mg/m ³
Absorption coefficient	1.010 mm ⁻¹
F(000)	2812
Crystal size	0.107x 0.097 x 0.057 mm ³
Theta range for data collection	1.33 to 25.00°.
Index ranges	-19<=h<=19, -21<=k<=20, -35<=l<=35
Reflections collected	62546
Independent reflections	15509 [R(int) = 0.0560]
Completeness to theta = 25.00°	100.0 %
Refinement method	Full-matrix least-squares on F ²
Data / restraints / parameters	15509 / 66 / 627
Goodness-of-fit on F ²	1.107
Final R indices [I>2sigma(I)]	R1 = 0.0491, wR2 = 0.1496
R indices (all data)	R1 = 0.0770, wR2 = 0.1615
Largest diff. peak and hole	1.445 and -0.444 e.Å ⁻³

Atomic coordinates ($\times 10^4$) and equivalent isotropic displacement parameters ($\text{\AA}^2 \times 10^3$)

for $[\text{Li}(\text{N}, \text{N}'\text{-tmeda})]_2[(\text{N}, \text{N}'\text{-tmeda})\text{Mn}_5(\text{SSiMe}_3)_6(\text{S})_3]$. $U(\text{eq})$ is defined as one third of the trace of the orthogonalized U^{ij} tensor.

	x	y	z	U(eq)
Mn(1)	3172(1)	5766(1)	3462(1)	27(1)
Mn(2)	4354(1)	7275(1)	3117(1)	24(1)
Mn(3)	2634(1)	7186(1)	2690(1)	25(1)
Mn(4)	1987(1)	7348(1)	3597(1)	25(1)
Mn(5)	3704(1)	7433(1)	4026(1)	25(1)
S(1)	5566(1)	8018(1)	3106(1)	30(1)
S(2)	3893(1)	6739(1)	2380(1)	27(1)
S(3)	1760(1)	7859(1)	2156(1)	31(1)
S(4)	769(1)	8064(1)	3496(1)	32(1)
S(5)	2453(1)	7104(1)	4382(1)	30(1)
S(6)	4620(1)	8237(1)	4458(1)	33(1)
S(7)	4374(1)	6364(1)	3717(1)	28(1)
S(8)	1966(1)	6246(1)	3123(1)	27(1)
S(9)	3162(1)	8036(1)	3310(1)	23(1)
Si(1)	6469(1)	7177(1)	3097(1)	33(1)
Si(2)	4185(1)	7585(1)	1898(1)	28(1)
Si(3)	1213(1)	7002(1)	1752(1)	33(1)
Si(4)	-126(1)	7267(1)	3644(1)	37(1)
Si(5)	2112(1)	8081(1)	4753(1)	35(1)
Si(6)	5153(1)	7522(1)	4960(1)	36(1)
Li(1)	5404(5)	8728(4)	3829(3)	35(2)
Li(2)	949(5)	8512(4)	2711(3)	34(2)
N(1)	3426(2)	4745(2)	3052(1)	31(1)
N(2)	2919(2)	4895(2)	3990(1)	37(1)
N(3)	4832(2)	9758(2)	3626(1)	33(1)
N(4)	6415(3)	9362(2)	4061(2)	44(1)
N(5)	1498(2)	9600(2)	2777(1)	34(1)
N(6)	-97(2)	9049(2)	2422(2)	45(1)
C(1)	6095(3)	6285(3)	2833(2)	51(2)
C(2)	6867(4)	6940(4)	3679(2)	66(2)
C(3)	7308(3)	7557(4)	2770(2)	62(2)
C(4)	3956(3)	8538(2)	2103(2)	35(1)
C(5)	5269(3)	7501(3)	1794(2)	36(1)
C(6)	3596(3)	7422(3)	1358(2)	39(1)
C(7)	1856(3)	6143(3)	1739(2)	58(2)
C(8)	235(3)	6716(3)	1971(2)	57(2)
C(9)	1032(4)	7366(3)	1164(2)	54(2)
C(10)	-530(4)	6765(4)	3125(2)	63(2)
C(11)	-963(3)	7786(4)	3900(2)	59(2)
C(12)	256(3)	6520(3)	4038(2)	56(2)
C(13)	2282(3)	8965(3)	4440(2)	49(1)
C(14)	1030(3)	7993(3)	4875(2)	49(1)
C(15)	2729(3)	8106(3)	5297(2)	50(1)
C(16)	6137(4)	7141(4)	4802(2)	75(2)
C(17)	5325(4)	8094(4)	5481(2)	59(2)
C(18)	4498(4)	6705(3)	5089(2)	55(2)

APPENDIX A.6.

Crystal data and structure refinement for [Li(*N,N'*-tmeda)]₂[(*N,N'*-tmeda)Mn₅(SeSiMe₃)₆(Se)₃], **3b**

Empirical formula	C ₄₂ H ₁₁₆ Li ₂ Mn ₅ N ₆ Se ₉ Si ₆	
Formula weight	1873.17	
Temperature	150(2) K	
Wavelength	0.71073 Å	
Crystal system	Monoclinic	
Space group	C2/c	
Unit cell dimensions	a = 16.6855(9) Å	α = 90°.
	b = 18.3900(9) Å	β = 91.3410(10)°.
	c = 26.4291(15) Å	γ = 90°.
Volume	8107.5(7) Å ³	
Z	4	
Density (calculated)	1.535 Mg/m ³	
Absorption coefficient	4.915 mm ⁻¹	
F(000)	3724	
Crystal size	0.085 x 0.084 x 0.020 mm ³	
Theta range for data collection	1.65 to 26.76°.	
Index ranges	-20 ≤ h ≤ 17, -23 ≤ k ≤ 14, -32 ≤ l ≤ 33	
Reflections collected	31175	
Independent reflections	8592 [R(int) = 0.0403]	
Completeness to theta = 26.76°	99.4 %	
Absorption correction	None	
Max. and min. transmission	0.675 and 0.498	
Refinement method	Full-matrix least-squares on F ²	
Data / restraints / parameters	8592 / 0 / 318	
Goodness-of-fit on F ²	1.095	
Final R indices [I > 2σ(I)]	R1 = 0.0505, wR2 = 0.1003	
R indices (all data)	R1 = 0.0845, wR2 = 0.1119	
Largest diff. peak and hole	0.897 and -0.773 e.Å ⁻³	

Atomic coordinates ($\times 10^4$) and equivalent isotropic displacement parameters ($\text{\AA}^2 \times 10^3$)

for $[\text{Li}(\text{N}, \text{N}'\text{-tmeda})]_2[(\text{N}, \text{N}'\text{-tmeda})\text{Mn}_5(\text{SeSiMe}_3)_6(\text{Se})_3]$. $U(\text{eq})$ is defined as one third of the trace of the orthogonalized U^{ij} tensor.

	x	y	z	U(eq)
Se(1)	218(1)	1513(1)	4084(1)	42(1)
Se(2)	1788(1)	2745(1)	3150(1)	37(1)
Se(3)	-2290(1)	1584(1)	3221(1)	39(1)
Se(4)	-658(1)	3323(1)	3246(1)	33(1)
Se(5)	0	1525(1)	2500	30(1)
Mn(1)	0	3870(1)	2500	31(1)
Mn(2)	-1267(1)	2301(1)	2726(1)	33(1)
Mn(3)	348(1)	2299(1)	3305(1)	33(1)
Si(1)	212(1)	2395(1)	4684(1)	49(1)
Si(2)	2536(1)	1784(1)	3446(1)	46(1)
Si(3)	-3089(1)	2501(1)	3495(1)	48(1)
Li(1)	-1181(7)	991(6)	3838(5)	54(3)
N(1)	766(3)	4789(3)	2793(2)	41(1)
N(2)	-1740(4)	461(4)	4431(3)	81(2)
N(3)	-929(3)	-53(3)	3515(3)	61(2)
C(1)	568(6)	1971(5)	5292(3)	80(3)
C(2)	-814(5)	2756(5)	4772(3)	76(2)
C(3)	887(5)	3163(4)	4527(3)	63(2)
C(4)	2613(5)	1860(5)	4152(3)	68(2)
C(5)	3557(4)	1878(4)	3177(3)	64(2)
C(6)	2074(4)	903(3)	3260(3)	48(2)
C(7)	-2731(5)	2901(5)	4105(4)	85(3)
C(8)	-3155(5)	3257(5)	3032(4)	88(3)
C(9)	-4106(4)	2115(5)	3592(4)	92(3)
C(10)	1486(4)	4873(4)	2483(3)	55(2)
C(11)	1026(4)	4714(4)	3325(3)	52(2)
C(12)	241(4)	5438(3)	2742(3)	53(2)
C(13)	-1262(6)	401(7)	4895(4)	112(4)
C(14)	-2522(5)	707(6)	4563(4)	94(3)
C(15)	-1887(8)	-278(6)	4159(5)	136(5)
C(16)	-1227(8)	-557(6)	3864(4)	108(4)
C(17)	-96(5)	-222(5)	3420(4)	85(3)
C(18)	-1359(5)	-183(5)	3018(3)	80(3)
C(1S)	1249(11)	5102(10)	5821(7)	205(8)
C(2S)	511(10)	4755(9)	5636(6)	185(7)
C(3S)	391(8)	5123(9)	5072(6)	165(6)

APPENDIX A.7.Crystal data and structure refinement for [Li(*N,N'*-tmeda)]₂[Mn(SSiMe₃)₄], **4**.

Empirical formula	C ₂₄ H ₆₈ Li ₂ Mn N ₄ S ₄ Si ₄
Formula weight	722.24
Temperature	150(2) K
Wavelength	0.71073 Å
Crystal system	Tetragonal
Space group	P4(1)
Unit cell dimensions	a = 11.1899(3) Å α = 90° b = 11.1899(3) Å β = 90° c = 35.4570(10) Å γ = 90°
Volume	4439.7(2) Å ³
Z	4
Density (calculated)	1.081 Mg/m ³
Absorption coefficient	0.612 mm ⁻¹
F(000)	1564
Crystal size	0.18 x 0.10 x 0.08 mm ³
Theta range for data collection	1.82 to 25.04°
Index ranges	-3 ≤ h ≤ 13, -9 ≤ k ≤ 11, -42 ≤ l ≤ 29
Reflections collected	9628
Independent reflections	6117 [R(int) = 0.0395]
Completeness to theta = 25.04°	98.0 %
Max. and min. transmission	0.9527 and 0.8979
Refinement method	Full-matrix least-squares on F ²
Data / restraints / parameters	6117 / 1 / 362
Goodness-of-fit on F ²	1.030
Final R indices [I > 2σ(I)]	R1 = 0.0398, wR2 = 0.0904
R indices (all data)	R1 = 0.0466, wR2 = 0.0943
Absolute structure parameter	0.00
Largest diff. peak and hole	0.325 and -0.317 e.Å ⁻³

Atomic coordinates ($\times 10^4$) and equivalent isotropic displacement parameters ($\text{\AA}^2 \times 10^3$)

for $[\text{Li}(\text{N},\text{N}'\text{-tmeda})]_2[\text{Mn}(\text{SSiMe}_3)_4]$. $U(\text{eq})$ is defined as one third of the trace of the orthogonalized U^{ij} tensor.

	x	y	z	U(eq)
Mn(1)	1000(1)	-6465(1)	698(1)	28(1)
S(1)	891(1)	-4327(1)	845(1)	31(1)
S(2)	3137(1)	-6573(1)	555(1)	32(1)
S(3)	-360(1)	-7218(1)	219(1)	42(1)
S(4)	337(1)	-7822(1)	1192(1)	36(1)
Si(1)	33(1)	-4108(1)	1371(1)	36(1)
Si(2)	3415(1)	-7415(1)	31(1)	38(1)
Si(3)	-1281(1)	-5858(1)	-65(1)	41(1)
Si(4)	1808(1)	-8681(1)	1447(1)	35(1)
N(1)	4289(3)	-3889(4)	1106(1)	39(1)
N(2)	3649(3)	-3090(3)	356(1)	37(1)
N(3)	-2685(4)	-8888(4)	1016(2)	50(1)
N(4)	-1367(4)	-10241(3)	454(1)	40(1)
C(1)	-1531(5)	-4622(7)	1336(2)	71(2)
C(2)	60(6)	-2487(5)	1502(2)	64(2)
C(3)	733(5)	-4928(5)	1766(2)	51(1)
C(4)	2583(8)	-8810(6)	-17(2)	98(3)
C(5)	3034(12)	-6477(7)	-369(2)	139(5)
C(6)	5030(7)	-7725(12)	-11(3)	175(7)
C(7)	-2347(6)	-5059(7)	247(2)	75(2)
C(8)	-245(6)	-4738(6)	-261(2)	71(2)
C(9)	-2123(6)	-6597(6)	-458(2)	63(2)
C(10)	1242(5)	-9464(5)	1878(2)	49(1)
C(11)	2526(5)	-9784(5)	1127(2)	58(2)
C(12)	2973(5)	-7587(5)	1590(2)	45(1)
C(13)	3682(6)	-3176(6)	1398(2)	71(2)
C(14)	5019(6)	-4821(6)	1284(2)	70(2)
C(15)	5065(5)	-3112(5)	883(2)	54(2)
C(16)	4371(5)	-2363(5)	610(2)	56(2)
C(17)	2709(5)	-2345(5)	184(2)	57(2)
C(18)	4376(5)	-3612(5)	49(2)	57(2)
C(19)	-3488(6)	-7875(5)	1037(2)	61(2)
C(20)	-2375(6)	-9256(6)	1402(2)	71(2)
C(21)	-3228(5)	-9903(5)	830(2)	65(2)
C(22)	-2294(5)	-10816(5)	701(2)	61(2)
C(23)	-1852(5)	-10066(5)	72(2)	58(2)
C(24)	-333(5)	-11032(5)	428(2)	54(2)
Li(2)	-1072(7)	-8591(7)	715(3)	39(2)
Li(1)	3024(6)	-4447(6)	712(3)	31(2)

APPENDIX A.8.**Crystal data and structure refinement for [Li(N,N'-tmeda)]₄[Mn₄(SeSiMe₃)₄(Se)₄], 5**

Empirical formula	C ₃₆ H ₁₀₀ Li ₄ Mn ₄ N ₈ Se ₈ Si ₄	
Formula weight	1636.80	
Temperature	150(2) K	
Wavelength	0.71073 Å	
Crystal system	Triclinic	
Space group	P-1	
Unit cell dimensions	a = 12.1008(3) Å	α = 99.7010(10)°.
	b = 14.1392(4) Å	β = 90.315(2)°.
	c = 22.2136(6) Å	γ = 104.171(10)°.
Volume	3627.95(17) Å ³	
Z	2	
Density (calculated)	1.498 Mg/m ³	
Absorption coefficient	4.787 mm ⁻¹	
F(000)	1624	
Crystal size	0.30 x 0.20 x 0.18 mm ³	
Theta range for data collection	1.74 to 27.58°.	
Index ranges	-15 ≤ h ≤ 15, -18 ≤ k ≤ 18, -28 ≤ l ≤ 28	
Reflections collected	57627	
Independent reflections	16647 [R(int) = 0.0811]	
Completeness to theta = 27.58°	99.0 %	
Max. and min. transmission	0.4795 and 0.3277	
Refinement method	Full-matrix least-squares on F ²	
Data / restraints / parameters	16647 / 0 / 604	
Goodness-of-fit on F ²	1.039	
Final R indices [I > 2σ(I)]	R1 = 0.0534, wR2 = 0.1208	
R indices (all data)	R1 = 0.1040, wR2 = 0.1418	
Largest diff. peak and hole	1.973 and -1.125 e.Å ⁻³	

Atomic coordinates ($\times 10^4$) and equivalent isotropic displacement parameters ($\text{\AA}^2 \times 10^3$)

for $[\text{Li}(\text{N}, \text{N}'\text{meda})]_4[\text{Mn}_4(\text{SeSiMe}_3)_4(\text{Se})_4]$. $U(\text{eq})$ is defined as one third of the trace of the orthogonalized U^{ij} tensor.

	x	y	z	$U(\text{eq})$
Mn(1)	2952(1)	3748(1)	3204(1)	34(1)
Mn(2)	3339(1)	3222(1)	1799(1)	35(1)
Mn(3)	4872(1)	5192(1)	2637(1)	35(1)
Mn(4)	2338(1)	5011(1)	2253(1)	34(1)
Se(1)	4747(1)	3362(1)	2687(1)	36(1)
Se(2)	1436(1)	3206(1)	2336(1)	35(1)
Se(3)	3937(1)	4976(1)	1536(1)	35(1)
Se(4)	3363(1)	5645(1)	3335(1)	35(1)
Se(5)	2742(1)	3030(1)	4186(1)	42(1)
Se(6)	788(1)	5902(1)	2161(1)	42(1)
Se(7)	2864(1)	1839(1)	871(1)	49(1)
Se(8)	6891(1)	6281(1)	2673(1)	45(1)
Si(1)	1250(2)	1697(1)	3947(1)	45(1)
Si(2)	1620(2)	7027(1)	1595(1)	45(1)
Si(3)	3730(2)	742(1)	1167(1)	53(1)
Si(4)	6740(2)	7752(1)	3191(1)	51(1)
Li(1)	870(9)	1954(8)	1370(5)	48(3)
Li(2)	4641(8)	2747(7)	3724(5)	42(2)
Li(3)	1558(9)	6280(8)	3283(4)	45(2)
Li(4)	6063(9)	5913(9)	1553(5)	52(3)
N(1)	244(4)	5571(4)	3761(3)	55(1)
N(2)	1570(5)	7604(4)	3831(2)	59(2)
N(3)	5450(5)	1579(4)	3732(3)	56(1)
N(4)	5980(4)	3676(4)	4300(2)	45(1)
N(5)	-642(5)	936(4)	1500(3)	60(2)
N(6)	13(4)	2399(4)	705(2)	47(1)
N(7)	6301(5)	6848(5)	897(3)	67(2)
N(8)	6943(5)	5012(5)	1029(3)	67(2)
C(1)	-103(6)	2088(5)	3881(3)	60(2)
C(2)	1396(6)	884(5)	3224(3)	54(2)
C(3)	1144(6)	964(5)	4582(3)	60(2)
C(4)	1697(7)	6405(5)	800(3)	65(2)
C(5)	730(6)	7951(5)	1608(3)	65(2)
C(6)	3085(6)	7688(5)	1893(3)	62(2)
C(7)	3273(7)	442(5)	1923(3)	66(2)
C(8)	5306(7)	1253(6)	1218(4)	80(2)
C(9)	3353(8)	-417(5)	574(3)	82(3)
C(10)	5576(7)	8168(6)	2850(4)	86(3)
C(11)	8109(6)	8696(6)	3154(5)	88(3)
C(12)	6439(9)	7674(7)	4004(4)	108(4)
C(13)	1074(9)	8211(7)	3482(4)	102(3)
C(14)	2673(9)	8167(6)	4112(4)	99(3)
C(15)	-126(8)	6385(8)	4101(5)	99(3)
C(16)	807(9)	7294(7)	4302(4)	96(3)
C(17)	616(7)	4982(6)	4153(4)	77(2)
C(18)	-703(7)	4901(7)	3353(4)	85(3)

APPENDIX A.9.Crystal data and structure refinement for [Li(*N,N'*-tmeda)]₄[Mn(Se₄)₃], **6**.

Empirical formula	C ₂₄ H ₆₄ Li ₄ Mn N ₈ Se ₁₂	
Formula weight	1495.05	
Temperature	150(2) K	
Wavelength	0.71073 Å	
Crystal system	Monoclinic	
Space group	P2(1)/n	
Unit cell dimensions	a = 18.8776(8) Å	α = 90°.
	b = 14.5127(4) Å	β = 108.080(2)°.
	c = 19.4562(8) Å	γ = 90°.
Volume	5067.1(3) Å ³	
Z	4	
Density (calculated)	1.960 Mg/m ³	
Absorption coefficient	8.906 mm ⁻¹	
F(000)	2836	
Crystal size	0.22 x 0.20 x 0.18 mm ³	
Theta range for data collection	1.78 to 27.55°.	
Index ranges	-22 ≤ h ≤ 24, -18 ≤ k ≤ 16, -25 ≤ l ≤ 24	
Reflections collected	35722	
Independent reflections	11633 [R(int) = 0.1203]	
Completeness to theta = 27.55°	99.4 %	
Max. and min. transmission	0.2970 and 0.2447	
Refinement method	Full-matrix least-squares on F ²	
Data / restraints / parameters	11633 / 0 / 442	
Goodness-of-fit on F ²	0.998	
Final R indices [I > 2σ(I)]	R1 = 0.0695, wR2 = 0.1669	
R indices (all data)	R1 = 0.1264, wR2 = 0.2026	
Largest diff. peak and hole	1.771 and -2.148 e.Å ⁻³	

Atomic coordinates ($\times 10^4$) and equivalent isotropic displacement parameters ($\text{\AA}^2 \times 10^3$)

for $[\text{Li}(\text{N}, \text{N}'\text{-tmeda})_4][\text{Mn}(\text{Se}_4)_3]$. $U(\text{eq})$ is defined as one third of the trace of the orthogonalized U^{ij} tensor.

	x	y	z	U(eq)
Mn	2427(1)	2392(1)	4783(1)	33(1)
Se(1)	3704(1)	2534(1)	5893(1)	39(1)
Se(2)	2962(1)	923(1)	4155(1)	39(1)
Se(3)	2032(1)	1220(1)	5726(1)	38(1)
Se(4)	1172(1)	2183(1)	3708(1)	42(1)
Se(5)	2919(1)	3703(1)	4070(1)	41(1)
Se(6)	1741(1)	3689(1)	5419(1)	43(1)
Se(7)	954(1)	494(1)	4982(1)	45(1)
Se(8)	4258(1)	990(1)	4694(1)	43(1)
Se(9)	4465(1)	2494(1)	5146(1)	45(1)
Se(10)	1071(1)	583(1)	3818(1)	49(1)
Se(11)	1749(1)	4390(1)	3630(1)	56(1)
Se(12)	1611(1)	4995(1)	4693(1)	60(1)
C(1)	3820(8)	495(9)	7210(6)	83(4)
C(2)	4227(8)	-802(8)	6651(7)	77(4)
C(3)	2450(6)	-1272(7)	5217(9)	87(5)
C(4)	-315(6)	3749(7)	4219(7)	69(3)
C(5)	904(7)	2758(8)	6682(6)	65(3)
C(6)	-755(6)	2216(8)	3852(6)	65(3)
C(7)	131(6)	1496(6)	6179(6)	60(3)
C(9)	3623(6)	-1319(6)	5032(6)	61(3)
C(10)	-765(6)	2763(7)	5034(6)	51(3)
C(13)	-268(7)	3024(7)	5762(6)	64(3)
C(14)	3541(9)	-1269(7)	6255(8)	84(4)
C(16)	3235(9)	4003(10)	7333(7)	99(5)
C(17)	2636(7)	5390(8)	6827(6)	71(3)
C(18)	4672(6)	4821(7)	5817(7)	65(3)
C(19)	3939(7)	5239(11)	7015(7)	91(5)
C(20)	4000(7)	5823(9)	6402(8)	85(4)
C(21)	3744(7)	5878(7)	5125(7)	78(4)
C(22)	4892(6)	617(7)	6800(6)	61(3)
C(25)	1475(13)	1217(17)	1991(10)	250(18)
C(26)	4022(11)	3022(18)	2953(10)	222(16)
C(28)	3046(9)	2646(12)	1909(9)	106(5)
C(29)	1394(10)	2862(14)	1899(8)	150(9)
C(31)	2361(6)	2052(9)	1613(6)	62(3)
C(32)	3787(12)	1551(16)	2648(11)	171(9)
Li(1)	739(9)	2349(10)	5061(8)	42(4)
Li(2)	3331(9)	532(10)	5609(8)	42(4)
Li(4)	2587(10)	2275(10)	3156(8)	46(4)
N(1)	1898(5)	2019(8)	2096(5)	68(3)
N(2)	4152(4)	219(5)	6647(4)	44(2)
N(6)	357(4)	2410(5)	6002(4)	43(2)
N(7)	3232(5)	4749(7)	6810(4)	59(2)
N(8)	3956(4)	5278(5)	5762(5)	48(2)

APPENDIX A.10.Crystal data and structure refinement for of $(N,N'$ -tmeda) $_6$ Zn $_{12.3}$ Mn $_{1.7}$ S $_{13}$ Cl $_2$, **7a**

Empirical formula	C ₄₅ H ₁₁₄ Cl ₂₀ Mn ₂ N ₁₂ S ₁₃ Zn ₁₂	
Formula weight	2843.58	
Temperature	150(2) K	
Wavelength	0.71073 Å	
Crystal system	Triclinic	
Space group	P-1	
Unit cell dimensions	a = 13.5003(7) Å	α = 99.918(2)°.
	b = 13.7288(7) Å	β = 93.060(3)°.
	c = 28.6237(14) Å	γ = 93.835(2)°.
Volume	5202.8(5) Å ³	
Z	2	
Density (calculated)	1.815 Mg/m ³	
Absorption coefficient	3.754 mm ⁻¹	
F(000)	2852	
Crystal size	0.31 x 0.30 x 0.20 mm ³	
Theta range for data collection	0.72 to 26.73°.	
Index ranges	-16<=h<=17, -17<=k<=17, -36<=l<=36	
Reflections collected	84312	
Independent reflections	22061 [R(int) = 0.0678]	
Completeness to theta = 26.73°	99.7 %	
Refinement method	Full-matrix least-squares on F ²	
Data / restraints / parameters	22061 / 0 / 937	
Goodness-of-fit on F ²	1.039	
Final R indices [I>2sigma(I)]	R1 = 0.0543, wR2 = 0.1178	
R indices (all data)	R1 = 0.1076, wR2 = 0.1355	
Largest diff. peak and hole	1.491 and -1.248 e.Å ⁻³	

Atomic coordinates ($\times 10^4$) and equivalent isotropic displacement parameters ($\text{\AA}^2 \times 10^3$)

for $(N,N'$ -tmeda) $_6\text{Zn}_{12,3}\text{Mn}_{1,7}\text{S}_{13}\text{Cl}_2$. $U(\text{eq})$ is defined as one third of the trace of the orthogonalized U^{ij} tensor.

	x	y	z	U(eq)
Zn(10)	-950(1)	3430(1)	1998(1)	20(1)
Zn(8)	1830(1)	4142(1)	2592(1)	20(1)
Zn(5)	-733(1)	7340(1)	3339(1)	20(1)
Zn(6)	1722(1)	4086(1)	3791(1)	19(1)
Zn(1)	2690(1)	6182(1)	2180(1)	20(1)
Zn(3)	-1397(1)	5236(1)	1337(1)	19(1)
Zn(4)	-2415(1)	3166(1)	2957(1)	19(1)
Zn(2)	1005(1)	1996(1)	1809(1)	19(1)
Zn(12)	1072(1)	4315(1)	1383(1)	14(1)
Zn(9)	-464(1)	4914(1)	3389(1)	20(1)
Zn(11)	-1828(1)	5331(1)	2530(1)	12(1)
Zn(7)	251(1)	6227(1)	2291(1)	20(1)
Zn(13)	1762(1)	6454(1)	3379(1)	15(1)
Zn(14)	68(1)	2820(1)	2899(1)	12(1)
Mn(12)	1072(1)	4315(1)	1383(1)	14(1)
Mn(11)	-1828(1)	5331(1)	2530(1)	12(1)
Mn(13)	1762(1)	6454(1)	3379(1)	15(1)
Mn(14)	68(1)	2820(1)	2899(1)	12(1)
S(6)	236(1)	5790(1)	1467(1)	19(1)
S(13)	100(1)	4634(1)	2581(1)	17(1)
S(3)	24(1)	2845(1)	1379(1)	19(1)
S(8)	-1411(1)	2213(1)	2479(1)	18(1)
S(4)	1547(1)	2400(1)	2591(1)	19(1)
S(9)	-1248(1)	6950(1)	2552(1)	20(1)
S(5)	-2289(1)	4346(1)	1809(1)	19(1)
S(11)	2588(1)	4968(1)	3325(1)	20(1)
S(2)	2524(1)	4516(1)	1911(1)	18(1)
S(7)	-2222(1)	4833(1)	3229(1)	19(1)
S(10)	235(1)	6460(1)	3763(1)	20(1)
S(1)	1693(1)	7114(1)	2665(1)	20(1)
S(12)	71(1)	3526(1)	3688(1)	19(1)
Cl(1)	2829(1)	7617(1)	3927(1)	28(1)
Cl(2)	1710(1)	4024(1)	618(1)	25(1)
Cl(2S)	-3525(2)	9277(2)	2653(1)	53(1)
Cl(1S)	-3432(2)	9406(2)	1658(1)	65(1)
Cl(3S)	-4769(2)	3928(2)	1294(1)	56(1)
Cl(5S)	-1169(2)	645(2)	5072(1)	65(1)
Cl(6S)	-438(2)	2357(2)	4687(1)	63(1)
Cl(7S)	3782(2)	-906(2)	5360(1)	75(1)
Cl(4S)	-5473(2)	4404(2)	406(1)	83(1)
C(24)	-4534(6)	3537(5)	2709(3)	44(2)
C(17)	-3135(5)	6514(5)	1392(3)	33(2)
C(36)	2760(6)	5506(6)	4628(3)	44(2)
C(15)	-2601(5)	5125(5)	463(3)	29(2)
C(20)	-2326(6)	1570(5)	3565(3)	37(2)

APPENDIX A.11.**Crystal data and structure refinement for $(N,N'$ -tmeda) $_6$ Zn $_{6.2}$ Mn $_{7.8}$ S $_{13}$ Cl $_2$, **7d****

Empirical formula	C ₄₄ H ₁₁₂ Cl ₁₈ Mn _{7.8} N ₁₂ S ₁₃ Zn _{6.2}	
Formula weight	2736.75	
Temperature	150(2) K	
Wavelength	0.71073 Å	
Crystal system	Triclinic	
Space group	P-1	
Unit cell dimensions	a = 13.6025(16) Å	$\alpha = 99.144(5)^\circ$.
	b = 13.7947(16) Å	$\beta = 92.894(6)^\circ$.
	c = 28.380(3) Å	$\gamma = 95.830(6)^\circ$.
Volume	5218.4(11) Å ³	
Z	2	
Density (calculated)	1.742 Mg/m ³	
Absorption coefficient	3.462 mm ⁻¹	
F(000)	2747	
Crystal size	0.35 x 0.15 x 0.14 mm ³	
Theta range for data collection	0.73 to 25.00°.	
Index ranges	-16 ≤ h ≤ 16, -16 ≤ k ≤ 16, -33 ≤ l ≤ 33	
Reflections collected	73480	
Independent reflections	18298 [R(int) = 0.0363]	
Completeness to theta = 25.00°	99.6 %	
Absorption correction	None	
Refinement method	Full-matrix least-squares on F ²	
Data / restraints / parameters	18298 / 0 / 988	
Goodness-of-fit on F ²	0.745	
Final R indices [I > 2σ(I)]	R1 = 0.0672, wR2 = 0.2059	
R indices (all data)	R1 = 0.0794, wR2 = 0.2142	
Largest diff. peak and hole	2.209 and -1.854 e.Å ⁻³	

Atomic coordinates ($\times 10^4$) and equivalent isotropic displacement parameters ($\text{\AA}^2 \times 10^3$)

for $(N,N'$ -tmeda) $_6$ Zn $_{6,2}$ Mn $_{7,8}$ S $_{13}$ Cl $_2$. U(eq) is defined as one third of the trace of the orthogonalized U^{ij} tensor.

	x	y	z	U(eq)
Mn(1)	11724(1)	1330(1)	3431(1)	18(1)
Mn(2)	11029(1)	-759(1)	1378(1)	16(1)
Mn(7)	10242(1)	1127(1)	2304(1)	19(1)
Mn(8)	9943(1)	-2326(1)	2912(1)	22(1)
Mn(9)	8151(1)	177(1)	2535(1)	21(1)
Mn(10)	8958(1)	-1715(1)	1996(1)	20(1)
Mn(11)	9452(1)	-254(1)	3420(1)	19(1)
Mn(12)	11759(1)	-979(1)	2618(1)	19(1)
Zn(1)	12685(1)	1100(1)	2202(1)	21(1)
Zn(2)	10902(1)	-3112(1)	1814(1)	21(1)
Zn(3)	8572(1)	138(1)	1338(1)	19(1)
Zn(4)	7465(1)	-2007(1)	2953(1)	20(1)
Zn(5)	9258(1)	2170(1)	3366(1)	19(1)
Zn(6)	11562(1)	-1110(1)	3837(1)	20(1)
Zn(7)	10242(1)	1127(1)	2304(1)	19(1)
Zn(8)	9943(1)	-2326(1)	2912(1)	22(1)
Zn(9)	8151(1)	177(1)	2535(1)	21(1)
Zn(10)	8958(1)	-1715(1)	1996(1)	20(1)
Zn(11)	9452(1)	-254(1)	3420(1)	19(1)
Zn(12)	11759(1)	-979(1)	2618(1)	19(1)
S(1)	11712(2)	2005(2)	2690(1)	21(1)
S(2)	12482(2)	-558(2)	1931(1)	20(1)
S(3)	9947(2)	-2277(2)	1376(1)	21(1)
S(4)	11415(2)	-2733(2)	2606(1)	20(1)
S(5)	7658(2)	-785(2)	1806(1)	20(1)
S(6)	10206(2)	723(2)	1465(1)	20(1)
S(7)	7700(2)	-350(2)	3236(1)	20(1)
S(8)	8451(2)	-2949(2)	2486(1)	20(1)
S(9)	8764(2)	1816(2)	2569(1)	20(1)
S(10)	10158(2)	1306(2)	3814(1)	21(1)
S(11)	12483(2)	-201(2)	3380(1)	21(1)
S(12)	9918(2)	-1685(2)	3718(1)	21(1)
S(13)	10030(1)	-506(1)	2599(1)	18(1)
Cl(1)	12818(2)	2529(2)	3974(1)	32(1)
Cl(2)	11683(2)	-1016(2)	603(1)	29(1)
N(1)	13077(6)	1958(6)	1646(3)	33(2)
N(2)	14237(5)	1445(6)	2446(3)	29(2)
N(3)	10291(6)	-4651(6)	1647(3)	30(2)
N(5)	7775(6)	1323(6)	1164(3)	28(2)
Cl(15)	5859(14)	-3758(13)	934(5)	146(7)
Cl(16)	7485(9)	-4179(9)	457(7)	146(6)
Cl(17)	16020(20)	3320(20)	193(10)	93(8)
Cl(17)	15570(70)	2940(40)	341(17)	280(50)
Cl(18)	14340(70)	3710(50)	400(30)	330(50)
Cl(18)	14190(20)	3940(30)	679(12)	135(15)

APPENDIX A.12.Crystal data and structure refinement for of $(N,N'$ -tmeda) $_6$ Zn $_{12}$ Mn $_2$ Se $_{13}$ Cl $_2$, **8a**

Empirical formula	C ₄₅ H ₁₁₀ Cl ₂₀ Mn ₂ N ₁₂ Se ₁₃ Zn ₁₂	
Formula weight	3449.25	
Temperature	150(2) K	
Wavelength	0.71073 Å	
Crystal system	Triclinic	
Space group	P-1	
Unit cell dimensions	a = 13.5535(7) Å	α = 99.455(2)°.
	b = 13.7519(7) Å	β = 92.747(2)°.
	c = 28.9793(15) Å	γ = 93.280(2)°.
Volume	5310.2(5) Å ³	
Z	2	
Density (calculated)	2.157 Mg/m ³	
Absorption coefficient	7.878 mm ⁻¹	
F(000)	3312	
Crystal size	0.34 x 0.28 x 0.22 mm ³	
Theta range for data collection	0.71 to 29.19°.	
Index ranges	-18<=h<=16, -18<=k<=18, -39<=l<=39	
Reflections collected	261422	
Independent reflections	28609 [R(int) = 0.0883]	
Completeness to theta = 29.19°	99.6 %	
Refinement method	Full-matrix least-squares on F ²	
Data / restraints / parameters	28609 / 0 / 945	
Goodness-of-fit on F ²	1.090	
Final R indices [I>2σ(I)]	R1 = 0.0592, wR2 = 0.1389	
R indices (all data)	R1 = 0.1000, wR2 = 0.1564	
Largest diff. peak and hole	2.134 and -2.239 e.Å ⁻³	

Atomic coordinates ($\times 10^4$) and equivalent isotropic displacement parameters ($\text{\AA}^2 \times 10^3$)

for $(N,N'$ -tmeda) $_6\text{Zn}_{12}\text{Mn}_2\text{Se}_{13}\text{Cl}_2$. $U(\text{eq})$ is defined as one third of the trace of the orthogonalized U^{ij} tensor.

	x	y	z	$U(\text{eq})$
Zn(1)	2229(1)	-1186(1)	2830(1)	18(1)
Zn(2)	5795(1)	-2452(1)	1645(1)	19(1)
Zn(3)	3294(1)	947(1)	1159(1)	18(1)
Zn(4)	7558(1)	1868(1)	2012(1)	18(1)
Zn(5)	3988(1)	3136(1)	3194(1)	18(1)
Zn(6)	6465(1)	-251(1)	3702(1)	17(1)
Zn(7)	6016(1)	1605(1)	2999(1)	20(1)
Zn(8)	3146(1)	925(1)	2396(1)	18(1)
Zn(9)	4777(1)	-1283(1)	2725(1)	19(1)
Zn(10)	5543(1)	79(1)	1592(1)	21(1)
Zn(11)	6902(1)	-367(1)	2468(1)	15(1)
Zn(12)	4974(1)	2234(1)	2081(1)	15(1)
Zn(13)	3216(1)	-1492(1)	1609(1)	16(1)
Zn(14)	3914(1)	720(1)	3638(1)	14(1)
Mn(11)	6902(1)	-367(1)	2468(1)	15(1)
Mn(12)	4974(1)	2234(1)	2081(1)	15(1)
Mn(13)	3216(1)	-1492(1)	1609(1)	16(1)
Mn(14)	3914(1)	720(1)	3638(1)	14(1)
Cl(1)	3283(2)	1016(2)	4390(1)	24(1)
Cl(2)	2161(2)	-2635(2)	1082(1)	29(1)
Se(13)	4927(1)	367(1)	2416(1)	15(1)
Se(11)	4769(1)	-837(1)	3574(1)	18(1)
Se(1)	2403(1)	559(1)	3100(1)	17(1)
Se(12)	7418(1)	655(1)	3207(1)	18(1)
Se(6)	2353(1)	68(1)	1650(1)	18(1)
Se(5)	5008(1)	1525(1)	1262(1)	18(1)
Se(7)	6512(1)	2885(1)	2507(1)	18(1)
Se(4)	6334(1)	-2069(1)	2459(1)	18(1)
Se(2)	3281(1)	-2201(1)	2345(1)	18(1)
Se(3)	4798(1)	-1512(1)	1204(1)	19(1)
Se(8)	7373(1)	123(1)	1741(1)	18(1)
Se(10)	5016(1)	2240(1)	3642(1)	19(1)
Se(9)	3426(1)	2733(1)	2385(1)	18(1)
N(1)	1812(6)	-1964(5)	3398(3)	28(2)
N(2)	698(5)	-1546(5)	2573(3)	24(2)
N(3)	5289(6)	-3993(5)	1487(3)	26(2)
N(4)	7024(5)	-2923(6)	1220(3)	26(2)
N(5)	3016(6)	306(5)	430(2)	23(2)
N(6)	2484(6)	2157(6)	971(3)	27(2)
N(7)	9051(6)	2344(5)	2277(3)	25(2)
N(8)	7941(5)	2524(5)	1406(3)	21(1)
N(9)	2726(6)	3673(5)	3552(3)	24(2)
N(10)	4566(6)	4673(5)	3349(3)	25(2)
N(11)	6812(5)	429(5)	4413(2)	18(1)
N(12)	7263(5)	-1462(5)	3890(3)	23(2)
C(1S)	7775(8)	-4367(8)	2799(4)	41(2)

APPENDIX A.13.Crystal data and structure refinement for $(N,N'$ -tmeda) $_6$ Zn $_{8.2}$ Mn $_{5.8}$ Se $_{13}$ Cl $_2$, **8d**

Empirical formula	C39.50 H103 Cl6.50 Mn5.60 N12 Se13 Zn8.40
Formula weight	2860.02
Temperature	150(2) K
Wavelength	0.71073 Å
Crystal system	Trigonal
Space group	P 31 2 1
Unit cell dimensions	a = 25.525(4) Å $\alpha = 90^\circ$. b = 25.525(4) Å $\beta = 90^\circ$. c = 27.953(6) Å $\gamma = 120^\circ$.
Volume	15772(4) Å ³
Z	6
Density (calculated)	1.807 Mg/m ³
Absorption coefficient	7.217 mm ⁻¹
F(000)	8211
Crystal size	0.175 x 0.15 x 0.075 mm ³
Theta range for data collection	2.16 to 25.02°.
Index ranges	-30 ≤ h ≤ 30, -25 ≤ k ≤ 25, -33 ≤ l ≤ 31
Reflections collected	32468
Independent reflections	18498 [R(int) = 0.0828]
Completeness to theta = 25.02°	99.8 %
Absorption correction	Semi-empirical from equivalents
Max. and min. transmission	0.582 and 0.294
Refinement method	Full-matrix least-squares on F ²
Data / restraints / parameters	18498 / 0 / 813
Goodness-of-fit on F ²	0.948
Final R indices [I > 2σ(I)]	R1 = 0.0636, wR2 = 0.1667
R indices (all data)	R1 = 0.1254, wR2 = 0.2065
Absolute structure parameter	0.004(19)
Largest diff. peak and hole	1.917 and -1.255 e.Å ⁻³

Atomic coordinates ($\times 10^4$) and equivalent isotropic displacement parameters ($\text{\AA}^2 \times 10^3$)

for $(N,N'$ -tmeda) $_6\text{Zn}_{8,2}\text{Mn}_{5,8}\text{Se}_{13}\text{Cl}_2$. U(eq) is defined as one third of the trace of the orthogonalized U^{ij} tensor.

	x	y	z	U(eq)
Mn(1)	9115(1)	3420(1)	10222(1)	33(1)
Mn(2)	8917(1)	2992(1)	7972(1)	35(1)
Mn(7)	8640(1)	3781(1)	9011(1)	35(1)
Mn(8)	11040(1)	4504(1)	8930(1)	39(1)
Mn(9)	9639(1)	5188(1)	8840(1)	44(1)
Mn(10)	10199(1)	4610(1)	8118(1)	38(1)
Mn(11)	10346(1)	4914(1)	9681(1)	37(1)
Mn(12)	9858(1)	3184(1)	9097(1)	38(1)
Zn(1)	8301(1)	2278(1)	9223(1)	42(1)
Zn(2)	10600(1)	3476(1)	7941(1)	40(1)
Zn(3)	8742(1)	4401(1)	7814(1)	38(1)
Zn(4)	11249(1)	5986(1)	8767(1)	42(1)
Zn(5)	8935(1)	4796(1)	10016(1)	38(1)
Zn(6)	10795(1)	3887(1)	10124(1)	42(1)
Zn(7)	8640(1)	3781(1)	9011(1)	35(1)
Zn(8)	11040(1)	4504(1)	8930(1)	39(1)
Zn(9)	9639(1)	5188(1)	8840(1)	44(1)
Zn(10)	10199(1)	4610(1)	8118(1)	38(1)
Zn(11)	10346(1)	4914(1)	9681(1)	37(1)
Zn(12)	9858(1)	3184(1)	9097(1)	38(1)
Se(1)	8207(1)	3029(1)	9666(1)	40(1)
Se(2)	9021(1)	2370(1)	8640(1)	41(1)
Se(3)	9916(1)	3744(1)	7582(1)	41(1)
Se(4)	10891(1)	3500(1)	8761(1)	40(1)
Se(5)	9730(1)	5254(1)	7962(1)	41(1)
Se(6)	8239(1)	3428(1)	8187(1)	39(1)
Se(7)	10502(1)	5898(1)	9329(1)	42(1)
Se(8)	11321(1)	5245(1)	8287(1)	40(1)
Se(9)	8626(1)	4744(1)	9198(1)	39(1)
Se(10)	9639(1)	4551(1)	10368(1)	38(1)
Se(11)	9818(1)	3034(1)	9981(1)	40(1)
Se(12)	11310(1)	4868(1)	9752(1)	41(1)
Se(13)	9804(1)	4180(1)	8971(1)	35(1)
Cl(1)	8729(2)	2983(2)	10991(2)	49(1)
Cl(2)	8397(2)	2262(2)	7360(2)	52(1)
N(1)	7396(6)	1678(7)	8951(5)	53(4)
N(2)	8109(7)	1511(6)	9688(5)	47(4)
N(3)	10429(7)	2644(7)	7627(5)	49(4)
N(4)	11430(6)	3859(7)	7518(5)	44(4)
N(5)	8119(6)	4760(7)	7761(5)	42(4)
N(6)	8624(7)	4302(6)	7035(5)	42(4)
N(7)	12105(7)	6568(7)	9096(6)	51(4)
N(8)	11494(8)	6751(7)	8306(6)	58(4)
N(9)	8109(6)	4429(7)	10439(5)	41(4)
N(10)	9125(7)	5650(7)	10306(5)	44(4)
N(11)	11400(7)	3529(7)	10196(5)	44(4)

APPENDIX A.14.Crystal data and structure refinement for $(N,N'$ -tmeda) $_6$ Zn $_{14}$ S $_{13}$ Cl $_2$, **9a**

Empirical formula	C ₄₅ H ₁₁₄ Cl ₂₀ N ₁₂ S ₁₃ Zn ₁₄	
Formula weight	2864.44	
Temperature	150(2) K	
Wavelength	0.71073 Å	
Crystal system	Triclinic	
Space group	P1	
Unit cell dimensions	a = 13.4610(19) Å	α = 100.000(6)°.
	b = 13.7110(19) Å	β = 93.060(7)°.
	c = 28.542(4) Å	γ = 93.710(8)°.
Volume	5165.7(12) Å ³	
Z	2	
Density (calculated)	1.842 Mg/m ³	
Absorption coefficient	4.001 mm ⁻¹	
F(000)	2872	
Crystal size	0.25 x 0.23 x 0.20 mm ³	
Theta range for data collection	0.73 to 30.12°.	
Index ranges	-18<=h<=18, -19<=k<=19, -39<=l<=39	
Reflections collected	107666	
Independent reflections	29573 [R(int) = 0.0379]	
Completeness to theta = 30.12°	97.1 %	
Absorption correction	None	
Refinement method	Full-matrix least-squares on F ²	
Data / restraints / parameters	29573 / 0 / 961	
Goodness-of-fit on F ²	2.293	
Final R indices [I>2sigma(I)]	R1 = 0.0462, wR2 = 0.0962	
R indices (all data)	R1 = 0.0676, wR2 = 0.1012	
Largest diff. peak and hole	2.488 and -1.657 e.Å ⁻³	

Atomic coordinates ($\times 10^4$) and equivalent isotropic displacement parameters ($\text{\AA}^2 \times 10^3$)

for $(N,N'$ -tmeda) $_6$ Zn $_{14}$ S $_{13}$ Cl $_2$. U(eq) is defined as one third of the trace of the orthogonalized U^{ij} tensor.

	x	y	z	U(eq)
Zn(1)	2680(1)	11172(1)	2178(1)	17(1)
Zn(2)	1003(1)	6996(1)	1807(1)	16(1)
Zn(3)	-1404(1)	10231(1)	1334(1)	16(1)
Zn(4)	-2415(1)	8164(1)	2958(1)	16(1)
Zn(5)	-734(1)	12343(1)	3334(1)	17(1)
Zn(6)	1724(1)	9090(1)	3790(1)	16(1)
Zn(7)	244(1)	11218(1)	2288(1)	16(1)
Zn(8)	-954(1)	8431(1)	1997(1)	16(1)
Zn(9)	-464(1)	9913(1)	3385(1)	16(1)
Zn(10)	1821(1)	9138(1)	2590(1)	15(1)
Zn(11)	-1839(1)	10331(1)	2528(1)	18(1)
Zn(12)	1066(1)	9311(1)	1382(1)	16(1)
Zn(13)	68(1)	7813(1)	2899(1)	18(1)
Zn(14)	1755(1)	11451(1)	3374(1)	17(1)
S(1)	1681(1)	12106(1)	2665(1)	16(1)
S(2)	2506(1)	9501(1)	1907(1)	15(1)
S(3)	19(1)	7853(1)	1378(1)	16(1)
S(4)	1548(1)	7399(1)	2591(1)	16(1)
S(5)	-2300(1)	9342(1)	1807(1)	16(1)
S(6)	235(1)	10778(1)	1464(1)	16(1)
S(7)	-2224(1)	9835(1)	3228(1)	16(1)
S(8)	-1412(1)	7209(1)	2477(1)	16(1)
S(9)	-1252(1)	11950(1)	2547(1)	17(1)
S(10)	244(1)	11458(1)	3755(1)	16(1)
S(11)	2576(1)	9976(1)	3318(1)	16(1)
S(12)	72(1)	8526(1)	3688(1)	16(1)
S(13)	94(1)	9630(1)	2578(1)	14(1)
Cl(1)	2816(1)	12604(1)	3921(1)	24(1)
Cl(2)	1697(1)	9020(1)	620(1)	21(1)
N(1)	3057(3)	12009(2)	1618(1)	22(1)
N(2)	4234(2)	11518(2)	2421(1)	20(1)
N(3)	2276(2)	6429(2)	1452(1)	21(1)
N(4)	399(2)	5453(2)	1646(1)	22(1)
N(5)	-1793(2)	9559(2)	614(1)	18(1)
N(6)	-2180(2)	11468(2)	1156(1)	21(1)
N(7)	-3918(2)	7674(2)	2681(1)	21(1)
N(8)	-2812(2)	7506(2)	3565(1)	19(1)
N(9)	-259(2)	13907(2)	3491(1)	19(1)
N(10)	-1976(2)	12794(3)	3761(1)	22(1)
N(11)	2591(2)	7888(2)	3950(1)	20(1)
N(12)	1998(2)	9674(2)	4538(1)	19(1)
C(1)	3102(4)	11341(3)	1156(2)	39(1)
C(2)	2345(3)	12754(3)	1558(2)	34(1)
C(3)	4055(3)	12505(3)	1782(2)	30(1)
C(4)	4702(3)	11838(3)	2012(2)	28(1)
C(5)	4349(3)	12315(3)	2840(2)	30(1)

APPENDIX A.15.Crystal data and structure refinement for $(N,N'$ -tmeda) $_6$ Zn $_{14}$ Se $_{13}$ Cl $_2$, **9b**

Empirical formula	C ₄₅ H ₁₀₅ Cl ₂₀ N ₁₂ Se ₁₃ Zn ₁₄	
Formula weight	3465.07	
Temperature	150(2) K	
Wavelength	0.71073 Å	
Crystal system	Triclinic	
Space group	P-1	
Unit cell dimensions	a = 13.5553(2) Å	$\alpha = 99.4740(7)^\circ$.
	b = 13.7348(2) Å	$\beta = 92.7150(7)^\circ$.
	c = 28.9568(4) Å	$\gamma = 93.1470(8)^\circ$.
Volume	5300.89(13) Å ³	
Z	2	
Density (calculated)	2.171 Mg/m ³	
Absorption coefficient	8.106 mm ⁻¹	
F(000)	3322	
Crystal size	0.28x 0.25x 0.20mm ³	
Theta range for data collection	2.06 to 29.21°.	
Index ranges	-18<=h<=18, -18<=k<=18, -39<=l<=39	
Reflections collected	50814	
Independent reflections	28166 [R(int) = 0.0503]	
Completeness to theta = 29.21°	98.1 %	
Absorption correction	None	
Refinement method	Full-matrix least-squares on F ²	
Data / restraints / parameters	28166 / 0 / 958	
Goodness-of-fit on F ²	0.854	
Final R indices [I>2sigma(I)]	R1 = 0.0632, wR2 = 0.1871	
R indices (all data)	R1 = 0.1011, wR2 = 0.2370	
Largest diff. peak and hole	1.476 and -2.377 e.Å ⁻³	

Atomic coordinates ($\times 10^4$) and equivalent isotropic displacement parameters ($\text{\AA}^2 \times 10^3$)

for $(N,N'$ -tmeda) $_6\text{Zn}_{14}\text{Se}_{13}\text{Cl}_2$. $U(\text{eq})$ is defined as one third of the trace of the orthogonalized U^{ij} tensor.

	x	y	z	U(eq)
Zn(1)	2237(1)	8817(1)	2830(1)	24(1)
Zn(2)	5788(1)	7548(1)	1647(1)	26(1)
Zn(3)	3286(1)	10939(1)	1162(1)	24(1)
Zn(4)	7548(1)	11866(1)	2013(1)	24(1)
Zn(5)	3982(1)	13123(1)	3195(1)	24(1)
Zn(6)	6462(1)	9748(1)	3701(1)	24(1)
Zn(7)	3149(1)	10919(1)	2399(1)	23(1)
Zn(8)	5535(1)	10080(1)	1596(1)	24(1)
Zn(9)	6009(1)	11598(1)	2998(1)	25(1)
Zn(10)	4778(1)	8723(1)	2725(1)	24(1)
Zn(11)	4967(1)	12240(1)	2081(1)	26(1)
Zn(12)	3216(1)	8508(1)	1611(1)	25(1)
Zn(13)	6908(1)	9630(1)	2469(1)	26(1)
Zn(14)	3915(1)	10715(1)	3636(1)	24(1)
Cl(1)	2165(2)	7374(2)	1084(1)	33(1)
Cl(2)	3290(1)	11007(1)	4384(1)	29(1)
Se(1)	2415(1)	10560(1)	3103(1)	23(1)
Se(2)	3289(1)	7808(1)	2342(1)	24(1)
Se(3)	4785(1)	8493(1)	1210(1)	24(1)
Se(4)	6332(1)	7936(1)	2461(1)	24(1)
Se(5)	5002(1)	11521(1)	1265(1)	24(1)
Se(6)	2358(1)	10056(1)	1656(1)	23(1)
Se(7)	6503(1)	12881(1)	2509(1)	24(1)
Se(8)	7365(1)	10119(1)	1742(1)	24(1)
Se(9)	3419(1)	12723(1)	2384(1)	24(1)
Se(10)	5009(1)	12223(1)	3642(1)	24(1)
Se(11)	4763(1)	9170(1)	3571(1)	23(1)
Se(12)	7415(1)	10654(1)	3206(1)	24(1)
Se(13)	4927(1)	10368(1)	2416(1)	22(1)
N(1)	1840(5)	8032(5)	3395(2)	29(1)
N(2)	701(5)	8467(5)	2569(2)	28(1)
N(3)	5285(5)	6012(5)	1497(2)	32(2)
N(4)	7015(5)	7082(5)	1220(3)	33(2)
N(5)	2470(5)	12149(5)	978(3)	33(2)
N(6)	3006(5)	10305(5)	431(2)	27(1)
N(7)	7930(5)	12515(5)	1409(2)	27(1)
N(8)	9037(5)	12346(5)	2274(3)	30(1)
N(9)	2712(5)	13668(5)	3561(2)	29(1)
N(10)	4567(5)	14661(5)	3356(2)	31(1)
N(11)	7239(5)	8514(5)	3894(2)	27(1)
N(12)	6821(5)	10426(5)	4413(2)	27(1)
C(1)	2556(7)	7308(7)	3472(4)	45(2)
C(2)	1724(8)	8722(7)	3827(3)	46(2)
C(3)	861(6)	7501(7)	3214(3)	40(2)
C(4)	219(6)	8148(7)	2972(3)	37(2)
C(5)	615(6)	7673(6)	2164(3)	36(2)

APPENDIX A.16.

Atomic coordinates ($\times 10^4$) and equivalent isotropic displacement parameters ($\text{\AA}^2 \times 10^3$)

for 07062b. $U(\text{eq})$ is defined as one third of the trace of the orthogonalized U_{ij} tensor.

	x	y	z	$U(\text{eq})$
Ag(1)	4284(1)	-776(1)	3845(1)	45(1)
Ag(2)	6086(1)	2791(1)	-13(1)	46(1)
Ag(3)	5390(1)	3391(1)	-2866(1)	47(1)
Ag(4)	5267(1)	2592(1)	-181(1)	45(1)
Ag(5)	8582(1)	-2782(1)	397(1)	48(1)
Ag(6)	4492(1)	3786(1)	-1822(1)	49(1)
Ag(7)	8692(1)	-2164(1)	990(1)	46(1)
Ag(8)	2657(1)	-598(1)	4096(1)	46(1)
Ag(9)	7901(1)	-1760(1)	1999(1)	48(1)
Ag(10)	4825(1)	-2133(1)	4041(1)	44(1)
Ag(11)	6775(1)	-1179(1)	2744(1)	48(1)
Ag(12)	5600(1)	-1346(1)	3518(1)	46(1)
Ag(13)	5714(1)	-75(1)	2568(1)	50(1)
Ag(14)	7381(1)	1604(1)	-546(1)	48(1)
Ag(15)	6462(1)	1312(1)	1134(1)	44(1)
Ag(16)	7680(1)	579(1)	528(1)	48(1)
Ag(17)	2022(1)	802(1)	3565(1)	48(1)
Ag(18)	5368(1)	3696(1)	-1099(1)	48(1)
Ag(19)	2635(1)	-1505(1)	3696(1)	48(1)
Ag(20)	1114(1)	442(1)	2372(1)	49(1)
Ag(21)	1713(1)	-301(1)	3287(1)	48(1)
Ag(22)	7033(1)	-2516(1)	2993(1)	46(1)
Ag(23)	1204(1)	1106(1)	2973(1)	52(1)
Ag(24)	3631(1)	-1926(1)	4097(1)	48(1)
Ag(25)	5275(1)	2392(1)	1147(1)	50(1)
Ag(26)	670(1)	1861(1)	1133(1)	47(1)
Ag(27)	7958(1)	-3023(1)	1666(1)	47(1)
Ag(28)	2486(1)	-1350(1)	2645(1)	50(1)
Ag(29)	4402(1)	470(1)	2943(1)	52(1)
Ag(30)	6958(1)	-28(1)	1831(1)	48(1)
Ag(31)	6254(1)	3044(1)	-2272(1)	49(1)
Ag(32)	5930(1)	-2942(1)	3561(1)	47(1)
Ag(33)	972(1)	533(1)	1336(1)	48(1)
Ag(34)	4077(1)	3812(1)	-545(1)	53(1)
Ag(35)	3802(1)	-854(1)	3164(1)	55(1)
Ag(36)	3195(1)	1600(1)	2872(1)	55(1)
Ag(37)	1856(1)	-604(1)	1787(1)	52(1)
Ag(38)	3995(1)	3628(1)	-2537(1)	57(1)
Ag(39)	8412(1)	-696(1)	741(1)	52(1)
Ag(40)	3977(1)	2390(1)	1802(1)	54(1)
Ag(41)	3375(1)	-2484(1)	3203(1)	52(1)
Ag(42)	4557(1)	3446(1)	401(1)	53(1)
Ag(43)	7053(1)	-1884(1)	1782(1)	54(1)
Ag(44)	8435(1)	324(1)	-665(1)	52(1)
Ag(45)	3201(1)	311(1)	3734(1)	52(1)
Ag(46)	9102(1)	-1378(1)	-169(1)	50(1)

Ag(47)	5953(1)	-1834(1)	2641(1)	54(1)
Ag(48)	957(1)	2097(1)	1954(1)	53(1)
Ag(49)	2752(1)	1(1)	2896(1)	56(1)
Ag(50)	3185(1)	3401(1)	626(1)	55(1)
Ag(51)	5154(1)	1226(1)	1959(1)	53(1)
Ag(52)	7235(1)	1814(1)	-1720(1)	56(1)
Ag(53)	5290(1)	2669(1)	-1266(1)	58(1)
Ag(54)	2973(1)	3349(1)	-1499(1)	54(1)
Ag(55)	4116(1)	1234(1)	1834(1)	62(1)
Ag(56)	4704(1)	-3035(1)	3650(1)	56(1)
Ag(57)	8810(1)	-2834(1)	-755(1)	53(1)
Ag(58)	6581(1)	2798(1)	-1238(1)	56(1)
Ag(59)	1791(1)	1177(1)	1425(1)	58(1)
Ag(60)	6224(1)	1461(1)	129(1)	58(1)
Ag(61)	6915(1)	-3347(1)	2622(1)	52(1)
Ag(62)	7199(1)	727(1)	-672(1)	65(1)
Ag(63)	7180(1)	-706(1)	1190(1)	63(1)
Ag(64)	2286(1)	3067(1)	-237(1)	60(1)
Ag(65)	3196(1)	2476(1)	366(1)	64(1)
Ag(66)	3319(1)	3494(1)	-745(1)	60(1)
Ag(67)	6241(1)	1859(1)	-1935(1)	68(1)
Ag(68)	2664(1)	2729(1)	1856(1)	65(1)
Ag(69)	1995(1)	3082(1)	1014(1)	68(1)
Ag(70)	8181(1)	-1544(1)	-280(1)	69(1)
Ag(71)	4978(1)	-664(1)	2550(1)	69(1)
Ag(72)	2838(1)	1196(1)	2363(1)	74(1)
Ag(73)	1761(1)	2155(1)	2551(1)	70(1)
Ag(74)	6031(1)	459(1)	1216(1)	79(1)
Ag(75)	4216(1)	2296(2)	671(1)	89(1)
Ag(76)	4262(1)	2650(2)	-1375(1)	91(1)
Ag(77)	2517(2)	-54(2)	2002(2)	130(2)
Ag(78)	5810(2)	-503(2)	1291(1)	106(1)
Ag(79)	3943(3)	1379(3)	196(3)	99(2)
Ag(80)	4151(2)	-1896(2)	2845(2)	34(1)
Ag(81)	4043(2)	-1172(2)	720(2)	60(1)
Ag(82)	2712(3)	1578(3)	1235(2)	79(2)
Ag(83)	7172(2)	-1953(3)	709(2)	58(1)
Ag(84)	3178(2)	140(2)	588(2)	64(1)
Ag(85)	4273(2)	-1607(2)	2472(3)	69(2)
Ag(86)	3025(3)	292(3)	949(3)	96(2)
Ag(87)	5392(2)	-2488(2)	2593(2)	32(1)
Ag(88)	5363(3)	-2164(3)	2258(3)	84(2)
Ag(89)	6741(2)	-1339(2)	-325(2)	65(1)
Ag(90)	7017(3)	-1351(3)	-81(3)	105(2)
Ag(91)	7780(2)	-502(2)	10(2)	46(1)
Ag(92)	7377(3)	-499(3)	40(3)	81(2)
Ag(93)	6003(3)	-1544(3)	1107(3)	91(2)
Ag(94)	5770(4)	-1670(4)	1404(4)	107(2)
Ag(95)	4312(2)	1791(2)	-209(2)	68(1)
Ag(96)	4998(2)	939(2)	806(2)	65(1)
Ag(97)	3482(3)	1217(3)	1234(3)	82(2)
A (98)	4038(4)	-127(4)	1994(4)	108(2)
Ag(99)	4398(3)	172(3)	319(3)	103(2)
Ag(100)	4169(3)	127(3)	1792(3)	75(2)
Ag(101)	4759(4)	51(4)	708(4)	140(3)
Ag(102)	2265(2)	1899(2)	1537(2)	47(1)

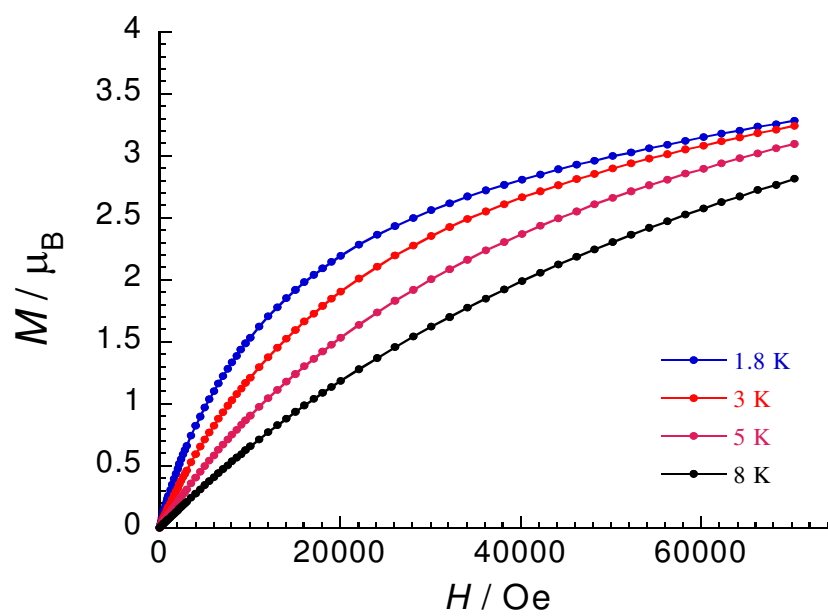
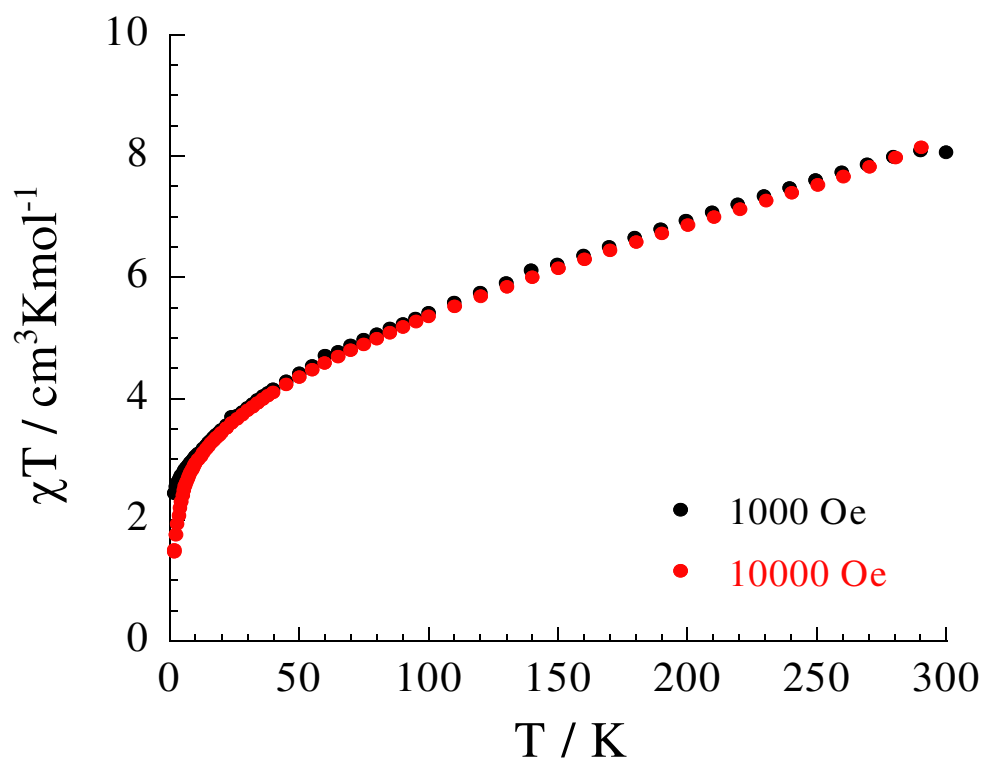
Ag(103)	4628(4)	603(4)	1023(4)	130(3)
Ag(104)	7293(3)	-2259(3)	864(3)	67(2)
Ag(105)	4481(4)	755(4)	-381(4)	133(3)
Ag(106)	3925(2)	-808(2)	1696(2)	65(1)
Ag(107)	5010(3)	1064(3)	-735(3)	88(2)
Ag(108)	5713(3)	249(3)	194(3)	104(2)
Ag(109)	4070(4)	-820(4)	1344(4)	118(3)
Ag(110)	3818(5)	-640(5)	366(5)	166(4)
S(1)	6355(4)	-658(4)	355(4)	72(3)
S(2)	2136(3)	883(3)	2256(3)	42(2)
S(3)	6136(3)	769(3)	2120(3)	44(2)
S(4)	3131(3)	-828(3)	1444(3)	36(2)
S(5)	5249(3)	2484(3)	-2101(3)	37(2)
S(6)	4839(3)	-1650(3)	3054(3)	42(2)
S(7)	7870(3)	-2076(3)	-589(3)	44(2)
S(8)	5049(3)	302(3)	1788(3)	39(2)
S(9)	7769(3)	-1570(3)	765(3)	38(2)
S(10)	3460(3)	2260(3)	-549(3)	41(2)
S(11)	7891(3)	-796(3)	1717(3)	49(2)
S(12)	8085(3)	1270(3)	-1335(3)	48(2)
S(13)	1450(3)	-606(3)	2795(3)	52(2)
S(14)	6296(3)	-933(3)	2090(3)	45(2)
S(15)	3609(4)	502(5)	1121(4)	91(3)
S(16)	9334(3)	-2339(3)	-171(3)	43(2)
S(17)	5015(3)	-368(3)	3559(3)	48(2)
S(18)	4910(4)	-880(4)	1518(3)	56(2)
S(19)	3624(3)	274(3)	2780(3)	44(2)
S(20)	5204(3)	1765(3)	840(3)	44(2)
S(21)	5381(3)	3724(3)	-284(3)	53(2)
S(22)	3196(3)	-1016(3)	2773(3)	46(2)
S(23)	6876(3)	1964(3)	244(3)	50(2)
S(24)	6459(3)	-2478(3)	1956(3)	42(2)
S(25)	3497(3)	-1186(3)	4397(3)	46(2)
S(26)	1989(3)	443(3)	990(3)	46(2)
S(27)	4359(3)	2802(3)	-412(3)	48(2)
S(28)	8107(3)	-3510(3)	1068(3)	44(2)
S(29)	4152(3)	1589(3)	2644(3)	51(2)
S(30)	7990(3)	-2772(3)	2355(3)	46(2)
S(31)	499(3)	1456(3)	2124(3)	52(2)
S(32)	3514(3)	4038(3)	-1785(3)	47(2)
S(33)	5420(4)	3834(3)	-2010(3)	53(2)
S(34)	9079(4)	-510(3)	-175(3)	51(2)
S(35)	6982(3)	374(3)	406(3)	40(2)
S(36)	5699(3)	-3612(3)	3467(3)	50(2)
S(37)	6181(3)	-2368(3)	3768(3)	46(2)
S(38)	2534(4)	3645(3)	152(3)	52(2)
S(39)	5091(5)	999(9)	-44(5)	176(9)
S(40)	2197(3)	1678(3)	3292(4)	56(2)
S(41)	2827(4)	-2428(3)	2714(3)	53(2)
S(42)	1716(3)	-24(3)	3979(3)	47(2)
S(43)	3299(3)	1985(3)	1390(3)	50(2)
S(44)	3693(4)	3358(3)	1136(4)	60(2)
S(45)	3665(3)	-2734(3)	3981(4)	56(2)
S(46)	1246(3)	2820(3)	1881(4)	57(2)
S(47)	6188(3)	2056(3)	-901(3)	52(2)

APPENDIX B:

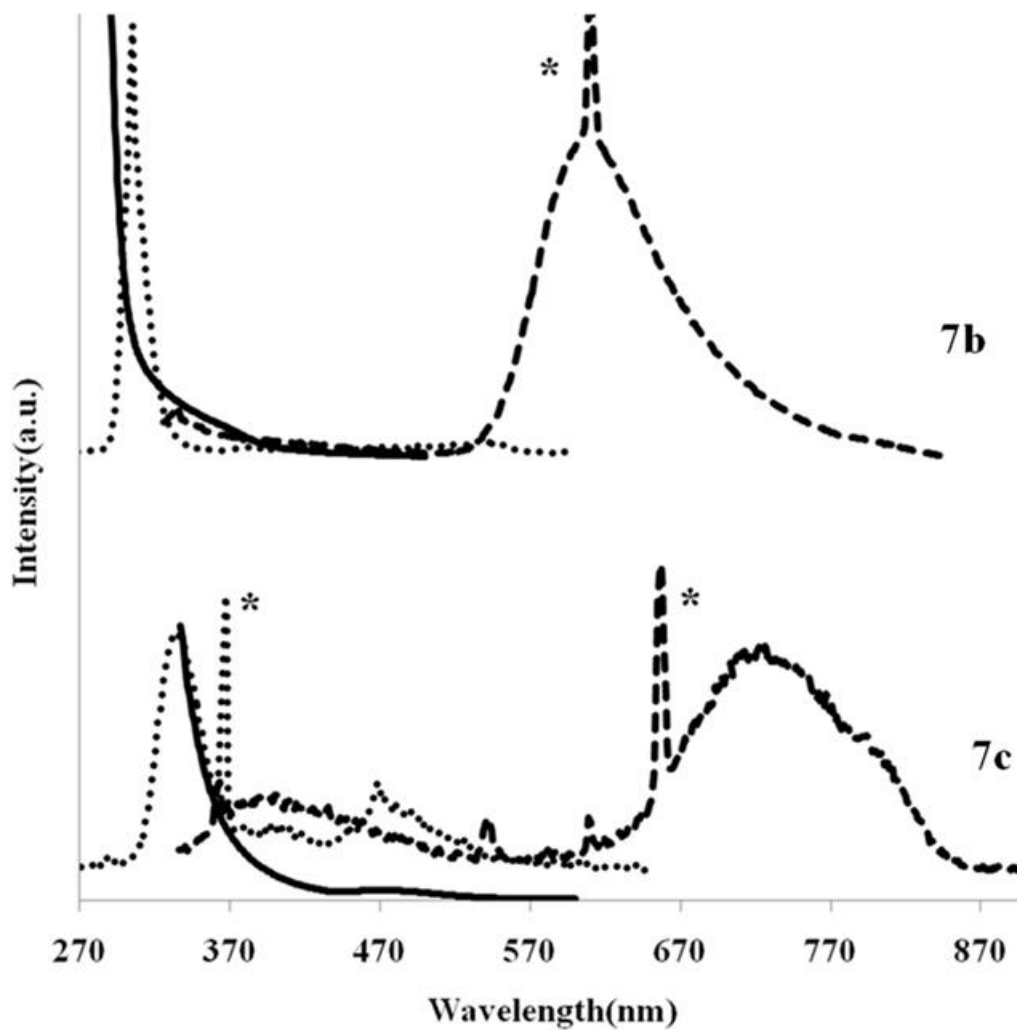
Magnetic data for Complex **3b**

Uv-Visible absorption, PL and PLE for Complexes **7b**, **7c**, **8b** and **8c**

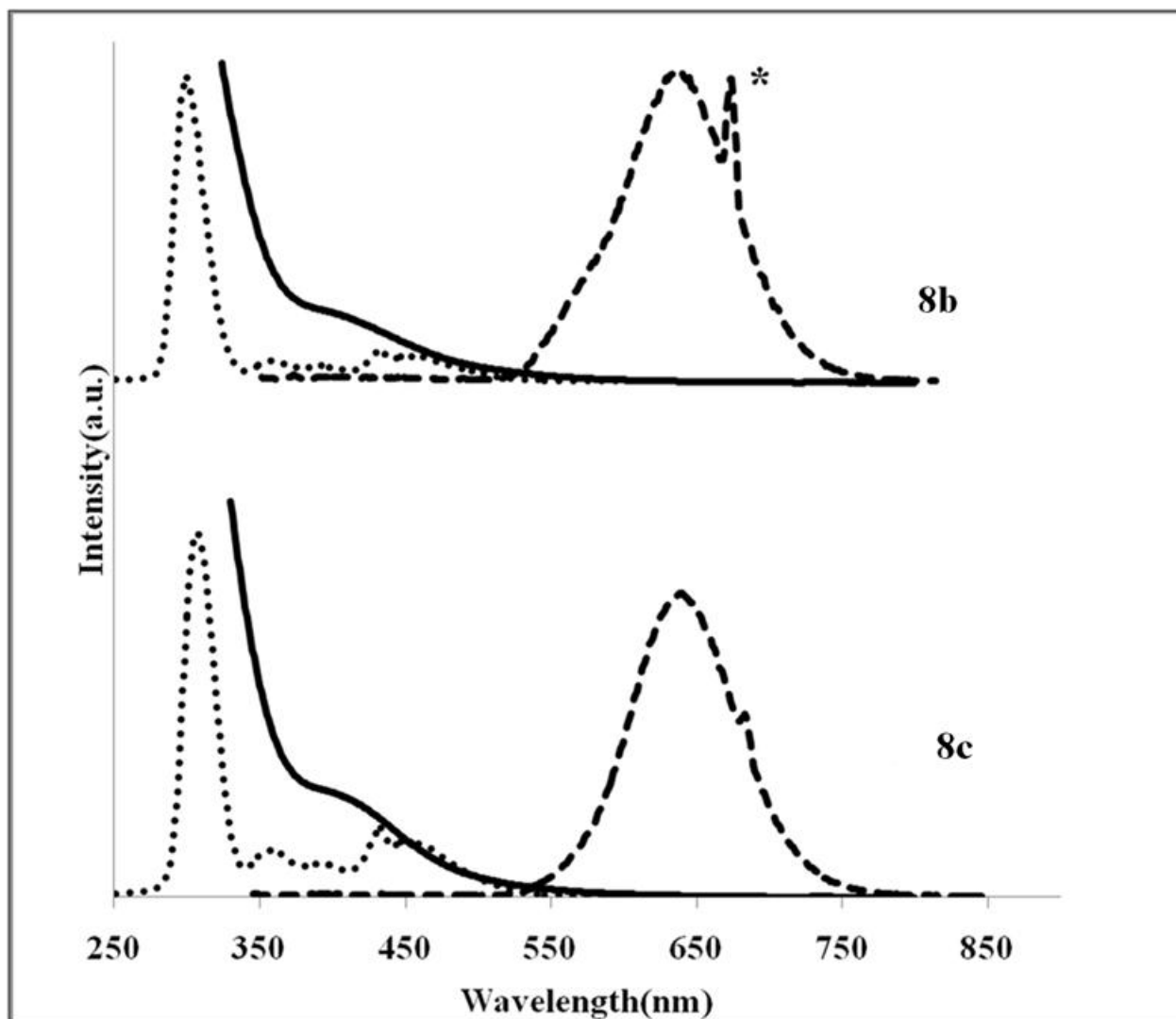
Quantum chemical calculations data for Complexes **7-8**



Appendix B.1. Plots of χT vs T (top) and M vs H (bottom) for complex **3b**



Appendix B.2. Normalized room temperature UV-Visible absorption (—), PLE (•••) and PL (---) spectra of Complexes **7b** and **7c** in DMSO and DMF respectively. *denotes harmonic vibration and/or solvent peaks.



Appendix B.3. Normalized room temperature UV-Visible absorption (—), PLE (•••) and PL (---) spectra of Complexes **8b** and **8c** in DCM. *denotes harmonic vibration and/or solvent peaks.

Appendix B.4. Metal type assignment by quantum chemical calculations

Table 1: Relative energies E_1 (in E_H) of Mn1Zn13 for Mn located at positions $i=1,2..8$ calculated with B3-LYP/SV(P) for the X-ray structure parameters.

i	E_1
1	-.0110506
2	-.01002373
3	-.00449731
4	-.00071944
5	0
6	-.00535679
7	-.00504896
8	-.00482102

Table 2: Energy differences for Mn2Zn12, E_2 (in E_H), of the high-spin state (5 spin-up electrons at each of the Mn atoms at positions i and j) and the broken-symmetry low-spin state (5 spin-up electrons at i , 5 spin-down electrons at j) in E_H (column 4). Column 3: distance between i and j in pm.

ij	dist	E_2
1 2	605.84	.00001857
1 3	364.98	.00188927
1 4	531.71	.00006029
1 5	533.86	.00005325
1 6	617.89	.00012459
1 7	359.38	.00189763
1 8	362.93	.00169763
2 3	367.43	.00170837
2 4	536.82	.00005509
2 5	536.29	.00005546
2 6	363.81	.00181547
2 7	624.17	.00009654
2 8	367.64	.00182620
3 4	530.34	.00149189
3 5	315.20	.00375144
3 6	406.72	.00092221
3 7	408.15	.00097781
3 8	391.69	.00083892
4 5	465.12	.00046851
4 6	313.69	.00378899

4 7 314.19 .00419088
 4 8 316.59 .00376144
 5 6 313.68 .00429144
 5 7 316.76 .00366583
 5 8 531.68 .00149912
 6 7 420.81 .00120260
 6 8 407.74 .00101501
 7 8 408.13 .00097345

Table 3: Reaction energies E (in kJ/mol) for all reactions $\text{Mn}(i)\text{Zn}(14-i) \rightarrow a*\text{Mn}(j)\text{Zn}(14-j)+b*\text{Mn}(k)\text{Zn}(14-k)$

i	a	j	b	k	E	i	a	j	b	k	E
1	0.50000	*0	+0.50000	*2	: +1.3544	3	0.50000	*1	+0.50000	*5	: +8.7427
1	0.66667	*0	+0.33333	*3	: +4.2243	3	0.60000	*1	+0.40000	*6	: +8.3013
1	0.75000	*0	+0.25000	*4	: +6.0745	3	0.66667	*1	+0.33333	*7	: +8.8120
1	0.80000	*0	+0.20000	*5	: +8.5662	3	0.71429	*1	+0.28571	*8	: +9.2154
1	0.83333	*0	+0.16667	*6	: +8.7392	3	0.75000	*1	+0.25000	*9	: +16.4209
1	0.85714	*0	+0.14286	*7	: +9.2078	3	0.50000	*2	+0.50000	*4	: +0.8305
1	0.87500	*0	+0.12500	*8	: +9.5761	3	0.66667	*2	+0.33333	*5	: +3.4101
1	0.88889	*0	+0.11111	*9	: +12.9305	3	0.75000	*2	+0.25000	*6	: +2.4677
2	0.33333	*0	+0.66667	*3	: +5.7397	3	0.80000	*2	+0.20000	*7	: +2.3852
2	0.50000	*0	+0.50000	*4	: +9.4401	3	0.83333	*2	+0.16667	*8	: +2.3527
2	0.60000	*0	+0.40000	*5	: +14.4236	3	0.85714	*2	+0.14286	*9	: +6.2741
2	0.66667	*0	+0.33333	*6	: +14.7695	4	0.20000	*0	+0.80000	*5	: +9.9670
2	0.71429	*0	+0.28571	*7	: +15.7067	4	0.33333	*0	+0.66667	*6	: +10.6590
2	0.75000	*0	+0.25000	*8	: +16.4433	4	0.42857	*0	+0.57143	*7	: +12.5332
2	0.77778	*0	+0.22222	*9	: +23.1522	4	0.50000	*0	+0.50000	*8	: +14.0065
2	0.50000	*1	+0.50000	*3	: +3.6275	4	0.55556	*0	+0.44444	*9	: +27.4243
2	0.66667	*1	+0.33333	*4	: +5.3904	4	0.25000	*1	+0.75000	*5	: +7.8255
2	0.75000	*1	+0.25000	*5	: +7.9989	4	0.40000	*1	+0.60000	*6	: +7.1633
2	0.80000	*1	+0.20000	*6	: +7.7782	4	0.50000	*1	+0.50000	*7	: +7.9294
2	0.83333	*1	+0.16667	*7	: +8.0335	4	0.57143	*1	+0.42857	*8	: +8.5345
2	0.85714	*1	+0.14286	*8	: +8.2352	4	0.62500	*1	+0.37500	*9	: +19.3427
2	0.87500	*1	+0.12500	*9	: +11.8380	4	0.33333	*2	+0.66667	*5	: +5.1592
3	0.25000	*0	+0.75000	*4	: +5.5506	4	0.50000	*2	+0.50000	*6	: +3.2742
3	0.40000	*0	+0.60000	*5	: +13.0258	4	0.60000	*2	+0.40000	*7	: +3.1092
3	0.50000	*0	+0.50000	*6	: +13.5448	4	0.66667	*2	+0.33333	*8	: +3.0443
3	0.57143	*0	+0.42857	*7	: +14.9505	4	0.71429	*2	+0.28571	*9	: +10.8870
3	0.62500	*0	+0.37500	*8	: +16.0555	4	0.50000	*3	+0.50000	*5	: +3.4541
3	0.66667	*0	+0.33333	*9	: +26.1188	4	0.66667	*3	+0.33333	*6	: +1.6291
3	0.33333	*1	+0.66667	*4	: +3.5258	4	0.75000	*3	+0.25000	*7	: +1.3204

4 0.80000*3+0.20000*8 : +1.1621
4 0.83333*3+0.16667*9 : +5.6586
5 0.16667*0+0.83333*6 : +0.8650
5 0.28571*0+0.71429*7 : +3.2078
5 0.37500*0+0.62500*8 : +5.0494
5 0.44444*0+0.55556*9 : +21.8216
5 0.20000*1+0.80000*6 : -0.8829
5 0.33333*1+0.66667*7 : +0.1385
5 0.42857*1+0.57143*8 : +0.9453
5 0.50000*1+0.50000*9 : +15.3563
5 0.25000*2+0.75000*6 : -2.8274
5 0.40000*2+0.60000*7 : -3.0749
5 0.50000*2+0.50000*8 : -3.1723
5 0.57143*2+0.42857*9 : +8.5918
5 0.33333*3+0.66667*6 : -3.6500
5 0.50000*3+0.50000*7 : -4.2675
5 0.60000*3+0.40000*8 : -4.5839
5 0.66667*3+0.33333*9 : +4.4091
5 0.50000*4+0.50000*6 : -4.4645
5 0.66667*4+0.33333*7 : -5.1477
5 0.75000*4+0.25000*8 : -5.4555
5 0.80000*4+0.20000*9 : -0.1178
6 0.14286*0+0.85714*7 : +2.8114
6 0.25000*0+0.75000*8 : +5.0213
6 0.33333*0+0.66667*9 : +25.1480
6 0.16667*1+0.83333*7 : +1.2768
6 0.28571*1+0.71429*8 : +2.2853
6 0.37500*1+0.62500*9 : +20.2990
6 0.20000*2+0.80000*7 : -0.3299
6 0.33333*2+0.66667*8 : -0.4598
6 0.42857*2+0.57143*9 : +15.2256
6 0.25000*3+0.75000*7 : -0.9262

6 0.40000*3+0.60000*8 : -1.4009
6 0.50000*3+0.50000*9 : +12.0886
6 0.33333*4+0.66667*7 : -1.3663
6 0.50000*4+0.50000*8 : -1.9819
6 0.60000*4+0.40000*9 : +8.6934
6 0.50000*5+0.50000*7 : +1.2075
6 0.66667*5+0.33333*8 : +1.6551
6 0.75000*5+0.25000*9 : +8.7818
7 0.12500*0+0.87500*8 : +2.5782
7 0.22222*0+0.77778*9 : +26.0594
7 0.14286*1+0.85714*8 : +1.2102
7 0.25000*1+0.75000*9 : +22.8267
7 0.16667*2+0.83333*8 : -0.1623
7 0.28571*2+0.71429*9 : +19.4444
7 0.20000*3+0.80000*8 : -0.6329
7 0.33333*3+0.66667*9 : +17.3531
7 0.25000*4+0.75000*8 : -0.9234
7 0.40000*4+0.60000*9 : +15.0896
7 0.33333*5+0.66667*8 : +0.8951
7 0.50000*5+0.50000*9 : +15.1485
7 0.50000*6+0.50000*8 : +0.0676
7 0.66667*6+0.33333*9 : +9.2940
8 0.11111*0+0.88889*9 : +26.8356
8 0.12500*1+0.87500*9 : +25.2193
8 0.14286*2+0.85714*9 : +23.5281
8 0.16667*3+0.83333*9 : +22.4824
8 0.20000*4+0.80000*9 : +21.3507
8 0.25000*5+0.75000*9 : +21.3802
8 0.33333*6+0.66667*9 : +18.4529
8 0.50000*7+0.50000*9 : +13.8059

Appendix B.5. Copyright information and permissions

American Chemical Society's Policy on Theses and Dissertations

This is regarding request for permission to include **your** paper(s) or portions of text from **your** paper(s) in your thesis. Permission is now automatically granted; please pay special attention to the **implications** paragraph below. The Copyright Subcommittee of the Joint Board/Council Committees on Publications approved the following:

Copyright permission for published and submitted material from theses and dissertations ACS extends blanket permission to students to include in their theses and dissertations their own articles, or portions thereof, that have been published in ACS journals or submitted to ACS journals for publication, provided that the ACS copyright credit line is noted on the appropriate page(s).

Publishing implications of electronic publication of theses and dissertation material
Students and their mentors should be aware that posting of theses and dissertation material on the Web prior to submission of material from that thesis or dissertation to an ACS journal may affect publication in that journal. Whether Web posting is considered prior publication may be evaluated on a case-by-case basis by the journal's editor. If an ACS journal editor considers Web posting to be "prior publication", the paper will not be accepted for publication in that journal. If you intend to submit your unpublished paper to ACS for publication, check with the appropriate editor prior to posting your manuscript electronically.

Reuse/Republication of the Entire Work in Theses or Collections: Authors may reuse all or part of the Submitted, Accepted or Published Work in a thesis or dissertation that the author writes and is required to submit to satisfy the criteria of degree-granting institutions. Such reuse is permitted subject to the ACS' "Ethical Guidelines to Publication of Chemical Research" (<http://pubs.acs.org/page/policy/ethics/index.html>); the author should secure written confirmation (via letter or email) from the respective ACS journal editor(s) to avoid potential conflicts with journal prior publication*/embargo policies. Appropriate citation of the Published Work must be made. If the thesis or dissertation to be published is in electronic format, a direct link to the Published Work must also be included using the ACS Articles on Request author-directed link – see

<http://pubs.acs.org/page/policy/articlesonrequest/index.html>

* Prior publication policies of ACS journals are posted on the ACS website at <http://pubs.acs.org/page/policy/prior/index.html>

If your paper has **not** yet been published by ACS, please print the following credit line on the first page of your article: "Reproduced (or 'Reproduced in part') with permission from [JOURNAL NAME], in press (or 'submitted for publication'). Unpublished work copyright [CURRENT YEAR] American Chemical Society." Include appropriate information.

If your paper has already been published by ACS and you want to include the text or portions of the text in your thesis/dissertation, please print the ACS copyright credit line on the first page of your article: "Reproduced (or 'Reproduced in part') with permission

from [FULL REFERENCE CITATION.] Copyright [YEAR] American Chemical Society." Include appropriate information.

Submission to a Dissertation Distributor: If you plan to submit your thesis to UMI or to another dissertation distributor, you should not include the unpublished ACS paper in your thesis if the thesis will be disseminated electronically, until ACS has published your paper. After publication of the paper by ACS, you may release the entire thesis (**not the individual ACS article by itself**) for electronic dissemination through the distributor; ACS's copyright credit line should be printed on the first page of the ACS paper.

Title: Trimethylsilylchalcogenolates
of Co(II) and Mn(II): From
Mononuclear Coordination
Complexes to Clusters
Containing –ESiMe₃ Moieties
(E = S, Se)

Author: Chhatra B. Khadka et al.

Publication: Inorganic Chemistry

Publisher: American Chemical Society

Date: Aug 1, 2010

Copyright © 2010, American Chemical
Society

Permission for this particular request is granted for print and electronic formats at no charge. Figures and tables may be modified. Appropriate credit should be given. Please print this page for your records and provide a copy to your publisher. Requests for up to 4 figures require only this record. Five or more figures will generate a printout of additional terms and conditions. Appropriate credit should read: "Reprinted with permission from {COMPLETE REFERENCE CITATION}. Copyright {YEAR} American Chemical Society." Insert appropriate information in place of the capitalized

Title: Bistrimethylsilylamide Transition-
Metal Complexes as Starting
Reagents in the Synthesis of Ternary
Cd–Mn–Se Cluster Complexes

Author: Andreas Eichhoffer et al.

Publication: Inorganic Chemistry

Publisher: American Chemical Society

Date: Aug 1, 2010

Copyright © 2010, American Chemical Society

RSC Publications Permission guidelines

Material in RSC and other publishers' publications is subject to all applicable copyright, database protection, and other rights. Therefore for any article, whether printed or electronic, permission must be obtained to use material for which the author(s) does not already own the copyright. This material may be, for example, a figure, diagram, table, photo or some other image. Note that permission is not needed to re-use your own figures, diagrams, etc, which were originally published in an RSC publication. However, permission should be requested for use of the whole article or chapter.

Use of Third Party Material in RSC Publications

The RSC must ensure that the material we publish does not infringe the copyright of others. We require the author(s) to obtain, at the earliest opportunity, the relevant permissions that might be needed from third parties to include material that belongs to someone else. Please complete and submit the Permission Request Form for non-RSC Material. Please plan to submit your request well ahead of publication of your material.

If you are submitting a book typescript, you should enclose a completed Books Permission Confirmation Form to confirm that all permissions have been received.

Use of RSC Material in Non-RSC Publications

If you require permission to use material from an RSC publication you must complete and submit the online Permission Request Form (or the printed Permission Request Form for RSC Material). Requests are usually for use of a figure or diagram, but they may also be for use of the entire paper. Requests to use individual figures or diagrams are invariably granted as long as the figure has come from the original RSC author and not from another author from whom permission had to be obtained. Permission for another publisher to print an entire RSC paper may be granted in special circumstances. Please plan to submit your request well ahead of publication of your material and allow at least seven working days for your request to be processed. Please note that the RSC is unable to supply artwork for the material you may wish to reproduce.

Permission requests are handled by the Contracts & Copyright Department. The RSC is a signatory to the STM Guidelines on Permissions.

The Royal Society of Chemistry hereby grants permission for the use of the material specified below in the work described and in all subsequent editions of the work for distribution throughout the world, in all media including electronic and microfilm. You may use the material in conjunction with computer-based electronic and information retrieval systems, grant permissions for photocopying, reproductions and reprints, translate the material and to publish the translation, and authorize document delivery and abstracting and indexing services. The Royal Society of Chemistry is a signatory to the STM Guidelines on Permissions (available on request).

Article/Chapter Title : Optical Properties of Quantum Confined Nanoparticles
Journal/Book Title : THESIS TITTLE: Manganese containing Semiconductor Nanoclusters
Editor/Author(s) : Chhatra B. Khadka
Publisher : The University of Western Ontario, Canada

Journal/Book Title : JOURNAL OF MATERIALS CHEMISTRY
Editor/Author(s) : Nikolai Gaponik
Volume Number : 20
Year of Publication : 2010
Description of Material : Figure 1 (page 5175)
Page(s) : 5174-5181

Copyright © 2010, The Royal Society of Chemistry

TERMS AND CONDITIONS John Wiley & Sons, Inc.

1. The materials you have requested permission to reproduce (the "Materials") are protected by copyright.
2. You are hereby granted a personal, non-exclusive, non-sublicensable, non-transferable, worldwide, limited license to reproduce the Materials for the purpose specified in the licensing process. This license is for a one-time use only with a maximum distribution equal to the number that you identified in the licensing process. Any form of republication granted by this licence must be completed within two years of the date of the grant of this licence (although copies prepared before may be distributed thereafter). The Materials shall not be used in any other manner or for any other purpose. Permission is granted subject to an appropriate acknowledgement given to the author, title of the material/book/journal and the publisher. You shall also duplicate the copyright notice that appears in the Wiley publication in your use of the Material. Permission is also granted on the understanding that nowhere in the text is a previously published source acknowledged for all or part of this Material. Any third party material is expressly excluded from this permission.

3. With respect to the Materials, all rights are reserved. Except as expressly granted by the terms of the license, no part of the Materials may be copied, modified, adapted (except for minor reformatting required by the new Publication), translated, reproduced, transferred or distributed, in any form or by any means, and no derivative works may be made based on the Materials without the prior permission of the respective copyright owner. You may not alter, remove or suppress in any manner any copyright, trademark or other notices displayed by the Materials. You may not license, rent, sell, loan, lease, pledge, offer as security, transfer or assign the Materials, or any of the rights granted to you hereunder to any other person.

4. The Materials and all of the intellectual property rights therein shall at all times remain the exclusive property of John Wiley & Sons Inc or one of its related companies (WILEY) or their respective licensors, and your interest therein is only that of having possession of and the right to reproduce the Materials pursuant to Section 2 herein during the continuance of this Agreement. You agree that you own no right, title or interest in or to the Materials or any of the intellectual property rights therein. You shall have no rights hereunder other than the license as provided for above in Section 2. No right, license or interest to any trademark, trade name, service mark or other branding ("Marks") of WILEY or its licensors is granted hereunder, and you agree that you shall not assert any such right, license or interest with respect thereto.

5. NEITHER WILEY NOR ITS LICENSORS MAKES ANY WARRANTY OR REPRESENTATION OF ANY KIND TO YOU OR ANY THIRD PARTY, EXPRESS, IMPLIED OR STATUTORY, WITH RESPECT TO THE MATERIALS OR THE ACCURACY OF ANY INFORMATION CONTAINED IN THE MATERIALS, INCLUDING, WITHOUT LIMITATION, ANY IMPLIED WARRANTY OF MERCHANTABILITY, ACCURACY, SATISFACTORY QUALITY, FITNESS FOR A PARTICULAR PURPOSE, USABILITY, INTEGRATION OR NON-INFRINGEMENT AND ALL SUCH WARRANTIES ARE HEREBY EXCLUDED BY WILEY AND ITS LICENSORS AND WAIVED BY YOU.

6. WILEY shall have the right to terminate this Agreement immediately upon breach of this Agreement by you.

7. You shall indemnify, defend and hold harmless WILEY, its Licensors and their respective directors, officers, agents and employees, from and against any actual or threatened claims, demands, causes of action or proceedings arising from any breach of this Agreement by you.

8. IN NO EVENT SHALL WILEY OR ITS LICENSORS BE LIABLE TO YOU OR ANY OTHER PARTY OR ANY OTHER PERSON OR ENTITY FOR ANY SPECIAL, CONSEQUENTIAL, INCIDENTAL, INDIRECT, EXEMPLARY OR PUNITIVE DAMAGES, HOWEVER CAUSED, ARISING OUT OF OR IN CONNECTION WITH THE DOWNLOADING, PROVISIONING, VIEWING OR USE OF THE MATERIALS REGARDLESS OF THE FORM OF ACTION, WHETHER FOR BREACH OF CONTRACT, BREACH OF WARRANTY, TORT, NEGLIGENCE, INFRINGEMENT

OR OTHERWISE (INCLUDING, WITHOUT LIMITATION, DAMAGES BASED ON LOSS OF PROFITS, DATA, FILES, USE, BUSINESS OPPORTUNITY OR CLAIMS OF THIRD PARTIES), AND WHETHER OR NOT THE PARTY HAS BEEN ADVISED OF THE POSSIBILITY OF SUCH DAMAGES. THIS LIMITATION SHALL APPLY NOTWITHSTANDING ANY FAILURE OF ESSENTIAL PURPOSE OF ANY LIMITED REMEDY PROVIDED HEREIN.

9. Should any provision of this Agreement be held by a court of competent jurisdiction to be illegal, invalid, or unenforceable, that provision shall be deemed amended to achieve as nearly as possible the same economic effect as the original provision, and the legality, validity and enforceability of the remaining provisions of this Agreement shall not be affected or impaired thereby.

10. The failure of either party to enforce any term or condition of this Agreement shall not constitute a waiver of either party's right to enforce each and every term and condition of this Agreement. No breach under this agreement shall be deemed waived or excused by either party unless such waiver or consent is in writing signed by the party granting such waiver or consent. The waiver by or consent of a party to a breach of any provision of this Agreement shall not operate or be construed as a waiver of or consent to any other or subsequent breach by such other party.

11. This Agreement may not be assigned (including by operation of law or otherwise) by you without WILEY's prior written consent.

12. Any fee required for this permission shall be non-refundable after thirty (30) days from receipt.

13. These terms and conditions together with CCC's Billing and Payment terms and conditions (which are incorporated herein) form the entire agreement between you and WILEY concerning this licensing transaction and (in the absence of fraud) supersedes all prior agreements and representations of the parties, oral or written. This Agreement may not be amended except in writing signed by both parties. This Agreement shall be binding upon and inure to the benefit of the parties' successors, legal representatives, and authorized assigns.

14. In the event of any conflict between your obligations established by these terms and conditions and those established by CCC's Billing and Payment terms and conditions, these terms and conditions shall prevail.

15. WILEY expressly reserves all rights not specifically granted in the combination of (i) the license details provided by you and accepted in the course of this licensing transaction, (ii) these terms and conditions and (iii) CCC's Billing and Payment terms and conditions.

16. This Agreement will be void if the Type of Use, Format, Circulation, or Requestor Type was misrepresented during the licensing process.

17. This Agreement shall be governed by and construed in accordance with the laws of the State of New York, USA, without regards to such state's conflict of law rules. Any legal action, suit or proceeding arising out of or relating to these Terms and Conditions or the breach thereof shall be instituted in a court of competent jurisdiction in New York County in the State of New York in the United States of America and each party hereby consents and submits to the personal jurisdiction of such court, waives any objection to venue in such court and consents to service of process by registered or certified mail, return receipt requested, at the last known address of such party.

This is a License Agreement between Chhatra B Khadka ("You") and John Wiley and Sons ("John Wiley and Sons") provided by Copyright Clearance Center ("CCC"). The license consists of your order details, the terms and conditions provided by John Wiley and Sons, and the payment terms and conditions.

License Number: 2726180749058

License date: Aug 11, 2011

Licensed content publisher: John Wiley and Sons

Licensed content publication: Angewandte Chemie International Edition

Licensed content title: Syntheses and Crystal Structures of the New Ag-S Clusters [Ag₇O₁₆(SPh)₃₄(PhCO₂)₄(triphos)₄] and [Ag₁₈S₉₄(PR₃)₃₀]

Licensed content author: Xiu-Jian Wang, Timo Langetepe, Claudia Persau, Bei-Sheng Kang, George M. Sheldrick, Dieter Fenske

Licensed content date: Oct 18, 2002

Start page: 3818

End page: 3822

Type of use: Dissertation/Thesis

Requestor type: University/Academic

Format: Print and electronic

Portion: Figure/table

Number of figures/tables: 1

Number of extracts: 1

Original Wiley figure/table number(s) : Figure 4

Will you be translating? : No

Copyright © 2002, WILEY-VCH Verlag GmbH & Co

License Number: 2738900329152

License date: Aug 30, 2011

Licensed content publisher: John Wiley and Sons

Licensed content publication: Advanced Functional Materials

Licensed content title: Mn²⁺-Doped CdSe Quantum Dots: New Inorganic Materials for Spin-Electronics and Spin-Photonics

Licensed content author: Rémi Beaulac, Paul I. Archer, Stefan T. Ochsenbein, Daniel R. Gamelin

Licensed content date: Dec 22, 2008

Start page: 3873

End page: 3891

Type of use: Dissertation/Thesis

Requestor type: University/Academic

Format: Print and electronic

Portion: Figure/table

Number of figures/tables: 1

Original Wiley figure/table number(s): Figure 2

Will you be translating?: No

Copyright © 2008 WILEY-VCH Verlag GmbH & Co

CURRICULUM VITAE

Chhatra B. Khadka

Education

2005 - Present Ph. D. Candidate, Department of Chemistry, *The University of Western Ontario*, London, Canada

2000 - 2004 Bachelors of Science, Honours Environmental Chemistry, Trent University, Peterborough, Ontario, Canada

Publications

Khadka, C.B.; Eichhöfer, A.; Weigend, F.; Corrigan, J.F. “Zinc chalcogenolate complexes as molecular precursors to Mn²⁺ containing ZnE (E= S, Se) nanoclusters”. Submitted to *Inorganic Chemistry*, **2011**, Manuscript ID ic-2011-00307g

Khadka, C.B.; Macdonald, D. G.; Lan, Y.; Powell, A. K.; Fenske, D.; Corrigan, J.F. “Trimethylsilylchalcogenolates of Co(II) and Mn(II): From mononuclear coordination complexes to clusters containing -ESiMe₃ moieties (E= S,Se)”. *Inorganic Chemistry*, **2010**, *49*, 7289-7297

Niebel, T.; Macdonald, D.G.; **Khadka, C.B.**; Corrigan, J.F. “Synthesis and characterization of trans-Pd(II)-trimethylsilylchalcogenolates”. *Zeitschrift für Anorganische und Allgemeine Chemie*, **2010**, *636*, 1095-1099

Degroot, M.W.; **Khadka, C.B.**; Rösner, H.; Corrigan, J. F. “ZnS and ZnSe nanoparticles via solid-state and solution thermolysis of zinc silylchalcogenolate complexes”. *Journal of Cluster Science*, **2006**, *17*, 97-110

Oral Presentations

Khadka, C.B.; Corrigan, J.F. “Zinc chalcogenolate complexes as molecular precursors to Mn²⁺ containing ZnE (E= S, Se) nanoclusters”. 93rd Canadian Society for Chemistry Conference and Exhibition. Toronto, Ontario. **May 29- June 2, 2010**.

Khadka, C.B.; Corrigan, J.F. “Zinc chalcogenolate complexes as molecular precursors to Mn²⁺ containing ZnE (E= S, Se) nanoclusters”. 42nd Annual Inorganic Discussion Weekend. Guelph, Ontario. **Nov 27- 29, 2009**.

Khadka, C.B.; Corrigan, J.F. Synthesis of Trimethylsilylchalcogenolate complexes of Manganese (II) and Cobalt (II): Precursors to Ternary Nanoclusters. 40th Annual Inorganic Discussion Weekend. Toronto, Ontario. **Nov 2-4, 2007**.

Poster Presentations

Khadka, C.B.; Corrigan, J.F.; Powell, A. K. Manganese (II) and Cobalt (II) Trimethylsilylchalcogenolates: Precursors to Ternary Nanomaterials. 92nd Canadian Society for Chemistry Conference and Exhibition. Hamilton, Ontario. **May 30- June 3, 2009.**

Khadka, C.B.; Corrigan, J.F. Coordination complexes of manganese with reactive trimethylsilylchalcogenolate ligands: precursor to ternary Mn-XII-XVI nanomaterials. 39th Annual Inorganic Discussion Weekend. Ottawa, Ontario. **Oct 27-29, 2006.**

Teaching experience

2009 - 2010 Teaching Assistant, *The University of Western Ontario*, London, Canada.

Instructed and supervised 2nd and 3rd year undergraduate students in the synthesis and characterization of inorganic compounds.

2005 - 2009 Discovering chemistry (1050)

Supervised and assisted students in first year general chemistry.

Awards

Western Graduate Research Scholarship (WGRS). The University of Western Ontario. **Sept 2005-Sep 2010.**

A Special International Research Experience (**ASPIRE**) Award, **2007**. Worked with Prof. Annie K. Powell's Group at the Institut für Anorganische Chemie, Universität Karlsruhe, Karlsruhe, Germany.

Nominated for graduate teaching assistant award (for first year undergraduate lab course). **2005.**

Trent International Program (TIP) Entrance Scholarship. **Sept 2000- May 2004.**